ABSTRACT

Name: Naw May Pearl

Department: Chemistry and Biochemistry

Title: Cytochrome *c* Binding to Cytochrome *c* Peroxidase: Mutagenesis and Kinetic Studies

Major: Chemistry

Degree: Doctor of Philosophy

Approved by:

Date:

James Erman

Dissertation Director

October 24, 2007

NORTHERN ILLINOIS UNIVERSITY

ABSTRACT

The interaction between cytochrome *c* peroxidase (CcP) and cytochrome *c* is investigated through the characterization of charge-reversal mutations on CcP. Forty-four point mutants involve converting an acidic residue to a lysine residue, while two mutants involve positive-to-negative charge reversal, R31E and K149D.

The mutants are characterized by uv-visible spectroscopy. The ratios of the absorbance in the Soret band to that in the protein band near 280 nm, A_{Soret}/A_{280}, are comparable to those of wild-type enzyme, with few exceptions. Many of the charge-reversal mutations induce changes in the heme coordination, from predominantly penta-coordinate heme as found in wild-type CcP to predominantly hexa-coordinate heme in D37K, K149D, D241K, and E267K. At pH 7.5, the fraction of hexa-coordinated heme increases for all mutants, indicating a pH-dependent shift in the binding of the sixth ligand.

Analyses of the circular dichroic spectra for representative samples indicate that neither single-site mutations nor changes in heme coordination produce significant changes in the secondary structure of the proteins.

Determination of the rates of the hydrogen peroxide reactions from stopped-flow studies indicate that penta-coordinate mutants have bimolecular rate constants similar to the wild type enzyme, while increases in hexa-coordination produce species which are less reactive toward hydrogen peroxide.

Steady-state kinetic studies of the H_2O_2 oxidation of yeast cytochrome *c* catalyzed by CcP and its mutants yield the maximum turnover number, V_{max}/e_0, and the Michaelis constant, K_M. Values of V_{max}/e_0 show a general correlation with the fraction of active enzyme, with turnover numbers decreasing with decreases in the fraction of active enzyme. The Michaelis constant, K_M, correlates well with the equilibrium constant for protein-protein binding. Five mutants, R31E, D34K, D37K, E118K, and E290K, show at least a twenty-four-fold increase in K_M, indicating a decrease in affinity for cytochrome *c* in these mutants. These five mutants are clustered at or near the crystallographically determined binding site. These results indicate the presence of a single cytochrome *c* binding domain on the surface of CcP.

NORTHERN ILLINOIS UNIVERSITY

CYTOCHROME *c* BINDING TO CYTOCHROME *c* PEROXIDASE: MUTAGENESIS AND KINETIC STUDIES

A DISSERTATION SUBMITTED TO THE GRADUATE SCHOOL

IN PARTIAL FULFILLMENT OF THE REQUIREMENTS

FOR THE DEGREE

DOCTOR OF PHILOSOPHY

DEPARTMENT OF CHEMISTRY AND BIOCHEMISTRY

BY

NAW MAY PEARL

DEKALB, ILLINOIS

DECEMBER 2007

Certification:

In accordance with departmental and Graduate School policies, this dissertation is accepted in partial fulfillment of degree requirements.

James Erman

Dissertation Director

October 24, 2007

Date

TABLE OF CONTENTS

Chapter Page

LIST OF TABLES

LIST OF FIGURES

Figure Page

Figure Page

Figure Page

Figure Page

LIST OF APPENDICES

CHAPTER I

INTRODUCTION

Heme proteins carry out a variety of functions in living organisms and are generally classified into three main groups, namely, the (A) oxygen transport/storage proteins such as myoglobin, (B) electron transfer proteins such as cytochrome *c*, and (C) heme enzymes such as cytochrome *c* peroxidase (CcP). Heme enzymes catalyze the oxidation of a wide variety of organic and inorganic compounds by utilizing either molecular oxygen or hydrogen peroxide as oxidant (1). Heme sensors such as FixL and guanylate cyclase are contained in a fourth class of heme proteins that is of recent discovery. Heme sensors can detect the presence of ligands such as O_2, CO, and NO and regulate physiological processes based on the presence or absence of ligands (1). Hemoproteins contain two components, the protein and the heme prosthetic group. "A heme is an octahedral complex of iron with porphyrin, in which the iron is held in the plane of porphyrin by four pyrrole nitrogens" (2). A porphyrin is a conjugated π system composed of four pyrrole rings connected by methine bridges (3). Coordination of an iron to the porphyrin ring produces heme, Figure 1.1. Naturally occurring hemes have different groups on the two β carbons of each of the four pyrrole groups of the porphyrin ring, positions that are labeled 1 through 8 in Figure 1.1. The most common heme is based on protoporphyrin IX, which has methyl groups at positions 1, 3, 5, and 8, vinyl

groups at positions 2 and 4, and propionate groups at positions 6 and 7. This heme is called either protoheme IX or heme *b*. Other relatively common hemes are heme *a* and heme *c*. Apart from these three major heme groups, there are additional, less common heme groups. Heme *a* is found in the *a*-type cytochromes and has a long isoprenoid tail attached to position 2 and an aldehyde group in position 8 of the porphyrin ring. In heme *c*, the vinyl groups at positions 2 and 4 in protoporphyrin IX are reduced to ethyl groups and attached to the protein via thioether linkages between the ethyl substituents from the heme and cysteinyl sulfurs from the protein (3, 4).

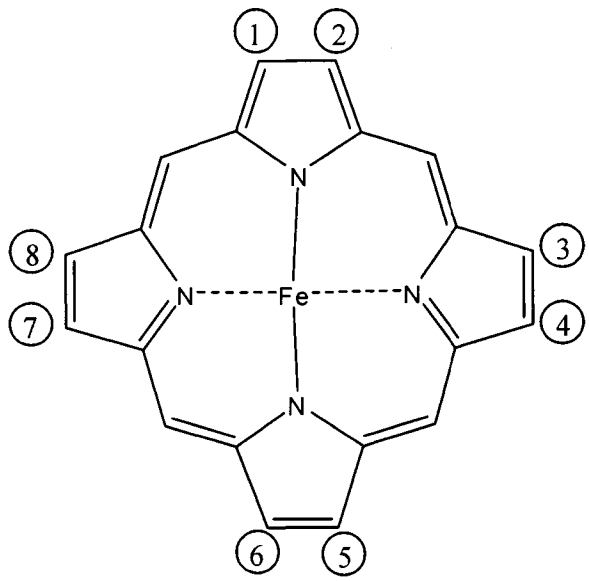

Figure 1.1. Basic structure of a heme group showing the coordination of the iron to the porphyrin ring. Different heme groups have different substituents on the β carbons of the pyrrole rings. The positions for the substituent groups are labeled 1 through 8 in the diagram.

Binding of the heme prosthetic group to the protein occurs in different ways. The heme iron forms an octahedral complex with the four nitrogen atoms of the porphyrin

ring occupying four equatorial positions. Generally, at least one of the two axial sites on the heme iron is coordinated to an amino acid side chain residue such as histidine, cysteine, tyrosine, or methionine, and in some cases both axial positions are coordinated to amino acid side chains. The porphyrin ring can be covalently attached to the protein as in the example of heme *c*, where the ethyl substituents of the heme are covalently linked through thioether linkages with the cysteinyl sulfurs of the protein (4). In general, the heme groups of most heme proteins are non-covalently bound to the polypeptide. How the polypeptide chain and heme group interact is considered important in determining the intrinsic reactivity of the heme group and allows the various heme proteins to carry out different functions. For instance, the heme group in myoglobin is located near the protein surface while the heme group in CcP is deeply buried inside the protein (5, 6). Molecular oxygen diffuses into the myoglobin structure by displacing atoms of the polypeptide chain (7) while in CcP there is an access channel for the entry of hydrogen peroxide (6). The relative positions of heme groups within polypeptide chains have evolved to optimize the functions of the various heme proteins.

The porphyrin ring has a conjugated double bond system, Figure 1.1, with low-lying electronic energy levels. Transitions between these energy levels account for the absorption of visible light by the heme and the production of highly colored heme proteins (2-4, 8). Heme proteins exhibit selective absorption over a broad spectral range between 200 to 1000 nm. The spectral range can be subdivided into four regions: (A) the near IR from about 800 to 1000 nm, which contains weak absorption bands associated with vibronic interactions between the axial ligands and the heme iron, (B) the visible region between about 450 and 700 nm, which contains absorbances associated with the α

and β bands of the heme group and ligand-to-metal charge transfer bands in some heme derivatives, (C) the near UV region between 300 and 450 nm, which contains the γ, or Soret, band and the δ band, and (D) the ultra-violet region below 300 nm, which contains absorbances due to the polypeptide chain (8). The visible and near UV spectral regions, between about 700 and 240 nm, are the most frequently examined and have been used to characterize various types of heme derivatives. The spectral characterization of heme proteins will be discussed in greater detail in Chapter III.

Cytochrome *c* Peroxidase Catalysis, Structure, and Reactivity

Yeast Cytochrome *c* peroxidase (Enzyme Commission number: EC 1.11.1.5, ferrocytochrome *c*: hydrogen-peroxide oxidoreductase), a heme enzyme, was first discovered in brewer's yeast in 1940 and is localized between the inner and outer membrane of yeast mitochondria (9-12). The function of the enzyme is detoxification of high concentrations of hydrogen peroxide to protect the organism (13). CcP decreases toxic levels of hydrogen peroxide by catalyzing its reduction to water using reducing equivalents from ferrocytochrome *c* according to Equation 1.1. C^{2+} and C^{3+} in Equation

$$2C^{2+} + H_2O_2 + 2H^+ \xrightarrow[CcP]{} 2C^{3+} + 2H_2O \qquad (1.1)$$

1.1 represent the Fe(II) and Fe(III) forms of cytochrome *c*. In exploring the mechanism of CcP catalysis, Yonetani found that CcP can be converted to a stable enzyme intermediate by the addition of a stoichiometric amount of hydrogen peroxide (14).

Yonetani called this intermediate Compound ES. Titration of Compound ES with either ferrocyanide or ferrocytochrome *c* indicated that Compound ES contained two oxidizing equivalents per enzyme hematin unit (14).

The catalytic mechanism involves oxidation of the native enzyme by hydrogen peroxide to the enzyme intermediate initially called Compound ES by Yonetani (14). This intermediate, the first enzyme intermediate in the catalytic cycle, is now called CcP Compound I, CcP-I (15). CcP-I contains two oxidized sites, an oxyferryl Fe (IV) heme group and a tryptophan π-cation radical located within van der Waals distance of the heme (16). Interaction with ferrocytochrome *c* and intracomplex electron transfer reduces CcP-I back to the native state via a second enzyme intermediate, CcP Compound II, CcP-II (13). A minimal catalytic mechanism of CcP is shown in Equations 1.2-1.4.

$$CcP + H_2O_2 \rightarrow CcP\text{-}I + H_2O \quad (1.2)$$

$$CcP\text{-}I + C^{2+} + H^{+} \rightarrow CcP\text{-}II + C^{3+} \quad (1.3)$$

$$CcP\text{-}II + C^{2+} + H^{+} \rightarrow CcP + C^{3+} + H_2O \quad (1.4)$$

In the above equations, CcP represents the native Fe (III) enzyme, CcP-I represents an intermediate oxidized two equivalents above the Fe (III) state and CcP-II is the one electron reduction product of CcP-I. CcP-II can exist as either an oxyferryl, Fe (IV) species ($CcP\text{-}II_F$) or the Trp-191 radical form ($CcP\text{-}II_R$) (15, 17). Steps 2 and 3, Equations 1.3 and 1.4, involve complex formation between cytochrome *c* and CcP and intracomplex electron transfer between these two proteins. Electron transfer from

ferrocytochrome *c* to either of the two oxidized sites in CcP-I and CcP-II is essentially irreversible.

The structure of CcP and its active site structure are shown in Figures 1.2 and 1.3 (6). The heme group is buried inside the protein with the heme edge about 10 Å from the nearest molecular surface. The proximal heme pocket contains His-175, Asp-235 and Trp-191. Trp-191 is in van der Waals contact with both His-175 and the porphyrin ring. The Asp-235 carboxylate group is hydrogen bonded to the side chains of both His-175 and Trp-191. The N_δ of the proximal His-175 is in close contact and hydrogen bonded with the carboxylate of Asp-235. This imparts greater anionic character to the imidazole in the stabilization of the higher oxidation states of the heme (6). A study by Goodin and McRee (18) indicates that the Asp-His-Fe interaction, which is similar to the catalytic triad of serine proteases, found in CcP is believed to modulate the character of histidine as a metal ligand. The distal heme pocket is composed of Arg-48, Trp-51 and His-52 (6).

CcP reacts rapidly with hydrogen peroxide, defining its function as a peroxidase, and produces the stable enzyme intermediate Compound I (Equation 1.2). The proposed mechanism for the reaction between CcP and hydrogen peroxide is shown in Figure 1.4. The mechanism for the formation of CcP-I was proposed by Poulos and Kraut (19) based upon the initial CcP crystal structure. In Figure 1.4, the top left corner represents native CcP and the distal heme pocket, which is above the heme plane. The distal heme pocket contains Arg-48, Trp-51 and His-52 in the active site. The proximal histidine, His-175 coordinated to heme iron, and Trp-191 are shown below the heme plane. The first step of the reaction occurs when hydrogen peroxide diffuses into the heme pocket and binds to the heme iron while His-52 accepts a proton from the hydrogen peroxide. Here His-52

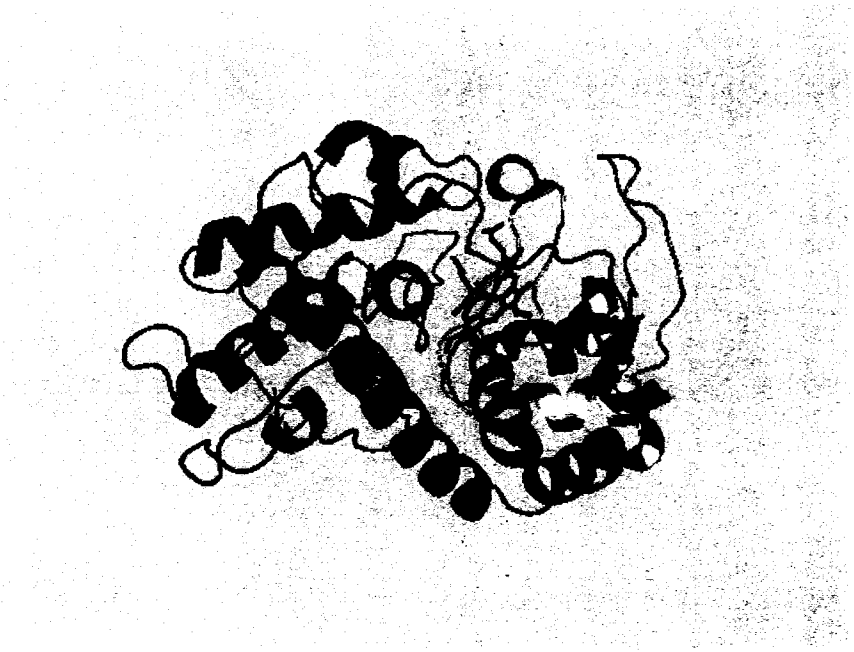

Figure 1.2. A representation of the three-dimensional structure of CcP determined by x-ray crystallography (6). The coordinates were obtained from the Protein Data Bank (PDB identification number 2CYP). PyMol was used to generate this image.

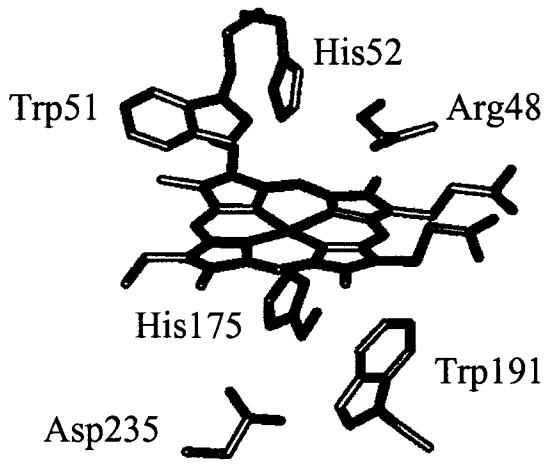

Figure 1.3. Active site structure of CcP (6). The proximal histidine, His-175, is coordinated to heme iron and Trp-191 and Asp-235 are in the proximal heme pocket. The distal pocket residues are Arg-48, Trp-51 and His-52.

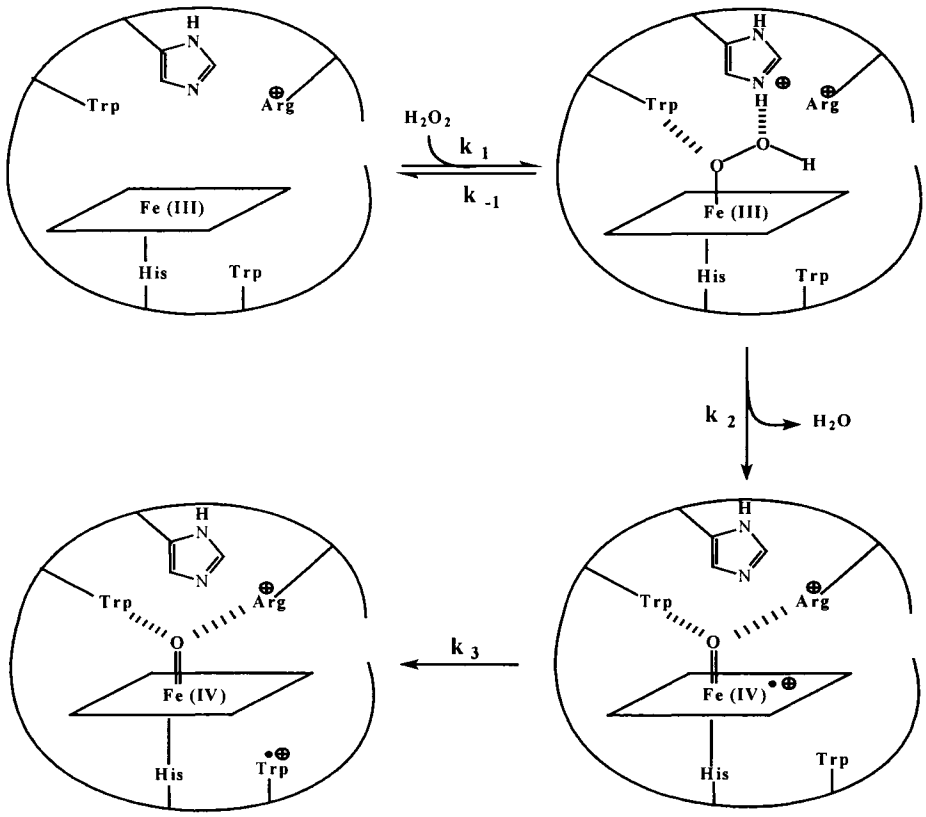

Figure 1.4. Proposed mechanism for CcP compound I formation. CcP (upper left) reacts with H_2O_2 to form a peroxy complex (upper right). His-52 acts as a base and accepts a proton from H_2O_2 to facilitate peroxide binding. The positively charged Arg-48 and His-52 stabilize the transition state for heterolytic cleavage of the oxygen-oxygen bond of the bound peroxide to form an oxyferryl Fe(IV) porphyrin π-cation radical species (lower right). This intermediate state is stabilized by hydrogen bonding between the iron-bound oxygen and both Arg-48 and Trp-51. Trp-191 reduces the porphyrin π-cation radical to generate CcP compound I (lower left).

acts as a base by accepting the proton. In the second step, the positive charges on His-52 and Arg-48 stabilize the transition state. This results in the heterolytic cleavage of the bound peroxide to produce a hydroxide ion. The distal histidine acts as an acid and donates a proton to the hydroxide ion for the release of water. The oxygen-oxygen bond cleaves heterolytically and leaves an electron-deficient oxene bound to the heme iron. In the lower right, electron transfer from the heme iron and the porphyrin ring stabilizes the oxene and generates the classic peroxidase compound I with an oxyferryl Fe(IV) and a porphyrin π-cation radical. The porphyrin π-cation radical is reduced by Trp-191, resulting in the CcP-I with oxyferryl Fe(IV) and Trp-191 π-cation radical species shown in the lower left panel (13, 19).

The 1.7 Å resolution refined crystal structure of yeast cytochrome *c* peroxidase by Finzel *et al.* (6) identified two factors which might contribute to the ability of the enzyme to stabilize the high oxidation state of the heme iron during catalysis. The first finding was the formation of a hydrogen bond between the proximal histidine and Asp-235, which contributes to the electronegative character of the coordinating histidine side chain. Asp-235 is also hydrogen bonded to Trp-191. The position and orientation of the proximal histidine, with little conformational flexibility, seems to be important for catalysis in constraining the high-spin iron in the heme plane. The second finding was that the heme environment in cytochrome *c* peroxidase is more polar than in cytochrome *c* or in the globins due to the presence of Arg-48 and five water molecules in close proximity of the heme. The positive charge on the heme iron seems to be stabilized by the increased polarity of the heme environment (6).

A comparison of the active site structures of metmyoglobin (5) and cytochrome *c* peroxidase (6) is shown in Figure 1.5. Both metmyoglobin and cytochrome *c* peroxidase have a protoporphyrin IX prosthetic group with a proximal histidine coordinated to the heme, His-175 in CcP and His-93 in myoglobin. On the distal side of the heme, the region where H_2O_2 and O_2 react with the heme, the two proteins have essentially equivalent histidine residues, His-52 in CcP and His-64 in myoglobin, which carry out important roles in determining the reactivity of the heme (1). In CcP, replacing His-52 with Leu decreased the rate of reaction with H_2O_2 by five orders of magnitude, which implies that His-52 is important for enzymatic activity (20). The functional differences between CcP and myoglobin might be due to the relative polarity of the heme environment in CcP due to the presence of Arg-48 in the distal heme pocket, which retains a positive charge to quite high pH. On the other hand, the distal heme pocket of myoglobin is relatively nonpolar due to the presence of Phe-43 and Val-67. There is also a difference between the two heme proteins on the proximal side of the heme with the histidine in myoglobin hydrogen-bonded to a peptide carbonyl group while CcP has His-175 hydrogen-bonded to the carboxylate group of Asp-235. The differences in heme environment in CcP and myoglobin contribute to the different relative stabilities of the Fe(III) and Fe(II) redox states in the two proteins (1).

As shown in Equation 1.2, CcP reacts with H_2O_2 to form CcP-I. The bimolecular rate constant for CcP and hydrogen peroxide reaction is $4.5 \times 10^7\ M^{-1}\ s^{-1}$ in the neutral pH region (21). The reaction rate is pH dependent, decreasing at both high and low pH. Protonation of His-52 is responsible for the low pH transition (21). The nature of the buffer contributes to the pK_A of His-52. The apparent pK_A of His-52 is 4.0 in buffers

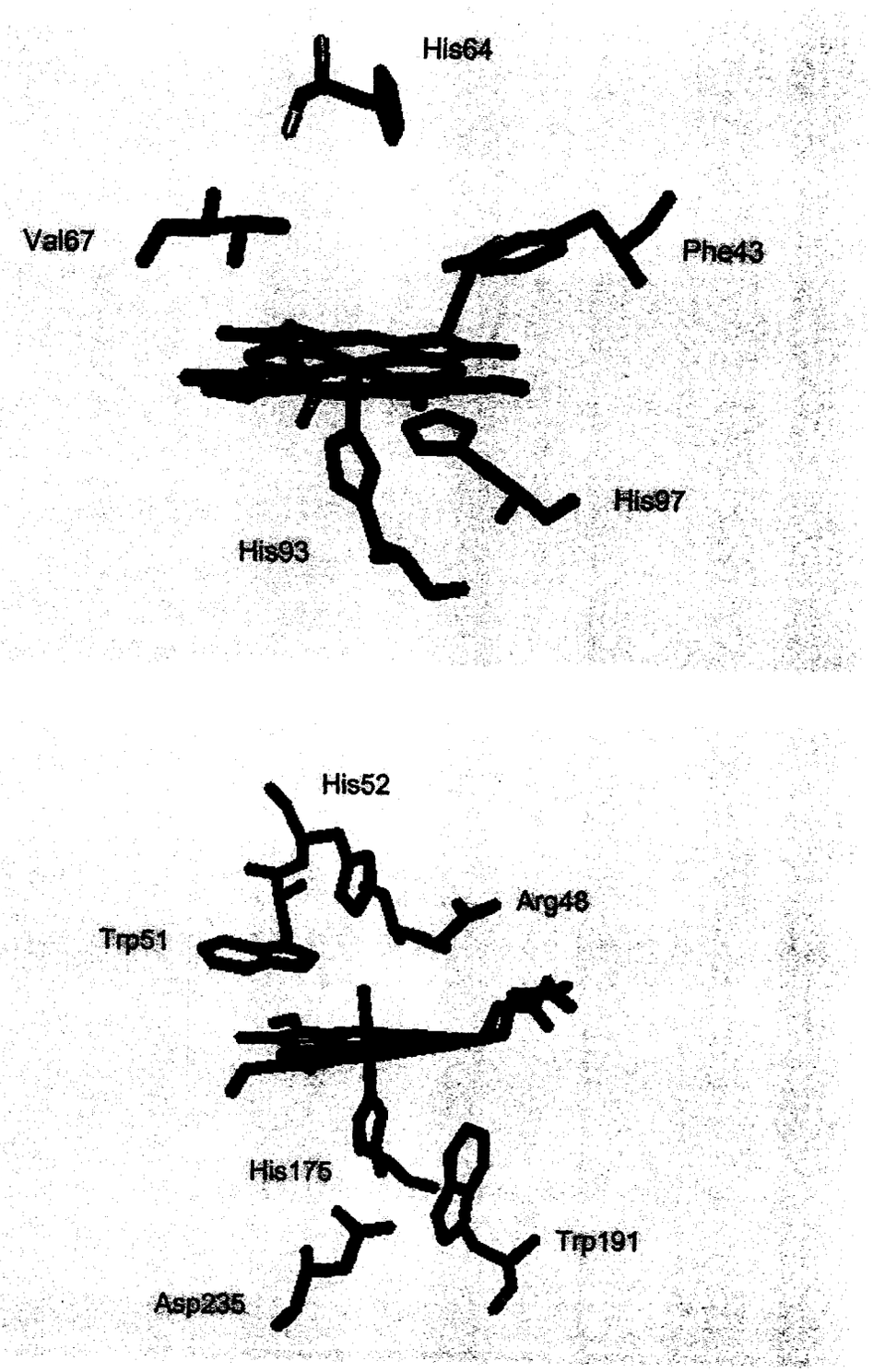

Figure 1.5. Active site structures of metmyoglobin (top) and cytochrome *c* peroxidase (bottom). The PyMol program was used for the image generation. PDB ID for myoglobin is 104M and that for CcP is 2CYP.

using phosphate to control ionic strength and 5.5 in buffers containing ~0.1M nitrate. Interaction of the protonated form of His-52 with the positively charged ferric heme iron and Arg-48 is responsible for the low apparent pK_A of the distal histidine. Replacing Arg-48 with a leucine residue by mutagenesis suggests that nitrate binds to Arg-48, neutralizing the positive charge associated with this residue, and shifting the His-52 pK_A toward the more common value of ~6 (22). There is also a decrease in the reaction rate between CcP and hydrogen peroxide at high pH with an apparent pK_A of 9.8 (23). Above pH 8, CcP undergoes a complex series of transformations that give rise to at least three distinct forms of the enzyme at alkaline pH. Observations from neutral to alkaline pH-jump experiments indicate that the initial spectroscopic changes in CcP are consistent with the conversion of the penta-coordinate, high-spin Fe (III) heme group found at neutral pH to a hexa-coordinate, low-spin Fe (III) group at alkaline pH (24). The conversion rate is very fast and occurs within the mixing time of the stopped-flow apparatus. It has an apparent pK_A of 9.7 ± 0.2, identical to the pH transition seen in the hydrogen peroxide reaction (24). This spectroscopic change is thought to be due to hydroxide ion binding to CcP at alkaline pH.

In the mid-1960s, attempts to investigate the properties and mechanism of CcP increased substantially due to the simple isolation procedure and high yield of purified enzyme (25, 26). CcP can be crystallized by dialysis against distilled water (27) and it became a routine purification step for CcP preparation. The first three-dimensional structure of CcP was first reported in 1980 (28) and since then CcP has played an important role in elucidating the structural basis for heme protein reactivity, especially in

the activation of hydrogen peroxide (19, 29), long-range electron transfer between heme proteins (30, 31), and protein-protein interactions (32, 33).

In 1982, the yeast CcP gene was isolated and cloned into *Escherichia coli* (34). The yeast CcP gene contains a coding region for a 68 amino-acid leader sequence used for importing the nuclear encoded enzyme into the intermembrane space of the mitochondria (11). Upon importation into the mitochondrial intermembrane space, the leader sequence is cleaved off, giving rise to the mature protein containing 294 amino acid residues (13).

In 1986, a site-directed mutagenesis study of the CcP gene was reported for the first time (35). A yeast strain lacking a functional CcP gene was transformed with a yeast expression vector containing either the wild-type CcP gene or one of several CcP mutant genes. This expression system yielded approximately 80 μg of purified enzyme per liter of yeast culture (35, 36). A CcP expression system in *E. coli* that yielded more than 8 mg of purified CcP per liter of culture was developed by Fishel *et al.* (37). The CcP gene engineered by Fishel *et al.* does not contain the leader sequence but has a Met residue at the -2 position to allow bacterial expression of the protein and Ile at the -1 position. This construct is called CcP (MI). CcP (MI) also differs from baker's yeast CcP in two other places, namely Ile-53 and Gly-152 instead of the Thr-53 and Asp-152 found in baker's yeast CcP (13, 37). Bacterial expression systems with very high yields of purified CcP protein were developed by Goodin *et al.* (38) and Darwish *et al.* (39) which yielded approximately 100 mg and 80 mg per liter, respectively.

CcP is a relatively stable protein and can be investigated by a vast array of techniques, including most spectroscopic methods, thermodynamics techniques, kinetic

methods, and structural studies (4, 8, 13, 6, 40-43). With the availability of large quantities of easily purified enzyme, an efficient mutagenesis system and easily crystallized enzyme, CcP has become an important model heme protein to investigate many aspects of structure/function relationships in this class of proteins (13).

The interaction between yeast CcP and its physiological partner cytochrome *c*, the CcP/cytochrome *c* system, is very useful for detailed investigation of heme protein structure/function relationships, long-range electron transfer between heme proteins, and protein-protein interactions. The nature of the cytochrome *c*/ CcP interaction during catalysis is still under active investigation with a number of questions still unresolved, including the number of cytochrome *c* binding sites on CcP, the cytochrome *c* affinity at each binding site, the location of the binding sites, the dynamic nature of the cytochrome *c* bound at each site, and the electron transfer activity of the cytochrome *c* bound at the various sites (13, 30).

Complex Formation between Cytochrome *c* and CcP

Early Studies – 1970 to 1980

Early investigation of complex formation between cytochrome *c* and CcP was carried out by Mochan and Nicholls using physical chemistry techniques (44, 45). Using gel-filtration and sedimentation velocity experiments, they demonstrated formation of a one-to-one (1:1) complex between CcP and cytochrome *c*. Polycation addition and modification of the lysine residues of cytochrome *c* inhibited the complex formation

between CcP and cytochrome *c*, implying that electrostatic interactions are important for the complex formation (44, 45). In addition, CcP is an acidic protein with an isoelectric point between 4.9 and 5.25 while cytochrome *c* is a basic protein with an isoelectric point of 10.05 (1).

Leonard and Yonetani synthesized a fluorescent CcP derivative by replacing the native heme group with protoporphyrin IX. They used the quenching of the porphyrin fluorescence upon addition of either ferro- or ferricytochrome *c* to monitor complex formation. Their results indicated formation of a 1:1 complex (46). Perturbation of the optical absorption spectrum by complex formation between CcP and ferricytochrome *c* also indicated a 1:1 complex according to the study by Erman and Vitello (47). Sedimentation equilibrium studies by Dowe *et al.* (48) and NMR spectroscopy by Gupta and Yonetani (49) also agree with the 1:1 complex formation between the two proteins.

Equilibrium Dissociation Constants for Cytochrome *c*/CcP Complex

It is universally accepted that CcP and cytochrome *c* form a high-affinity 1:1 complex with an equilibrium dissociation constant, K_{D1}, that increases upon increasing the ionic strength (1). Recent studies show that both 1:1 and 2:1 CcP/cytochrome *c* complexes can exist under certain experimental conditions (13, 42, 50-54). CcP and cytochrome *c* form a high-affinity 1:1 complex with the equilibrium dissociation constant, K_{D1}, which is 10^3 to 10^4 times smaller than the equilibrium dissociation constant, K_{D2}, for the 2:1 complex at low ionic strength. Figure 1.6 shows the ionic

strength dependence of the equilibrium dissociation constants K_{D1} and K_{D2} for the CcP and cytochrome *c* binding (13).

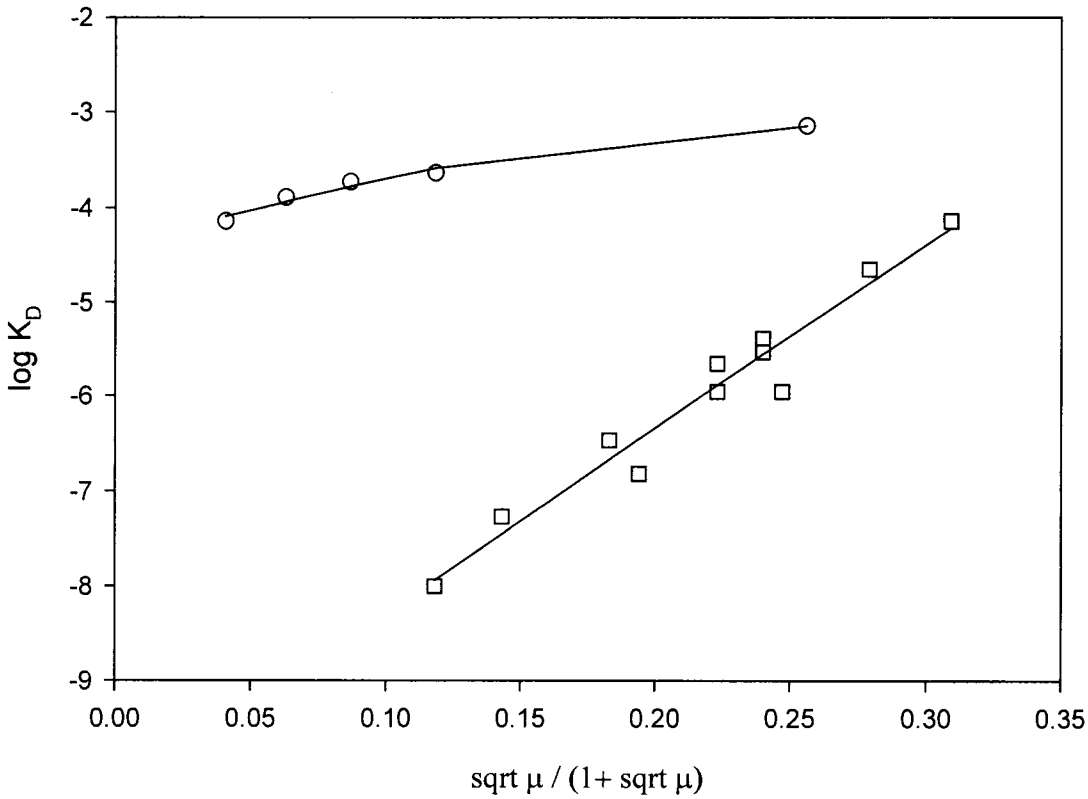

Figure 1.6. Ionic strength dependence of K_D. Open circles represent K_{D2} values and open squares represent K_{D1} values (data from references 50-54).

The K_{D1} values (open squares) were obtained from proton liberation studies (50) and isothermal titration calorimetry (51, 52). There are relatively few equilibrium data for K_{D2} (50) so data from transient-state kinetic studies using zinc-substituted CcP and cytochrome *c* (53, 54) are also included for K_{D2} values in Figure 1.6. Formation of the 2:1 complex is very weak, which makes accurate characterization difficult. The plots in Figure 1.6 show that the log of the equilibrium dissociation constants increase with

increasing ionic strength, indicating that electrostatic interactions between the two proteins are important for binding (55).

Evidence for Multiple Cytochrome *c* Binding Sites

The first suggestion of multiple cytochrome *c* binding sites on the surface of CcP came from the steady-state velocity studies of Margoliash and co-workers in 1977 (56). Their analysis shows that the oxidation of ferrocytochrome *c* by yeast CcP is biphasic under most conditions (56). The concept of multiple binding sites remained controversial initially due to alternative explanations for the biphasic steady state velocity data (57). In the late 1980s and early 1990s, the idea of multiple cytochrome *c* binding sites on CcP was reintroduced by Northrup and colleagues (58). Northrup *et al.* carried out Brownian dynamic computer simulations of the electrostatic interaction between the positively charged cytochrome *c* molecule and the negatively charged CcP molecule. Northrup and co-workers identified three potential energy minima areas on the surface of CcP that may form productive electron transfer complexes with cytochrome *c*. The areas identified as binding cytochrome *c* with high-affinity are located near Asp-34, Asp-148, and Asp-217. Stemp and Hoffman (53) investigated photoinitiated electron transfer between zinc-substituted CcP and a variety of cytochromes from different sources and analyzed their data based on the involvement of both 1:1 and 2:1 cytochrome *c*/CcP complexes.

The first non-kinetic evidence for the formation of a 2:1 cytochrome *c*/CcP came from proton linkage studies of the binding by Mauk *et al.* (50), who studied the electrostatic character of cytochrome *c*/CcP complex formation by potentiometric

titration between pH 5.5 and 7.75. Mauk *et al.* found that the data obtained at ≥ 100 mM ionic strength were adequately analyzed in terms of 1:1 complex formation, while fitting of data at lower ionic strength involves the assumption of two inequivalent binding sites for the cytochrome *c* on the peroxidase. As shown in Figure 1.6, the K_{D2} values are much larger than K_{D1}, which indicates the large difference in affinity between binding the first cytochrome *c* and binding the second.

Wang and Margoliash (59) constructed several cysteine mutants of CcP and labeled the cysteine residues with a photoactive cross-linking agent, 4-azidophenacyl bromide. They performed cross-linking experiments in the presence of cytochrome *c* and generated a mixture of 1:1 covalent cytochrome *c*/CcP complexes, which were purified and characterized. Wang and Margoliash suggest that their data support the hypothesis of multiple forms of the 1:1 cytochrome *c*/CcP complex in solution.

The current status on the interaction between cytochrome *c* and CcP is that there is a general consensus that CcP has at least two cytochrome *c* binding sites and that both 1:1 and 2:1 cytochrome *c*/CcP complexes are possible in solution. However, there is still significant disagreement concerning the cytochrome *c* affinity at each of the binding sites, the location of the second binding site, and the electron transfer activity of cytochrome *c* bound at the two sites.

Binding Models

Various models can be used to explain the binding of cytochrome *c* to the multiple binding sites on CcP ranging from a unique, non-interacting site model to an identical, interacting site model. The unique, non-interacting site model postulates that there is a primary high-affinity cytochrome *c* binding site and a secondary binding site with much weaker affinity for cytochrome *c*. The identical, interacting site model postulates that there are two (or more) binding sites with equal (or nearly equal) affinity for cytochrome *c*. This model explains the weaker formation of the 2:1 complex by invoking strong electrostatic repulsion between bound cytochromes. Figure 1.7 shows the general two-binding site scheme for cytochrome *c* and CcP, which can accommodate both the unique, non-interacting site model and the identical, interacting site model.

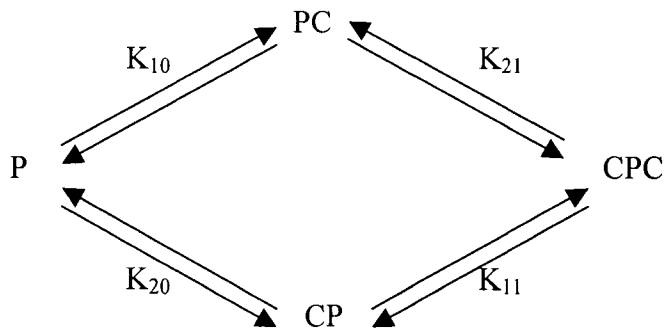

Figure 1.7. Two-binding site model for interaction between cytochrome *c* and CcP. P and C represent CcP and cytochrome *c*. PC and CP represent two different 1:1 complexes with cytochrome *c* bound either to Site 1 (PC) or Site 2 (CP) while CPC represents the 2:1 complex with both sites occupied. K_{10}, K_{20}, K_{11}, and K_{21} are microscopic equilibrium association constants, with the first subscript identifying the binding site, Site 1 or Site 2, and the second subscript indicating the number of previously bound cytochromes, either 0 or 1.

The general two-binding site model defines four microscopic (or site) equilibrium association constants, K_{ij}, where the subscript *i* indicates the identity of the binding site, either site 1 or site 2, and the subscript *j* indicates the number of previously bound cytochromes, either 0 for free CcP (species P in Figure 1.7) or 1 for either of the two 1:1 complexes, PC or CP, as defined in Figure 1.7. Equations 1.5 and 1.6 show the relationships between the observed equilibrium dissociation constants, K_{D1} and K_{D2}, and the microscopic equilibrium association constants defined in Figure 1.7.

$$K_{D1} = 1/(K_{10} + K_{20}) \quad (1.5)$$

$$K_{D2} = (K_{11} + K_{21}) / (K_{11} K_{21}) \quad (1.6)$$

In terms of the general two-binding site mode, Figure 1.7, the unique, non-interacting site model postulates unique high- and low-affinity binding sites for cytochrome *c* on the surface of CcP with binding at one site having no effect on the binding at the other site (13). This postulate means that $K_{10} = K_{11}$ and $K_{20} = K_{21}$ since there is no interaction between bound cytochromes and the affinity is solely determined by the properties of the two unique sites. In addition, $K_{10} >> K_{20}$, *i.e.*, the microscopic equilibrium association constant for the high-affinity site, is much larger than that for the low-affinity site. With these considerations, Equations 1.5 and 1.6 reduce to Equations 1.7 and 1.8 for the unique, non-interacting site model.

$$K_{D1} = 1/K_{10} \quad (1.7)$$

$$K_{D2} = 1/K_{20} \quad (1.8)$$

A consequence of the postulates for the unique, non-interacting site model is that there is essentially only one form of the 1:1 complex, i.e., in Figure 1.7, the lower pathway is not populated and the concentration of CP is less than 10^{-3} that of PC.

The postulates of the identical, interacting site model, is that $K_{10} = K_{20}$ (identical sites) and that $K_{11} = K_{21} = K_{10}e^{(-\Delta Gi/RT)}$, where ΔG_i is the interaction energy between bound cytochromes. The interaction energy is positive, indicating a repulsive electrostatic interaction between the bound cytochromes making $K_{11} << K_{10}$, where K_{10} is the intrinsic site constant. Note that $K_{21} = K_{11}$ since the interaction energy between the two sites is the same. In terms of the postulates of the identical, interacting site model, Equations 1.5 and 1.6 reduce to Equations 1.9 and 1.10.

$$K_{D1} = 1/2K_{10} \tag{1.9}$$

$$K_{D2} = 2/K_{10}e^{(-\Delta Gi/RT)} \tag{1.10}$$

In this model, K_{D2} is much larger than K_{D1} due to the repulsive interaction energy. For the identical, interacting site model, both pathways in Figure 1.7 are equally populated and the concentration of PC and CP are identical under all conditions, *i.e.*, there are two forms of the 1:1 complex.

In addition to the two extreme models presented above, there is a continuum of binding models depending upon the number of binding sites, the cytochrome *c* affinity at each site, and the interaction between sites. Consensus has not been reached as to the operative binding model for the cytochrome *c*/CcP system (13, 30).

Evidence for the unique site model comes from the crystallographic study of Pelletier and Kraut (32). Pelletier and Kraut have determined the structures of two cytochrome *c*/CcP complexes, a 1:1 complex between yeast cytochrome *c* peroxidase and yeast iso-1-cytochrome *c* and a 1:1 complex between yeast cytochrome *c* peroxidase and horse heart cytochrome *c*. The observation of a single crystal form of the 1:1 complex strongly supports a unique high-affinity binding site, although this is not definitive. The crystallographically-identified site will be called Site 1 in this dissertation.

The strongest evidence for the identical interacting site model comes from the computer simulation work of Northrup and colleagues (55), which suggests three potential energy minima areas on the surface of CcP, each of which has three or four inter-protein ionic contacts that stabilize encounter complexes at any given time.

Localization of Cytochrome *c* Binding Sites

A number of studies have been designed to identify the location of the cytochrome *c* binding sites on the surface of CcP. The first site, Site 1, has been identified through X-ray crystallography. The crystal structure of the 1:1 horse cytochrome *c*/CcP complex and the 1:1 yeast iso-1 cytochrome *c*/CcP complex provides information about Site 1 (32). The two cytochromes bind in the same general area on the surface of CcP. The horse cytochrome *c*/CcP complex includes salt bridges between Glu-35 and Glu-290 on CcP and Lys-87 and Lys-72 on cytochrome *c*, respectively. Pelletier and Kraut report no direct salt bridges in the yeast cytochrome *c*/ CcP complex, but that the carboxyl groups of Asp-34 and Glu-290 on CcP are within 4.2 and 4.4 Å of the amino

group of Lys-87 and Lys-73 on cytochrome *c*, and small adjustments of the side chains would allow salt-bridge formation (30). The software program iMolTalk at http://i.imoltalk.org analyzes interfaces between protein subunits and identifies the Glu-290/Lys-73 as a salt-bridge in the CcP/yeast cytochrome *c* complex, with an interaction distance of 3.2 Å. Apparently, the crystal structures have been further refined since the initial publication. The crystal structures demonstrated that Site 1 spans the surface of CcP between the Asp-34/Glu-35 pair and Glu-290. The 2.3 Å resolution crystal structure of 1:1 complex between yeast cytochrome *c* peroxidase and yeast iso-1-cytochrome *c* reveals a possible electron transfer pathway which includes Ala-194, Ala-193, Gly-192, and Trp-191, as the shortest straight line between the two hemes. Figure 1.8 shows the CcP/cytochrome *c* complex determined by Pelletier and Kraut with residues at or near Site 1 highlighted.

Early studies on possible locations for cytochrome *c* binding sites came from computer modeling studies (60, 61) and from chemical modification of CcP in the presence and absence of cytochrome *c* (62). The computer modeling studies suggested a binding site encompassing Asp-33, Asp-34, Asp-37, Asp-79 and Asp-217 on CcP while the chemical modification studies indicate that carboxylate groups in three regions on the surface of CcP were protected from modification by binding cytochrome *c*; these regions included residues 33 to 37, residues 221-224, and residues 290-294. The Brownian dynamic simulations of Northrup *et al.* (58) suggested cytochrome *c* binding regions near Asp-148 and Asp-217 on CcP in addition to the region near Asp-34. These studies provide some information on where Site 2 and possibly other sites may be located.

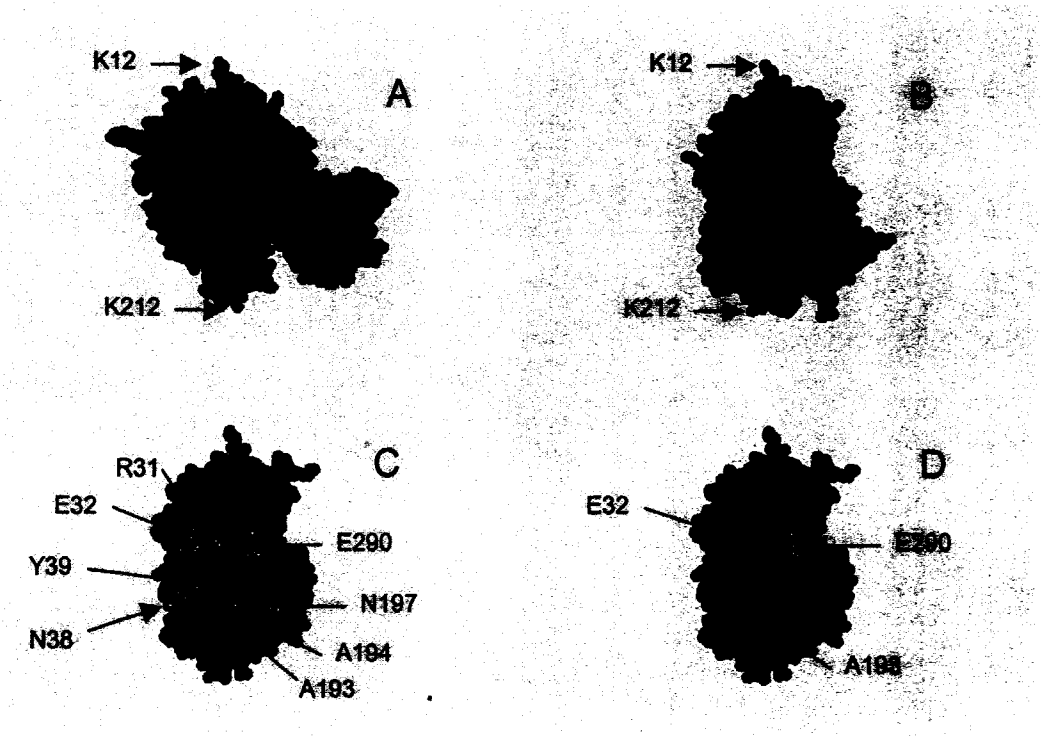

Figure 1.8. Space-filling rendering of the yeast iso-1 cytochrome *c*/CcP complex. Data from Pelletier, H. and Kraut, J. (1992) Science 258, 1748-1755 and the Protein Data Bank ID number: 2PCC. This site is defined as Site 1 in this dissertation. **A** - Model showing the left-hand face of CcP (green) and yeast cytochrome *c* (blue). Lys-12 and Lys-212 of CcP are indicated to orient the reader. **B** – Same rendering as shown in A but rotated 90° clockwise about a vertical axis extending approximately from Lys-12 to Lys-212. This view defines the front-face of CcP, the CcP surface that contains the cytochrome *c* binding site identified in this crystal structure. **C** - same view as in B but with the cytochrome *c* removed. Eleven atoms on the surface of CcP are within 3.6Å of an atom in bound cytochrome *c* and these are highlighted in gray and identified by the amino acid residues in which they reside. **D** - Same view as in C but with three residues highlighted, Glu-32, Ala-193, and Glu-290. These residues will be used to define Site 1 throughout this dissertation. The PyMol program was used for the image generation.

Long-Range Electron Transfer Reaction Debate

There are different views on biological, long-range electron transfer reactions (63). Gray and colleagues view the electron transfer process as a pathway process where the electron migrates along covalent and hydrogen bonds with some short through-space hops. They modified electron-transfer proteins and found that the rate of electron transfer did not correlate with the absolute distance between the redox centers but rather, the shortest distances through the bonding network. Based on their experience, they developed a theory for analyzing electron transfer pathways through proteins. An alternative model is provided by Dutton and colleagues (63), who believe that the distance between the two reaction centers is the major factor and not the covalent pathways. The crystal structure of the physiological partners, cytochrome *c* and CcP, reveals a possible electron transfer pathway as reported by Pelletier and Kraut, and their results support the pathway model. Dutton argues that the complex determined by Pelletier and Kraut represents only a small fraction of the cytochrome *c*-CcP conformations that exist in solution.

Goals

It is generally accepted that both 1:1 and 2:1 complexes of cytochrome *c* and CcP can exist at low ionic strength (30, 50), but only the 1:1 complex exists in significant quantities at ionic strengths above 0.100 M (64). There is experimental evidence that suggests that only Site 1 is electron-transfer active during steady-state catalysis (64). At

low ionic strength, binding of cytochrome *c* to Site 2 can increase the rate of product dissociation from Site 1, increasing the rate of catalytic turnover (64-67). On the other hand, there is experimental evidence that has been interpreted as indicating that cytochrome *c* bound at Site 1 is electron-transfer inactive while the cytochrome *c* bound at Site 2 is highly electron-transfer active (30, 66, 68). These studies also suggest that the very small amount of 2:1 complex formed at high ionic strength is responsible for the observed electron transfer activity. These latter studies use photoinitiated electron transfer reactions from zinc-substituted CcP to ferricytochrome *c*, which may not be a good model for the thermally activated catalytic reaction. Besides the aforementioned two different schools of thought, the binding interface for the second binding site, Site 2, is not well localized. There are computational models and some experimental evidence that suggest possible locations for Site 2, but consensus has not been reached on whether there is only one other binding site or whether there are multiple secondary interaction sites.

Full characterization of the interaction between CcP and cytochrome *c* is required for a complete understanding of the catalytic mechanism of the enzyme and to fully realize the potential of this system as a model for protein-protein interaction and long-range electron transfer in heme protein systems. This dissertation involves the systematic investigation of the binding interactions between cytochrome *c* and CcP. The primary objectives of this research project are as follows:

1. Construct a library of charge-reversal mutants of CcP in which each of the aspartate and glutamate residues in CcP are individually converted to lysine residues.

2. Characterize each of the charge-reversal mutants with respect to their expression, purification, and electronic absorption spectrum.
3. Determine the hydrogen peroxide reactivity of each of the charge-reversal mutants.
4. Determine the steady-state kinetic parameters for the catalytic oxidation of yeast iso-1 ferrocytochrome *c* by hydrogen peroxide for each of the mutants.
5. Map the interaction site, or sites, for formation of the 1:1 cytochrome *c*/CcP complex using the Michaelis constants from the steady-state catalysis studies.

Site-directed mutagenesis will be used as a tool to construct the surface mutants. Forty-seven CcP charge reversal mutants will be constructed by protocols described in Chapter II. Each acidic residue, aspartate or glutamate, will be converted to a lysine residue, one residue at a time, to generate a library of charge-reversal mutants in which the mutation sites are scattered over the entire surface of CcP. After the mutant genes are constructed and verified, the mutant proteins will be expressed and characterized by spectroscopy, including electronic absorption spectra and circular dichroism spectra, hydrogen peroxide reactivity, and catalysis of yeast iso-1 ferrocytochrome *c* oxidation by hydrogen peroxide using steady-state kinetics to examine the effect of each single-site mutation on the structure and function of the enzyme.

Heme proteins have characteristic absorption bands in the UV and visible region. Effects of single-site mutation as well as pH changes will be determined by absorption spectroscopy between 240-700nm. This will allow us to determine the RZ (Reinheitzahl) or purity index, the estimation of the heme coordination states, and any changes in mutant

spectra compared to rCcP. In addition, circular dichroism will be used to determine if selected charge-reversal mutations can alter the secondary structure of the protein. CcP reacts with its first substrate, H_2O_2, very rapidly and the rate of the reaction can be determined by stopped-flow techniques. Results from these transient-state kinetics analyses will be used to determine whether single-site mutations have any effect on the reaction with H_2O_2. After confirming that the mutants are active toward H_2O_2, steady-state analysis will be used to investigate the overall catalytic activity of the mutants. It has been shown (65) that the Michaelis constants, K_{M1}, from steady-state analysis correlate well with the equilibrium dissociation constants, K_{D1}, and the Michaelis constants will be used to map the effects of the charge-reversal mutations on the binding interaction with the second substrate, ferrocytochrome *c*.

Initial predictions are: (A) that the single-site mutations will have no effect on the overall structure of the enzyme, because the structure of the enzyme is robust and until now, no single-site mutation has affected the overall structure of the enzyme, (B) that mutation of residues involved in binding cytochrome *c* to form 1:1 complexes will affect the Michaelis constant, (C) that mutations with altered K_M values will cluster around Site 1 if the unique, non-interacting site binding model is correct, and (D) that mutations with altered K_M values will be scattered over at least two binding domains if the identical, interacting site model is more nearly correct.

References

1. Erman, J. E., and Vitello, L. B. (1998) Cytochrome *c* peroxidase: a model heme protein, *J. Biochem. Mol. Biol. 31*, 307-327.

2. Iizuka, T., and Yonetani, T. (1970) Spin changes in hemoproteins, *Adv. Biophys. 1,* 157-182.

3. Nelson, D. L., and Cox, M. M. (2000) *Lehninger Principles of Biochemistry*, third edition, Worth Publishers, New York, *p 205.*

4. Adar, F. (1978) Electronic absorption spectra of hemes and hemoproteins, in *The Porphyrins, Vol. III,* Dolphin, D., ed., Academic Press, New York, pp 167-209.

5. Takano, T. (1977) Structure of myoglobin refined at 2.0 Å resolution. I. Crystallographic refinement of metmyoglobin from sperm whale, *J. Mol. Biol. 110*, 537-568.

6. Finzel, B. C., Poulos, T. L., and Kraut, J. (1984) Crystal structure of yeast cytochrome *c* peroxidase refined at 1.7-Å resolution, *J. Biol. Chem. 259*, 13027-13036.

7. Case, D. A., and Karplus, M. (1979) Dynamics of ligand binding to heme proteins, *J. Mol. Biol. 132*, 343-368.

8. Drabkin, D. (1961) Analysis and interpretation of absorption spectra of haemin chromoproteins in *Haematin Enzymes, Part I,* Falk, J. E., Lemberg, R., and Morton, R. K., eds., Pergamon Press Ltd, London, pp 142-172.

9. Yonetani, T., and Ohnishi, T. (1966) Cytochrome *c* peroxidase, a mitochondrial enzyme of yeast, *J Biol. Chem. 241*, 2983-2984.

10. Altschul, A. M., Abrams, R., Hogness, T. R. (1940) Cytochrome *c* peroxidase, *J. Biol. Chem. 136*, 777-794.

11. Kaput, J., Goltz, S. and Blobel, G. (1982) Nucleotide sequence of the yeast nuclear gene for cytochrome *c* peroxidase precursor: functional implications of the pre-sequence for protein transport into mitochondria, *J. Biol. Chem. 257*, 15054-15058.

12. Reid, G. A., Yonetani, T., and Schatz, G. (1982) Import of proteins into mitochondria: import and maturation of the mitochondrial intermembrane space enzymes cytochrome b_2 and cytochrome *c* peroxidase in intact yeast cells, *J. Biol. Chem. 257*, 13068-13074.

13. Erman, J. E., and Vitello, L. B. (2002) Yeast cytochrome *c* peroxidase: mechanistic studies via protein engineering, *Biochim. Biophys. Acta 1597*, 193-220.

14. Yonetani, T. (1966) Studies on cytochrome *c* peroxidase IV. A comparison of peroxide-induced complexes of horseradish and cytochrome *c* peroxidases, *J. Biol. Chem. 241*, 2562-2571.

15. Coulson, A. F.W., Erman, J. E., and Yonetani, T. (1971). Studies on cytochrome *c* peroxidase XVII. Stoichiometry and mechanism of the reaction of compound ES with donors, *J. Biol. Chem. 246*, 917-924.

16. Erman, J. E., Vitello, L. B., Mauro. J. M., and Kraut, J. (1989). Detection of an oxyferryl porphyrin π-cation radical intermediate in the reaction between hydrogen peroxide and a mutant yeast cytochrome *c* peroxidase: evidence for tryptophan-191 involvement in the radical site of compound I, *Biochemistry 28*, 7992-7995.

17. Summers, F. E., and Erman, J. E. (1988). Reduction of cytochrome *c* peroxidase compound I and II by ferrocytochrome *c*. A stopped-flow kinetic investigation, *J. Biol. Chem. 263*, 14267-14275.

18. Goodin, D. B., and McRee, D. E. (1993) The Asp-His-Fe triad of cytochrome *c* peroxidase controls the reduction potential, electronic structure, and coupling of the tryptophan free radical to the heme, *Biochemistry 32*, 3313-3324.

19. Poulos, T. L., and Kraut, J. (1980) The stereochemistry of peroxidase catalysis, *J. Biol. Chem. 255*, 8199-8205.

20. Erman, J. E., Vitello, L. B., Miller, M. A., and Kraut, J. (1992) Active site mutations in cytochrome *c* peroxidase: a critical role for histidine-52 in the rate of formation of compound I, *J. Am. Chem. Soc. 114*, 6592-6593.

21. Loo, S., and Erman, J. E. (1975) A kinetic study of the reaction between cytochrome *c* peroxidase and hydrogen peroxide. Dependence on pH and ionic strength, *Biochemistry 14*, 3467-3470.

22. Vitello, L. B., Erman, J. E., Miller, M. A., Wang, J., and Kraut, J. (1993) Effect of arginine-48 replacement on the reaction between cytochrome *c* peroxidase and hydrogen peroxide, *Biochemistry 32*, 9807-9818.

23. Vitello, L. B., Erman, J. E., Miller, M. A., Mauro, J. M., and Kraut, J. (1992) Effect of asp-235 → asn substitution on the absorption spectrum and hydrogen peroxide reactivity of cytochrome *c* peroxidase, *Biochemistry 31*, 11524-11535.

24. Dhaliwal, B. K., and Erman, J. E. (1985) A kinetic study of the alkaline transitions in cytochrome *c* peroxidase, *Biochim. Biophys. Acta 827*, 174-182.

25. Yonetani, T., and Ray, G. S. (1965) Studies on cytochrome *c* peroxidase: I. Purification and some properties, *J. Biol. Chem. 240*, 4503-4508.

26. Yonetani, T., and Ray, G. S. (1966) Studies on cytochrome *c* peroxidase: III. Kinetics of the peroxidatic oxidation of ferrocytochrome *c* catalyzed by cytochrome *c* peroxidase, *J. Biol. Chem. 241*, 700-706.

27. Yonetani, T., Schleyer, H., Chance, B. (1966). Crystalline cytochrome *c* peroxidase and its enzyme-substrate complex, *Science 152*, 678.

28. Poulos, T. L., Freer, S. T., Alden, R. A., Edwards, S. L., Skogland, U., Takio, K., Eriksson, B., Xuong, N., Yonetani, T., and Kraut, J. (1980) The crystal structure of cytochrome *c* peroxidase, *J. Biol. Chem. 255*, 575-580.

29. Erman, J. E., Vitello, L. B., Miller, M. A., Shaw, A., Brown, K. A., and Kraut, J. (1993) Histidine 52 is a critical residue for rapid formation of cytochrome *c* peroxidase compound I, *Biochemistry 32*, 9798-9806.

30. Nocek, J. M., Zhou, J. S., De Forest, S., Priyadarshi, S., Beratan, D. N., Onuchic, J. N., and Hoffman, B. M. (1996) Theory and practice of electron transfer within protein-protein complexes: application to the multidomain binding of cytochrome *c* by cytochrome *c* peroxidase, *Chem. Rev. 96*, 2459-2489.

31. Bendall, D. S. (Ed) (1996) *Protein electron transfer*, Bios Scientific Publishers, Oxford.

32. Pelletier, H., and Kraut, J. (1992) Crystal structure of a complex between electron transfer partners, cytochrome *c* peroxidase and cytochrome *c*, *Science 258*, 1748-1755.

33. Mathews, F. S., Mauk, A. G., and Moore, G. R. (2000) Protein-protein complexes formed by electron transfer proteins, in *Protein-protein recognition* (Kleanthous, C., Ed.) pp 60-101, Oxford University Press, Oxford.

34. Goltz, S., Kaput, S., and Blobel, G. (1982) Isolation of the yeast nuclear gene encoding the mitochondrial protein, cytochrome *c* peroxidase, *J. Biol. Chem. 257*, 11186-11190.

35. Goodin, D. B., Mauk, A. G., and Smith, M. (1986) Studies of the radical species in compound ES of cytochrome *c* peroxidase altered by site-directed mutagenesis, *Proc. Natl. Acad. Sci. U.S.A. 83*, 1295-1299.

36. Goodin, D. B., Mauk, A. G., and Smith, M. (1987) The peroxide complex of yeast cytochrome *c* peroxidase contains two distinct radical species, neither of which resides at methionine 172 or tryptophan 51, *J. Biol. Chem. 262*, 7719-7724.

37. Fishel, L. A., Villafranca, J. E., Mauro, J. M., and Kraut, J. (1987) Yeast cytochrome *c* peroxidase: mutagenesis and expression in *Escherichia coli* show tryptophan-51 is not the radical site in compound I, *Biochemistry 26*, 351-360.

38. Goodin, D. B., Davidson, M. G., Roe, J. A., Mauk, A. G., and Smith, M. (1991) Amino acid substitutions at tryptophan-51 of cytochrome *c* peroxidase: effects on coordination, species preference for cytochrome *c* and electron transfer, *Biochemistry 30,* 4953-4962.

39. Darwish, K., Li, H., and Poulos, T. L. (1991) Engineering proteins, subcloning and hyperexpressing oxidoreductase genes, *Protein Eng. 4,* 701-708.

40. Asakura, T., and Yonetani, T. (1972) Studies on cytochrome *c* peroxidase: XVIII. Recombination of apoenzyme with protoporphyrin and protoheme monomethyl esters, *J. Biol. Chem. 247,* 2278-2282.

41. Kresheck, G. C., Vitello, L. B., and Erman, J. E. (1995) Calorimetric studies on the interaction of horse ferricytochrome *c* and yeast cytochrome *c* peroxidase, *Biochemistry 34,* 8398-8405.

42. Matthis, A. L., and Erman, J. E. (1995) Cytochrome *c* peroxidase-catalyzed oxidation of yeast iso-1 ferrocytochrome *c* by hydrogen peroxide. Ionic strength dependence of the steady-state parameters, *Biochemistry 34*, 9985-9991.

43. Takio, K., Titani, K., Ericsson, L. H., and Yonetani, T. (1980) Primary structure of yeast cytochrome *c* peroxidase II. The complete amino acid sequence, *Arch. Biochem. Biophys. 203*, 615-629.

44. Mochan, E. (1970) The nature of complex formation between cytochrome *c* and cytochrome *c* peroxidase, *Biochim. Biophys. Acta 216*, 80-95.

45. Mochan, E., and Nicholls, P. (1971) Complex-formation between cytochrome *c* and cytochrome *c* peroxidase: Equilibrium and titration studies, *Biochem. J. 121*, 69-82.

46. Leonard, J. J., and Yonetani, T. (1974) Interaction of cytochrome *c* peroxidase with cytochrome *c*, *Biochemistry 13*, 1465-1468.

47. Erman, J. E., and Vitello, L. B. (1980) The binding of cytochrome *c* peroxidase and ferricytochrome *c*: A spectrophotometric determination of the equilibrium association constant as a function of ionic strength, *J. Biol. Chem. 255*, 6224-6227.

48. Dowe, R. J., Vitello, L. B., and Erman, J. E. (1984) Sedimentation equilibrium studies on the interaction between cytochrome *c* and cytochrome *c* peroxidase, *Arch. Biochem. Biophys. 232*, 566-573.

49. Gupta, R. K., and Yonetani, T. (1973) Nuclear magnetic resonance study of the interaction of cytochrome *c* with cytochrome *c* peroxidase, *Biochim. Biophys. Acta. 292,* 502-508.

50. Mauk, M. R., Ferrer, J. C., and Mauk, A. G. (1994) Proton linkage in formation of the cytochrome *c*-cytochrome *c* peroxidase complex: electrostatic properties of the high- and low-affinity cytochrome binding sites on the peroxidase, *Biochemistry 33*, 12609-12614.

51. Wang, X., and Pielak, G. J. (1999) Equilibrium thermodynamics of a physiologically-relevant heme-protein complex, *Biochemistry 38*, 16876-16881.

52. Pielak, G. J., and Wang, X. (2001) Interactions between yeast iso-1-cytochrome *c* and its peroxidase, *Biochemistry 40*, 422-428.

53. Stemp, E. D. A., and Hoffman, B. M. (1993) Cytochrome *c* peroxidase binds two molecules of cytochrome *c*: evidence for a low-affinity, electron-transfer-active site on cytochrome *c* peroxidase, *Biochemistry 32*, 10848-10865.

54. Zhou, J. S., and Hoffman, B. M. (1994) Stern-Volmer in reverse: 2:1 stoichiometry of the cytochrome *c*-cytochrome *c* peroxidase electron-transfer complex. *Science 265,* 1693-1696.

55. Mei, H., Wang, K., McKee, S., Wang, X., Waldner, J. L., Pielak, G. J, Durham, B., and Millett, F. (1996) Control of formation and dissociation of the high affinity complex between cytochrome *c* and cytochrome *c* peroxidase by ionic strength and the low affinity binding site, *Biochemistry 35,* 15800-15806.

56. Kang, C. H., Ferguson-Miller, S., and Margoliash, E. (1977) Steady state kinetics and binding of eukaryotic cytochromes *c* with yeast cytochrome *c* peroxidase, *J. Biol. Chem. 252*, 919-926.

57. Kang, D. S., and Erman, J. E. (1982) The cytochrome *c* peroxidase-catalyzed oxidation of ferrocytochrome *c* by hydrogen peroxide. Steady state kinetic mechanism, *J. Biol. Chem. 257*, 12775-12779.

58. Northrup, S. H., Boles, J. O., and Reynolds, J. C. L. (1988) Brownian dynamics of cytochrome *c* and cytochrome *c* peroxidase association, *Science 241*, 67-70.

59. Wang, Y., and Margoliash, E. (1995) Enzymatic activities of covalent 1:1 complexes of cytochrome *c* and cytochrome *c* peroxidase, *Biochemistry 34,* 1948-1958.

60. Poulos, T. L., and Kraut, J. (1980) A hypothetical model of the cytochrome *c* peroxidase · cytochrome *c* electron transfer complex, *J. Biol. Chem. 255*, 10322-10330.

61. Poulos, T. L., and Finzel, B. C. (1984) Heme enzyme structure and function, *Peptide and Protein Reviews 4*, 115-171.

62. Bechtold, R., and Bosshard, H. R. (1985) Structure of an electron transfer complex. II. Chemical modification of carboxyl groups of cytochrome *c* peroxidase in presence and absence of cytochrome *c*, *J. Biol. Chem. 260*, 5191-5200.

63. Baum, R. M. (1993) Views on biological, long-range electron transfer stir debate, *C&EN News,* February 22, pp 20-23.

64. Nakani, S., Viriyakul, T., Mitchell, R., Vitello, L. B., and Erman, J. E. (2006) Characterization of a covalently-linked yeast cytochrome *c*-cytochrome *c* peroxidase complex: Evidence for a single, catalytically-active cytochrome *c* binding site on cytochrome *c* peroxidase, *Biochemistry 45,* 9887-9893.

65. Nakani, S., Vitello, L. B., and Erman, J. E. (2006) Characterization of four covalently-linked yeast cytochrome *c*/cytochrome *c* peroxidase complexes: Evidence for electrostatic interaction between bound cytochrome *c* molecules, *Biochemistry 45*, 14371-14378.

66. Leesch, V. W., Bujons, J., Mauk, A. G., and Hoffman, B. M. (2000) Cytochrome *c* peroxidase-cytochrome *c* complex: locating the second binding domain on cytochrome *c* peroxidase with site-directed mutagenesis, *Biochemistry 39*, 10132-10139.

67. Hirota, S., Tsukazaki, T., and Yamauchi, O. (2000) Interactions of cytochrome *c* peroxidase with lysine peptides, *Biochem. Biophys. Res. Commun. 268,* 395-397.

68. Zhou, J. S., and Hoffman, B. M. (1993) Cytochrome *c* peroxidase simultaneously binds cytochrome *c* at two different sites with strikingly different reactivities: titrating a "substrate" with an enzyme, *J. Am. Chem. Soc. 115,* 11008-11009.

CHAPTER II

CONSTRUCTION, EXPRESSION, AND ISOLATION OF CcP CHARGE-REVERSAL MUTANTS

Overview

The gene for yeast CcP was isolated in 1982 and cloned into *Escherichia coli* by Goltz *et al.* (1). The gene contains a 68 amino-acid leader sequence that is used for importing the nuclear-encoded enzyme into the intermembrane space of mitochondria (2). Upon importation into the intermembrane space, the leader sequence is cleaved from the protein giving a mature yeast CcP (yCcP) with 294 amino acid residues. The molecular weight of yCcP is 34.2 kDa, including the noncovalently bound heme. It was later discovered that the CcP gene isolated from the strain of yeast used by Goltz *et al.* gave an altered amino acid sequence compared to the CcP isolated and sequenced by Takio *et al.* (3) and from which the original crystal structure of CcP was determined (4). The discrepancies are Ile-53 and Gly-152 in the sequence by Goltz *et al.* (1) and Thr-53 and Asp-152 in the sequence by Takio *et al.* (3). The amino acid sequencing was done on commercial baker's yeast protein and the nuclear gene was isolated from yeast strain D273-10B (ATCC 25657) (5). Kaput *et al.* (2) also noted that Takio *et al.* (3) missed Asn-164 in their sequence. The amino acid sequence of CcP used in this dissertation is that determined by Takio *et al.* (3) with the addition of Asn-164.

Goodin *et al.* (6) were the first to report on studies using site-directed mutagenesis of the CcP gene. Mutants M172S and M172C were constructed in order to determine if Met-172 was the site of the free radical center in Compound ES (Compound I). (Note: The nomenclature for specifying mutants of CcP, and of cytochrome *c* later, is to give the one-letter abbreviation and primary sequence position of the amino acid residue in the wild-type protein followed by the one-letter abbreviation for the amino acid residue in the mutant protein. Thus, M172S indicates that Met-172 in wild-type CcP was replaced by a serine residue in the mutant protein.) Goodin *et al.* found that these mutants had little effect on the free radical in Compound I and concluded that Met-172 was not the site of the free radical. The mutated proteins were produced using a yeast expression system that yielded only 80 μg of purified CcP per liter of yeast culture (6).

Fishel *et al.* (7) reported the cloning of CcP in *E. coli* and described the addition of an extra Met and Ile at the N-terminus of the gene in order to obtain bacterial expression. This construct of the CcP gene is known as CcP(MI), where the 'M' represents the methionine at primary sequence position -2 and the 'I' represents the isoleucine at primary sequence position -1. Fishel *et al.* received the CcP gene from Goltz *et al.* (1) and CcP(MI) also contains the T53I and D152G mutations compared to baker's yeast CcP. This clone produced about 200 times as much CcP as did the yeast expression system described by Goodin *et al.* (6), about 15 mg of purified CcP per liter of culture, of which 90% is apoCcP and 10% is holo-CcP(MI). Fishel *et al.* found that purified CcP(MI) has the same spectra and catalytic activity as baker's yeast CcP.

Goodin *et al.* (8) constructed a CcP clone for expression in *E. coli* and optimized the N-terminal sequence of the gene for high levels of expression. Their clone is named

CcP(MKT) because they replaced the first three amino acid residues in the primary sequence of CcP, Thr-1, Thr-2, and Pro-3, by Met-1, Lys-2, and Thr-3. This clone produced about 80 mg of crystalline CcP(MKT) per liter of culture.

Darwish *et al.* (9) constructed a plasmid, pT7CCPZf1, for an expression system that produces a recombinant CcP with no N-terminal alterations. The Met at position -1 is cleaved from the protein by the expression system and the recombinant protein only differs from baker's yeast CcP in terms of the internal mutations T53I and D152G. This recombinant protein was not given a special name since it was not used extensively in the published literature.

Choudhury *et al.* (10) repaired the internal mutation in pT7CCPZf1 to make a clone with a sequence identical to that of baker's yeast CcP. This clone is now called rCcP for recombinant CcP. In their initial studies with rCcP, Choudhury and coworkers carried out site-directed mutagenesis on His-175 with or without a Trp-191 mutation to determine the role of the proximal ligand in peroxidase catalysis.

Teske *et al.* (11) obtained two genes for CcP in their original hosts, pT7CCPZf1, from the Poulos group (9, 10) and cloned them into pET24a+ (Novagen). The two genes corresponded to the correct baker's yeast-isolated 294-amino-acid enzyme sequence and the nuclear gene sequence that contained the T53I and D152G mutations. The proteins were expressed in *E. coli* strain BL21(DE3) that efficiently removed the N-terminal methionine required for bacterial expression. Teske *et al.* developed a more efficient 2-day isolation and purification method for recombinant yeast CcP produced from *E. coli* and extensively characterized both recombinant proteins (11, 12). All of their results

indicate that the purified recombinant wild-type enzymes are functionally and spectroscopically identical to the native, yeast-isolated wild-type enzyme.

The rCcP gene constructed in Dr. Satterlee's laboratory (11, 12) that has the same sequence as that of baker's yeast CcP was given to us and it was used for the expression and characterization of wild-type and mutant proteins in this project.

This chapter describes the experimental methods used in this research project for the site-directed mutagenesis of cytochrome *c* peroxidase surface residues and selected internal residues, protein expression, and isolation of the charge-reversal mutants. The details of the methods, preparation of buffers, broths, and reagents are given in Appendix A.

Experimental Procedures

Recombinant CcP

The plasmid pET24a+ that carries the wild-type gene for cytochrome *c* peroxidase from baker's yeast was a gift from Dr. James Satterlee, Washington State University, WA (11, 12). This plasmid has the same sequence as baker's yeast CcP. The abbreviations used throughout this dissertation are: (1) CcP, generic abbreviation for cytochrome *c* peroxidase whatever the source, (2) yCcP, authentic yeast cytochrome *c* peroxidase isolated from baker's yeast, *Saccharomyces cerevisiae*, (3) rCcP, recombinant CcP expressed in *Escherichia coli* with an amino acid sequence identical to that of yCcP, and

(4) CcP (MI), recombinant CcP expressed in *E. coli* with four amino-acid variations compared to yCcP, a Met-Ile N-terminal extension and mutations T53I and D152G.

Site-Directed Mutagenesis of CcP

The Stratagene QuikChange site-directed mutagenesis kit (Stratagene, La Jolla, CA) was used to perform the mutations. The plasmid pET24a+ carrying the rCcP gene along with two complementary oligonucleotide primers containing the desired mutation were subjected to the polymerase chain reaction using the Stratagene RoboCycler® Gradient 40 (Stratagene, La Jolla, CA).

The wild-type CcP gene was used as the template for designing the oligonucleotide primers. The oligo analyzer program offered by Integrated DNA Technologies (Coralville, IA www.idtdna.com) was used to construct primers. The primers were synthesized by MWG Biotech Inc. (High Point, NC). The primer sequences are listed in Appendix B. Agarose gel electrophoresis was used to detect the correct amplification reaction. Following the PCR reaction, the product obtained was digested with DpnI endonuclease to remove any methylated parental strands. After DpnI digestion, the PCR products were transformed into *E. coli* XLI blue for the generation of multiple copies of the plasmid. The reaction mixture containing the transformed plasmids was plated on agar plates containing kanamycin for the selection of the correct clones. Three colonies were selected and each was cultured overnight at 37 °C and 250 rpm in 5 mL LB broth with 5 μL of 30 mg/ml kanamycin. Glycerol stocks were prepared and stored at -70°C. The QIAprep Spin Miniprep kit (QUIAGEN Inc., Valencia, CA)

was used to extract the plasmids. DNA sequencing was performed by Dr. Scott Greyburn (DNA Core Facility, Department of Biological Sciences, Northern Illinois University) or by MWG Biotech (Hight Point, NC) using five primers to ensure that the entire CcP gene could be read.

The DNA sequencing results were analyzed using the Sequencher program demonstration version (www.genecodes.com). If the correct mutation was obtained, the plasmid was transformed into *E. coli* BL21(DE3) Gold for the expression of protein. Glycerol stocks were also prepared and stored at -70°C.

Expression of CcP and Charge-Reversal Mutants

A culture tube containing 5 mL Luria Bertani (LB) broth and 5 μL of 30 mg/mL kanamycin was inoculated with the desired *E. coli* BL21(DE3) glycerol stock. The culture tube was incubated at 37 °C with shaking at 250 rpm. One mL of the 5 mL culture was added to 100 mL of Terrific Broth (TB) containing 100 μL of 30 mg/mL kanamycin. The culture was grown to an optical density (OD) of 1.0-1.2 at 600 nm.

Twenty-four mL of the above culture was added to each of four Fernbach flasks containing 1 L TB broth and 1 mL of 30 mg/mL kanamycin. The 1 L culture flasks were incubated at 37 °C with shaking at 250 rpm and grown to an OD of 1.0 to 1.2 at 600 nm. Protein expression was induced by adding 2.5 mL of 0.4 M isopropyl-1-thio-β-D-galactopyranoside (IPTG). The temperature was reduced to 30 °C and the cultures were grown overnight with 250 rpm shaking. The cells were harvested by centrifuging at 4000xg (Beckman J2-21 Centrifuge, Palo Alto, CA) and stored at -20 °C.

Isolation of CcP and the Charge-Reversal Mutants

Stored cells were thawed at room temperature and 10-30 mL of lysis buffer, 0.8 mg lysozyme per gram of cell, about 4 mg each of DNAse and RNAse were added to the thawed cells. The mixture was stirred on ice in the cold room (4 °C) for 10 to 30 minutes. The sample was frozen at -70 °C for 1-2 hrs and then thawed at 4 °C overnight. For 25 – 30 g of wet cells, 8.3 mL 5% Brij58 solution (polyoxyethylene(20) cetyl ether) was added and the solution shaken gently at 4 °C for 1.5 hours. After incubation in Brij58, the sample was centrifuged at 43000xg for 35 minutes. The pellet was discarded and the supernatant was dialyzed against distilled water. The dialyzed sample was centrifuged for 30 min at 43000xg and the supernatant was collected.

The sample was applied to a Sephadex G75 column (Sigma, St. Louis, MO), 90 x 3 cm, equilibrated in 0.050 M potassium phosphate buffer, pH 6.2. Five-minute fractions, approximately 10 mL each, were collected using an LKB 2111 Multirac fraction collector. The spectra of the fractions were recorded and the fractions corresponding to the molecular weight of apoCcP were pooled and the volume was recorded.

To convert apoCcP to the holo protein, a 5-fold (mol/mol) excess of hemin (Sigma, St Louis, MO) was added to the apoCcP solution and allowed to react in the dark for 1.5 hrs. The sample was dialyzed against distilled water, and centrifuged for 30 min at 43000xg. The supernatant was applied to a DEAE Sepharose Fast Flow (Amersham Biosciences, Uppsala, Sweden) column equilibrated in 0.050 M potassium phosphate, pH

6.2. Under these conditions, CcP binds to the resin and impurities can be eluted by extensive washing with low ionic strength buffer. CcP is eluted using a potassium phosphate buffer linear gradient between 0.050 M and 1.0 M, pH 6.2. Five to 8 mL fractions were collected using an LKB 2211 SuperRac. The spectrum of each fraction was determined and used to pool the fractions containing CcP. The pooled sample was dialyzed against distilled water and concentrated using a small (10 cm) DEAE Sepharose Fast Flow column equilibrated in 0.010 M potassium phosphate buffer, pH 6.2. CcP is eluted with 1.0 M potassium phosphate buffer, pH 6.2. The spectrum of the purified protein was recorded and the sample was dialyzed against distilled water for 2 to 3 days at 4 °C, with frequent water changes. If crystals formed, they were collected and the supernatant was lyophilized. If no crystallization occurred, the solution was lyophilized. Both the crystals and lyophilized samples were stored at -20 °C.

Results

A total of forty-seven charge-reversal mutants were constructed during this work and these mutants are listed in Table 2.1 in order of the primary sequence position of the mutation. Forty-two of the forty-seven mutants constructed in this study were the conversion of either negatively-charged aspartate or glutamate residues on the surface of CcP to positively-charged lysine residues. It is expected that if a particular aspartate or glutamate is important for cytochrome *c* binding, that mutation to lysine will weaken the interaction. Three internal acidic residues were also converted to lysine residues, E76K, D106K and D235K, and these are specifically indicated in Table 2.1. With the inclusion

of the three internal residues, every aspartate and glutamate residue in CcP has been individually converted to a lysine residue.

Table 2.1. rCcP Charge-Reversal Mutations Constructed for this Study.[a]

E11K	E17K	D18K	R31E (+ to -)
E32K	D33K	D34K	E35K
D37K	D58K	D61K	E76K (internal)
D79K	E93K	E98K	D106K (internal)
E118K	D132K	E135K	D136K
D140K	D146K	D148K	K149D (+ to -)
D150K	D152K	D165K	E167K
E188K	E201K	E209K	D210K
E214K	D217K	E221K	D224K
D235K (internal)	D241K	E250K	D254K
D256K	D261K	E267K	E271K
D279K	E290K	E291K	

[a] The internal residue mutations and the positive-to-negative charge-reversal mutations are specifically indicated in the table.

In addition to the negative-to-positive charge-reversal mutations, two mutants with positive-to-negative charge reversals were also constructed, R31E and K149D. These two unique charge-reversal mutants are specifically noted in Table 2.1. Arg-31 precedes a negative cluster in which five out of six residues have carboxylate side chains beginning with Glu-32 and ending with Asp-37. This negative cluster has been

implicated in cytochrome *c* binding (13). It was thought that an Arg-31 to glutamate mutation might strengthen the binding of cytochrome *c*; therefore the R31E mutant was included in this study.

There is evidence in the literature that a second binding site for cytochrome *c* may be located near Asp-148 and it has been shown that a K149E mutation promotes formation of the 2:1 cytochrome *c*/CcP complex (14). It was decided to include a K149D mutation in this study to determine if it would enhance formation of the 1:1 complex.

Forty-seven plasmids, based on the pET24a(+) vector, were constructed with each of these plasmids containing the CcP gene with one of the mutations listed in Table 2.1. The vectors were transformed into *E. coli*, selected, re-isolated, and their sequences confirmed. The plasmids were then transformed into *E. coli* BL21(DE3) Gold for protein expression. The yield of the wet cells was about 7-15 g/L culture and the typical yield of the purified mutant proteins was 10 to 100 mg/L culture. All of the CcP mutants express well except one of the internal mutants, D106K. Three attempts to express D106K failed and it was suspected that the internal aspartate-to-lysine mutation led to protein misfolding and rapid proteolytic degradation of D106K.

In the process of single-site mutant construction, it was found that the original D152K mutant had an additional alteration and is actually a double mutant, D152K/D165Y. This double mutant was partially characterized but the data are not included in this dissertation. A single-site mutant was reconstructed and all the experiments were carried out with the single-site mutant of D152K. Comparison of steady-state kinetic data for D152K and the double mutant indicates that the results are essentially the same.

Several undergraduate students worked on this project and their efforts are gratefully acknowledged. Mutations E32K, D33K, D34K, E35K and D37K were introduced by Cassandra Meyen. Mutant E135K was prepared by Eric Choi and mutants E167K, E250K and D261K were constructed by Anthony Clementz.

Location of the Mutation Sites Relative to the Crystallographic Cytochrome *c* Binding Site

The main goal of this research project is to map the cytochrome *c* binding site (or sites) of the surface of CcP. One binding site, Site 1, has been identified by x-ray crystallography as described in Chapter I (13). Site 1 defines the "front-face" of CcP (see Figure 1.8). Figure 2.1 shows the location of Site 1, as identified by the crystal structure of the yeast iso-1 cytochrome *c*/CcP complex. Site 1 is indicated by the residues shown in black, Glu-32, Ala-193, and Glu-290. Note that both Glu-32 and Glu-290 were individually mutated to lysine residues in this study. In addition to Glu-32 and Glu-290 shown in black, all other aspartates and glutamates visible on the front face of CcP were individually converted to lysine residues and these are shown in blue in Figure 2.1. Arg-31 is located on the front-face of CcP and this residue was converted to a glutamate, a positive-to-negative charge reversal; this mutant site is shown in yellow in Figure 2.1.

Figures 2.2, 2.3, and 2.4 show the locations of all the mutation sites on the "left-hand" face, the "right-hand" face, and the "back" face of CcP, respectively. For easy reference, Table 2.2 lists the mutation sites on the four faces of CcP in order of their

primary sequence position. The two internal mutations that were expressed, E76K and D235K, are not listed in Table 2.2 nor shown in Figures 2.1 through 2.4.

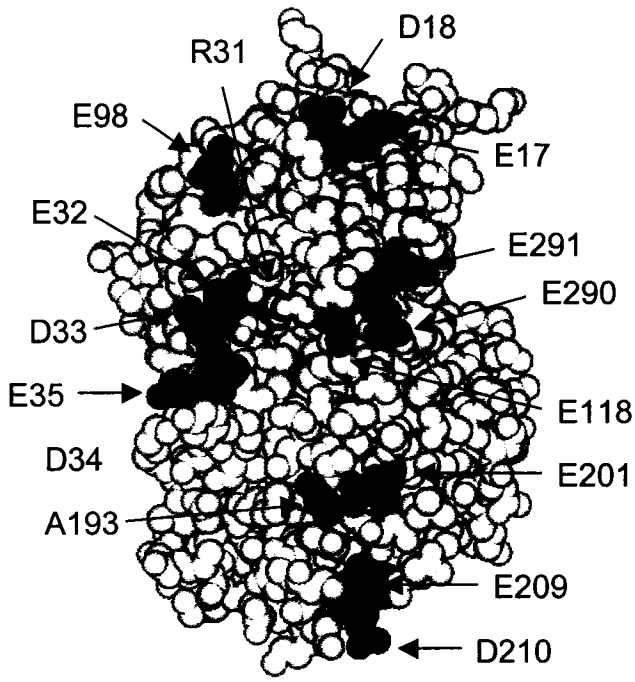

Figure 2.1. Front-face of CcP. Residues in black (Glu-32, Ala-193, and Glu-290) define the crystallographically-identified cytochrome *c* binding site, Site 1 (13). Note that Glu-32 and Glu-290 were individually mutated to lysine residues as part of this study. Other negative-to-positive charge reversal mutation sites are shown in blue, either aspartate (D) or glutamate (E) to lysine mutations. The R31E mutation site is shown in yellow.

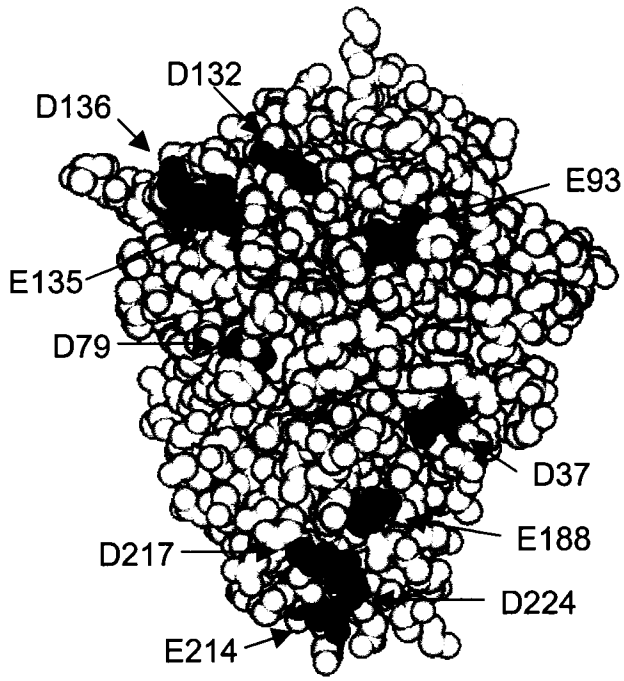

Figure 2.2. Left-face of CcP. This view of the surface of CcP is generated from that shown in Figure 2.1 by a 90° counter-clockwise rotation about a vertical axis. The negative-to-positive charge reversal mutation sites are shown in blue, either aspartate (D) or glutamate (E) to lysine mutations.

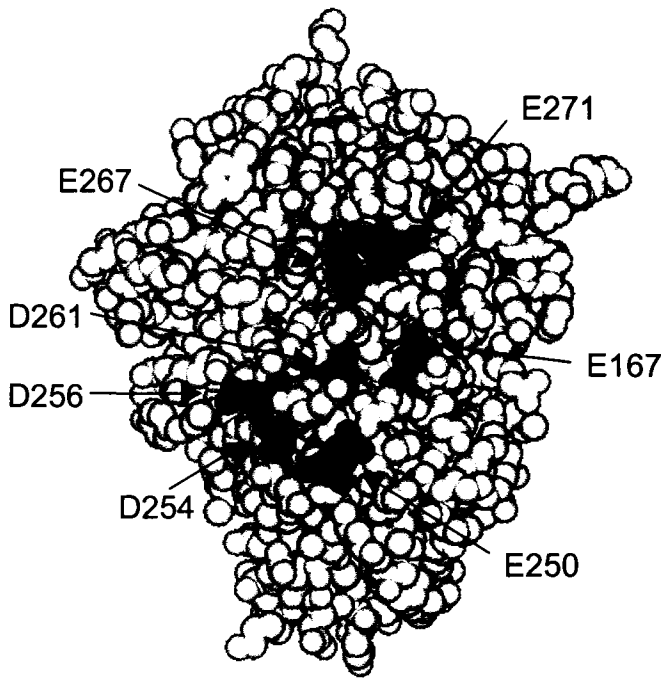

Figure 2.3. Right-face of CcP. This view of the surface of CcP is generated from that shown in Figure 2.1 by a 90° clockwise rotation about a vertical axis. The negative-to-positive charge reversal mutation sites are shown in blue, either aspartate (D) or glutamate (E) to lysine mutations.

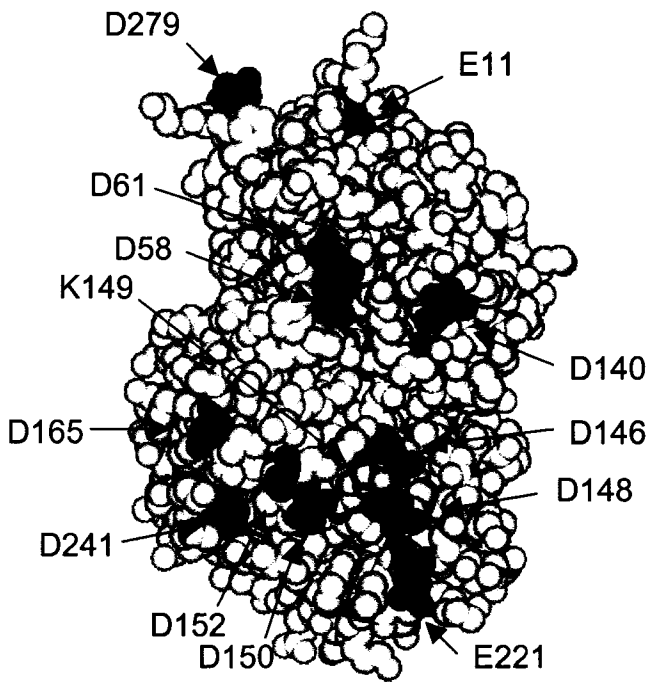

Figure 2.4. Back-face of CcP. This view of the surface of CcP is generated from that shown in Figure 2.1 by a 180° clockwise rotation about a vertical axis. The negative-to-positive charge reversal mutation sites are shown in blue, either aspartate (D) or glutamate (E) to lysine mutations. The K149D mutation site is shown in yellow.

Table 2.2. Location of the Charge-Reversal Mutants on the Four Faces of CcP. [a]

Front-Face (Figure 2.1)	Left-hand Face (Figure 2.2)	Right-hand Face (Figure 2.3)	Back Face (Figure 2.4)
E17K	D37K	E167K	E11K
D18K	D79K	E250K	D58K
R31E (+ to -)	E93K	D254K	D61K
E32K	D132K	D256K	D140K
D33K	E135K	D261K	D146K
D34K	D136K	E267K	D148K
E35K	E188K	E271K	K149D (+ to -)
E98K	E214K		D150K
E118K	D217K		D152K
E201K	D224K		D165K
E209K			E221K
D210K			D241K
E290K			D279K
E291K			

[a] The internal mutations, E76K and D235K, are not listed in the table. The positive-to-negative (+ to -) mutations are explicitly indicated in the table.

References

1. Glotz, S., Kaput, J., and Blobel, G. (1982) Isolation of the yeast nuclear gene encoding the mitochondrial protein, cytochrome *c* peroxidase, *J. Biol. Chem. 257*, 11186-11190.

2. Kaput, J., Goltz, S., and Blobel, G. (1982) Nucleotide sequence of the yeast nuclear gene for cytochrome *c* peroxidase precursor: functional implications of the pre-sequence for protein transport into mitochondria, *J. Biol. Chem. 257*, 15054-15058.

3. Takio, K., Titani, K., Ericsson, L. H., and Yonetani, T. (1980) Primary structure of yeast cytochrome *c* peroxidase: II. The complete amino acid sequence, *Arch. Biochem. Biophys. 203*, 615-629.

4. Finzel, B. C., Poulos, T. L., and Kraut, J. (1984) Crystal structure of yeast cytochrome *c* peroxidase refined at 1.7-Å resolution, *J. Biol. Chem. 259*, 13027-13036.

5. Erman, J. E., and Vitello, L. B. (2002) Yeast cytochrome *c* peroxidase: mechanistic studies via protein engineering, *Biochim. Biophys. Acta 1597*, 193-220.

6. Goodin, D. B., Mauk, A. G., and Smith, M. (1986) Studies of the radical species in compound ES of cytochrome *c* peroxidase altered by site-directed mutagenesis, *Proc. Natl. Acad. Sci. U.S.A. 83*, 1295-1299.

7. Fishel, L. A., Villafranca, J. E., Mauro, J. M., and Kraut, J. (1987) Yeast cytochrome *c* peroxidase: mutagenesis and expression in *Escherichia coli* show tryptophan-51 is not the radical site in compound I, *Biochemistry 26*, 351-360.

8. Goodin, D. B., Davidson, M. G., Roe, J. A., Mauk, A. G., and Smith, M. (1991) Amino acid substitutions at tryptophan-51 of cytochrome *c* peroxidase: Effects on coordination, species preference for cytochrome *c* and electron transfer, *Biochemistry 30*, 4953-4962.

9. Darwish, K., Li, H., and Poulos, T. L. (1991) Engineering proteins, subcloning and hyperexpressing oxidoreductase genes, *Protein Eng. 4*, 701-708.

10. Choudhury, K., Sundaramoorthy, M., Hickman, A., Yonetani, T., Woehl, E., Dunn, M. F., and Poulos, T. (1994) Role of the proximal ligand in peroxidase catalysis: Crystallographic, kinetic, and spectral studies of cytochrome *c* peroxidase proximal ligand mutants, *J. Biol. Chem. 269*, 20239-20249.

11. Teske, J. G., Savenkova, M. I., Mauro, J. M., Erman, J. E., and Satterlee, J. D. (2000) Yeast cytochrome *c* peroxidase expression in *Escherichia coli* and rapid isolation of various highly pure holoenzymes, *Protein Exprs. Purif. 19*, 139-147.

12. Savenkova, M. I., Satterlee, J. D., Erman, J. E., Siems, W. F., and Helms, G. L. (2001) Expression, purification, characterization, and NMR studies of highly deuterated recombinant cytochrome *c* peroxidase, *Biochemistry 40*, 12123-12131.

13. Pelletier, H., and Kraut, J. (1992) Crystal structure of a complex between electron transfer partners, cytochrome *c* peroxidase and cytochrome *c*, *Science 258*, 1748-1755.

14. Leesch, V. W., Bujons, J., Mauk, A. G., and Hoffman, B. M. (2000) Cytochrome *c* peroxidase-cytochrome *c* complex: Locating the second binding domain on cytochrome *c* peroxidase with site-directed mutagenesis, *Biochemistry 39*, 10132-10139.

CHAPTER III

CHARACTERIZATION OF THE CHARGE-REVERSAL MUTANTS – ELECTRONIC ABSORPTION SPECTROSCOPY

Introduction

Overview of Ferric Heme Protein Spectroscopic Properties

The electronic absorption spectra of heme proteins are sensitive to the coordination and spin state of the iron in the heme and to the nature of the heme ligands (1-4). As such, the absorption spectrum is a useful monitor of changes occurring near the active site of heme proteins. Heme is an iron-porphyrin complex with the iron in an approximate octrahedral field. The four pyrrole nitrogens of the porphyrin ring coordinate to the four equatorial positions of the iron leaving the two axial positions, the fifth and sixth coordination sites, available for coordinating to the protein and/or exogenous ligands. The fifth coordination site is typically coordinated to an amino acid residue of the protein and this is called the "proximal" residue. The proximal residue defines the proximal heme pocket. The sixth coordination site can be occupied by an amino acid residue, giving rise to a six-coordinate heme group, or it can be vacant, giving rise to a five-coordinate heme. For those heme proteins that react with exogenous ligands such as molecular oxygen, nitric oxide, carbon monoxide or hydrogen peroxide, the sixth

coordination site of the heme is either vacant or occupied by an easily displaced ligand such as water.

Iron(III), ferric iron, has five *d* electrons and Fe(III) heme proteins can have one of two spin states, either a high-spin state with five unpaired *d* electrons or a low-spin state with one unpaired and four paired *d* electrons. The number of unpaired electrons is related to the field strength of the heme ligands, which determine the splitting of the *d* orbitals of the heme iron. Weak-field ligands, such as fluoride, produce small splittings of the *d* orbitals, allowing each of the five *d* electrons to occupy a separate orbital and giving rise to the high-spin state with total spin of 5/2. Strong-field ligands, such as cyanide, give rise to large splittings of the *d* orbitals such that it is energetically favorable to pair four of the five *d* electrons in the lowest energy orbitals, leaving a single unpaired d electron and giving the low-spin state with total spin of 1/2. An intermediate spin state of 3/2 is theoretically possible but has not been unequivocally demonstrated in ferric heme proteins.

The combination of possible coordination and spin states leads to three common heme species in Fe(III) heme proteins: (A) a five-coordinate, high-spin (5c-hs) heme, (B) a six-coordinate, high-spin (6c-hs) heme, and (C) a six-coordinate, low-spin (6c-ls) heme. A five-coordinate, low-spin heme has never been observed since a vacant sixth coordination site causes very little splitting of the *d* orbitals. (The vacant site can be considered a very weak-field "ligand"). The theoretical interpretation of ferric heme proteins optical spectra is complex but several investigators have noted correlations between the optical spectra and the nature of the heme ligands and spin state (1-4). These

correlations, although empirical, are useful in qualitative interpretation of heme protein spectra.

Ferric heme proteins typically have up to six resolvable absorption bands in the near UV and visible region of the spectrum due to the heme group and an absorption band near 280 nm due to the absorption properties of the aromatic amino acids. The six heme bands are designated CT2, α, β, CT1, γ (Soret), and δ bands in order of increasing energy. CT1 and CT2 designate two ligand-to-metal charge transfer bands and these are most prominent in the spectra of high-spin hemes (4). Representative heme protein spectra are illustrated in Figures 3.1 to 3.3 for CcP and its complexes with fluoride and cyanide, respectively (5-8).

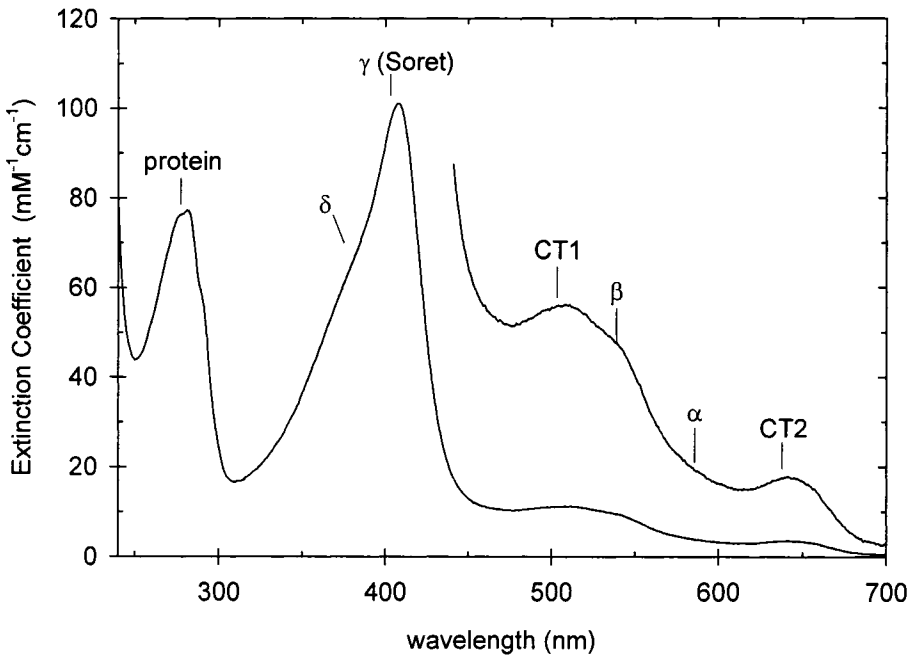

Figure 3.1. Spectrum of CcP at pH 6.0. The positions of the α, β, γ (Soret), and δ bands as well at the two charge transfer bands, CT1 and CT2, and the protein band near 280 nm are identified in the figure. Experimental conditions: 0.100 M ionic strength potassium phosphate buffer, pH 6.0, and room temperature.

The spectrum of wild type CcP, shown in Figure 3.1, is characteristic of five-coordinate, high-spin CcP. Native CcP has a five-coordinated heme iron with the fifth coordination site bonded to the ε- nitrogen of His-175 in the proximal heme pocket (see Figure 1.3). The sixth position is vacant. The main features of this spectrum include the protein band centered at 280 nm, the δ band at 380 nm, the γ or Soret band at 408 nm and the charge transfer bands, CT1 and CT2, at 506 and 646 nm, respectively. In addition, the α and β bands appear as shoulders on CT1 in this spectrum and are centered at 590 and 544 nm, respectively. Table 3.1 lists the absorption bands and their extinction coefficients.

Table 3.1. Spectroscopic Properties of CcP and its Complexes [a]

Ligand	Spin State	δ	γ (Soret)	CT1	β	α	CT2
none	hs	380 (63.6)	408 (98.0)	506 (11.1)	544 (8.3 sh)	590 (3.4 sh)	646 (3.5)
F^-	hs	350 (32.0)	405 (133.6)	493 (9.2)	544 (5.0 sh)	578 (5.3 sh)	618 (7.5)
CN^-	ls	361 (29.4)	423 (105.6)	-	544 (11.8)	576 (8.1 sh)	-

[a] The wavelengths of the band maxima are given in nm with the extinction coefficients, in units of mM^{-1} cm^{-1}, given in parenthesis.

The addition of a sixth ligand can generate a high-spin or low-spin six-coordinate protein depending on the field strength of the ligand. The spectrum of a high-spin, six-coordinate system is shown in Figure 3.2, represented by the fluoride complex of

cytochrome *c* peroxidase. The major spectroscopic changes observed in going from a 5c-hs heme protein such as rCcP to a 6c-hs heme protein such as the CcP/fluoride complex include a decrease in the absorptivity in the δ band, an increase in absorptivity in the Soret band, and a blue shift of most of the absorption bands. These characteristics are exemplified by the spectrum of fluoro-CcP, Figure 3.2. Values of the band positions and the extinction coefficients for fluoro-CcP are collected in Table 3.1.

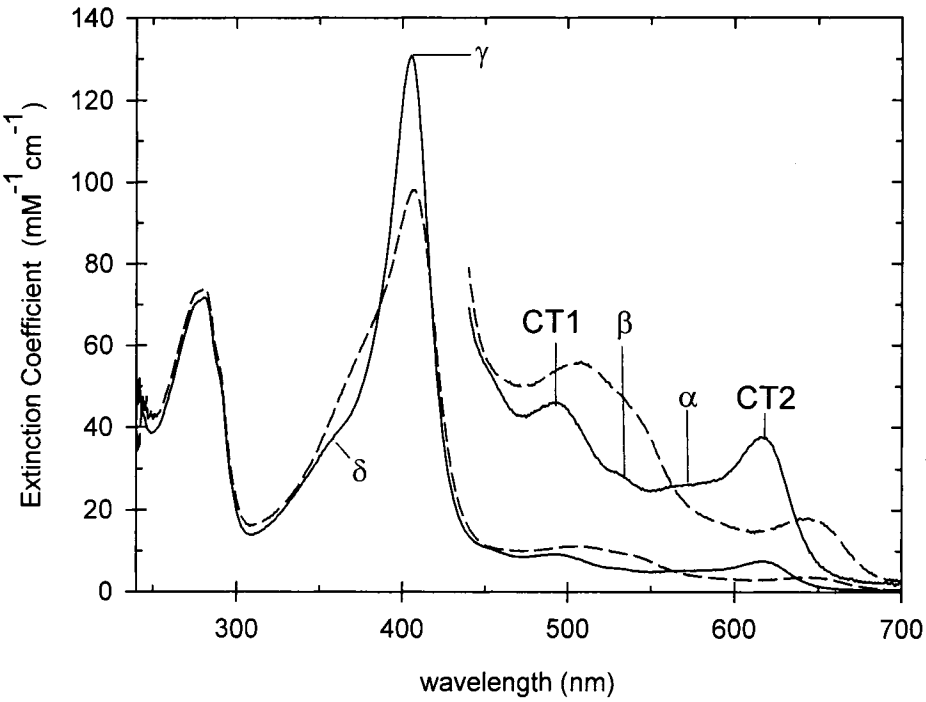

Figure 3.2. Spectrum of fluoro-CcP. The spectrum of fluoro-CcP (solid line) is shown in comparison to that of CcP (dashed line). The bands associated with the heme absorption in fluoro-CcP are indicated on the figure.

The cytochrome *c* peroxidase/cyanide complex is representative of a hexa-coordinate low-spin system. The major spectroscopic changes that occur on going from a 6c-hs heme to a 6c-ls heme include a red-shift in the Soret band and a loss of absorptivity in the charge-transfer bands. The spectrum of the CcP/cyanide is shown in Figure 3.3. Compared to CcP, the Soret band is red-shifted to 423 nm and the β band dominates the visible region of the spectrum. The α band exists as a shoulder on the β band. The charge transfer bands are very small in the CcP/cyanide spectrum. Values for the extinction coefficients for these absorption bands are collected in Table 3.1.

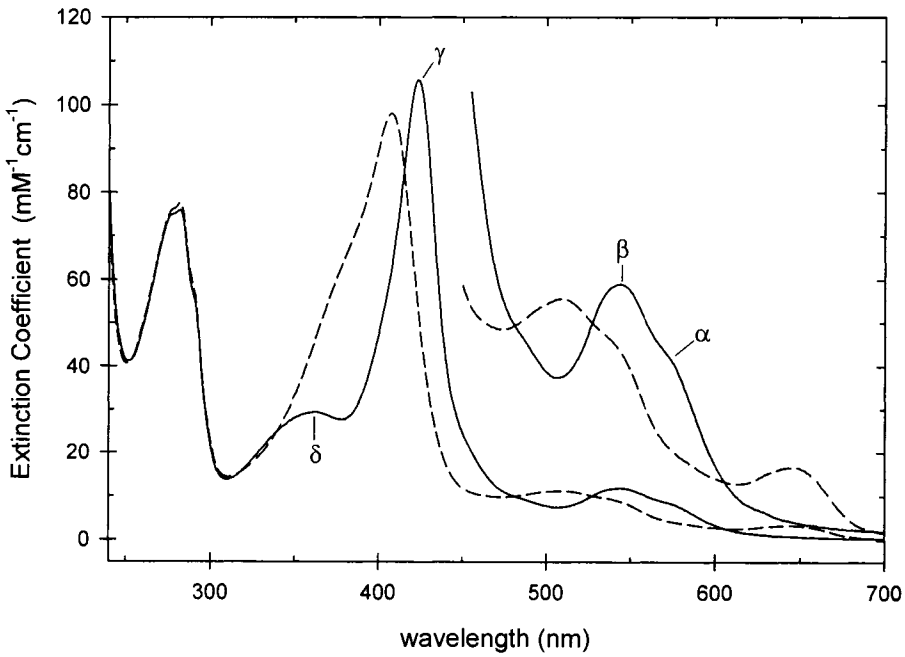

Figure 3.3. Spectrum of cyano-CcP. The spectrum of cyano-CcP (solid line) is shown in comparison to that of CcP (dashed line). The bands associated with the heme absorption in cyano-CcP are indicated on the figure. The charge transfer bands, CT1 and CT2, are generally inconspicuous in 6c-ls Fe(III) heme proteins.

In addition to the three types of ferric heme protein spectra described above, more complex spectra can occur. Intermediate field strength ligands such as water and hydroxide ion can produce equilibrium mixtures of six-coordinate, high- and low-spin forms (3). Heme proteins can also exist as equilibrium mixtures of five- and six-coordinate forms depending upon pH and ligand concentration.

Spectroscopic Characterization of Charge-Reversal Mutants

Initial characterization of the charge-reversal mutants of CcP was done by absorption spectroscopy. In addition to determining whether or not a mutation perturbs the heme ligation and spin-state of CcP, absorption spectroscopy can also provide information about the purity of the isolated mutants and the completeness of heme reconstitution. These latter two properties affect the ratio of the heme absorbance in the Soret band relative to the protein absorbance near 280 nm.

The RZ (Reinheitzahl) value (9) is the ratio of the maximum absorbance in the Soret band to the maximum absorbance in the protein band near 280 nm and is sometimes called the purity index or purity number. The RZ value should be constant for a specific heme protein under defined conditions of coordination and spin state. Decreased values of RZ suggest that the protein isolates contain impurities that absorb near 280 nm. In the case of the charge-reversal mutants, low values of RZ can also indicate incomplete heme incorporation during isolation. The *E. coli* expression system used in this study does not synthesize enough heme to produce 100% holoenzyme and

exogenous heme must be added during the isolation procedure. It is possible that the heme incorporation does not go to completion for some mutant proteins.

Experimental Methods

A Cary model 3E spectrophotometer was used to determine the spectra of wild-type and mutant proteins. The absorbance for each protein was acquired at 1 nm intervals between 240 nm and 700 nm in 100 mM potassium phosphate buffer. Spectra were obtained at both pH 6.0 and 7.5 to observe any changes in absorption due to pH. Spectra of authentic yeast CcP, yCcP, and recombinant CcP, rCcP, are included for comparison with the mutants. The extinction coefficients for yCcP and rCcP are 98 ± 3 mM^{-1} cm^{-1} and 101 ± 3 mM^{-1} cm^{-1}, respectively (8, 10).

Results

The spectroscopic properties of wild-type CcP and all the charge-reversal mutants are characterized at pH 6.0, the center of the pH region where CcP is stable, and at pH 7.5, the pH at which the steady-state and transient-state kinetic studies are performed. The spectra of all 46 mutants characterized in this study are given in Appendix C. Spectra are presented at both pH 6.0 and 7.5. In this section, selected spectroscopic parameters are presented in Table 3.2 with the mutants listed in order of the primary sequence position beginning with mutant E11K and ending with mutant E291K. At pH 6.0, the selected spectroscopic parameters included in Table 3.2 are the positions of the

Table 3.2. Spectroscopic Properties for CcP and the Charge-Reversal Mutants [a]

	pH 6.0				pH 7.5	
Mutant	$\lambda_{protein}$(nm)	λ_{Soret}(nm)	RZ	A_{Soret}/A_{380}	λ_{Soret}(nm)	A_{Soret}/A_{380}
yCcP	282	408	1.28±0.03	1.52±0.04	409	1.60±0.04
rCcP	282	408	1.28±0.03	1.60±0.05	410	1.79±0.24
E11K	279	408	1.08	1.64	412	2.19
E17K	280	408	1.22	1.61	411	2.00
D18K	281	408	1.28	1.60	410	1.74
R31E	277	406	1.18	1.59	410	1.98
E32K	282	409	1.29	1.58	409	1.62
D33K	282	409	1.29	1.60	410	1.69
D34K	282	408	1.29	1.57	408	1.63
E35K	282	408	1.30	1.58	408	1.63
D37K	283	411	1.34	2.23	414	2.59
D58K	281	408	1.31	1.80	410	2.06
D61K	281	407	1.31	1.56	410	1.77
E76K	280	409	1.19	1.73	413	2.46
D79K	280	408	1.23	1.66	410	2.33
E93K	282	408	1.33	1.55	410	1.65
E98K	281	408	1.31	1.55	409	1.62

(continued on the following page)

Table 3.2 (continued)

Mutant	pH 6.0				pH 7.5	
	$\lambda_{protein}$(nm)	λ_{Soret}(nm)	RZ	A_{Soret}/A_{380}	λ_{Soret}(nm)	A_{Soret}/A_{380}
E118K	279	409	1.12	1.62	410	1.76
D132K	279	409	1.25	1.84	414	2.74
E135K	278	409	1.24	1.71	412	1.99
D136K	281	408	1.31	1.56	412	2.05
D140K	281	407	1.32	1.49	411	1.91
D146K	281	407	1.31	1.50	409	1.64
D148K	281	408	1.26	1.66	410	1.81
K149D	280	411	1.27	2.15	413	2.74
D150K	280	408	1.30	1.77	411	2.04
D152K	281	409	1.24	1.70	411	1.95
D165K	280	410	1.25	1.72	412	1.90
E167K	278	410	1.23	1.67	410	1.70
D188K	281	409	1.21	1.85	411	2.14
E201K	280	409	0.73	1.60	410	1.75
E209K	280	409	1.22	1.87	411	2.12
D210K	281	409	1.27	1.71	411	1.93
E214K	281	408	1.27	1.59	409	1.71

(Continued on following page)

Table 3.2. (continued)

Mutant	pH 6.0				pH 7.5	
	$\lambda_{protein}$(nm)	λ_{Soret}(nm)	RZ	A_{Soret}/A_{380}	λ_{Soret}(nm)	A_{Soret}/A_{380}
D217K	282	408	1.32	1.58	408	1.64
E221K	281	408	1.30	1.58	409	1.72
D224K	282	408	1.26	1.63	409	1.74
D235K	279	411	1.32	2.53	412	2.66
D241K	277	412	1.28	2.04	413	2.33
E250K	2.77	407	1.27	1.44	409	1.57
D254K	277	407	1.18	1.64	410	1.84
D256K	282	408	1.32	1.57	409	1.66
D261K	281	407	1.37	1.48	409	1.61
E267K	279	412	1.44	2.27	412	2.47
E271K	281	408	1.29	1.57	411	1.76
D279K	281	408	1.28	1.54	411	1.85
E290K	281	407	1.26	1.57	410	1.84
E291K	281	408	1.23	1.53	411	1.87

[a] Spectra were acquired in 0.100 M ionic strength potassium phosphate buffers at pH 6.0 and 7.5 at ambient temperature. Mutant D106K did not express stable protein and is not included in the table.

Soret and the protein bands, the RZ value, and the ratio of the Soret absorbance relative to the absorbance at 380 nm, A_{Soret}/A_{380}. At pH 7.5, only the position of the Soret band and the A_{Soret}/A_{380} are tabulated. The A_{Soret}/A_{380} value reflects variation in the fraction of five- and six-coordinate heme in the various mutants and justification for including this parameter will be given in the Discussion section.

Discussion

Purity Number and Heme Incorporation in Charge Reversal Mutations

The RZ values for all 46 charge-reversal mutants are plotted in Figure 3.4 as a function of the mutant number, listed in order of their primary sequence position, *i.e.*, the left-most data point in Figure 3.4 represents the RZ value of the E11K mutant and the right-most data point represents the RZ value of the E291K mutant. The solid line in Figure 3.4 represents the average RZ value for six preparations of rCcP, 1.28 ± 0.03. The average RZ value for rCcP is identical to the average RZ value for authentic yCcP at pH 6.0 reported earlier (8). The RZ values for most mutants are within 8 % of that of rCcP ranging between 1.18 and 1.37, Figure 3.4. The similarity of RZ values between mutant enzymes and both yCcP and rCcP suggest that the purity of the samples, the extent of heme incorporation, and the extinction coefficient at the Soret maximum of the mutants are similar to those of wild-type yCcP. Figure 3.5 compares the spectrum of a typical charge-reversal mutant, D34K, with that of rCcP, with both spectra normalized to the

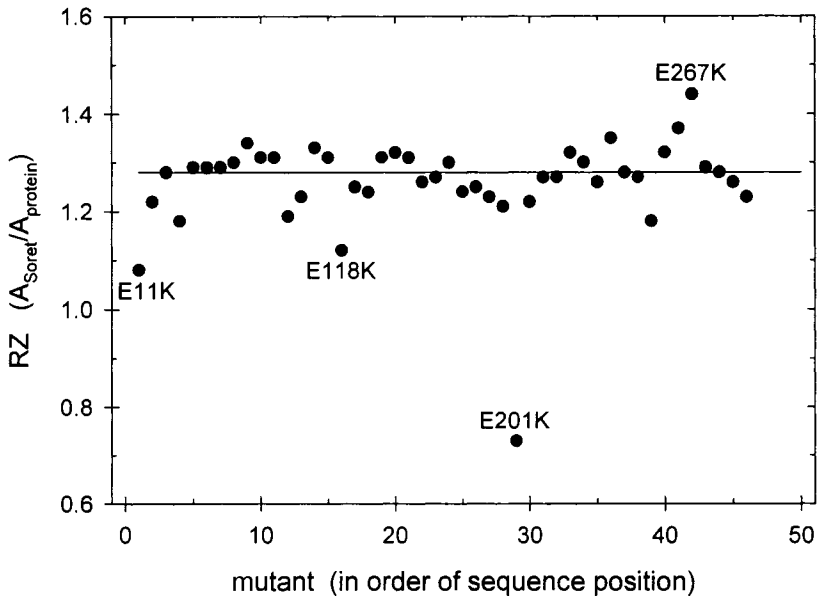

Figure 3.4. Plot of RZ, the ratio of the absorbance at the Soret maximum to that at the maximum of the protein band, for 46 charge-reversal mutants in order of primary sequence position of the mutation. The solid line is the RZ value for both yCcP and rCcP, 1.28. The four mutants with the greatest deviation from 1.28 are indicated in the figure: E11K, E118K, E201K, and E267K.

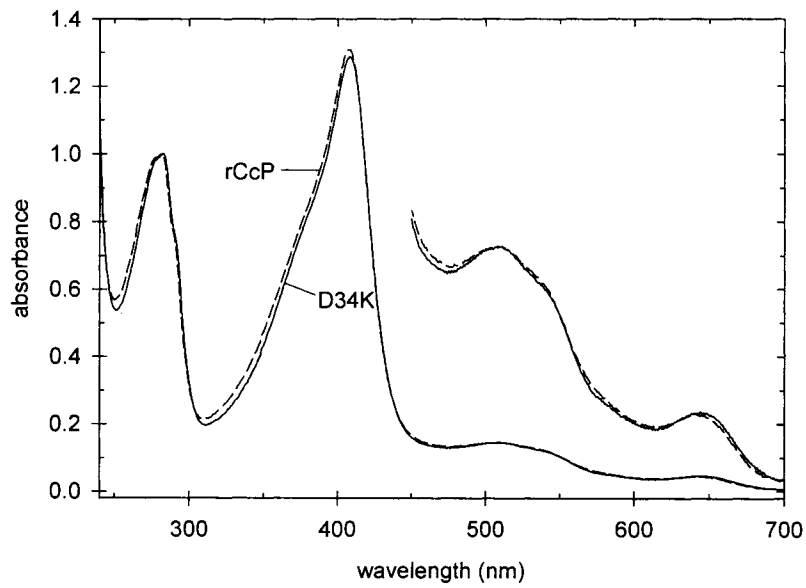

Figure 3.5 Comparison of the spectra of D34K (solid line) and rCcP (dashed line) at pH 6.0. Both spectra have been normalized to the maximum absorbance in the protein band near 280 nm.

absorbance maximum in the protein band. The spectroscopic properties are essentially identical, as are those of almost all of the charge-reversal mutants at pH 6.0. However, there are four significant outliers in the data shown in Figure 3.4 and these mutants are identified in the figure. Three of the mutants, E11K, E118K and E201K, have significantly smaller RZ values than rCcP and E267K has a significantly higher RZ. Figure 3.6 shows the spectrum of E201K as an example of a mutant with a very low RZ number and Figure 3.7 shows the spectrum of E267K as an example of a mutant with a larger than normal RZ value. In both Figures 3.6 and 3.7, the spectra are normalized to the maximum absorbance in the protein band.

The smaller RZ value for E201K, Figure 3.6, is attributed to incomplete heme incorporation into the apoenzyme during the purification rather than the co-purification of a non-heme protein impurity. This conclusion is based on the shape of the protein peak, which shows band structure characteristic of CcP, and on SDS PAGE, which does not show significant protein impurities in the samples with low RZ values. Based on the RZ values, E11K, E118K and E201K contain approximately 24%, 12% and 43% apoenzyme, respectively. For those samples that contain significant apoenzyme, the apoenzyme should not interfere with determination of the kinetic properties of these mutants since the concentration of the active enzyme is based on the heme concentration. Only the heme-containing mutant will react with hydrogen peroxide in the transient state studies and only the heme-containing mutant will be active in the steady-state oxidation of ferrocytochrome *c*, to be described in subsequent chapters.

The increase in RZ value for E267K compared to rCcP, Figure 3.7, is related to a change in heme coordination and spin state. As will be discussed in the next section,

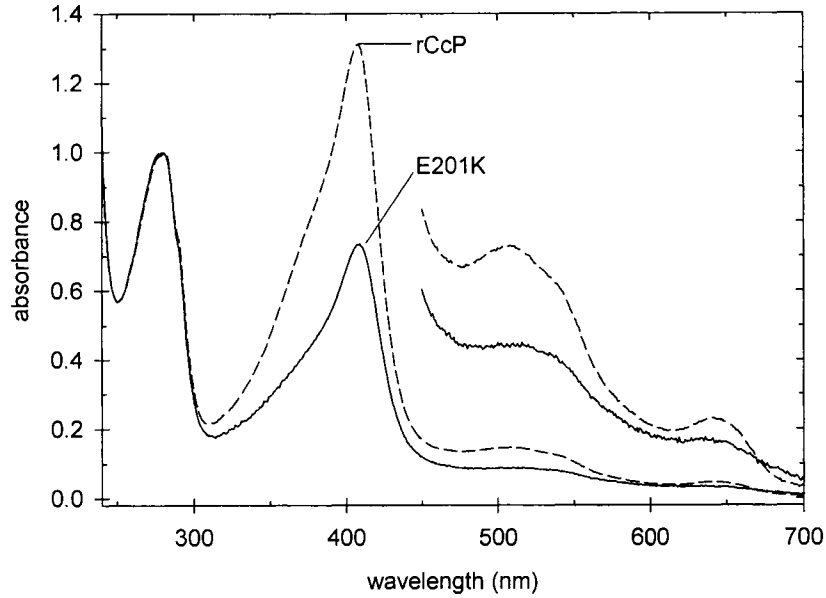

Figure 3.6. Comparison of the spectra of E201K (solid line) and rCcP (dashed line) at pH 6.0. The two spectra are normalized to the maximum absorption in the protein band near 280 nm. The low heme absorbance in E201K is attributed to incomplete heme insertion into the mutant apoprotein during isolation.

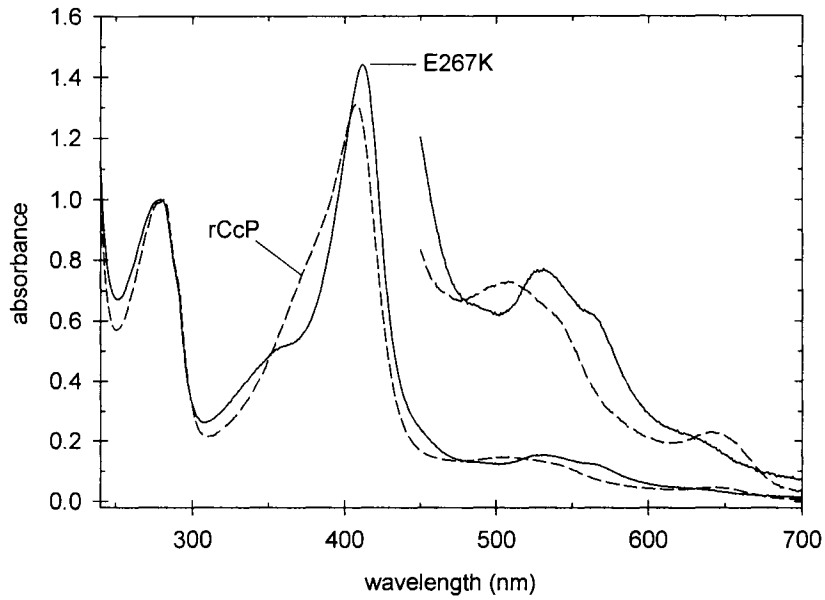

Figure 3.7. Spectrum of E267K (solid line) compared to that of rCcP (dashed line) at pH 6.0. Both spectra are normalized to the maximum in the protein band near 280 nm. The spectrum of E267K has a higher fraction of 6c-ls heme than rCcP as exemplified by the lower absorptivity in the δ band near 350 nm for E267K and near 380 nm for rCcP.

the spectrum of E267K at pH 6.0 is characteristic of a predominantly 6c-ls heme protein and this is associated with an increase in the extinction coefficient of the Soret maximum. A larger extinction coefficient in the Soret band will give a larger RZ value. One can estimate the extinction coefficient of E267K at pH 6.0 and it is ~114 mM^{-1} cm^{-1}, about 13% larger than that of rCcP.

It is possible that RZ values higher than about 1.30 for the charge-reversal mutants indicate some hexa-coordination in the protein sample and that these mutants have Soret extinction coefficients greater than the value of 98 ± 3 mM^{-1} cm^{-1} determined for yCcP and the value of 101 ± 3 mM^{-1} cm^{-1} determined for rCcP. This would be especially true if the A_{Soret}/A_{380} ratio indicates an increase in the amount of hexa-coordinate heme in the sample, as will be discussed in the next section.

Effect of Charge-Reversal Mutations on the Spectrum of CcP

The spectra of yCcP, CcP (MI), and rCcP are independent of pH between pH 4 and 7 in the absence of buffer components that bind in the heme pocket such as high concentrations of acetate and nitrate (5, 8, 11). The heme group of CcP is predominantly penta-coordinate and high-spin in the pH 4 to 7 region, Figure 3.1. There are detectable changes in the absorption spectrum above pH 7.0. Yonetani *et al.* have observed that above pH 7.5, the Soret band is red-shifted, with increased absorption at 540 and 590 nm and concomitant decreased absorption at 505 and 645 nm (5). These changes are associated with a complex series of transformations at alkaline pH leading to formation of two distinct low spin forms of CcP, followed by complete denaturation of the enzyme

at pH 12 (12, 13). The two low-spin forms of CcP have absorption spectra at alkaline pH that are consistent with a hydroxy-ligated heme and a form in which His-52 is coordinated to the heme iron (13). The five- and six-coordinate species exist in a pH-dependent equilibrium with an apparent pK_A of 9.7, with the five-coordinate form predominating at low pH and the six-coordinate forms predominating at high pH (12).

The spectral properties of the charge-reversal mutants presented in Table 3.2 do change somewhat between pH 6.0 and 7.5 consistent with a pH-dependent change in heme ligation and spin-state. The changes observed at pH 7.5 relative to that at pH 6.0 include a red-shift in the position of the Soret band and a decrease in the absorbance at the δ band position near 380 nm relative to that at the Soret maximum. The average red-shift in the Soret maximum for the mutants is about 2 nm, from an average of approximately 408 nm to 410 nm between pH 6.0 and 7.5, and is indicative of an increased amount of hexa-coordinate, low-spin heme in the mutant samples at pH 7.5.

The ratio of the absorbance at Soret maximum to that at 380 nm is also an indicator of five and six coordination (8, 11). At pH 6, yCcP has a heme group which is essentially 100% five-coordinate, high-spin and the A_{Soret}/A_{380} ratio is 1.52 ± 0.04, averaged over a large number of preparations (8). The relatively small value of the A_{Soret}/A_{380} ratio is due to the high absorptivity of the δ band that occurs near 380 nm in the 5c-hs heme proteins like CcP, Figure 3.1. Upon coordination of a ligand to the sixth coordination site, whether a weak-field ligand like fluoride or a strong-field ligand like cyanide, the δ band shifts to the blue and loses significant absorptivity. The A_{Soret}/A_{380} ratio for fluoro-CcP is 2.31and for cyano-CcP is 3.80, Figures 3.2 and 3.3. Thus,

regardless of the nature of the sixth ligand, the A_{Soret}/A_{380} ratio will increase upon conversion of five-coordinate heme in CcP to a hexa-coordinate form.

The rCcP samples isolated in our laboratory have an average A_{Soret}/A_{380} ratio of 1.60 ± 0.05, averaged over six preparations, Table 3.2. This slight variation in the A_{Soret}/A_{380} ratio for wild-type enzyme may indicate that the recombinant protein has a slightly greater tendency to form a hexa-coordinate heme than yCcP, although the change is small and similar to the experimental error in determining the absorbance ratio.

The A_{Soret}/A_{380} ratio for all of the charge-reversal mutants are plotted as a function of the primary sequence position in Figure 3.8 for the data at pH 6.0 and in Figure 3.9 for the data at pH 7.5. At pH 6.0, the A_{Soret}/A_{380} ratios tend to be close to that of rCcP with an average value of 1.67 ± 0.19 for the 46 charge-reversal mutants. However, the average is affected by four distinct outliers on the high side of the plot shown in Figure 3.8. E267K has the highest A_{Soret}/A_{380} ratio at pH 6.0 with a value of 2.26 while D37K, K149D, and D241K all have A_{Soret}/A_{380} ratios greater than 2.0.

The spectrum of E267K relative to that of rCcP is shown in Figure 3.7. The variation in the spectroscopic parameters between E267K and rCcP, Figure 3.7, is similar to that seen between cyano-rCcP and rCcP shown in Figure 3.3, providing evidence that the spectrum of E267K is that of a predominantly hexa-coordinate low-spin heme complex, as suggested in the previous section when it was shown that E267K has a higher RZ value than rCcP. All of the charge-reversal mutants with A_{Soret}/A_{380} ratios greater than the value of 1.52 ± 0.04 observed for yCcP most likely have equilibrium mixtures of penta- and hexa-coordinate heme groups with the penta-coordinate form

dominating at pH 6.0 except for D37K, K149D, D241K, and E267K which are predominantly hexa-coordinate.

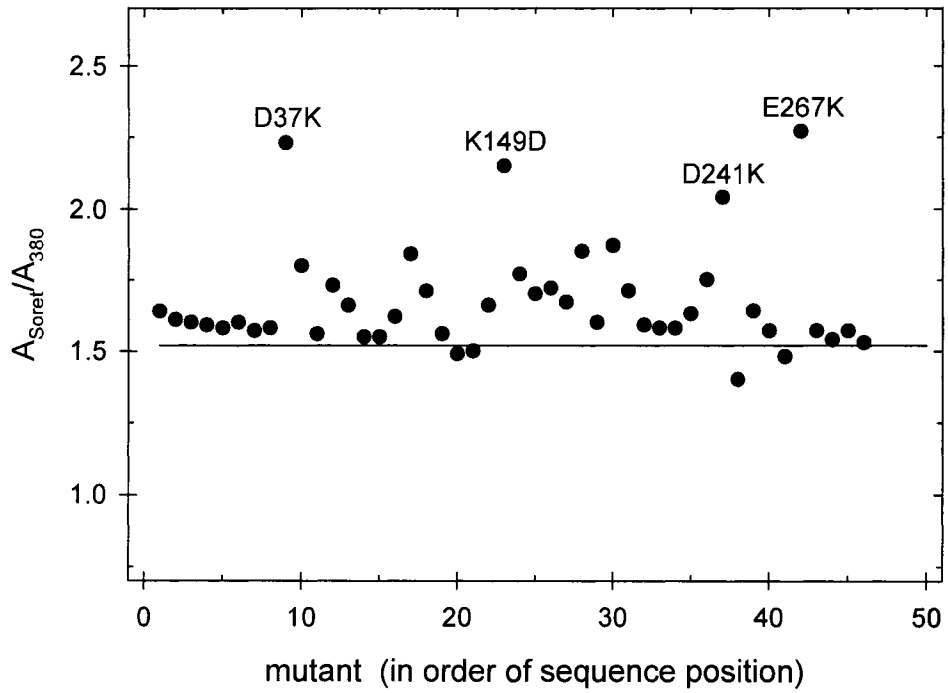

Figure 3.8. Plot of A_{Soret}/A_{380} ratio at pH 6.0 for 46 charge-reversal mutants in order of primary sequence position of the mutation. The solid line is the A_{Soret}/A_{380} ratio for yCcP at pH 6.0, 1.52. Four mutants have A_{Soret}/A_{380} values greater than 2.0 and these are D37K, K149D, D241K, and E267K.

At pH 7.5, the A_{Soret}/A_{380} ratio is larger than the ratio at pH 6.0 for all the proteins included in Table 3.2, indicating a higher concentration of six-coordinate forms at the higher pH. Both the average value of the A_{Soret}/A_{380} ratio and its standard deviation are much larger at pH 7.5, Figure 3.9, than at pH 6.0, Figure 3.8. The average A_{Soret}/A_{380} ratio for the 46 mutants is 1.91 ± 0.31 at pH 7.5 compared to the average of 1.67 ± 0.19 at

pH 6.0. The A_{Soret}/A_{380} ratio varies between 1.56 for the E250K mutant at the low end of the scale to 2.74 for both D132K and K149D at the high end of the scale, Figure 3.9.

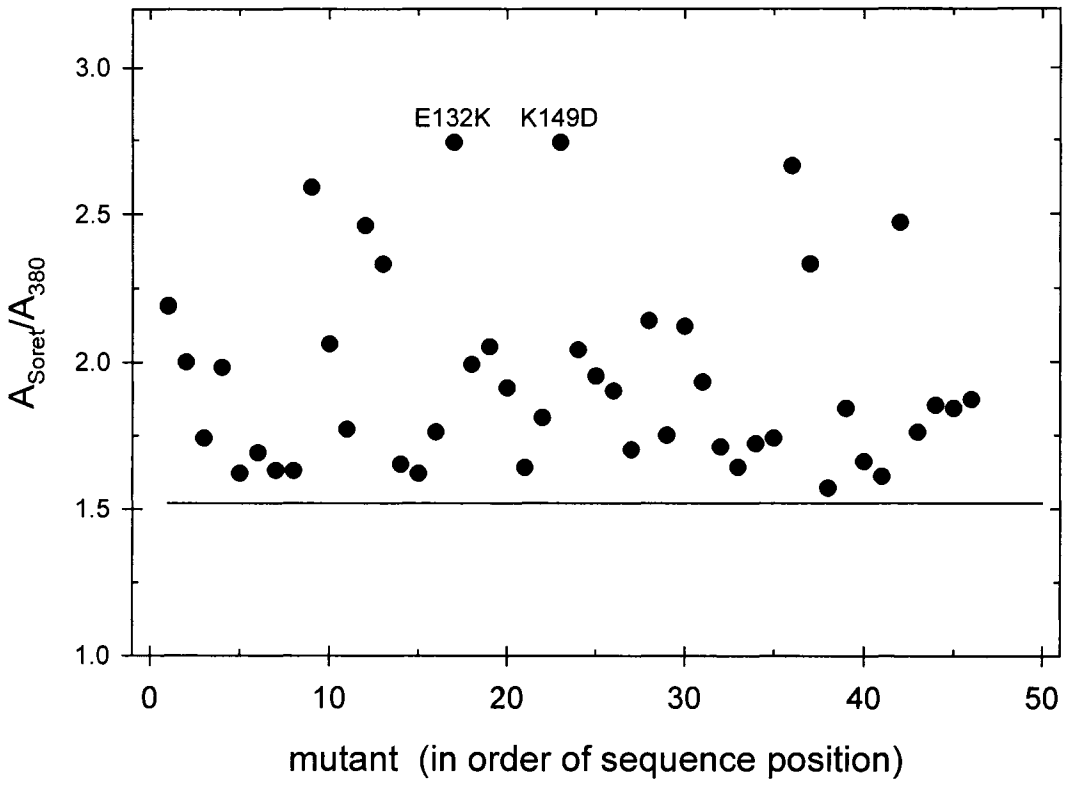

Figure 3.9. Plot of A_{Soret}/A_{380} ratio at pH 7.5 for 46 charge-reversal mutants in order of primary sequence position of the mutation. The solid line is the A_{Soret}/A_{380} ratio for yCcP at pH 6.0, 1.52, representing the A_{Soret}/A_{380} ratio for a 100% 5c-hs complex. Two mutants, E132K and K149D, have the largest values for A_{Soret}/A_{380} ratio observed in this study, a value of 2.74.

The spectra of D132K and K149D at pH 7.5 have the highest A_{Soret}/A_{380} ratio observed for any of the mutants examined in this study and these two spectra are essentially identical, Figure 3.10. Since the spectra of D132K and K149D are most

similar to that of an authentic six-coordinate, low-spin compound, cyano-CcP (Figure 3.3), the spectra of D132K and K149D could represent that for the 100% six-coordinate, low-spin form of rCcP. Two previous studies of alkaline transitions in yCcP (12) and CcP(MI) (11) have demonstrated that two different low-spin alkaline forms of CcP exist above pH ~7.5 and these two forms have been attributed to a hydroxy-ligated heme and to a heme group in which the distal histidine, His-52, is coordinated to the heme, giving a bis-imidazole-like complex. Likewise, a distal pocket mutant of CcP(MI), D235N, shows two different six-coordinate, low-spin heme forms that can exist between pH 5 and 9, again attributed to the hydroxy-ligated and bis-imidazole forms of CcP (13). The spectrum of D132K and K149D at pH 7.5 is similar, but not identical, to the two low-spin forms of D235N (13). In spite of the slight differences in the spectrum of D132K and K149D compared to those of D235N, we postulate that the spectrum of both D132K and K149D represents that of a hydroxy-ligated heme in the charge-reversal mutants. In all three of the previous studies (11-13), it was postulated that hydroxy-ligation preceded formation of the bis-imidazole form and that the bis-imidazole form only occurred at high pH where the polypeptide chain had sufficient flexibility to allow the distal histidine to move about 6 Å in order to coordinate to the heme iron.

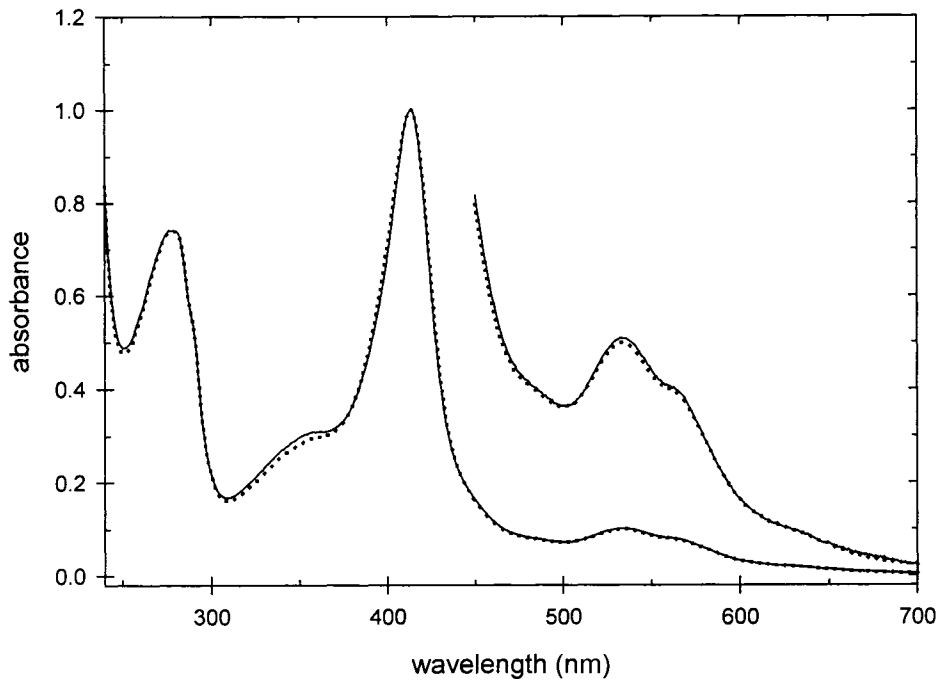

Figure 3.10 Spectra of K149D (solid line) and D132K (dotted line) at pH 7.5. These two mutants have the highest A_{Soret}/A_{380} ratio observed for the charge-reversal mutants with a value of 2.74. The spectra of these two mutants are essentially identical and may represent 100% 6c-ls complexes in which a hydroxide ion is bound to the heme in these mutants.

Possible Mechanism for Effect of Surface Mutations on Heme Ligation

The increase in hexa-coordinate forms at pH 7.5 compared to pH 6.0 as exemplified in the A_{Soret}/A_{380} ratio, Figures 3.8 and 3.9, is most likely due to the perturbation of the apparent pK_A for the five- to six-coordinate transition in the charge-reversal mutants compared to that in yCcP. In yCcP the apparent pK_A for the penta-coordinate to hydroxy-ligated CcP is 9.7. A shift in the apparent pK_A to smaller values in the charge-reversal mutants can be rationalized based on electrostatic considerations.

The initial hexa-coordinate CcP species formed during the alkaline transitions is thought to involve binding of a hydroxide ion to the heme in CcP (12, 13). Magnetic susceptibility studies have also shown that peroxidases can bind to hydroxide and form a complex that has higher percentages of low-spin form than some other heme proteins (3). Binding of hydroxide would change the net charge at the heme center from +1 in the five-coordinate, high-spin form to zero in the hydroxy-ligated species. Increasing the net charge on CcP by +2 through mutation of an aspartate or glutamate residue to a lysine residue would tend to destabilize the positively charged five-coordinate species, shifting the penta- to hexa-coordinate transition to lower pH.

Further studies will be needed in order to determine the pH dependence of heme-ligation in the charge-reversal mutants and to establish apparent pK_A values for the penta- to hexa-coordination of the heme group. If this transition occurs in the pH stability region of CcP, as seems likely for those mutants with high A_{Soret}/A_{380} ratios at pH 7.5, then kinetic studies can be undertaken to determine the equilibration rate between penta- and hexa-coordinate forms of the CcP mutants. The best candidates for initial studies are D37K, D132K, K149D, D241K, and E267K.

Conclusions

The spectra of the 46 charge-reversal mutants constructed, expressed, and purified in this study have been determined at both pH 6.0 and 7.5. Initial characterization of the mutants using absorption spectroscopy was done to monitor heme incorporation and purification of the mutants. The large changes in peak position and peak shape observed

for some of the mutants was unexpected since it was originally assumed that the charge-reversal mutations on the surface of the protein would have little effect on the spectroscopic properties of the heme group, which is deeply buried in the interior of the protein. The observed spectroscopic changes are consistent with a pH-dependent conversion of wild-type penta-coordinate CcP to a hydroxy-ligated form of CcP at more alkaline pH. Simple electrostatic arguments can rationalize how changes in the charge distribution on the surface of the enzyme can affect the relative stabilities of the penta- and hydroxy-ligated hemes. At pH 7.5, the ligation state of the mutants appear to range between ~90% penta-coordinate heme in mutants D34K and E35K to ~100% hexa-coordinate heme in D132K and K149D. The spectroscopic properties for 43 of the 46 mutants characterized in this study can be attributed to this penta- to hexa-coordinate equilibration. Three of the mutants have spectra that require additional considerations.

The three atypical mutants are E201K, E11K, and E118K. These three mutants have low RZ values that can be attributed to incomplete reconstitution of the apoprotein with heme. Based on the RZ values, the E201K, E11K and E118K samples contain approximately 43%, 24%, and 12% apoenzyme, respectively. The catalytic properties of these three mutants will be based on the amount of holoenzyme in the sample since the apoprotein will not react with hydrogen peroxide.

References

1. Drabkin, D. (1961) Analysis and interpretation of absorption spectra of haemin chromoproteins in *Haematin Enzymes, Part 1*, Falk, J. E., Lemberg, R., and Morton, R. K., eds., Pergamon Press Ltd, London, pp 142-172.

2. Smith, D. W., and Williams, R. J. P. (1968) Analysis of the visible spectra of some sperm-whale ferrimyoglobin derivatives, *Biochem. J. 110*, 297-301.

3. Iizuka, T., and Yonetani, T. (1970) Spin changes in hemoproteins, *Advan. Biophys. 1*, 157-182.

4. Adar, F. (1978) Electronic absorption spectra of hemes and hemoproteins, in *The Porphyrins, Vol. III*, Dolphin, D., ed., Academic Press, New York, pp 167-209.

5. Yonetani, T., Wilson, D. F., and Seamonds, B. (1966) Studies on cytochrome *c* peroxidase. VIII. The effect of temperature on light absorptions of the enzyme and its derivatives, *J. Biol. Chem. 241*, 5347-5352.

6. Erman, J. E. (1974) Kinetic studies of fluoride binding by cytochrome *c* peroxidase, *Biochemistry 13*, 34-39.

7. Erman, J. E. (1974) Kinetic and equilibrium studies of cyanide binding by cytochrome *c* peroxidase, *Biochemistry 13,* 39-44.

8. Vitello, L. B., Huang, M., Erman, J. E. (1990) pH-dependent spectral and kinetic properties of cytochrome *c* peroxidase: comparison of freshly isolated and stored enzyme, *Biochemistry 29*, 4283-4288.

9. Dunford, H. B. (1999) in *Heme Peroxidases*, Wiley-VCH, New York, p. 21.

10. Nakani, S., Viriyakul. T., Mitchell, R., Vitello, L. B. and Erman, J. E. (2006) Characterization of a covalently linked yeast cytochrome *c*-cytochrome *c* peroxidase complex: evidence for a single, catalytically active cytochrome *c* binding site on cytochrome *c* peroxidase, *Biochemistry 45*, 9887-9893.

11. Vitello, L. B., Erman, J. E., Mauro, J. M., and Kraut, J. (1990) Characterization of the hydrogen peroxide-enzyme reaction for two cytochrome *c* peroxidase mutants, *Biochim. Biophys. Acta 1038*, 90-97.

12. Dhaliwal, B. K., and Erman, J. E. (1985) A kinetic study of the alkaline transitions in cytochrome *c* peroxidase, *Biochim. Biophys. Acta 827*, 174-182.

13. Vitello, L. B., Erman, J. E., Miller, M. A., Mauro, J. M., and Kraut, J. (1992) Effect of Asp-235→Asn substitution on the absorption spectrum and hydrogen peroxide reactivity of cytochrome *c* peroxidase, *Biochemistry 31*, 11524-11535.

CHAPTER IV

CHARACTERIZATION OF THE CHARGE-REVERSAL MUTANTS – CIRCULAR DICHROISM SPECTROSCOPY

Introduction

The determination and analysis of the CD spectra of rCcP and some of its variants was undertaken to determine if there exists a large change in the secondary structure due to point mutations on the surface of CcP that could influence the coordination state of the heme. As observed in Chapter III, introduction of point mutations in CcP to produce the charge-reversal mutations caused approximately 28% of the mutants (13 of 46 mutants) to have spectra with A_{Soret}/A_{380} ratios greater than 2.0 at pH 7.5, indicating a significant increase in the amount of hexa-coordinated heme iron. It is surprising that changing one amino acid on the surface of the protein would change the coordination of the heme iron inside the protein matrix. In the steady-state analysis of the enzyme activity, Chapter VI, all of these hexa-coordinated mutants give turnover numbers significantly lower than that that of the wild-type rCcP. In an effort to determine if the increase in hexa-coordinate enzyme is associated with a significant change in the secondary structure of the mutant, two representative hexa-coordinate mutants, D37K and K149D, were investigated using CD spectroscopy along with wild-type rCcP and two mutants that had spectra typical of the penta-coordinate forms, D34K and E290K.

Circular dichroism is the difference in absorbance between left and right circularly polarized light. An asymmetric molecule contains no plane or center of symmetry and displays circular dichroism due to absorbing circularly polarized light of one rotation differently from circularly polarized light of the other rotation. Biomolecules such as proteins exhibit circular dichroism owing to the presence of asymmetric centers in the primary, secondary and tertiary structures (1). The primary structure contains amino acids which have chiral carbons, the secondary structure includes electronic transitions in the chain backbone or helically arrayed side groups, and the tertiary structure comprises symmetric molecules such as tyrosine, which may be in an asymmetric electronic field within a protein (1).

Circular dichroism (CD) analysis has many advantages that make it a very useful technique. It requires little sample and is relatively quick. It is relatively easy to interpret and can be used under a variety of conditions. One of the most successful applications of CD is the structural characterization of proteins. The far-UV CD has remarkable sensitivity to the backbone conformation of the proteins and generally reflects the secondary structure content (2). The drawback of the technique is that it gives a global average view of the molecule and the signal cannot be related to an exact structure. The measured spectrum is compared to either model polypeptides or reference protein data sets to predict each component of the secondary structures. Therefore it is very important that the reference data sets contain a wide variety of proteins and are representative of all possible secondary structures.

The secondary structure of yCcP obtained from analysis of the crystal structure (3, 4) is used as a reference throughout the Results and Discussion sections of this chapter.

Experimental Methods

Sample Preparation

All samples for CD spectroscopy were prepared in a 0.1 M ionic strength potassium phosphate buffer at pH 6.0. Stock samples of rCcP and the mutants were prepared by dissolving a small amount of lyophilized or crystalline enzyme in 2 mL buffer and centrifuged at 17400 xg at 4°C for 20 minutes to remove any undissolved material. After centrifugation, the supernates were decanted into a clean tube and stored on ice.

The spectrum of each protein sample was determined between 240 and 700 nm using an HP 8452A diode array spectrophotometer. A blank reading was initially taken using 2 mL of buffer followed by the addition of 20 to 50 μL of stock enzyme and measurement of the spectrum. The absorbance at the Soret maximum was used for the calculation of the protein concentration in the stock solution using an extinction coefficient of 101 mM^{-1} cm^{-1} (5). The spectra were also used to monitor the A_{Soret}/A_{380} value to confirm the level of hexa-coordination in the samples.

Circular Dichroism Spectra

An AVIV 215 Circular Dichroism Spectrophotometer was used for the all CD measurements. The instrument was turned on according to the instruction manual and purged with nitrogen to prevent absorbance due to oxygen below 200 nm. CD spectra were obtained between 450 and 195 nm at 25°C. Data were accumulated every 1 nm with an averaging time of 0.5 second and a bandwidth of 1 nm. Standard Fisherbrand Suprasil quartz fluorescence cuvettes, 10 x 10 mm, were used for the measurement.

Blank spectra were obtained using 3 mL of buffer added to a stoppered cuvette. The cuvette was placed in the sample chamber with the same orientation for every measurement. After the scanning was completed the experiment was saved for analysis. The appropriate amount of stock enzyme was added to the cuvette to give a 1 μM final concentration of the enzyme and mixed well. The cuvette was stoppered and the sample scanned 3 times. After the scanning was completed, the file was saved for structure analysis. A blank measurement was done for every sample.

Conversion to Molar Ellipticity

The experimentally measured ellipticity was converted to the molar ellipticity by the math function included in the software. The average of the three sample scans was calculated and the baseline was subtracted before any conversion was made. The following relationship was used for the conversion to molar ellipticity:

$$\text{ME} = \text{millidegrees} / (\#\ \text{AminoAcids} \cdot c \cdot l \cdot 10) \qquad (4.1)$$

where ME is the molar ellipticity, millidegrees is the ellipticity measured by the instrument, # Amino Acids is the number of amino acids in the protein sequence, *c* is the concentration of sample in molarity and *l* is the path length in cm, 1 cm for all determinations. The resulting value was called the mean residue ellipticity or molar ellipticity with units of deg cm^2 $dmol^{-1}$. The data were exported as text files for secondary structure prediction.

Results

Wild-type rCcP and the mutants D34K, E290K, D37K and K149D were chosen for CD analysis to determine whether the change in heme coordination of the enzymes was associated with observable changes in the secondary structure of the enzyme. Native rCcP has a penta-coordinated heme iron, whereas the mutants have a variable amount of penta- or hexa-coordination. D37K and K149D are mutants with significant hexa-coordinate heme while D34K and E290K were chosen to represent those mutants having predominantly penta-coordinated hemes. Table 4.1 summarizes the spectroscopic parameters for these proteins determined from samples used in the CD measurements at pH 6.0. The spectroscopic parameters are essentially identical to those reported in Table 3.2 of Chapter III. Note that in addition to an increased A_{Soret}/A_{380} ratio, the mutants with significant hexa-coordinate heme also have red-shifted Soret maxima, with D37K and K149D having its Soret maximum at 410 and 412 nm, respectively, in comparison to the Soret maxima at 408 nm for rCcP, D34Km and E290K.

Table 4.1. Spectroscopic Properties of rCcP and Selected Surface Mutants

Enzyme	pH	Soret Maximum (nm)	Absorbance at Soret Maximum (A_{Soret})	Absorbance at 380nm (A_{380})	A_{Soret}/A_{380}
rCcP	6	408	0.111	0.070	1.59
D34K	6	408	0.142	0.090	1.58
E290K	6	408	0.159	0.100	1.59
D37K	6	410	0.296	0.139	2.13
K149D	6	412	0.326	0.151	2.16

Figure 4.1 shows the CD spectra for rCcP and the mutants between 195 nm and 260 nm. When the CD spectra for the mutants are compared to that of the rCcP, there are no major changes, with all the spectra showing similar features and molar ellipticities. The molar ellipticities at 208 and 222 nm for the wild-type and mutant enzymes along with the mean and standard deviation are collected in Table 4.2. The similarity of the CD spectra indicates that there are no gross changes in secondary structure of the mutants when compared to rCcP even before the detailed analysis of the CD spectra is performed. The small variation in the molar ellipticity among the proteins, ~6% at 208 nm and ~3% at 222 nm Table 4.2, may be due to a variety of reasons including pipetting error, the assumption that the extinction coefficients are all the same, or the day-to-day reproducibility of sample preparation.

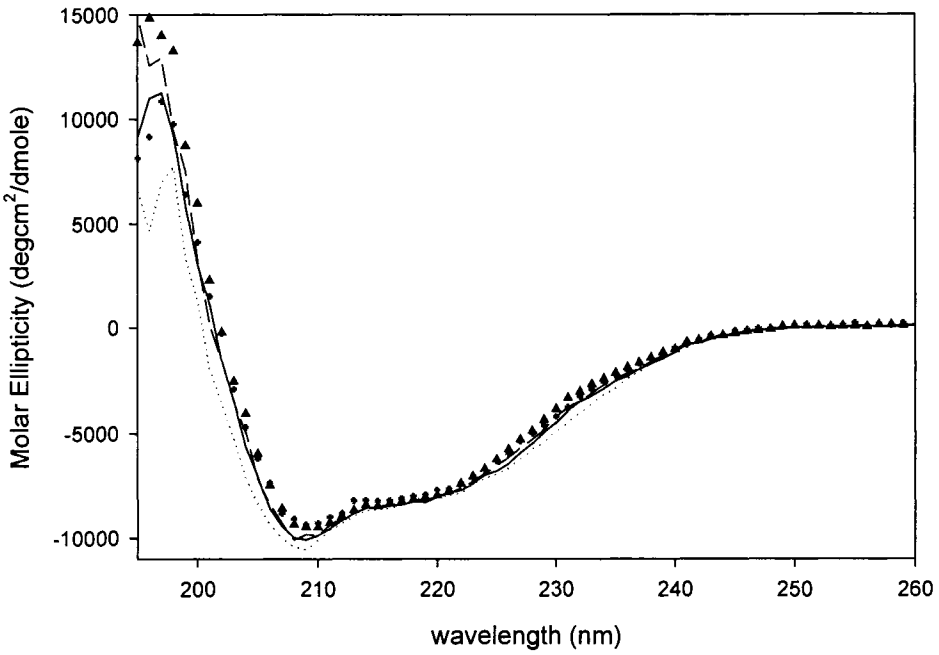

Figure 4.1. CD spectra of rCcP and four charge-reversal mutants. Solid line, rCcP; dashed line, E290K; dotted line, K149D; filled circles, D37K; and filled triangles, D34K.

Table 4.2. Molar Ellipticity of Wild Type and Mutant CcP at 208 nm and 222 nm

Protein	Molar Ellipticity at 208 nm (deg cm^2/dmole)	Molar Ellipticity at 222 nm (deg cm^2/dmole)
rCcP	-9969	-7696
D34K	-9349	-7393
E290K	-10080	-7596
D37K	-9080	-7372
K149D	-10453	-7860
Average	-9786	-7583
Standard Deviation	560	206

Analysis

The Secondary Structure of yCcP Predicted by PROCHECK

PROCHECK (4) is a software program used to check the stereochemical quality of protein structures. The PROCHEK program can also be used to determine the secondary structure of proteins based on the crystallographic structure deposited in the Protein Data Bank (3). Figure 4.2 represents the secondary structure of yCcP predicted by the PROCHECK analysis of the PDB entry: 2CYP.

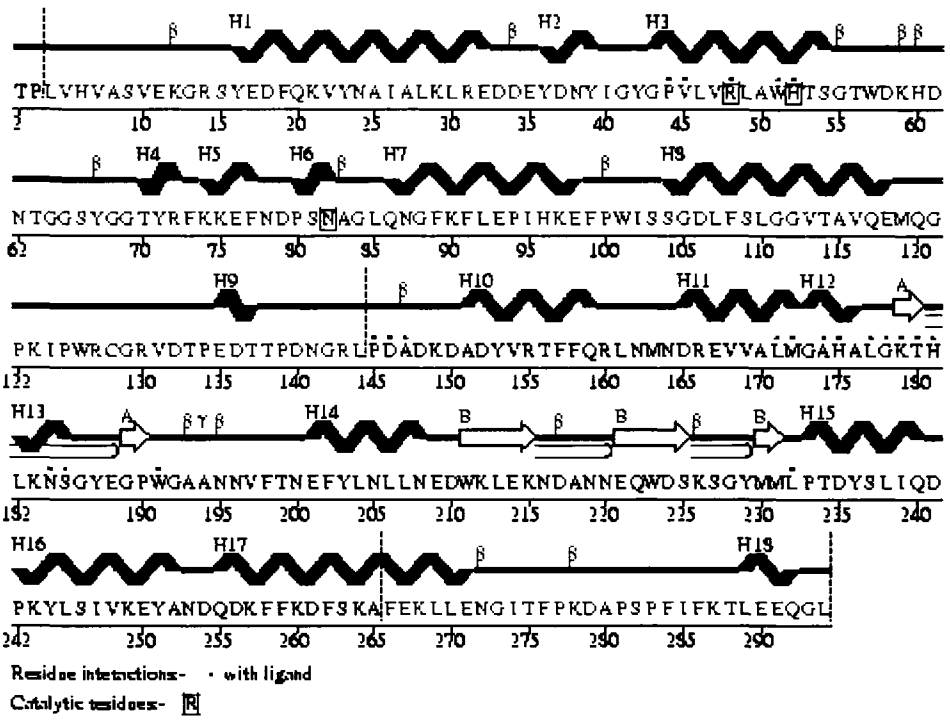

Figure 4.2. The secondary structure of yCcP. Predicted by PROCHECK analysis of the data file: PDB identification number 2CYP.

The PROCHECK analysis of yCcP predicts 18 helical sections and two beta sheets. The helical sections vary in length from a single turn of three residues to a five-turn helix involving 17 residues. The two beta sheets are labeled sheet A, which contains two anti-parallel strands, and sheet B, which contains three anti-parallel strands. Based on the number of residues with conformations associated with secondary structural elements, yCcP is 50% helix, 6% beta strand, 20% beta turns and 24% other forms of secondary structure including the random coil form. A cartoon structure of yCcP illustrating the secondary structure elements is shown in Chapter I, Figure 1.2.

The AVIV Structural Analysis Package

The AVIV CD spectrophotometer includes a structural analysis package named CDNN 2.1, a software program to analyze and quantify the far UV CD spectra. The output gives five different secondary structure components, namely, helix, parallel and anti-parallel β-sheet, β-turn and random coil (6). This CDNN 2.1 program uses a reference data set made up of eleven proteins whose structures are known and analyzes the CD data using neural network theory (6).

The results of the CDNN 2.1 analysis for rCcP and the four surface mutants are given in Table 4.3 along with a comparison of the secondary structure of wild-type yCcP predicted by the PROCHECK program from the X-ray crystallographic structure of yCcP. The X-ray analysis of yCcP is given in the first row of Table 4.3 and the CDNN 2.1 analysis of rCcP and the four mutants are given in the bottom five rows.

Table 4.3. Comparison of CcP Secondary Structures Predicted by X-ray and CDNN2.1

Protein	% Helix	% β sheet Anti-parallel	% β sheet Parallel	% β-Turn	% Random Coil	Coordination State
yCcP (X-ray)	50	6	0	20	24	5
rCcP	28	9	10	17	36	5
D34K	27	9	11	17	36	5
E290K	28	9	10	17	36	5
D37K	27	9	11	17	37	6
K149D	29	9	10	17	35	6

Two observations can be made from the data analysis given in Table 4.3. First, the CDNN2.1 analysis of the CD spectra predicts essentially identical secondary structures for rCcP and the four charge-reversal mutants, giving an average of 28 ± 1 % helix, 9 ± 0 % anti-parallel β-sheet, 10 ± 1 % parallel β-sheet, 17 ± 0 % β-turn and 36 ± 1 % random coil for the five proteins. This is consistent with the near identity of the CD spectra for rCcP and the four mutants shown in Figure 4.1.

The second significant observation is that the fraction of secondary structural elements obtained from the CDNN 2.1 analysis of the CD spectra does not agree with the PROCHECK analysis of the X-ray structure of yCcP. The CD analysis significantly underestimates the amount of helical structure and overestimates the amount of parallel beta sheet and random coil compared to the X-ray analysis. In terms of the helical structures, the CD analysis gives 28% compared to 50% from the X-ray analysis. Both

methods give reasonable agreement as to the anti-parallel beta sheet structure, 9% from the CD analysis and 6% from the X-ray structure. The CD analysis predicts 10% parallel beta sheet while the X-ray structure shows none. The percentage of β-turns is similar, with 17% from the CD analysis and 20% from the X-ray analysis, but the amount of random coil is overestimated by the CDNN 2.1 program, 36% from the CD analysis compared to 24% from the X-ray analysis.

With the discrepancy between the CD analysis of secondary structure using the CDNN 2.1 program and that based on the crystal structure of CcP, a number of other methods were used to estimate the secondary structure of rCcP and the four charge-reversal mutants from their CD spectra. These methods were those of Chen *et al.* (7) and the CDPro software package developed by Sreerama and Woody (8) which contains three different programs for secondary structural analysis, namely the CDSSTR, CONTIN/LL and SELCON3 programs. The CDPro package can be used with five different reference protein data sets ranging from 29 to 48 proteins and the protein data sets vary in the wavelength ranges they cover and whether they include or exclude denatured proteins (8). The detailed analyses using these additional software packages are included in Appendix D.

In general, all of the software packages for the analysis of CD spectra give essentially identical results for the secondary structure of rCcP and the four charge-reversal mutants and none of the software packages agree with the X-ray structure of yCcP. All of the CD analysis programs underestimate the amount of helix structure in CcP and overestimate the amount of beta sheet structure. A summary of the results for

secondary structure prediction from the various software packages is given in Table 4.4 where the % other category includes the % β-turns.

Table 4.4. Summary of Average Secondary Structural Elements from CD Analysis [a]

Method [b]	Reference Proteins [c]	% helix	% β sheet	% other[d]
yCcP (X-ray)	1	50	6	44
CDNN 2.1	11	28 ± 1	19 ± 1	53 ± 1
Chen *et al.*	5	26 ± 1	41 ± 7	34 ± 6
CDSSTR	37	24 ± 2	30 ± 4	46 ± 5
CDSSTR	43	35 ± 4	22 ± 3	43 ± 6
CONTIN/LL	37	22 ± 2	28 ± 2	50 ± 1
CONTIN/LL	43	27 ± 2	24 ± 2	49 ± 1
SELCON3	37	23 ± 2	27 ± 2	50 ± 1
SELCON3	43	25 ± 3	25 ± 2	50 ± 1

[a] The data in the table is the mean ± standard deviation of the percentage of each of the three major secondary structural elements averaged for the five proteins: rCcP, D34K, D37K, K149D, and E290K. [b] The methods are software packages from references 7 and 8. [c] The number of proteins in the reference data base used with each method of analysis. [d] including % β-turns.

Discussion

The wavelength dependence of the molar ellipticities for rCcP and the selected mutants have similar shapes and magnitudes, Figure 4.1. The average molar ellipticities at 208 nm and 222 nm are essentially the same, within experimental error (-9786 ± 560)

deg cm^2 $dmol^{-1}$ and (-7583 ± 206) deg cm^2 $dmol^{-1}$ respectively, Table 4.2. These results indicate that there are no gross conformational changes accompanying a change in heme coordination or the introduction of a charge-reversal mutation on the surface of CcP. Nevertheless, the secondary structure of rCcP and the selected mutants were determined from the CD spectra using several methods of analysis. In addition, these structures were compared with those predicted for wild-type yeast CcP, (yCcP) obtained from analysis of the crystal structure using the PROCHEK program (4).

Prediction of Secondary Structures from the Crystal Structure

Inspection of Tables 4.3 and 4.4 (and the tables in Appendix D) reveals that the % α-helix from the CD analyses is consistently lower than that obtained from the crystal structure and the % β structure is higher. Since the comparisons are made between results for the wild-type yeast enzyme and a series of recombinant systems, a survey of the secondary structures determined from the crystal structure of several CcP species was performed. The first group includes CcP(MI), a wild-type enzyme containing Met and Ile at the N-terminal (Chapter II) and six of its active site mutants, D235N, W191F, W51F, H52L, R48K and R48L (9-11). The second group is represented by yeast CcP Compound I, the fully oxidized enzyme intermediate containing a radical at tryptophan-191 and an oxyferryl heme iron (12). The third group contains CcP(MKT) mutants. CcP(MKT) is a recombinant enzyme with Met, Lys and Thr replacing the first three amino acid residues at the N-terminus of yCcP. The two mutants in this series are W191G, which introduces a cavity ~ 180 $Å^3$ in the proximal heme pocket and eliminates

the Trp-191 radical during formation of Compound I (13) and a second mutant that removes the electron transfer pathway in CcP to form a channel from the surface of the protein to the proximal heme surface. This construct was formed by mutations P190G and W191G and the removal of A193 and A194 (14). The secondary structures obtained for these proteins by PROCHECK analysis are given in Table 4.5. Review of these

Table 4.5. Secondary Structures of Selected CcP Species Determined by PROCHECK.

Protein	% α helix	% β Strand	% other	Ref.
yCcP	50	6	44	3
CcP(MI)	50	5	45	9
CcP(MI)D235N	49	6	45	9
CcP(MI)W191F	50	6	45	9
CcP(MI)W51F	50	6	45	9
CcP(MI)H52L	50	6	45	10
CcP(MI)R48K	50	5	45	11
CcP(MI)R48L	50	5	45	11
yCcP Cpd I	49	6	45	12
CcP(MKT)W191G	51	6	43	13
CcP(MKT)P190G W191G Δ(A193, A194)	50	8	42	14

results indicates that the secondary structure of CcP remains almost unchanged even though the catalytic activity of the mutants is severely altered. Mutations produce electron density changes localized at the site of the mutation but have little effect on the secondary and tertiary structure of CcP (9-14). Neither the formation of a cavity nor a channel lead to major changes in the structure (13,14): "It is remarkable that such extended channel can be introduced into the structure of a protein without significant collapse" (14). One can conclude that CcP is a very robust enzyme and that its secondary and tertiary structure is resistant to changes due to point mutations, either on the surface of the protein or in the protein interior.

Various methods have been used to analyze the CD spectra of wild-type and mutant proteins of CcP in order to estimate their secondary structure. These methods use different reference protein sets and different secondary structure assignments for the secondary structure prediction and as a result it is difficult to compare the data from different methods (8) For CcP, the CDSSTR method with 43 reference proteins gives the highest % helix and SELCON3 and CONTIN/LL methods with 37 reference proteins give the lowest % helix, Table 4.4. CDNN 2.1 predicts the lowest and the Chen method gives the highest % β structures. For the unordered forms, the Chen method estimates the lowest amount and CDNN 2.1 the highest.

Comparison of CD and X-ray Prediction of Secondary Structure

One of the more interesting observations is that the percentage of secondary structure estimated from CD does not agree with the amount of secondary structure determined

from the X-ray structure of CcP. Reasons for such discrepancies have been discussed by a number of authors. The secondary structure analysis by CD involves numerous assumptions. Manning (15) pointed out that the assumption that the secondary structure composition of the crystalline protein is retained in solution may not be true in every case. The detailed comparison of α-bungarotoxin in solution and crystal structure shows differences in both the backbone and side chain conformations and, more importantly, in the amount of secondary structure (15). The degree of protein aggregation may also differ in solution and crystal environment. The associated monomers can introduce perturbation to the CD spectrum and initiate changes in the conformation of the peptide backbone. Manning also indicated the possibility of protein crystallization in different forms, with unique secondary and tertiary structure (15). The resolution of the crystal structure to which the CD data is compared is also very important. Poor resolution structures can result in incorrect assignment of the secondary structures.

The assumption that contributions from the secondary structures are additive and that no contribution from the tertiary structure is included remains an open question (15). The lack of a reliable standard for the fully α-helical peptide complicates the analysis as well. The estimated value for the molar ellipticity of 100% α helix at 222 nm ranges from -26,000 to -38,000 deg cm^2 $dmol^{-1}$ (15). Since the molar ellipticity reflects the helix content, analysis can vary with the value used or the choice of protein reference sets (16). There is both experimental and theoretical evidence that varying helical chain length can affect the prediction of helical content (15). Chen *et al.* (7) assume an average value of 11 residues per helix for their calculations. In yCcP, the average number of residues per

helix is 8.1, with 12 out of the 18 helical segments having fewer than 10 residues. Therefore, the consideration of the length of the α helix may be important for the deconvolution algorithms.

The β structures with different strand length, the number of strands per sheet, and the extent of strand distortion may also have marked effects on the CD spectra (15). The assumption that the geometric variability does not affect the overall CD spectrum may not be true at all times. The number of geometric variables is greater in the β-sheets and β-turns, making the interpretation more difficult. The contribution of β-turns to the CD spectrum depends on the geometry of the bend. The most common types, I and II, have a strong positive band at about 208 nm, a weak positive band at 228 nm and a strong negative bands between 169 and 191 nm (17). In CcP there are 15 β-turns, ten of which are type I or II, accounting for 20% of the structure; however, in most analyses the contribution of the bends are included in the "other" category.

Manning (15) also pointed out that there are many conditions that can denature a protein and produce an unordered structure. However, estimation of the unordered or random structure is the most variable among the components of secondary structure.

The assumption that contributions from side chain chromophores in the far UV are negligible may not be true in all cases. Estimation of the molar ellipticity by the indole group of tryptophan range from 40,000 to 80,000 deg cm^2 $dmol^{-1}$ in the far UV region (15). Among the aromatic residues, tyrosine and tryptophan are considered the most significant contributors to the far UV CD spectra of proteins (15). The unusual CD spectrum with strong positive features near 230 nm is postulated to arise from the side chain contributions. Some of the proteins used in the reference set, concanavalin A,

avidin, and erabutoxin b, were found to show unusual CD spectra (15). Tyrosine, tryptophan and disulfide groups can all produce strong CD signals in the 222 nm region, and, therefore, can affect the estimation of the amount of helical structures.

The presence of aromatic amino acids in the α-helix can change the shape and ellipticity of a "pure" α-helix spectrum. Studies of model compounds show that Tyr induces the greatest change, essentially decreasing the ellipticity at 222 nm (18). The amino acid composition of CcP contains fourteen Tyr, twenty Phe and five Trp. Ten of the fourteen Tyr are present in α-helices and this may be one of the reasons that the ellipticity at 222 nm for CcP appears as a shoulder rather than a well-defined band, Figure 4.1.

The far UV CD spectra of proteins may also be affected by the prosthetic groups such as heme (6) because it contains an extended π-system with the large dipole moment. Therefore the changes in heme orientation and position may affect the far UV CD spectrum of heme proteins (15).

Interactions between secondary structural elements may produce alteration of the CD spectrum. Examples given by Manning (15) include two folding motifs, the four-helix bundle and the β sheet sandwich, that can form interactions between units. Significant interaction occurs between members of these tertiary structures, as indicated by the theoretical and experimental studies. Systems composed of two helices in close contact can result in a change in CD signal in proteins such as tropomyosin (15). Other proteins, such as those containing the leucine zipper found in certain DNA-binding proteins, show no disturbance in CD spectrum although they contain two parallel aligned α-helices (15). Therefore, helix-helix interaction may be modulating the CD signal in some cases. For

T4 dihydrofolate reductase, folding of secondary structures produces characteristic CD spectra that can be used to predict the type of tertiary structure present (19).

The quality of the CD spectra in the reference databases may not meet the standards required by the analyses. Janes (20) indicated that one inherent problem with the spectra used in the data sets is that some of the spectra were obtained from individual non-commercial CD instruments with limited cross reference calibration. Protein from the same source material, superoxide dismutase, measured in different laboratories resulted in considerably different spectra. Since it is not known which spectrum is representative of the individual protein, choosing and including an incorrect one in the reference protein data set might contribute to the error associated with the reference itself. It is important to do cross-calibration and cross checking on a diverse range of machines to ensure consistency, especially if the data will be used in a reference data set.

The wavelength range of the CD reference spectra is also very important since the information that can be extracted is proportional to the range. The larger the range, the more the information can be made available (15). The quality of the X-ray structures used in the reference databases is also very important. Many of the structures were acquired long before the systematic refinement protocols were available. Checking and validation programs like PROCHECK were not available at that time and some flaws went undetected. As indicated before, the assumption that protein crystal and solution structures are the same may need to be taken into account because the environments are different. Different concentrations, salts and pH may result in inaccuracies, which might be compounded in the data set (15).

X-ray structures with poor resolution can have regions with incorrectly assigned amino acids that can contribute error to the secondary structure. The more correct the conformation, the more correct the percentages of the secondary structure type that can be derived. Therefore, the reliability of the reference datasets is very important and inclusion of structures with serious mistakes may introduce a degree of inaccuracy (6).

The completeness of the structures determined from protein crystals also contribute to the reliability of the reference data set. Some structures contain undetermined regions due to the flexible nature of the region, especially in the N- and C-termini. If the missing number is significant, it may result in inaccurate predictions (15).

Experimentally, sample preparation is also very important. Bohm (6) commented on the importance of accurate concentration measurement and optically transparent solutions. The noise in the CD signal is also a source of possible error in CD analysis.

Prior Analysis of the CD spectrum of yCcP

Three different studies on the CD properties of CcP have been reported, including the work presented in this study (21, 22). The CD data were collected under slightly different conditions and analyzed using somewhat different parameters. In spite of the differences, the estimates of secondary structure are similar. For the yeast CcP wild-type and mutant proteins, CD measurements were done at a wavelength range between 195 and 450 nm. It covers more of the near UV than the far UV, which may be one of the reasons that the predictions are less accurate compared to the X-ray structure. The X-ray structure for yCcP was solved from 1.7Å resolution data (3) and therefore should give

accurate information on the secondary structure. Comparison of the data from the current study with that of Dowe and Erman (21) and Sievers (22), Table 4.6, indicates good agreement of the estimated helical content from CD measurements. The somewhat higher estimation of the helical content for the Siever data may be due to the fact that the author used an incorrect value for the molecular weight of CcP; therefore, the calculated molar concentrations and consequently the molar ellipticities are in error. Other factors that may give rise to differences in results includes the use of different experimental parameters, such as number of amino acids, wavelength at Soret maximum, and extinction coefficient at Soret maximum. The wavelength range and instruments are different among the three CD studies of CcP.

Table 4.6. Comparison of CcP Secondary Structures Predicted by Chen Method from Three Laboratories

Study	Protein	AA[a]	Soret Maximum (nm)	εSoret ($mM^{-1}cm^{-1}$)	CD Instrument	Wavelength range (nm)	% Helix	% β	% Unordered
This work	rCcP	294	408	98	AVIV 215	195-450	26	40	34
Dowe (21)	yCcP	294	408	95	JASCO ORD/UV5 with CD		26	24	50
Sievers (22)	yCcP	270	407	99	Cary 61	200-660	36	30	34

[a]Number of amino acids residues in CcP used in data analysis

Conclusions

Apart from all the possible error sources, which may contribute to the discrepancy between the X-ray data and the different structure deconvolution methods, all the CD

analyses predicted similar secondary structure for wild-type and mutant CcP molecules. This strongly suggests that there are no gross changes in the secondary structure in the mutant proteins, whether they are penta- or hexa-coordinate. None of the CD secondary structure analyses give a good prediction of the secondary structure in rCcP when compared to the secondary structure observed in the crystal structure.

There are several wild-type CcP structures and mutant CcP structures deposited in the Protein Data Bank and all predict the same secondary structure, Table 4.5. This indicates the robust nature of the CcP. The current data indicate that a single amino acid change on the surface of CcP can cause a change in heme iron coordination but that the mutation does not change the secondary structure of the protein. Therefore, reduction in the turnover number in the hexa-coordinated mutants, as will be discussed in Chapter VI, is more likely due to the presence of an inactive, hexa-coordinate form of the heme group in some of the mutant enzymes.

References

1. Beychok, S. (1966) Circular dichroism of biological macromolecules, *Science, 154,* 1288-1299.

2. Sreerama, N., Venyaminov, S. Y., and Woody, R. W. (2000) Estimation of proteinsecondary structure from circular dichrosim spectra: Inclusion of denatured proteins with native proteins in the analysis, *Analytical Biochem. 287*, 243-251.

3. Finzel, B. C., Poulos, T. L., and Kraut, J. (1984) Crystal structure of yeast cytochrome *c* peroxidase refined at 1.7 Å resolution, *J. Biol. Chem. 259*, 13027-13036.

4. www.ebi.ac.uk/Thornton-srv last used July 2007

5. Nakani, S., Viriyakul, T., Mitchell, R., Vitello, L. B., and Erman, J. E. (2006) Characterization of a covalently-linked yeast cytochrome *c*/cytochrome *c* peroxidase complex: Evidence for a single, catalytically-active cytochrome *c* binding site on cytochrome *c* peroxidase, *Biochemistry 45,* 9887-9893.

6. Bohm, G., Muhr, R., Jaenicke, R. (1992) Quantitative analysis of protein far UV circular dichroism spectra by neural networks, *Protein Eng. 5*, 191-195.

7. Chen, Y. H., Yang, J. T., Chau, K. H. (1974) Determination of the helix and β form of proteins in aqueous solution by circular dichroism, *Biochemistry 13*, 3350-3359.

8. Sreerama, N., and Woody, R.W. (2000) Estimation of protein secondary structure from circular dichroism spectra: Comparison of CONTIN, SELCON, and CDSSTR methods with an expanded reference set, *Analytical Biochem. 287*, 252-260.

9. Wang, J., Mauro, J. M., Edwards, S. L., Oatley, S. J., Fishel, L. A., Ashford, V. A., Xuong, N. H., and Kraut, J. (1990) X-ray structure of recombinant yeast cytochrome *c* peroxidase and three heme-cleft mutants prepared by site-directed mutagenesis, *Biochemistry 29*, 7160-7173.

10. Erman, J. E., Vitello, L. B., Miller, M. A., Shaw, A., Brown, K. A., and Kraut, J. (1993) Histidine 52 is a critical residue for rapid formation of cytochrome *c* peroxidase compound I, *Biochemistry 32*, 9798-9806.

11. Vitello, L. B., Erman, J. E., Miller, M. A., Wang, J., and Kraut, J. (1993) Effect of arginine-48 replacement on the reaction between cytochrome *c* peroxidase and hydrogen peroxide, *Biochemistry 32*, 9807-9818.

12. Fülöp, V., Phizackerley, R. P., Soltis, S. M., Clifton, I. J., Wakatsuki, S., Erman, J., Hajdu, J., and Edwards, S. L. (1994) Laue diffraction study on the structure of cytochrome *c* peroxidase compound I, *Structure 2*, 201-208.

13. Fitzgerald, M. M., Churchill, M. J., McRee, D. E., and Goodin, D. B. (1994) Small molecule binding to an artificially created cavity at the active site of cytochrome *c* peroxidase, *Biochemistry 33*, 3807-3818

14. Rosenfeld, R. J., Hays, A. M., Musah, R. A., and Goodin, D. B. (2002) Excision of a proposed electron transfer pathway in cytochrome *c* peroxidase and its replacement by a ligand binding channel, *Protein Sci. 11*, 1251-1259

15. Manning M.C. (1989), Underlying assumptions in the estimation of secondary structure content in proteins by circular dichroism spectroscopy- a critical review, *J. Pharm. Biomed. Anal. 7*, 1103-1119.

16. Baker, C. C., and Isenberg, I. (1976) On the analysis of circular dichroic spectra of proteins, *Biochemistry 15*, 629-634

17. Brahms, S., Brahms, J., Spach, G., and Brack, A. (1977) Identification of β, β-turns and unordered conformations in polypeptide chains by vacuum ultraviolet circular dichroism, *Proc. Natl. Acad. Sci. U.S.A. 74*, 3208-3212

18. Chakrabartty, A., Kortemme, T., Padmanabhan, S., and Baldwin, R. L. (1993) Aromatic side chain contribution to far-ultraviolet circular dichroism of helical peptides and its effect on measurement of helix propensities, *Biochemistry. 32*, 5560-5565

19. Compton, L. A., Mathews, C. K., and Johnson, Jr., W. C. (1987) The conformation of T4 bacteriophage dihydrofolate reductase from circular dichroism, *J. Biol. Chem. 262*, 13039-13043

20. Janes, R. W. (2005) Bioinformatics analyses of circular dichroism protein reference databases, *Bioinformatics 21*, 4230-4238

21. Dowe, R. J., and Erman, J. E. (1985) Physicochemical characterization of the alkaline denaturation of cytochrome *c* peroxidase, *Biochim. Biophys. Acta 827*, 183-189

22. Sievers, G. (1978) Circular dichroism studies on cytochrome *c* peroxidase from baker's yeast (*Saccharomyces cerevisiae*), *Biochim Biophys. Acta, 536*, 212-225.

CHAPTER V

CHARACTERIZATION OF THE CHARGE-REVERSAL MUTANTS – HYDROGEN PEROXIDE REACTIVITY

Introduction

Oxidation of CcP by Hydrogen Peroxide to Form CcP Compound I

In the study of enzyme kinetics, transient-state kinetics is the sub-field that studies fast reactions, the reactions that occur before the establishment of a steady-state during catalytic turnover (1). The first redox step in the CcP-catalyzed oxidation of ferrocytochrome *c* using H_2O_2 is the bimolecular reaction between CcP and H_2O_2 to form CcP Compound I, Equation 5.1. This reaction, and the mechanism of CcP catalysis, has

$$\text{CcP} + \text{H}_2\text{O}_2 \xrightarrow{k_1} \text{CcP-I} + \text{H}_2\text{O} \qquad (5.1)$$

been discussed in Chapter I. The reaction between H_2O_2 and CcP is very fast, irreversible, and generally studied using stopped-flow techniques (2-4). The first transient-state studies of the reaction between H_2O_2 and CcP were those of Loo and Erman in 1975 (2), who investigated the reaction as a function of pH and ionic strength, using KNO_3 to adjust the ionic strength. Loo and Erman found that the reaction had a

"bell-shaped" dependence upon pH with a maximum value of 45 ± 3 μM^{-1} s^{-1} near neutral pH. The rate of the reaction decreases at low and high pH with apparent pK_A values of 5.4 and 9.8 at 0.10 M ionic strength. The more acidic pK_A is attributed to ionization of the distal histidine residue, His-52 (5), and the more alkaline pK_A is attributed to conversion of penta-coordinate CcP to hydroxy-ligated CcP (6). The maximum rate of the reaction is independent of ionic strength but the apparent pK_A values depended upon ionic strength. It was later discovered that the more acidic pK_A was affected by nitrate binding to the active site of the enzyme (4). In the absence of nitrate, the apparent pK_A of the distal histidine is 4.0 at 0.10 M ionic strength (4, 5).

Slow Kinetic Phase of the Reaction between H_2O_2 and CcP

Previous reports indicate that some, but not all, preparations of yCcP show biphasic kinetics with hydrogen peroxide (2-4). For those preparations of yCcP that have biphasic kinetics, the amplitude of the second phase is small, usually less than 2% of the major phase, and the rate of the second phase is about ten times slower than the major phase of the reaction. Loo and Erman (2) and Vitello *et al.* (4) only observed the slow phase of the reaction at pH 6 or below and the amplitude of the slow reaction was generally less than 2% of the total absorbance change for the hydrogen peroxide reaction at 424 nm. The rate of the slow phase is about 2 s^{-1} at 25 °C and independent of the hydrogen peroxide concentration. Balny *et al.* (3) have studied the temperature dependence of the hydrogen peroxide/yCcP reaction and observed biphasic kinetics under all experimental conditions for their sample of yCcP. Balny *et al.* report that the rate for

the slow phase of the reaction is independent of hydrogen peroxide concentration, that the rate increases with increasing pH, and the amplitude varies from about 20% of the total absorbance change at low pH to less than 2% at pH 8. They report a rate of 0.14 s^{-1} at pH 6.1, 2 °C with an activation energy of 20.5 ± 0.2 kcal/mol (3).

Hydrogen Peroxide Reactivity of the Charge-Reversal Mutants

In this chapter, the reaction between hydrogen peroxide and the 46 charge-reversal mutants will be described. Stopped-flow studies were carried out at pH 6.0, the center of the pH stability region for CcP, and at pH 7.5, the pH at which the steady-state catalytic properties of the mutants were investigated. The steady-state results will be presented in the next chapter.

Experimental Methods

rCcP and the Charge-Reversal Mutants

Construction, expression, and isolation of rCcP and the 46 charge-reversal mutations are described in Chapter II of this dissertation. The concentration of rCcP and the charge-reversal mutants was determined spectrophotometrically using an extinction coefficient of 101 mM^{-1} cm^{-1} at the Soret maximum at pH 6.0 (7).

Hydrogen Peroxide

Hydrogen peroxide was reagent grade 30% (v/v) purchased from Aldrich Chemical Company, Inc. The concentration of hydrogen peroxide stock solutions were determined periodically by titration with standardized cerium(IV) sulfate (8).

Determination of Rate of Hydrogen Peroxide Reaction

The rate of CcP Compound I formation was measured using an Applied Photophysics Model DX.17MV stopped-flow spectrofluorimeter (Applied Photophysics Limited, Leatherhead, UK) with a dead time of 2 ms. All the reactions were carried out with ~1 μM solutions of the enzyme dissolved in 100 mM ionic strength potassium phosphate buffer, pH 6.0 or 7.5, at 25°C. The hydrogen peroxide concentrations were prepared from stock solutions and diluted into buffer. The final concentrations ranged between 3 and 30 μM H_2O_2. The enzyme solution was placed in one syringe of the stopped-flow instrument and the H_2O_2 solution in the second syringe. Upon mixing the two reactants, the reaction was followed at the wavelength of maximum difference, usually 424 nm, and at different time intervals. The time dependence of the absorbance was fitted to a one or two exponential equation in order to extract the observed rate constants, k^{obs}, using the software provided with the stopped-flow instrument.

The measured k^{obs} was then plotted against the hydrogen peroxide concentration to determine if the reaction was dependent upon, or independent, of H_2O_2. If the reaction

was dependent upon the hydrogen peroxide reaction, the bimolecular rate constant, k_{bi}, was determined from Equation 5.2.

$$k^{obs} = k_{bi}\,[\text{Hydrogen peroxide}] \qquad (5.2)$$

Estimation of Active Enzyme Fraction

The spectra of compound I for all the CcP surface mutants were determined using a Hewlett Packard 8452A diode array spectrophotometer. Two mL of an approximately 10 μM enzyme solution was used to record the spectrum of the resting enzyme. The formation of Compound I was initiated by addition of 15 μL of 2.1 mM H_2O_2 (final H_2O_2 concentration ~15 μM) and the spectrum recorded. Difference spectra were calculated to determine the wavelength of maximum difference between the mutant and the H_2O_2-oxidized mutant. The absorbance change at 424 nm was used to estimate the fraction of mutant enzyme that reacts with H_2O_2 using the assumption that the spectrum of Compound I of the mutant enzyme is identical to that of yCcP Compound I.

Results

Estimation of Fraction of Reactive Enzyme

During the investigation of the reaction between H_2O_2 and the mutant enzymes it became apparent that the absorbance changes associated with the H_2O_2 reaction were not consistent with complete formation of Compound I for many of the charge-reversal

mutants. This suggested that a significant fraction of some of the mutants did not react with H_2O_2. In order to estimate the fraction of each mutant that reacted with H_2O_2 it was assumed that the spectrum of Compound I for each of the mutants was identical to that of yCcP Compound I. This should be a valid assumption since the ligation state of Compound I will be the same in the mutants as in wild-type CcP with the proximal histidine bound to the fifth coordination site and an "oxo" oxygen atom covalently bound at the sixth coordination site on the heme. The fraction of each mutant enzyme that was oxidized to Compound I was estimated by comparing the spectrum of the mutant in the presence of a small excess of H_2O_2 with that of an equal concentration of authentic yCcP Compound I using Equation 5.3. In Equation 5.3, A_{424}^{mutant} is the absorbance of the

$$f_{active} = (A_{424}^{mutant+H2O2} - A_{424}^{mutant})/(A_{424}^{yCcP\text{-}I} - A_{424}^{mutant}) \quad (5.3)$$

mutant enzyme at 424 nm in the resting Fe(III) state, $A_{424}^{mutant + H2O2}$ is the absorbance of the mutant at 424 nm in the H_2O_2-oxidized state, and $A_{424}^{yCcP\text{-}I}$ is the absorbance of an equal concentration of yCcP Compound I.

Some of the mutant enzymes, such as E32K, react with H_2O_2 to form Compound I as well as does yCcP, Figure 5.1. The spectrum of E32K in the presence and absence of H_2O_2 is shown in Figure 5.1 at pH 7.5. The spectrum of an equal concentration of yCcP Compound I is shown for comparison in Figure 5.1. The absorbance for the E32K/H_2O_2 reaction product is actually about 4% larger than that calculated for an equal concentration of yCcP Compound I at 424, giving 107% active enzyme when using

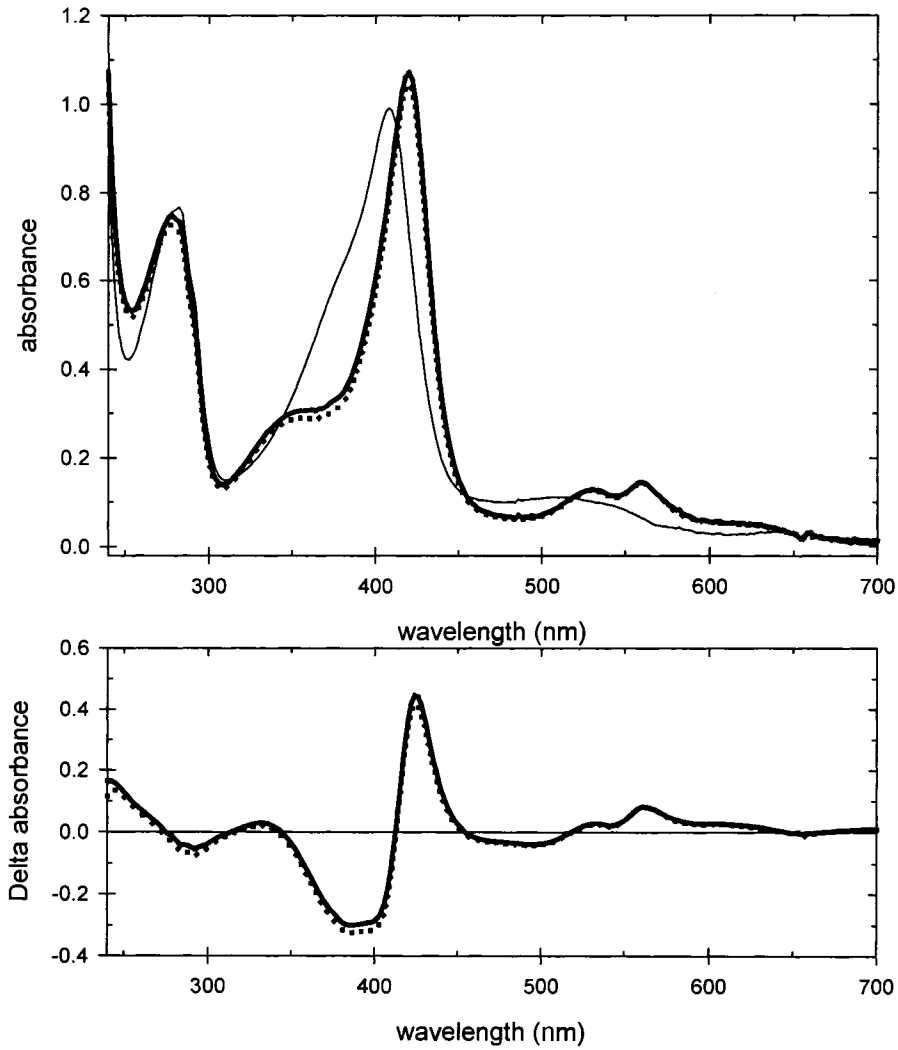

Figure 5.1 Upper Panel - Spectra of E32K mutant of rCcP in the absence (thin line) and presence (thick line) of a slight stoichiometric excess of hydrogen peroxide at pH 7.5. The spectrum of an equivalent concentration of yCcP compound I (dotted line). Bottom Panel - Difference spectrum of E32K+H_2O_2 minus E32K (thick line) and of yCcP Compound I minus E32K (dotted line).

Equation 5.3. E32K has the largest positive change in absorbance at 424 nm upon peroxide addition for any of the mutants investigated in this study and gives an upper limit for the accuracy of Equation 5.3. The larger absorbance change at 424 nm for the E32K mutant in comparison to yCcP-I could be due to a variety of reasons. First, the spectrum of yCcP Compound I and E32K Compound I could be slightly different such that E32K Compound I has a 4% higher extinction coefficient at 424 nm than yCcP Compound I. Second, the extinction coefficient at the Soret maximum for resting-state E32K could be slightly larger than that of rCcP such that the concentration of E32K is overestimated in these experiments. A 4% error is essentially within experimental error in determining the extinction coefficient of the charge-reversal mutants.

E35K, D33K, and E98K also gave absorbance changes that were 1 to 2% larger than predicted based on the spectrum of yCcP Compound I, which is within the experimental error of the measurement. All three of these mutants, along with E32K, are considered to be 100% active toward H_2O_2 at pH 6.0, Table 5.1. E32K is the only mutant that is considered to be 100% active toward H_2O_2 at pH 7.5, Table 5.2. One of the characteristics for these four mutants, E32K, E35K, D33K, and E98K is that all four are predominantly penta-coordinate with A_{Soret}/A_{380} values between 1.55 and 1.60 at pH 6.0, Table 3.2, Chapter III.

Some mutants, however, had very small absorbance changes upon addition of H_2O_2. At pH 7.5, five mutants actually gave small decreases in absorbance at 424 nm upon addition of H_2O_2 rather than the expected increase. These mutants are D132K, K149D, D235K, D241K, and E267K. K149D gave the largest decrease in absorbance at 424 nm upon addition of H_2O_2, about 9%, while the other four mutants gave decreases of

Table 5.1. Kinetic Parameters for Reaction of rCcP and Its Charge-Reversal Mutants with H_2O_2, pH 6.0

	Fast Phase		Slow Phase			Inactive
Mutant	% Enzyme	k_1 ($\mu M^{-1}s^{-1}$)	% Enzyme	k_2 ($\mu M^{-1}s^{-1}$)	k_3 (s^{-1})	% Enzyme
yCcP	98	45 ± 3	2	-	~2	0
CcP(MI)	82	47 ± 4	15	-	8 ± 2	3
rCcP	81	47 ± 1	8	2.2 ± 0.1	-	11
E11K	14	43 ± 12	56	2.0 ± 0.1	-	31
E17K	35	41 ± 7	37	2.0± 0.1	-	28
D18K	76	48 ± 1	13	2.5 ± 0.4	-	11
R31E	29	51 ± 3	17	2.5 ± 0.6	-	54
E32K	94	39 ± 7	6	1.5 ± 0.6	-	0
D33K	92	41 ± 4	8	-	34 ± 8	0
D34K	85	51 ± 12	12	-	27 ± 16	3
E35K	92	37 ± 7	8	1.9 ± 0.5	-	0
D37K	46	34 ± 5	9	-	14 ± 6	45
D58K	35	35 ± 11	17	2.0 ± 0.5	-	48
D61K	70	38 ± 3	23	3.5 ± 0.1	-	7
E76K	0		48	2.0 ± 0.2	-	52
D79K	0	-	42	1.6 ± 0.1		58
E93K	70	39 ± 7	17	-	25 ± 1	13
E98K	91	46 ± 7	9	-	35 ± 7	0

(Table continued on following page)

Table 5.1. (continued)

Mutant	Fast Phase % Enzyme	Fast Phase k_1 ($\mu M^{-1}s^{-1}$)	Slow Phase % Enzyme	Slow Phase k_2 ($\mu M^{-1}s^{-1}$)	Slow Phase k_3 (s^{-1})	Inactive % Enzyme
D106K	No Expression					
E118K	54	25 ± 6	20	-	25 ± 11	26
D132K	0		43	1.6 ±0.1	-	57
E135K	0		25	1.5 ± 0.2	-	75
D136K	34	41 ± 2	40	1.8 ± 0.1	-	26
D140K	39	38 ± 4	38	2.4 ± 0.3	-	23
D146K	53	46 ± 11	38	2.0 ± 0.1	-	9
D148K	64	41 ± 7	17	1.8 ± 0.2	-	19
K149D	4	19 ± 7	0	-	-	96
D150K	33	39 ± 4	8	2.2 ± 0.5	-	59
D152K	62	40 ± 5	25	2.4 ± 0.4	-	13
D165K	50	34 ± 15	0	-	-	50
E167K	49	55 ± 6	14	3.3 ± 0.9	-	37
E188K	58	39 ± 6	10	2.7 ± 0.8		32
E201K	61	36 ± 5	7	1.6 ± 0.2	-	32
E209K	38	29 ± 7	0	-	-	62
D210K	63	36 ± 7	8	-	23 ± 2	29
E214K	79	43 ± 4	11	2.6 ± 0.3	-	9
D217K	83	45 ± 3	10	-	30 ± 6	7

(Table continued on following page)

Table 5.1. (continued)

	Fast Phase		Slow Phase			Inactive
Mutant	% Enzyme	k_1 ($\mu M^{-1}s^{-1}$)	% Enzyme	k_2 ($\mu M^{-1}s^{-1}$)	k_3 (s^{-1})	% Enzyme
E221K	90	43 ± 0.4	8	2.5 ± 0.3	-	2
D224K	70	45 ± 5	21	2.6 ± 0.3	-	9
D235K	0	-	0	-	-	100
D241K	0	-	0	-	-	100
E250K	52	45 ± 5	16	2.5 ± 0.4	-	32
D254K	42	39 ± 4	24	2.5 ± 0.2	-	34
D256K	88	45 ± 4	10	3.0 ± 0.9	-	2
D261K	74	44 ± 7	9	2.8 ± 0.4	-	17
E267K	0	-	0	-	-	100
E271K	47	44 ± 7	37	2.0 ± 0.3	-	16
D279K	55	36 ± 7	40	1.8 ± 0.1	-	5
E290K	56	38 ± 5	28	1.7 ± 0.2	-	16
E291K	40	30 ± 7	35	1.7 ± 0.1	-	25

Table 5.2. Kinetic Parameters for Reaction of rCcP and Its Charge-Reversal Mutants with H_2O_2, pH 7.5

	Fast Phase		Slow Phase			Inactive
Mutant	% Enzyme	k_1 ($\mu M^{-1}s^{-1}$)	% Enzyme	k_2 ($\mu M^{-1}s^{-1}$)	k_3 (s^{-1})	% Enzyme
yCcP	96	45 ± 3	0	-	-	4
CcP(MI)	76	47 ± 4	12	-	11 ± 7	12
rCcP	83	48 ± 2	3	1.3 ± 0.1	-	14
E11K	14	33 ± 9	18	2.4 ± 0.1	-	68
E17K	31	38 ± 8	10	2.0 ± 0.3	-	59
D18K	68	43 ± 14	7	2.8 ± 1.5	-	25
R31E	25	44 ± 3	0	-	-	75
E32K	98	43 ± 6	2	2.1 ± 0.3	-	0
D33K	94	41 ± 7	0	-	-	6
D34K	94	49 ± 4	0	-	-	6
E35K	89	44 ± 6	3	2.2 ± 0.2	-	8
D37K	25	37 ± 6	5	-	6 ± 3	70
D58K	15	36 ± 10	5	2.0 ± 0.8	-	80
D61K	53	25 ± 20	16	2.7 ± 0.0	-	31
E76K	0		3	3.5 ± 1.6	-	97
D79K	0	-	0	-	-	100
E93K	52	37 ± 7	27	-	20 ± 7	21
E98K	93	42 ± 6	5	-	22 ± 7	2

(Table continued on following page)

Table 5.2. (continued)

Mutant	Fast Phase % Enzyme	Fast Phase k_1 ($\mu M^{-1}s^{-1}$)	Slow Phase % Enzyme	Slow Phase k_2 ($\mu M^{-1}s^{-1}$)	Slow Phase k_3 (s^{-1})	Inactive % Enzyme
D106K	No Expression					
E118K	57	44 ± 8	0	-	-	43
D132K	0	-	0	-	-	100
E135K	0		3	4.8 ± 0.1	-	97
D136K	26	50 ± 14	9	-	54 ± 24	65
D140K	27	30 ± 6	15	-	21 ± 4	58
D146K	63	49 ± 6	15	1.6 ± 0.4	-	22
D148K	62	51 ± 32	0	-	-	38
K149D	0	-	0	-	-	100
D150K	18	46 ± 13	0	-	-	82
D152K	62	36 ± 13	7	-	49 ± 6	31
D165K	amplitude too small to measure					86
E167K	46	66 ± 8	3	-	48 ± 42	51
E188K	38	39 ± 13	7	-	14 ± 3	55
E201K	42	43 ± 7	0	-	-	58
E209K	27	40 ± 12	0	-	-	73
D210K	58	39 ± 11	0	-	-	42
E214K	75	42 ± 7	7	2.4 ± 0.7	-	18
D217K	90	43 ± 6	0	-	-	10

(Table continued on following page)

Table 5.2. (continued)

	Fast Phase		Slow Phase			Inactive
Mutant	% Enzyme	k_1 ($\mu M^{-1}s^{-1}$)	% Enzyme	k_2 ($\mu M^{-1}s^{-1}$)	k_3 (s^{-1})	% Enzyme
E221K	81	47 ± 8	5	3.8 ± 0.6	-	14
D224K	74	45 ± 8	11	2.6 ± 0.3	-	15
D235K	0	-	0	-	-	100
D241K	0	-	0	-	-	100
E250K	60	50 ± 5	4	3.3 ± 0.8	-	36
D254K	39	39 ± 8	10	3.3 ± 0.7	-	51
D256K	84	42 ± 6	4	3.3 ± 0.1	-	12
D261K	59	43 ± 11	9	-	8 ± 4	32
E267K	0	-	0	-	-	100
E271K	33	28 ± 4	21	-	21 ± 5	46
D279K	52	37 ± 11	19	1.4 ± 0.3	-	29
E290K	61	51 ± 6	8	2.5 ± 0.4	-	31
E291K	40	36 ± 5	7	1.8 ± 0.2	-	53

between 1 and 7%. The spectrum of K149D in the presence and absence of a stoichiometric excess of H_2O_2 is shown in Figure 5.2. The two spectra are essentially superimposable. The difference spectrum for K149D in the presence of H_2O_2 minus the spectrum in the absence of H_2O_2 is shown in the lower panel of Figure 5.2. The most obvious feature is a negative absorbance centered at 420 nm that corresponds to a 9% decrease in the absolute absorbance of the resting state mutant at 420 nm. Although small, the 9% decrease in absorbance indicates that H_2O_2 interacts with K149D but it does not form a Compound I-like intermediate. This conclusion is supported by a calculated difference spectrum between equivalent concentrations of yCcP Compound I and resting state K149D. The calculated difference spectrum is shown by the dotted line in the lower panel of Figure 5.2 and the shape of this calculated difference spectrum is essentially opposite that of the observed difference spectrum for K149D in the presence and absence of H_2O_2. The most likely cause of the small decrease in absorbance near 420 nm is non-specific oxidation of the porphyrin ring in K149D. The five mutants that have small negative absorbance changes at 424 nm upon H_2O_2 addition are considered to be inactive toward H_2O_2 and not capable of producing a Compound I-like intermediate, Tables 5.1 and 5.2. One of the characteristics of these five mutants, D132K, K149D, D235K, D241K, and E267K, is that all have predominantly low-spin spectra with the A_{Soret}/A_{380} ratios varying between 1.91 and 2.74 at pH 7.5, Table 3.2, Chapter III. In addition, none of these five mutants had detectable reactions with H_2O_2 in the stopped-flow studies to be presented below and all have very low catalytic activities, as will be described in Chapter VI.

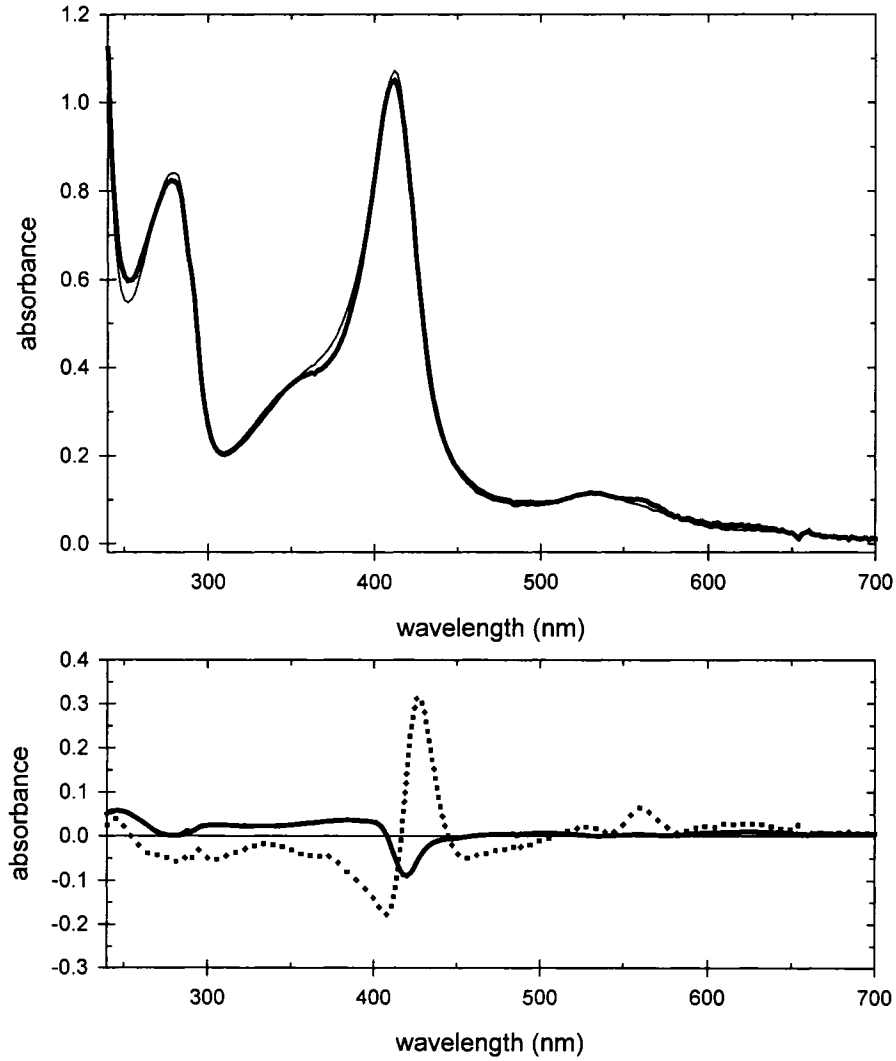

Figure 5.2 Upper Panel - Spectra of the K149D mutant of rCcP in the absence (thin line) and presence (thick line) of a slight stoichiometric excess of hydrogen peroxide at pH 7.5. These two spectra are almost superimposed. Lower Panel - Difference spectrum of K149D+H_2O_2 minus K149D (solid line). Difference spectrum of yCcP Compound I minus K149D (dotted line).

The spectrum of each mutant was determined in the presence and absence of H_2O_2 at both pH 6.0 and 7.5 and the fraction of enzyme that reacted with H_2O_2 was estimated from the absorbance change at 424 nm using Equation 5.1. These data,

converted to the percent inactive enzyme, are included in the last columns of Tables 5.1 and 5.2. Tables 5.1 and 5.2 summarize the H_2O_2 reactivity data at pH 6.0 and 7.5 respectively, including kinetic data obtained from the stopped-flow studies to be described in the next section.

The fraction of mutant enzyme that reacted with H_2O_2 varied dramatically, with some reacting stoichiometrically with H_2O_2 while others were totally inactive. The percentage of H_2O_2-reactive enzyme for each mutant is given in Table 5.1 (pH 6.0) and Table 5.2 (pH 7.5). Visual representations of the percentage of active enzyme are shown in Figures 5.3 and 5.4. At pH 6.0, the average percentage of active enzyme in the charge-reversal mutants is 67 ± 30% while at pH 7.5, the average amount of active mutant enzyme decreases to 49 ± 33%. As will be seen in the Discussion section, the percentage of inactive enzyme correlates with the amount of hexa-coordinate heme in the mutants and the mutants have a higher fraction of hexa-coordinate heme at pH 7.5 than at pH 6.0.

Rate of Reaction between Hydrogen Peroxide and the Charge-Reversal Mutants

The rate of reaction between the charge-reversal mutants and H_2O_2 was determined by stopped-flow techniques at both pH 6.0 and 7.5 under pseudo-first order conditions with hydrogen peroxide in excess. The reaction was monitored at the wavelength giving the largest absorbance changes upon reaction with hydrogen peroxide, generally 424 nm. In most cases, the transient absorbance changes were biphasic with observed rate constants, k_f^{obs} and k_s^{obs}, for the fast and slow kinetic phases, respectively. The rate of the fast phase of the reaction was generally ten times faster than the slow

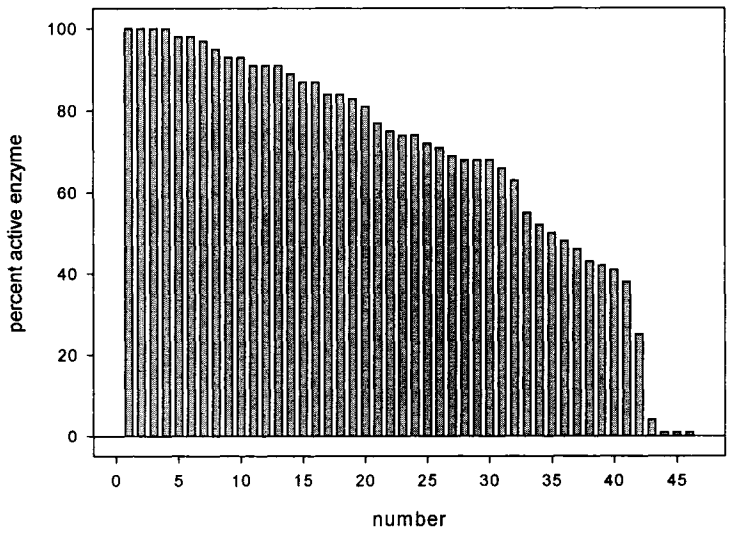

Figure 5.3. Distribution of active enzyme at pH 6.0. Bar graph showing the percentage of active enzyme for the 46 charge-reversal mutants listed in order of decreasing activity. Note that the abscissa values do not refer to specific mutations.

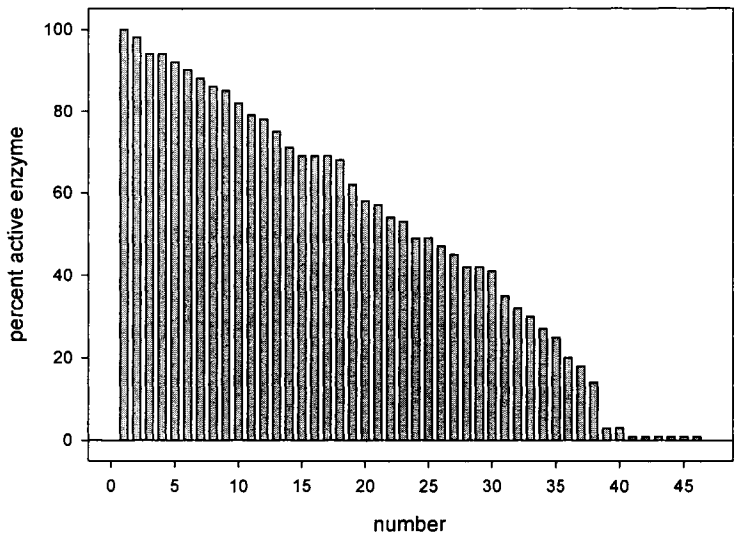

Figure 5.4. Distribution of active enzyme at pH 7.5. Bar graph showing the percentage of active enzyme for the 46 charge-reversal mutants listed in order of decreasing activity. Note that the abscissa values do not refer to specific mutations.

phase and the amplitude of the fast phase was generally larger than the slow phase. The fraction of the total absorbance change that occurs in the fast and slow kinetic phases as well as the fraction of enzyme that does not react with hydrogen peroxide are included in Tables 5.1 and 5.2.

In all cases, the fast phase of the reaction is linearly dependent upon the hydrogen peroxide concentration as illustrated in Figure 5.5 for the D37K mutant. The apparent bimolecular rate constant can be determined from the slope of plots such as that shown in Figure 5.5, by using Equation 5.2. The bimolecular rate constant for the fast phase of the reaction is designated k_1 and is included in Tables 5.1 and 5.2. At pH 6.0, k_1 could be determined for 39 of the 46 mutants while at pH 7.5, k_1 could be determined for 37 of the mutants. The average value of k_1 is $40 \pm 7\ \mu M^{-1}\ s^{-1}$ for the 39 reactive mutants at pH 6.0 and $42 \pm 7\ \mu M^{-1}\ s^{-1}$ for the 37 reactive mutants at pH 7.5. These average values are within experimental error of the k_1 values for bakers' yeast CcP (yCcP) and rCcP at pH 6.0 and 7.5, Tables 5.1 and 5.2. The observed range in k_1 for the charge-reversal mutants is between 19 $\mu M^{-1}\ s^{-1}$ for K149D at pH 6.0 and 66 $\mu M^{-1}\ s^{-1}$ for E167K at pH 7.5.

Slow Phase of Hydrogen Peroxide Reaction

The hydrogen peroxide dependence for the slow phase of the reaction is complex. For some of the mutants, k_s^{obs} is independent of the hydrogen peroxide concentration, as is observed for yCcP and CcP(MI), Table 5.1, while for other mutants, k_s^{obs} is linearly dependent upon the hydrogen peroxide concentration, as is observed for rCcP, Table 5.1.

If k_s^{obs} is linearly dependent upon the hydrogen peroxide concentration, as illustrated in Figure 5.6 for the E290K mutant, an apparent bimolecular rate constant designated k_2 is calculated and included in Tables 5.1 and 5.2. If k_s^{obs} is independent of the hydrogen peroxide concentration, as illustrated for the D210K mutant in Figure 5.7, the first order rate constant is designated k_3 in Tables 5.1 and 5.2.

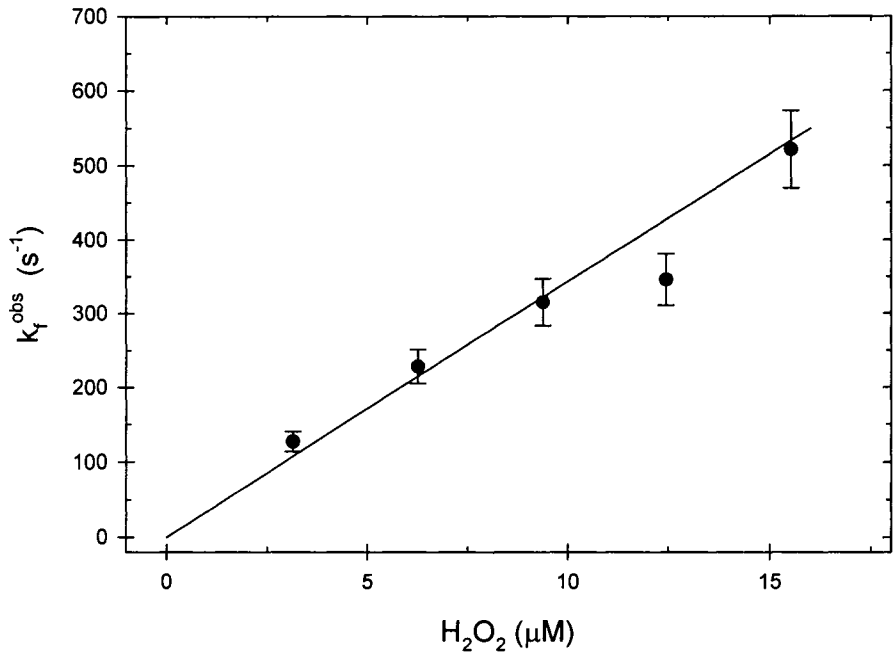

Figure 5.5. Variation of k_f^{obs} with hydrogen peroxide for the D37K mutant at pH 6.0. The slope of this plot gives the apparent bimolecular rate constant, k_1, for the reaction between H_2O_2 and the D37K mutant.

At pH 6.0, 32 of the 46 mutants have slow phases that depend upon the hydrogen peroxide concentration and the value of k_2 averages 2.2 ± 0.5 μM^{-1} s^{-1} for these 32 mutants. Eight of the mutants have hydrogen peroxide-independent slow phases with an average value for k_3 of 27 ± 7 s^{-1}. Seven of the mutants have monophasic reactions with

hydrogen peroxide, with three mutants having only the fast phase of the reaction, K149D, D165K, and E209K, while four of the mutants have only the slow phase of the reaction, E76K, D79K, D132K, and E135K. There is no detectable reaction with hydrogen peroxide for three of the mutants, D235K, D241K, and E267K.

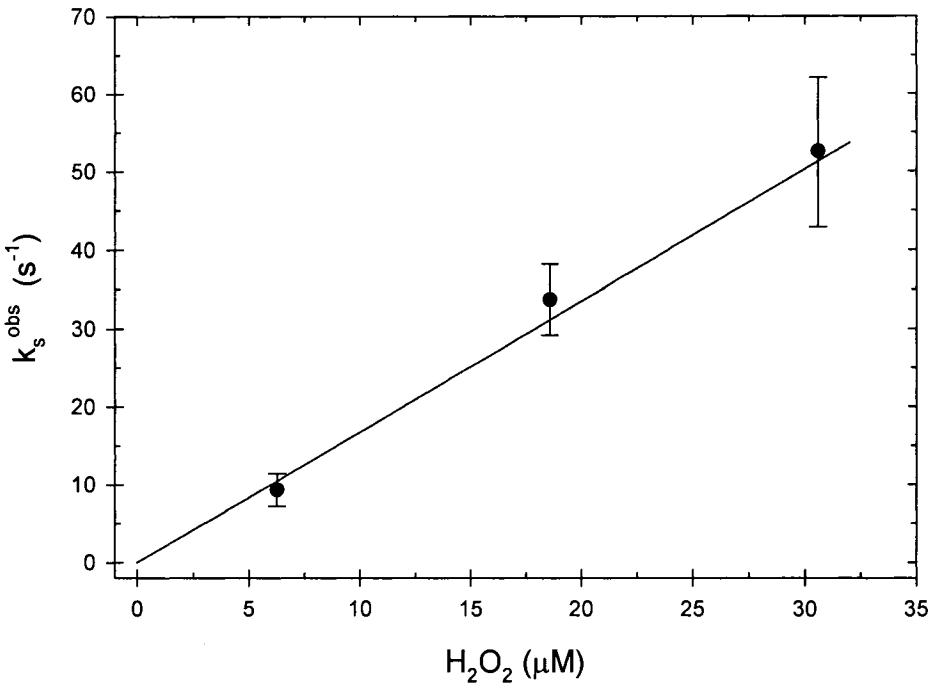

Figure 5.6. Variation of k_s^{obs} with hydrogen peroxide for the E290K mutant at pH 6.0. The slope of this plot gives the apparent bimolecular reaction, k_2, for the slow phase of the H_2O_2 reaction with the E290K mutant.

Similar results are obtained at pH 7.5, Table 5.2. There was no detectable reaction with H_2O_2 using stopped-flow techniques for seven of the mutants at pH 7.5, the same three that did not have detectable reactions at pH 6.0 (D235K, D241K, and E267K) and four additional mutants, D79K, D132K, K149D, and D165K. Twelve of the mutants reacted in a monophasic manner with H_2O_2, with ten of the twelve reacting rapidly with

H_2O_2 giving apparent k_1 values similar to that of yCcP. Two of the mutants, E76K and E135K, reacted in a monophasic manner but with bimolecular rate constants equal to k_2 rather than k_1. The remaining 27 mutants reacted with H_2O_2 in a biphasic manner with the rate of the slow phase of the reaction dependent upon the H_2O_2 concentration for seventeen of the mutants and independent of the H_2O_2 concentration for ten of the mutants.

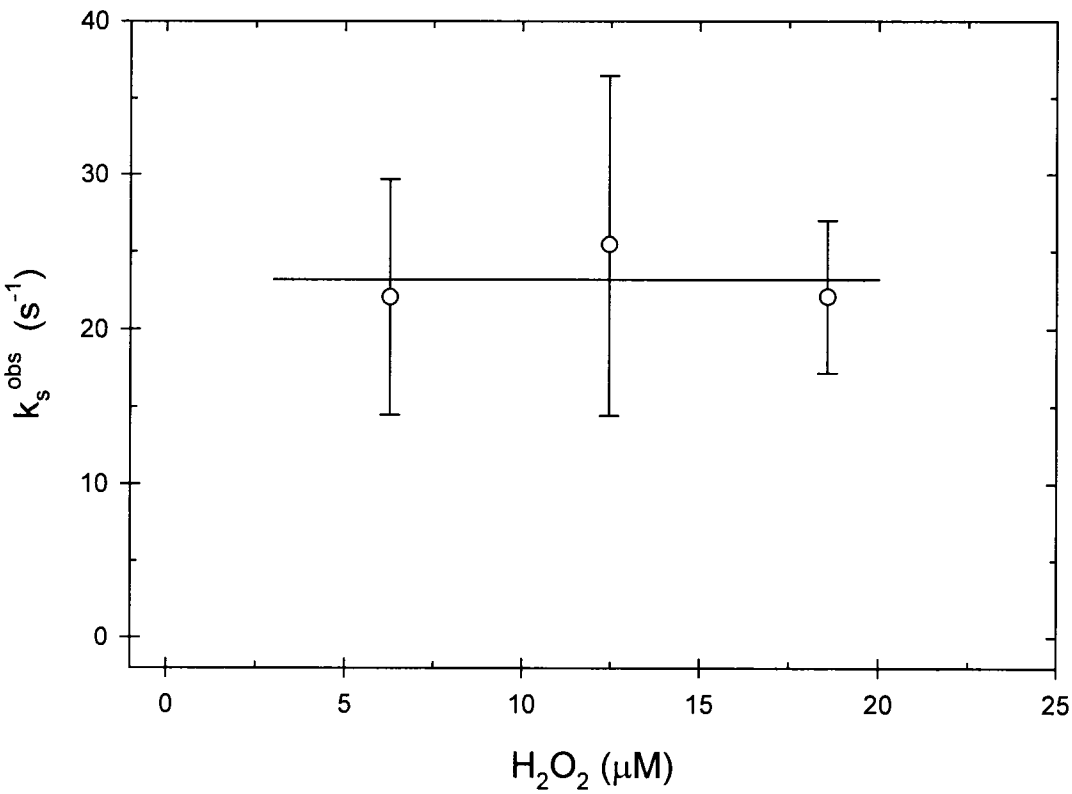

Figure 5.7. Variation of k_s^{obs} with hydrogen peroxide for the D210K mutant at pH 6.0. The observed rate constant is independent of the H_2O_2 concentration and the observed first-order rate constant is designated k_3.

Discussion

Fraction of H_2O_2-Reactive Enzyme for the Charge-Reversal Mutants

One of the unexpected findings of this research was the observation that the charge-reversal mutations on the surface of CcP could alter the heme ligation in the interior of the protein, Chapter III. Another unanticipated finding was that the charge-reversal mutations on the surface of the enzyme have a profound influence on the reaction with H_2O_2, with several of the mutants not reacting with H_2O_2 at all, and many others only partially reacting with H_2O_2. In retrospect, these two findings are correlated. It has previously been observed that, although yCcP and CcP(MI) react stoichiometrically with H_2O_2 between pH 4.5 and 7, the fraction of H_2O_2-reactive enzyme decreases at higher pH and this is correlated with conversion of CcP to the alkaline hexa-coordinate low-spin forms of the enzyme (9).

The most extensive study of the stoichiometry of the CcP/H_2O_2 reaction was that of Vitello *et al.* (9), who found a stoichiometric ratio ([H_2O_2]/[CcP]) of 1.01 ± 0.05 for ten titrations carried out. The stoichiometric ratio decreases to zero at high pH with an apparent pK_A of 9.0 ± 0.1 (9). This apparent pK_A value correlates well with the apparent pK_A of 8.7 ± 0.2 for the conversion of the penta-coordinate form of yCcP to the hexa-coordinate, low-spin forms (9). Previously, Yonetani and Ray (10) and Coulson *et al.* (11) had shown that H_2O_2 reacts essentially stoichiometrically in the neutral pH region. Coulson *et al.* (11) obtained a molar ratio of peroxide to CcP for the fully formed

Compound ES (former name of Compound I) to be 0.91 ± 0.07 for nine determinations at pH 6.0. Coulson *et al.* (11) discussed the potential errors in determining this stoichiometric ratio, especially in determining the concentration of CcP. Published extinction coefficients for yCcP vary between 93 mM^{-1} cm^{-1} (10) to 102 mM^{-1} cm^{-1} (12) at the Soret maximum in the neutral pH region. This range in extinction coefficients leads to a possible variation of 9% in determining the yCcP concentration and the stoichiometric ratio with H_2O_2. Yonetani (10) used an extinction coefficient of 93 mM^{-1} cm^{-1}, while Coulson *et al.* (11) used an extinction coefficient of 95 mM^{-1} cm^{-1} at the Soret maximum. In the Erman/Vitello laboratory, multiple determinations of the extinction coefficient for multiple isolations of yCcP give a value of 98 ± 3 mM^{-1} cm^{-1} at the Soret maximum, a standard deviation of 3% (4).

Vitello *et al.* (9) also examined the H_2O_2 stoichiometry for CcP(MI) and the W191F mutant of CcP(MI) and found that both reacted stoichiometrically with H_2O_2 in the neutral pH region. However, the stoichiometry for both CcP(MI) and the W191F mutant decreased to zero at alkaline pH with an apparent pK_A of 8.2, indicating that recombinant CcP(MI) is somewhat less resistant to conversion to the low-spin forms at alkaline pH than is yCcP. A second heme pocket mutation of CcP(MI) also provides evidence that the hexa-coordinate forms of CcP are not as reactive toward H_2O_2 as is the penta-coordinate form. The heme ligation of the D235N mutant of CcP(MI) is very complex, with three different coordination states existing between pH 4 and 8. At low pH, a high-spin, penta-coordinate state dominates but is converted to two different low-spin forms above pH 5 (13). The H_2O_2 stoichiometry of D235N reflects this complex heme ligation, with a maximum stoichiometry of ~0.8 at pH 5.5, decreasing to zero at pH

8. An Asp-235 mutant was constructed and investigated in this study, D235K, and it too has altered H_2O_2 reactivity. As seen in Tables 5.1 and 5.2, the D235K mutant of rCcP does not react with H_2O_2 at either pH 6.0 or pH 7.5, although the A_{Soret}/A_{380} ratio of 1.83 and 1.91 at pH 6.0 and 7.5, respectively (Table 3.2, Chapter III), suggests a mixture of penta- and hexa-coordinate forms.

There is a general correlation between the estimated fraction of H_2O_2-inactive enzyme and the amount of hexa-coordinate heme as estimated from the A_{Soret}/A_{380}, with some notable exceptions, Figures 5.8 and 5.9. The correlations at pH 6.0 and 7.5 are shown in Figures 5.8 and 5.9, respectively. In general, as the A_{Soret}/A_{380} ratio increases, the fraction of inactive enzyme generally increases. The correlation is not perfect for a number of reasons. First, the A_{Soret}/A_{380} ratio does not represent conversion of penta-coordinate wild-type enzyme to a single low-spin species with a specific H_2O_2 reactivity. There are at least three potential hexa-coordinate forms with either a water, hydroxide, or His-52 bound to the sixth heme site. Each of these different hexa-coordinated forms will have a different A_{Soret}/A_{380} value. While it has not been possible to obtain accurate spectra of the alkaline forms of yCcP due to the complex kinetic behavior at pH values greater than 9 (6), the two hexa-coordinate, low-spin forms of the D235N mutant of CcP(MI) observed between pH 5 and 8 have A_{Soret}/A_{380} values of ~2.5 and ~3.3 (13). The former has been assigned to the hydroxy-ligated form and the latter to the His-52 coordinated form. In addition to the nature of the sixth ligand affecting the A_{Soret}/A_{380} value, it is also possible that there are small variations in this ratio due to the environmental effects in the various mutants. Thus the spectrum of the hydroxy-ligated form in one mutant may be slightly different than the hydroxy-ligated form of

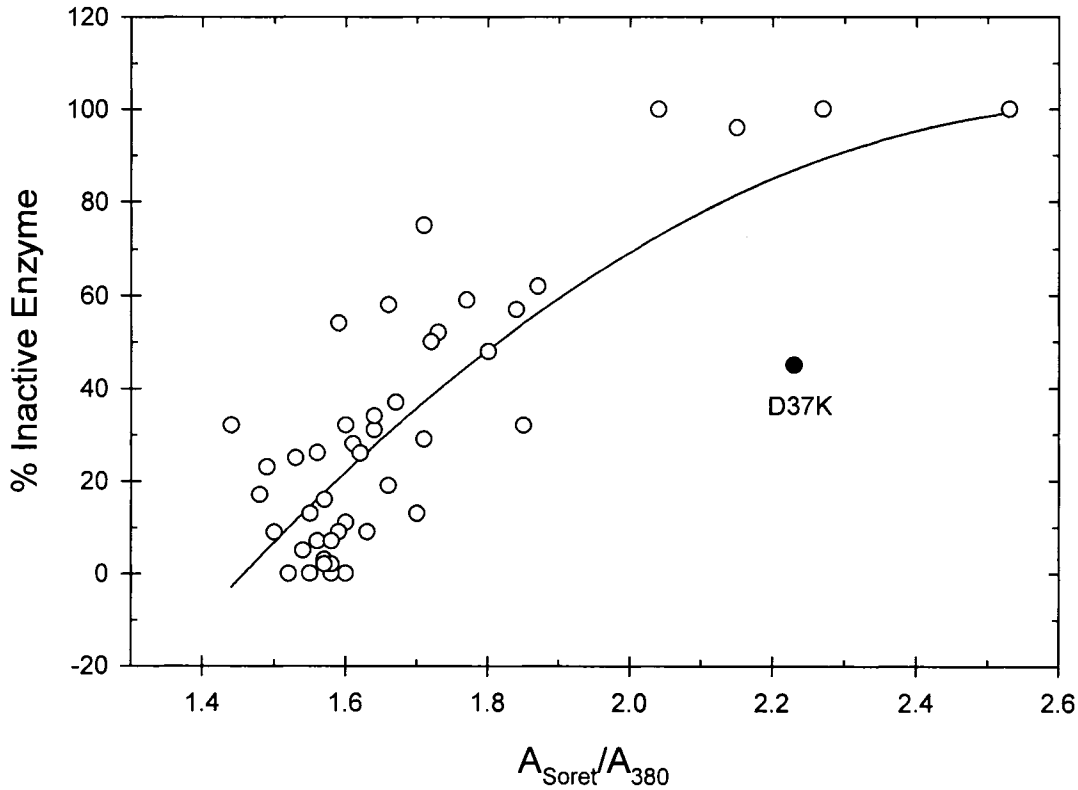

Figure 5.8. Plot of A_{Soret}/A_{380} *versus* the percentage of inactive enzyme for 46 charge-reversal mutants of rCcP at pH 6.0. The percentage of inactive enzyme was estimated from the absorbance change at 424 nm upon addition of a slight stoichiometric excess of hydrogen peroxide. The datum for D37K is labeled and shown as a solid point. The properties of D37K are discussed in the text. A second-order correlation line is included to show the trend in the data and has no physical significance.

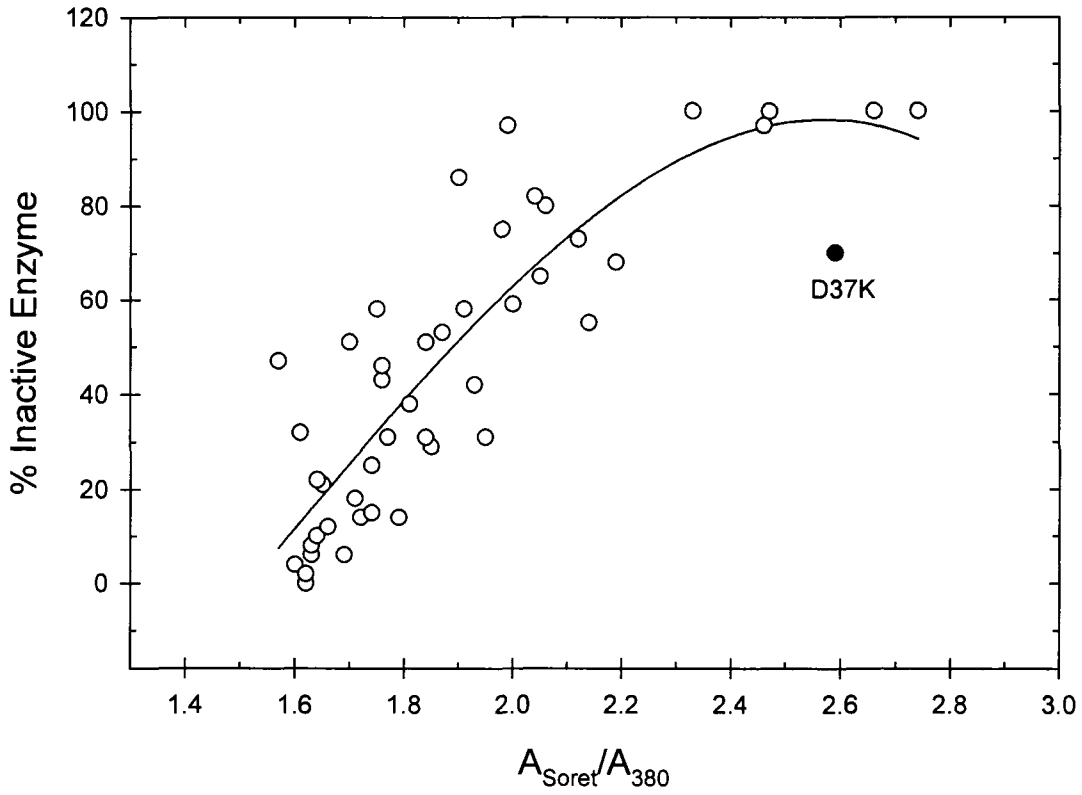

Figure 5.9. Plot of A_{Soret}/A_{380} *versus* the percentage of inactive enzyme for 46 charge-reversal mutants of rCcP at pH 7.5. The percentage of inactive enzyme was estimated from the absorbance change at 424 nm upon addition of a slight stoichiometric excess of hydrogen peroxide. The datum for D37K is labeled and shown as a solid point. The properties of D37K are discussed in the text. A second-order correlation line is included to show the trend in the data and has no physical significance.

another mutant, for example. The possibility of water existing as the sixth ligand also leads to variation in the correlation between the A_{Soret}/A_{380} value and the percentage of inactive enzyme. Water is an intermediate-strength field ligand, and in many heme proteins, water coordination leads to an equilibrium mixture of high- and low-spin forms (14). It is expected that water ligation would increase the A_{Soret}/A_{380} value over the penta-coordinated wild-type enzyme but it may not completely inactivate the enzyme. A water molecule should be more easily displaced from the heme iron than either a hydroxide ion or the distal histidine, as has been reported for other aquo-ligated heme proteins such as metmyoglobin, which reacts with hydrogen peroxide (15). It would be expected that an aquo-ligated mutant would react with H_2O_2 even though it will have an elevated A_{Soret}/A_{380} value.

The second factor that leads to variation in the correlation between the percentage of inactive enzyme and the A_{Soret}/A_{380} value is in the estimation of inactive enzyme. As a quick screen of the ability of the mutant to react with H_2O_2 to form a Compound I-like intermediate, the spectrum of the mutant was determined in the absence and presence of a slight stoichiometric excess of H_2O_2. The assumption was made that the spectrum of the H_2O_2-oxidized mutants would be identical to the spectrum of Compound I for yCcP. This assumption should be good since the ligation of the heme group in Compound I would be identical in yCcP and the mutants, with the proximal histidine bound at the first axial position and an "oxo" oxygen atom covalently bound to the second axial position of the heme (16). For the conversion of yCcP to yCcP Compound I, the largest change in absorbance occurs at 424 nm. The fractional change in the absorbance at 424 upon addition of H_2O_2 to the mutant compared to the change that would occur for 100%

formation of yCcP Compound I was used to calculate the fraction of the mutant converted to Compound I, Equation 5.1. As presented in the Results section, some of the mutants gave higher than predicted absorbance changes at 424 nm and some gave lower than expected absorbance changes. This suggests that the mutant Compound I spectra may be slightly different than that of yCcP Compound I, leading to small potential errors in the fraction of inactive enzyme.

In spite of the complexity of factors that can affect the correlation between the A_{Soret}/A_{380} values and the percentage of inactive enzyme, Figures 5.8 and 5.9 are useful in showing that the hexa-coordinate forms tend to be less active toward H_2O_2 than the penta-coordinate wild-type enzyme. D37K is a conspicuous outlier in Figures 5.8 and 5.9. The datum for D37K is shifted to the lower right in the correlation plot, Figures 5.8 and 5.9. This could be due to water binding to the heme iron in D37K, increasing the A_{Soret}/A_{380} value due to its hexa-coordination, but not substantially decreasing its reaction with H_2O_2 since the peroxide could displace the water ligand. Although Asp-37 is a surface residue in CcP, the carboxylate group of Asp-37 does not interact with the solvent but is hydrogen bonded to His-181 in the interior of CcP (17, 18). His-181 in turn is part of a hydrogen-bonding network that extends from the proximal side of the heme to the distal side of the heme and includes water-595, which is poised above the sixth coordination site of the heme iron but not bound in wild-type CcP (17-20). Parenthetically, it was initially reported that water-595 was coordinated to the heme iron with the oxygen-to-iron distance 2.4 Å (17). Later refinement of the crystal structure moved the distance to 2.7 Å, which is considered outside the coordination sphere of the heme iron (19, 20) and making the crystal structure consistent with the spectroscopic data

that indicates a penta-coordinate heme iron. Obviously, small movements of the residues within the heme pocket and mutations that alter the hydrogen-bonding network in the distal heme pocket can have a marked effect on whether water-595 is bound or not bound to heme iron (18-20). Mutation of His-181 to a glycine residue causes formation of a predominantly high-spin, hexa-coordinate heme, as monitored by the absorption spectrum with the most probable heme ligand water-595 (18-20).

More detailed studies of the spectroscopic properties and hydrogen peroxide reactivity of the charge-reversal mutants of CcP, especially as a function of pH and temperature, may ultimately determine the identify of the sixth heme ligand in the mutants, how the ligands may change with pH and temperature, and how they affect the H_2O_2 reactivity of CcP. Transient-state pH jump studies can give information about the kinetics of ligand exchange and could provide insight into why the hexa-coordinate, low-spin forms of CcP do not react with H_2O_2.

Rate of Reaction between H_2O_2 and the Charge-Reversal Mutants

The detailed summary of the percentage of each mutant that reacts rapidly with hydrogen peroxide at pH 6.0 and 7.5 along with the observed rate constant for the reaction with hydrogen peroxide is given in Tables 5.1 and 5.2. At pH 6.0, the percentage of rapidly-reacting enzyme varies from 0% for seven of the mutants, namely, E76K, D79K, D132K, E135K, D235K, D241K, and E267K to 94% for E32K. At pH 7.5, the number of unreactive mutants increases to eight, the same seven as observed at pH 6.0 plus one additional mutant, K149D. E32K is the most reactive mutant at pH 7.5, just

as it is at pH 6.0. In fact, the percentage of rapidly reacting E32K increases from 94% at pH 6.0 to 98% at pH 7.5, Tables 5.1 and 5.2.

At pH 6.0, the bimolecular rate constant for the fast reaction with H_2O_2, k_1, could be determined for 39 of the 46 mutants while at pH 7.5, k_1 could be determined for 37 of the mutants. The average value of k_1 is $40 \pm 7\ \mu M^{-1}\ s^{-1}$ for the 39 reactive mutants at pH 6.0 and $42 \pm 7\ \mu M^{-1}\ s^{-1}$ for the 37 reactive mutants at pH 7.5. These average values are within experimental error of the k_1 values for bakers' yeast CcP (yCcP) and rCcP at pH 6.0 and 7.5, Tables 5.1 and 5.2. The observed range in k_1 for the charge-reversal mutants is between 19 $\mu M^{-1}\ s^{-1}$ for K149D at pH 6.0 and 66 $\mu M^{-1}\ s^{-1}$ for E167K at pH 7.5. We can conclude that for the rapidly-reacting fraction of mutant enzyme, the rate of the reaction with hydrogen peroxide is essentially identical to that of wild-type yCcP.

Slow Kinetic Phase of the Reaction between H_2O_2 and the Charge-Reversal Mutants

The slow phase of the hydrogen peroxide reaction is generally a very minor phase of the reaction for the mutant enzymes and has not been studied in detail. A slow phase of the H_2O_2 reaction is observed for 40 of the 46 mutants at pH 6.0 and for 29 of the mutants at pH 7.5. This is consistent with the earlier findings of Balny *et al.* (3) and Vitello *et al.* (4), who report that the amplitude of the minor phase is largest at pH 6.0 and below. The slow phase of the reaction has been reported to be independent of the H_2O_2 concentration for yCcP and CcP(MI) (3, 4) and observed to be linearly dependent upon the H_2O_2 concentration for rCcP in this study. Since rCcP is the parental form of the charge-reversal mutants used in this study, the slow phase of the reaction is dependent

upon the H_2O_2 concentration for most of the charge-reversal mutants. Only eight of the 46 mutants have H_2O_2-independent slow rates at pH 6.0.

References

1. Cornish-Bowden, A. (1979) *Fundamentals of Enzyme Kinetics*, Butterworths, London, U.K.

2. Loo, S., and Erman, J. E. (1975) A kinetic study of the reaction between cytochrome *c* peroxidase and hydrogen peroxide. Dependence on pH and ionic strength, *Biochemistry 14*, 3467-3470.

3. Balny, C., Anni, H., and Yonetani, T. (1987) A stopped-flow study of the reaction of cytochrome *c* peroxidase with hydroperoxides, *FEBS Letts. 221*, 349-354.

4. Vitello, L. B. Huang, M., and Erman, J. E. (1990) pH-dependent spectral and kinetic properties of cytochrome *c* peroxidase: Comparison of freshly isolated and stored enzyme, *Biochemistry 29*, 4283-4288.

5. Erman, J. E., Vitello, L. B., Miller, M. A., Shaw, A., Brown, K. A., and Kraut, J. (1993) Histidine 52 is a critical residue for rapid formation of cytochrome *c* peroxidase compound I, *Biochemistry 32*, 9798-9806.

6. Dhaliwal, B. K., and Erman, J. E. (1985) A kinetic study of the alkaline transitions in cytochrome *c* peroxidase, *Biochim. Biophys. Acta 827*, 174-182.

7. Nakani, S., Viriyakul, T., Mitchell, R., Vitello, L. B., and Erman, J. E. (2006) Characterization of a covalently-linked yeast cytochrome *c*-cytochrome *c* peroxidase complex: Evidence for a single, catalytically-active cytochrome *c* binding site on cytochrome *c* peroxidase, *Biochemistry 45*, 9887-9893.

8. Kolthoff, I. M. and Belcher, R. (1957) Hydrogen peroxide, in *Volumetric Analysis*, Vol. 3, pp 75-76, Interscience, New York.

9. Vitello, L. B., Erman, J. E., Mauro, J. M., and Kraut, J. (1990) Characterization of the hydrogen peroxide-enzyme reaction for two cytochrome *c* mutants, *Biochim. Biophys. Acta 1038*, 90-97.

10. Yonetani, T. (1966) Studies on cytochrome *c* peroxidase. IV. A comparison of peroxide-induced complexes of horseradish and cytochrome *c* peroxidases, *J. Biol. Chem. 241*, 2562-2571.

11. Coulson, A. F. W., Erman, J. E., and Yonetani, T. (1971) Studies on cytochrome *c* peroxidase. XVII. Stoichiometry and mechanism of the reaction of compound ES with donors, *J. Biol. Chem. 246*, 917-924.

12. Nelson, C. E., Sitzman, E. V., Kang, C. H., and Margoliash, E. (1977) Preparation of cytochrome *c* peroxidase from baker's yeast, *Anal. Biochem. 83*, 622-631.

13. Vitello, L. B., Erman, J. E., Miller, M A., Mauro, J. M., and Kraut, J. (1992) Effect of Asp-235→Asn substitution on the absorption spectrum and hydrogen peroxide reactivity of cytochrome *c* peroxidase, *Biochemistry 31*, 11524-11535.

14. Iizuka, T., and Yonetani, T. (1970) Spin changes in hemoproteins, *Advan. Biophys. 1*, 157-182.

15. George, P., and Irvine, D. H. (1952) The reaction between metmyoglobin and hydrogen peroxide, *Biochem. J. 52*, 511-517.

16. Fülöp, V., Phizackerley, R. P., Soltis, S. M., Clifton, I. J., Wakatsuki, S., Erman, J., Hajdu, J., and Edwards, S. L. (1994) Laue diffraction study on the structure of cytochrome *c* peroxidase compound I, *Structure 2*, 201-208.

17. Finzel, B. C., Poulos, T. L., and Kraut, J. (1984) Crystal structure of yeast cytochrome *c* peroxidase refined at 1.7-Å resolution, *J. Biol. Chem. 259*, 13027-13036.

18. Miller, M. A., Hazzard, J. T., Mauro, J. M., Edwards, S. L., Simons, P. C., Tollin, G., and Kraut, J. (1988) Site-directed mutagenesis of yeast cytochrome *c* peroxidase shows histidine 181 is not required for oxidation of ferrocytochrome *c*, *Biochemistry 27*, 9081-9088.

19. Mauro, J. M., Miller, M. A., Edwards, S. L., Wang, J., Fishel, L. A., and Kraut, J. (1989) Exploring structure-function relationships in yeast cytochrome *c* peroxidase using mutagenesis and crystallography, in *Metal Ions in Biological Systems, Vol. 25*, Eds. Sigel, H., and Sigel, A., Marcel Dekker, New York, pp 477-503.

20. Miller, M. A., Shaw, A., and Kraut, J. (1994) 2.2 Å structure of oxy-peroxidase as a model for the transient enzyme:peroxide complex, *Struct. Biol. 1*, 524-531.

CHAPTER VI

STEADY-STATE OXIDATION OF FERROCYTOCHROME *c*

Introduction

The steady-state kinetic analysis of the CcP-catalyzed ferrocytochrome *c* oxidation by hydrogen peroxide provides information regarding maximum enzyme turnover rates, the interaction between cytochrome *c* and CcP, and places limits on possible mechanisms for CcP-I and CcP-II reduction by ferrocytochrome *c* (Equations 1.2 and 1.3 from Chapter I) (1).

Yonetani and Ray (2) carried out the first detailed steady-state measurements with highly purified enzyme for the oxidation of both horse heart and yeast iso-1 ferro-cytochrome *c* under a variety of conditions. Under the optimum condition, 23°C, pH 6.0 at 0.05 M ionic strength for horse heart cytochrome *c* and 0.2 M ionic strength for yeast cytochrome *c*, the kinetics were monophasic with K_M values equal to 4.5 μM and 25 μM for the horse heart and yeast cytochrome *c*, respectively . The maximum turnover rate of the enzyme was 1300 s^{-1} for horse heart cytochrome *c* and 7000 s^{-1} for yeast cytochrome *c* at pH 6.0.

Nicholls and Mochan (3) compared the properties of CcP isolated by the original procedure of Abrams in 1942 and the method of Yonetani from 1965. The activity of the

two preparations differ substantially using horse heart cytochrome *c* as substrate. The highest turnover rate for the Abrams preparation was 14.2 s^{-1} (measured as cytochrome *c* turnover) in 0.01 M potassium phosphate buffer, pH 7. Nicholls and Mochan also observed monophasic kinetics for the Yonetani preparation at both pH 6 and 7. They investigated the ionic strength dependence at pH 7 and found that both the K_M and the maximum turnover number varied with buffer concentration. K_M varied between 2.2 and 28 μM at 5 and 500 mM phosphate buffer, respectively, similar to the K_M values of the Abrams preparation. However, the maximum turnover numbers were much larger, with a turnover rate of 460 s^{-1} in 10 mM phosphate buffer. An important observation was that ferricytochrome *c* inhibited the reaction with the inhibition constant, K_i, about equal to K_M, suggesting that both ferri- and ferrocytochrome *c* bound to CcP with the same affinity.

Kang *et al.* (4) gave the first report of biphasic steady-state plots and the suggestion of the formation of both 1:1 and 2:1 cytochrome *c*/CcP complexes. The authors used cytochrome *c* from a variety of sources including yeast iso-1, yeast iso-2, horse, tuna, and cicada cytochromes and observed biphasic kinetics for all. They report that the experimental conditions required to obtain the highest enzyme turnover varied with the source of the cytochrome, with the highest turnover for horse cytochrome *c* occurring approximately at pH 6 and ionic strength about 0.05 M and for yeast cytochrome *c*, the optimum conditions were pH 7 and 0.2 M ionic strength. Kang *et al.* reported substantially smaller turnover numbers from those of Yonetani and Ray (2) under similar conditions. For yeast cytochrome *c* in 0.2 M acetate buffer, pH 6, Kang *et al.* report a maximum cytochrome *c* turnover of 1450 s^{-1}, compared to 14,000 s^{-1} for

Yonetani and Ray. For horse cytochrome *c* in 0.05 M acetate buffer, pH 6, Kang *et al.* report a maximum turnover of 730 s^{-1}, compared to 2,600 s^{-1} for Yonetani and Ray. Although the observation of biphasic kinetics was one of the most interesting results of their studies, Kang *et. al.* only report ranges of values for K_{M2} as a function of ionic strength and it is essentially impossible to extract the K_{M2} values and to compare these values with other studies.

Kang and Erman (5) investigated the oxidation of horse ferrocytochrome *c* as a function of both cytochrome *c* and hydrogen peroxide concentrations at pH 7.0 in a 0.010 M ionic strength buffer. They used a three-fold larger range of cytochrome *c* concentrations than had been used previously (0.27 to 104 μM) and observed biphasic kinetics under all experimental conditions investigated. They derived a steady-state velocity expression for a mechanism involving only a single cytochrome *c* binding site and demonstrated that this model could explain the biphasic steady-state velocity plots without the necessity of invoking a second cytochrome *c* binding site. The biphasic behavior in this model is due to multiple pathways for the two-substrate reaction to occur, *i.e.*, either ferrocytochrome *c* or hydrogen peroxide can react with the enzyme initially to start the catalytic cycle. The maximum enzyme turnover rate, extrapolated to infinite concentrations of both substrates, was 380 s^{-1}, which translates to a value of 760 s^{-1} for a cytochrome *c* turnover rate.

Kim *et al.* (6) investigated the ionic strength dependence of the steady-state oxidation of horse ferrocytochrome *c* at both pH 7.0 and 7.5. They investigated the rates as functions of both the ferrocytochrome *c* and hydrogen peroxide. Plots of the initial velocity as a function of the ferrocytochrome *c* concentration up to 100 μM were biphasic

although the deviation from monophasic kinetics was small. The biphasic nature was due to an initial phase of the reaction that saturated at low concentration of cytochrome *c* and had maximum turnover numbers between 3 and 54 s^{-1}. The low-affinity phase had apparent K_M values ranging between 8 and ~120 μM at 0.010 M and 0.10 M ionic strength, respectively, pH 7.5. The maximum enzyme turnover rates were independent of ionic strength with values of 470 ± 50 and 290 ± 30 s^{-1} at pH 7.0 and 7.5, respectively. Kim *et al.* favored a single binding-site mechanism to explain the oxidation of horse ferrocytochrome *c*.

Matthis and Erman (7) investigated the ionic strength dependence of the steady-state oxidation of yeast iso-1 ferrocytochrome *c* as a function of ionic strength at pH 7.5. Steady-state velocity plots were biphasic between 0.010 and 0.070 M ionic strength and monophasic at 0.10 and 0.20 M ionic strength. The apparent Michaelis constants, K_{M1} and K_{M2}, were similar to equilibrium dissociation constants for the 1:1 and 2:1 yeast cytochrome *c*/CcP complexes, K_{D1}, and K_{D2}, leading to the conclusion that a mechanism involving two cytochrome *c*-binding sites on CcP was consistent with the steady-state data. The maximum turnover rate varied between 1100 and 2700 s^{-1} over the ionic strength range, 0.010 and 0.070 M.

Miller (8) investigated the catalytic properties of CcP(MI) and five CcP(MI) mutants, E32Q, D34N, A193F, E290N, and E291Q, as a function of ionic strength at pH 6.0 using yeast cytochrome *c* as substrate. The mutation sites were within or near the cytochrome *c* binding site identified by Pelletier and Kraut (discussed in Chapter I of this dissertation). Miller indicated that the data were best interpreted based on a two-binding-site model, where the affinity of the two sites for yeast cytochrome *c* differed by 1000-

fold. Rapid electron transfer only occurs from the cytochrome *c* bound at the high-affinity site identified in the crystal structure of the 1:1 complex. At low ionic strength, the overall rate is limited by product dissociation and binding of cytochrome *c* at the low-affinity site facilitates product dissociation from the high-affinity site.

The primary goal of the steady-state investigation of the catalytic properties of cytochrome *c* peroxidase in this dissertation is to map the cytochrome *c* interaction site (or sites) for formation of 1:1 cytochrome *c*/CcP complexes using charge-reversal mutants of CcP. The plan is to use the Michaelis constants from steady-state studies as a measure of the binding affinity between cytochrome *c* and the CcP mutants. The validity of the use of steady-state kinetics to monitor interaction between CcP and cytochrome *c* comes from the observation that the Michaelis constants correlate very well with true equilibrium dissociation constants obtained in equilibrium studies (1,7-12). Figure 6.1 shows a plot of log K_{MI} (from kinetic studies) or K_{DI} (from equilibrium studies) as a function of square root of the ionic strength. It can be seen in Figure 6.1 that the values of K_{MI} and K_{DI} are comparable and that they increase with the ionic strength. The increasing value of both K_{MI} and K_{DI} with increasing ionic strength indicates that the binding of cytochrome *c* to CcP is dependent upon electrostatic interactions and that the binding becomes weaker at higher ionic strength.

A basic hypothesis in using charge-reversal mutations is that if a negatively charged amino acid residue on the surface of CcP is directly involved in binding cytochrome *c* (which has a net positive charge at pH 7.5), mutation of the residue to a positively charged lysine residue should weaken the interaction with cytochrome *c*. If a negatively charged residue is not directly involved in binding of cytochrome *c*, a charge-

reversal mutation at that site should have little effect on binding. By determining which amino acid residues on the surface of CcP affect the binding of cytochrome *c*, it should be possible to determine whether there is a single cytochrome *c* binding site or whether there are multiple binding sites with similar affinity for cytochrome *c*.

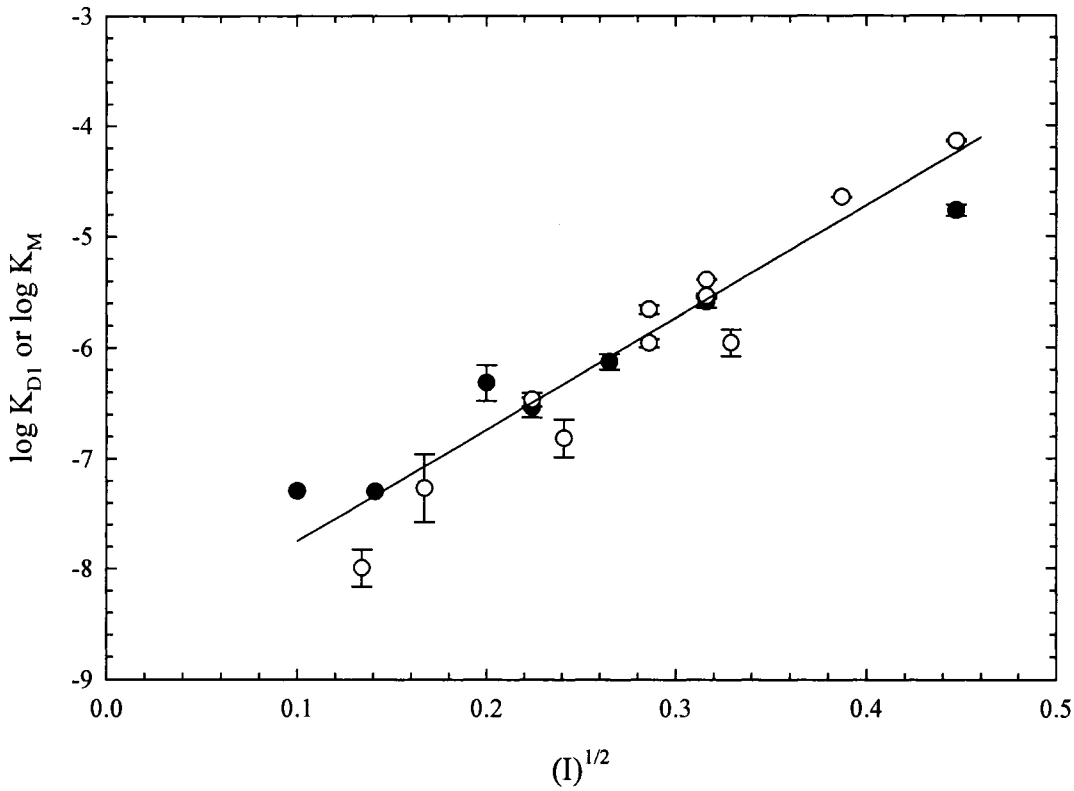

Figure 6.1. Ionic strength dependence of log K_{D1} and log K_{M1}. K_{M1} (open circles) and K_{D1} (filled circles) are comparable and increase with the ionic strength. Data for K_{M1} are from references 7 and 8 and data for K_{D1} are from references 10-12.

Since Pelletier and Kraut (13) have already determined the location of at least one of the cytochrome *c* binding sites, Site 1, from X-ray crystallography (See Chapter I), it is expected that charge-reversal mutations in the vicinity of Site 1 will affect the binding of cytochrome *c*. This will serve as a control experiment in that one would expect that the

residues identified by Pelletier and Kraut as potentially forming salt bridges between CcP and cytochrome *c*, namely Asp-34 and Glu-290, should affect the binding and the Michaelis constants determined from steady-state velocity measurements. The more interesting observations will be if mutations at sites elsewhere on the surface of CcP affect the Michaelis constants.

Experimental Methods

rCcP and the Charge-Reversal Mutants

Construction, expression, and isolation of rCcP and the 46 charge-reversal mutations that have been expressed are described in Chapter II of this dissertation.

Hydrogen Peroxide

Hydrogen peroxide was reagent grade 30% (v/v) and purchased from Aldrich Chemical Company, Inc. The concentration of the 30% hydrogen peroxide stock solution was determined periodically by titration with standardized cerium(IV) sulfate (14). Working solutions of hydrogen peroxide were prepared by volumetric dilution into deionized, distilled water and kept on ice during the experiment.

Preparation of Recombinant Yeast iso-1 Ferrocytochrome *c*(C102T)

Cytochrome *c* Plasmid The plasmid pBTR cloned with the wild type cytochrome *c* gene containing the C102T mutation and the heme lyase gene was a gift from Dr. Gary Pielak, University of North Carolina, NC (15, 16).

Expression of Yeast iso-1 Cytochrome *c*(C102T) Following the procedure described for CcP in Chapter II, the pBTR plasmid was transformed into and cultured in *E. coli* XL1 Blue cells. The plasmids were subsequently isolated and transformed into the *E. coli* BL21 (DE3) Gold cell line for protein expression.

The primary culture contained 100 mL TB broth, 200 μL 50 mg/mL ampicillin and a small amount of BL21 DE3 glycerol stock. It was grown at 37°C with shaking at 250 rpm. Four Fernbach flasks containing doubly concentrated TB broth were prepared and 100 mL of 0.10M potassium phosphate buffer, 1 mL 0.1 M δ -amino levulinic acid, 2 mL 50 mg/mL ampicillin and 10 mL cytochrome *c* culture were added to each flask. The flasks were incubated at 37°C with 250 rpm shaking for 48 hours.

Cells were collected by centrifugation in an identical manner as described for the CcP isolation.

Isolation and Purification of Yeast iso-1 Cytochrome *c*(C102T) The cell lysis procedure was the same as that for CcP except that no lysozyme was added to the cells. The lysed sample was centrifuged at 43000xg for 30 minutes and the supernatant was collected. The sample was dialyzed against distilled water with frequent changes of water. The

dialysate was centrifuged at 43000xg for 30 minutes and applied to a CM Sepharose Fast Flow column equilibrated with 10 mM potassium phosphate buffer, pH 7.2. After extensive washing with the equilibrating buffer, cytochrome *c* was eluted with 0.500 M potassium phosphate buffer, pH 7.2 and dialyzed against distilled water. After several changes of water, the protein was lyophilized and stored at -20°C. Details of the methods for expression, isolation, and purification of yeast iso-1 cytochrome *c*(C102T) are given in Appendix A.

Reduction of Yeast iso-1 Cytochrome *c*(C102T) Cytochrome *c* was reduced by the addition of sodium hydrosulfite and then applied to a small Sephadex G25 column equilibrated in the experimental buffer, to remove the excess sodium hydrosulfite and its oxidation products. The reduced cytochrome *c* solution was kept at room temperature under argon to minimize oxidation.

Protein Concentration Determinations

The concentration of the stock CcP solution was determined spectrophotometrically using an extinction coefficient of 101 mM^{-1} cm^{-1} at 408 nm (9). Similarly, the concentration of reduced stock cytochrome *c* was determined using an extinction coefficient of 131.9 mM^{-1} cm^{-1} at 418 nm or 30.9 mM^{-1} cm^{-1} at 548 nm (9).

For the steady-state experiments, CcP at a working concentration in the nanomolar range was mixed with reduced cytochrome *c* at concentrations ranging from 1.0 to 100 μM.

Determination of Steady-State Rate Parameters

The steady-state kinetic experiments were carried out primarily in 100 mM ionic strength potassium phosphate buffer at pH 7.5 and 25.0°C for both wild-type and mutant proteins. Both the cytochrome *c* solution and the buffer were kept at room temperature under argon to minimize oxidation. The enzyme and hydrogen peroxide solutions were kept on ice during the experiment. The experiments were performed on a Hewlett Packard 8452A diode array spectrophotometer equipped with the Hewlett Packard Peltier temperature controller (Hewlett Packard, Palo Alto, CA).

Initial velocities were determined as a function of yeast iso-1 ferrocytochrome *c* (C102T) concentration (generally 1 to 100 μM) at constant hydrogen peroxide (200 μM). The hydrogen peroxide concentration is sufficiently high so as not to limit the steady-state velocity. Initial velocities were determined by measuring the change in absorbance upon oxidation of recombinant yeast iso-1 ferrocytochrome *c* (C102T) at multiple wavelengths using the diode array spectrophotometer. Buffer, cytochrome *c*, and enzyme were thermally equilibrated at 25 °C in the spectrophotometer, initial absorbance readings made, then the reaction initiated by addition of the hydrogen peroxide. Five different wavelengths, generally chosen from 314, 362, 418, 448, 468, 478, 548, 564, and 574 nm depending upon the substrate concentration, were used to calculate the initial velocity at each set of experimental conditions using Equation 6.1.

$$\frac{v_0}{e_0} = \frac{1}{2(1-f_{ox})\Delta\varepsilon}\frac{\Delta A}{\Delta t} \qquad (6.1)$$

The symbols in Equation 6.1 include the initial velocity, v_0, the total enzyme concentration, e_0, the change in absorbance with time, $\Delta A/\Delta t$, and the difference in extinction coefficient, $\Delta\varepsilon$, between oxidized and reduced cytochrome *c*. Samples of the substrate may contain small amounts of oxidized cytochrome *c* that can inhibit the reaction; f_{ox} is the fraction of oxidized cytochrome *c* in the substrate and is used to make small corrections to the initial velocity. The factor of 2 in the denominator converts cytochrome *c* turnover to enzyme turnover. Details are given in Appendix A.

Results

Analysis of the data from steady-state velocity measurements indicate that rCcP and forty-three charged reversal mutants show simple Michaelis-Menten behavior, characterized by a maximum velocity, V_{max}/e_0, and a Michaelis constant, K_M. The steady-state velocity plots for yCcP and rCcP as a function of the yeast iso-1 ferrocytochrome *c* (C102T) are identical, within experimental error, and are shown in Figure 6.2. These data will serve as the reference when assessing the effect of the charge-reversal mutation on the steady-state catalytic properties of CcP. The steady-state parameters for both yCcP and rCcP, as well as those for the charge-reversal mutants, are tabulated in Table 6.1.

Data cannot be determined for two mutants, D106K, which cannot be expressed, and D235K, which is essentially inactive. The mutations in both D106K and D235K are at internal residue positions and are among the highest conserved residues in CcP, suggesting both are important for the structure or function of the enzyme.

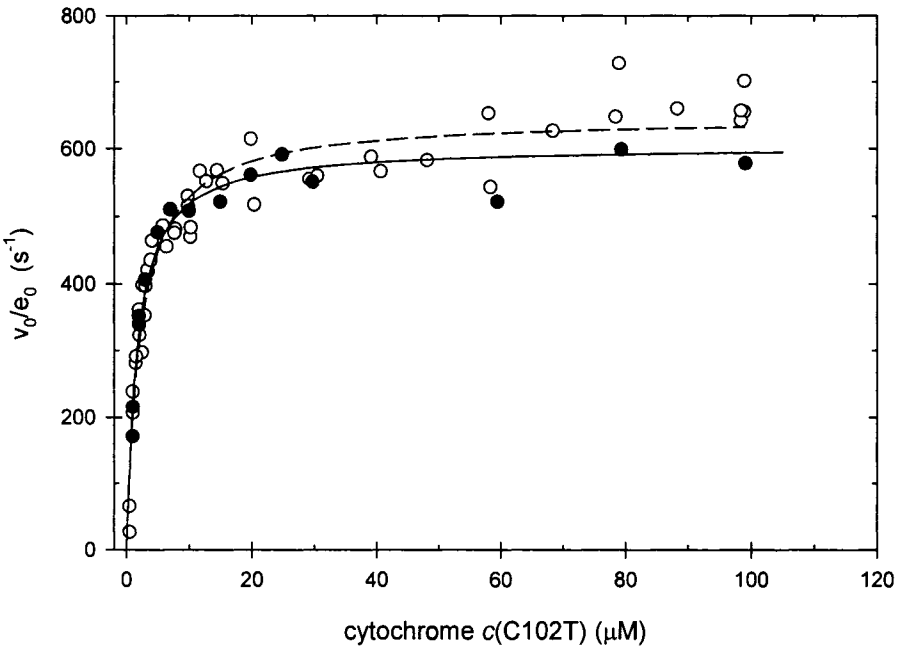

Figure 6.2 A comparison of hyperbolic plots for yCcP (filled circles) and rCcP (open circles). The experimental conditions are 100mM potassium phosphate buffer at pH 7.5, 1-100μM ferrocytochrome *c* C102T, 1-2nM CcP, 200 μM H_2O_2, and 25°C.

Two of the mutants, R31E and D34K, show biphasic kinetics with a minor phase characterized by V_{max}/e_0 and K_M values and a major phase in which the velocity increases with the ferrocytochrome *c* concentration up to the maxium amount, 100 μM, used in the experiment. The steady-state velocity plots for R31E and D34K are shown in Figure 6.3. Only lower limits for the V_{max}/e_0 and K_M values for the major phase could be determined. The parameters for the minor phase and the lower limits for the major phase are included in Table 6.1. The minor phase of the reaction contributes less than 20% of the activity of R31E and D34K based on the V_{max}/e_0 values.

Table 6.1. Steady-State Rate Parameters for rCcP and its Charge-Reversal Mutants at 0.100 M ionic strength, pH 7.5, 25°C

Enzyme	K_M (μM)	V_{max}/e_0 (s^{-1})	Enzyme	K_M (μM)	V_{max}/e_0 (s^{-1})
yCcP	1.7 ± 0.2	604 ± 14	rCcP	2.1 ± 0.2	640 ± 20
E11K	2.8 ± 0.5	400 ± 20	E17K	2.3 ± 0.4	420 ± 20
D18K	2.0 ± 0.3	380 ± 10	R31E-major -minor	> 100 1.2 ± 0.4	>170 30 ± 3
E32K	4.5 ± 0.5	750 ± 20	D33K	2.4 ± 0.3	680 ± 20
D34K-major -minor	>100 2.7 ± 0.8	>90 20 ± 2	E35K	4.4 ± 0.4	760 ± 20
D37K	82 ± 12	41 ± 3	D58K	1.0 ± 0.4	150 ± 5
D61K	1.2 ± 0.2	400 ± 10	E76K	1.0 ± 0.4	36 ± 3
D79K	0.75 ± 0.35	38 ± 3	E93K	1.1 ± 0.2	380 ± 10
E98K	3.1 ± 0.7	690 ± 40	D106K	ND[a]	ND[a]
E118K	51 ± 8	230 ± 20	D132K	4.1 ± 0.7	23 ± 1
E135K	4.9 ± 1.1	100 ± 10	D136K	1.4 ± 0.3	280 ± 10
D140K	1.7 ± 0.4	220 ± 10	D146K	0.43 ± 0.11	250 ± 10
D148K	1.6 ± 0.2	290 ± 10	K149D	2.9 ± 1.3	49 ± 5
D150K	2.6 ± 0.7	330 ± 20	D152K	2.3 ± 0.4	330 ± 10
D165K	2.4 ± 0.6	130 ± 6	E167K	1.6 ± 0.3	290 ± 10
E188K	2.9 ± 0.4	370 ± 5	E201K	2.9 ± 0.9	2.8 ± 0.2
E209K	2.8 ± 0.5	200 ± 10	D210K	1.9 ± 0.3	470 ± 10
E214K	2.7 ± 0.6	430 ± 20	D217K	0.84± 0.12	320 ± 10
E221K	2.1 ± 0.4	420 ± 20	D224K	3.6 ± 0.7	420 ± 20
D235K	ND[a]	<0.06±0.06	D241K	2.5 ± 0.6	32 ± 2
E250K	2.5 ± 0.4	240 ± 10	D254K	1.7 ± 0.3	540 ± 20
D256K	3.3 ± 0.6	600 ± 20	D261K	1.5 ± 0.3	370 ± 10
E267K	7.4 ± 6.6	0.3 ± 0.1	E271K	1.6 ± 0.3	280 ± 20
D279K	1.8 ± 0.3	350 ± 10	E290K	60 ± 11	140 ± 10
E291K	3.8 ± 0.4	520 ± 10			

[a] ND indicates that the parameter could not be determined.

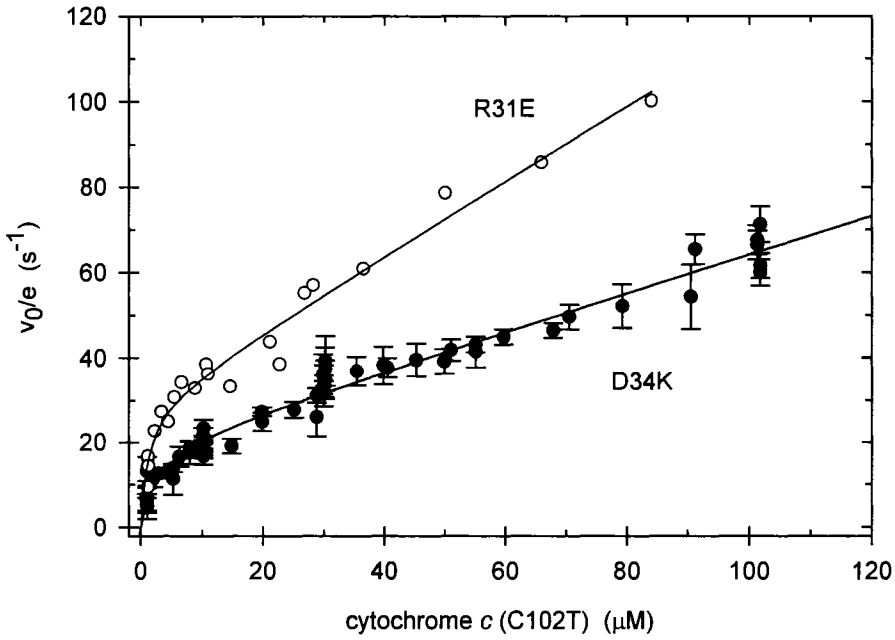

Figure 6.3. Steady-state velocity plots for two charge-reversal mutants, R31E (open circles) and D34K (filled circles). Experimental conditions: 0.100 M ionic strength potassium phosphate buffer, pH 7.5, 25 °C.

Forty-three of the forty-six purified charge-reversal mutants show simple Michaelis-Menten behavior that can be characterized by a Michaelis constant, K_M, and a maximum enzyme turnover number, V_{max}/e_0. The K_M values vary by 190-fold, from a low value of 0.43 ± 0.11 μM for D146K to a high value of 82 ± 12 μM for D37K (excluding the lower limits of 100 μM for the major phases of R31E and D34K). Surprisingly, the maximum turnover numbers have even larger variability, ranging from a low of 0.3 ± 0.1 s^{-1} for E267K to a high of 750 ± 20 for E32K, over 2200-fold (excluding the estimate for D235K of <0.06 ± 0.06 s^{-1}).

One of the unexpected findings of the steady-state studies is the very large variation in the V_{max}/e_0 values. This was not anticipated when this project began, but as the project unfolded, it became obvious that some of the charge-reversal mutants did not react with H_2O_2 as readily as did rCcP. A large part of the variability of V_{max}/e_0 can be attributed to the fraction of H_2O_2-inactive enzyme in some of the mutants, as determined in Chapter V. The correlation of V_{max}/e_0 with the fraction of inactive enzyme will be presented in the Discussion section of this chapter.

This study is most concerned with the effect of charge on the binding of cytochrome *c* as monitored by the Michaelis constants. Thirty-three of the forty-six expressed mutants have K_M values within a factor of two of that for rCcP, and these mutants are considered not to have a significant effect on the binding of cytochrome *c*. Of the remaining thirteen mutants, one, D235K, is inactive and no steady-state data are available, three have lower K_M values than rCcP, implying tighter cytochrome *c* binding, four have K_M values between two and 3.5 times larger than that of rCcP, suggesting weak perturbation of cytochrome *c* binding, and five have K_M values that are more than 24 times larger than that of rCcP, indicating significantly reduced affinity for cytochrome *c*.

The three mutants that have significantly smaller values of K_M compared to that of rCcP are D79K, D146K, and D217K with K_M values of 0.75 ± 0.35 μM, 0.43 ± 0.11 μM, and 0.84 0.12M, respectively. The D146K data is shown in Figure 6.4. It is very difficult to obtain accurate values of K_M less than about 1 μM since this is the lower limit of the ferrocytochrome *c* concentration used as the substrate to determine the initial velocities. It is not practical to go to lower substrate concentrations than ~1 μM cytochrome *c* and still measure accurate initial velocities. The maximum observed

absorbance change for the first 10% of the reaction occurs at 417 nm and is ~0.006 absorbance units. In order to obtain more accurate K_M values, these three mutants could be examined at higher ionic strengths, where the binding is weaker. Comparing the K_M values of rCcP and these three mutants at higher ionic strengths could determine whether they do, in fact, bind cytochrome *c* with greater affinity than rCcP. It is difficult to explain why an aspartate-to-lysine mutation in CcP would strengthen the binding of cytochrome *c*.

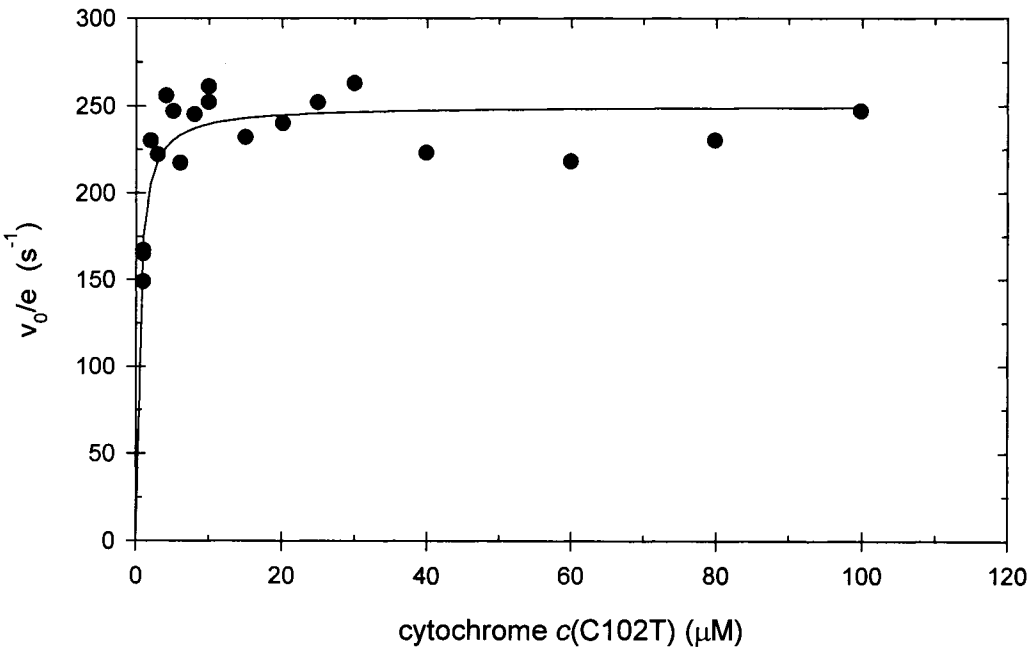

Figure 6.4. Steady-state velocity plot for D146K. The initial velocity achieves 90% of the maximum velocity below 2 μM ferrocytochrome *c*, making it difficult to determine an accurate value for K_M. Experimental conditions: 0.100 M ionic strength potassium phosphate buffer, pH 7.5, 25 °C.

Another consideration could affect the K_M value of D79K consideration. D79K is one of the mutants that did not form detectable Compound I upon addition of a stoichiometric excess of H_2O_2, Chapter V. Even though the formation of Compound I was not observed, the D79K mutant does have some catalytic activity, as shown in Figure 6.5. The V_{max}/e_0 of 38 ± 3 s^{-1} indicates that this mutant has about 6% of the activity of rCcP. Either it forms about 6% of a Compound I-like intermediate, which was not detected, perhaps because it decays too rapidly, or it forms some other type of activated H_2O_2 species that does not affect the spectrum but can oxidize ferrocytochrome *c* more rapidly than the uncatalyzed H_2O_2/ferrocytochrome *c* reaction. This is another mutant with intriguing properties and deserves further investigation.

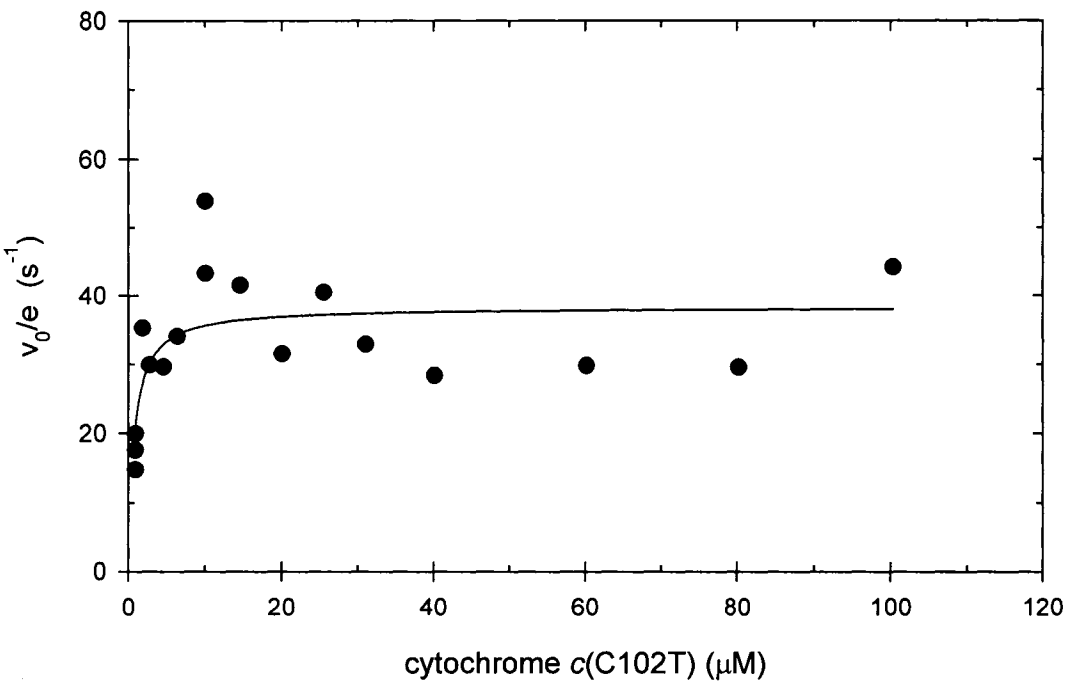

Figure 6.5. Steady-state velocity plot for D79K. The maximum velocity of this mutant is less than 6% that or rCcP. Experimental conditions: 0.100 M ionic strength potassium phosphate buffer, pH 7.5, 25 °C.

The four mutants with slightly larger K_M values than rCcP are E32K, E35K, E135K, and E267K with K_M values of 4.5 ± 0.5, 4.4 ± 0.4, 4.9 ± 1.1, and 7.4 ± 6.6, respectively, Table 6.1. E135K and E267K are similar to D79K in that they do not form significant Compound I upon addition of excess H_2O_2, Chapter V. E135K forms about 3% Compound I and E267K has no detectable Compound I formation based on the changes in absorbance at 424 nm upon addition of H_2O_2, Chapter V. In addition, the maximum turnover rate indicates that E135K is more active than estimated from the 424 nm absorbance change with the maximum turnover ~16 % that of rCcP. The K_M value of 4.9 ± 1.1 μM suggests a weak perturbation of cytochrome *c* binding by the E135K mutation.

There was no detectable formation of a Compound I-like intermediate for E267K upon addition of excess H_2O_2, Chapter V, and this mutant has the smallest detectable value of V_{max}/e_0 of any of the mutants investigated in this study, 0.34 ± 0.06 s^{-1}, Table 6.1, less than 0.06% as active as rCcP. In spite of the very low activity, steady-state data could be obtained but the error in determining K_M is quite large. The value for K_M of 7.4 ± 6.6 μM is within one standard deviation of the K_M value for rCcP and the difference between the two values may not be significant.

The K_M values for E32K and E35K are slightly greater than two times that of rCcP and these mutants are fully active, Table 6.1. Both Glu-32 and Glu-35 are close to the cytochrome *c* binding site observed in the crystal structure of the 1:1 yeast iso-1 cytochrome *c*/CcP complex (13) and it is entirely possible that these charge-reversal mutations affect cytochrome *c* binding.

Five mutants, R31E, D34K, D37K, E118K, and E290K have K_M values that are at least 24-times larger that that of rCcP and these mutants are considered to have a major effect on the binding of cytochrome c. The properties of these five mutants will be discussed in detail in the Discussion section of this chapter.

Discussion

Variation in V_{max}/e_0

It was unexpected that the charge-reversal mutants would have a large effect on the turnover number of the enzyme; however, the variation is enormous, with the observed V_{max}/e_0 varying by more than 2200-fold, from 0.34 s^{-1} for E267K to 760 s^{-1} for E35K, Table 6.1. A visual representation of the variation and distribution of V_{max}/e_0 for the charge-reversal mutants is given by a bar graph shown in Figure 6.6. Figure 6.7 shows the V_{max}/e_0 values as a function of the primary sequence position.

Part of the variation in V_{max}/e_0 is due to the presence of variable amounts of hexa-coordinated heme in these mutants. As shown in Chapter V, the hexa-coordinate, low-spin forms of CcP do not react with hydrogen peroxide, Tables 3.1, 3.2, 5.1, and 5.2 and Figures 5.6 and 5.7. Figure 6.8 shows the correlation between V_{max}/e_0 values in Table 6.1 and the estimated percent inactive enzyme from Table 5.2.

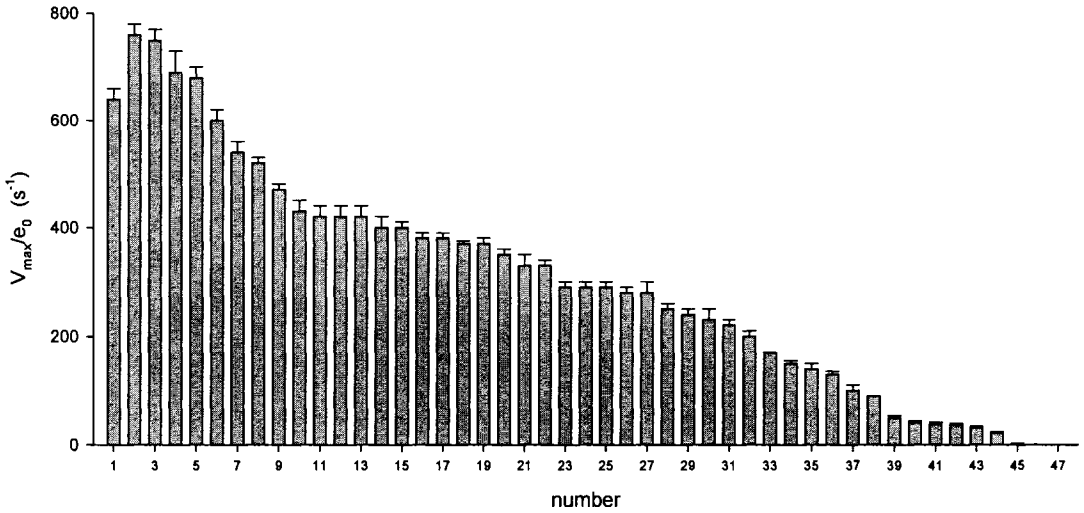

Figure 6.6. Bar graph showing the distribution of V_{max}/e_0 for rCcP and the forty-four charge-reversal mutants for which maximum velocities could be determined. The data excludes values for R31E, D34K, and D235K. The value of V_{max}/e_0 for rCcP is 640 ± 20 s^{-1} and is shown by the left-most bar. The V_{max}/e_0 values for the charge-reversal mutants follow those of rCcP and are shown in order of decreasing value, ranging from 760 ± 20 s^{-1} for E35K to 0.34 ± 0.06 s^{-1} for E267K.

In general, the maximum velocity of the mutants decreases as the percentage of inactive enzyme increases (open circles in Figure 6.8) with some significant downside outliers (filled circles in Figure 6.8). Four of the six outliers are mutations within or near Site 1 for cytochrome *c* binding, D34K, D37K, E201K, and E290K. Three of these, D34K, D37K, and E290K have very large effects upon cytochrome *c* binding, increasing K_M by more than 30-fold, and it is reasonable to assume that these mutations alter the orientation of bound cytochrome *c* such that the rate of ferrocytochrome *c* oxidation is severely inhibited, leading to lower turnover rates than predicted by the percentage of enzyme that reacts with H_2O_2. These data are consistent with the idea that oxidation of

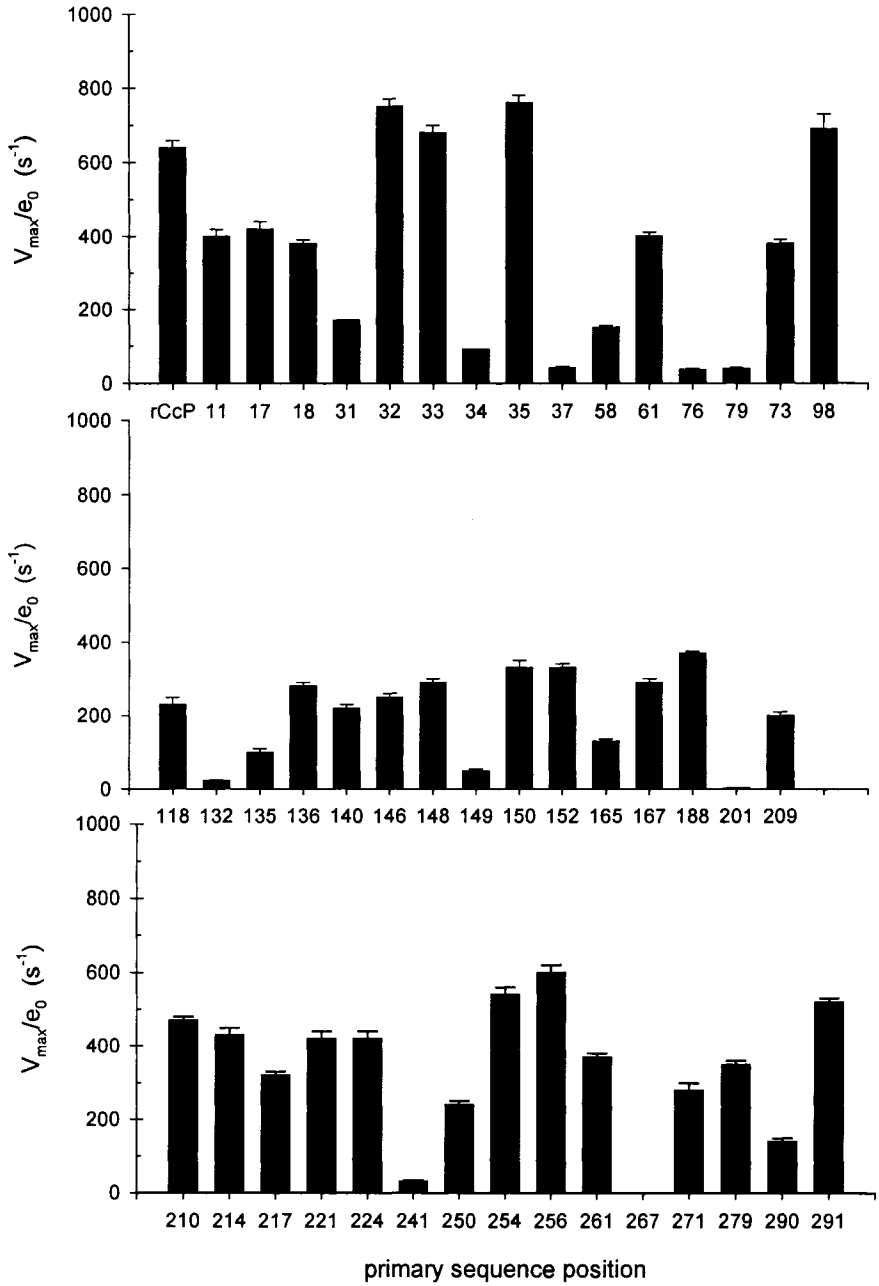

Figure 6.7. V_{max}/e_0 as a function of the primary sequence position. The V_{max}/e_0 value for rCcP is shown at the left-hand side of the top panel.

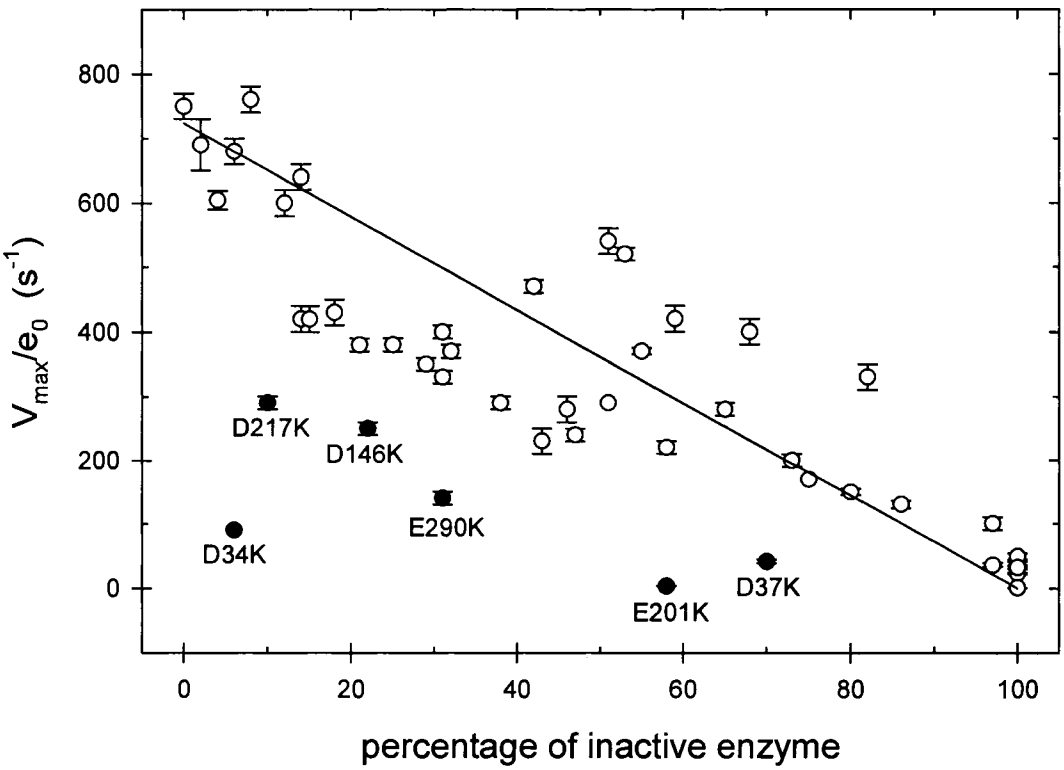

Figure 6.8. Correlation of V_{max}/e_0 with the percentage of inactive enzyme at pH 7.5. Significant outliers are labeled and shown with filled circles. The correlation line is calculated by the equation: $V_{max}/e_0 = (723\ s^{-1})$ (fraction of active enzyme).

cytochrome *c* by CcP Compound II, rather than product dissociation, is the rate-limiting process at high substrate concentrations and high ionic strength (17).

The E201K mutant has one of the largest effects on V_{max}/e_0, decreasing its value to $2.8 \pm 0.2\ s^{-1}$, less than 0.5 % of rCcP. Calculation of the percent active enzyme shows that 58% of E201K reacts with H_2O_2 to form Compound I with a rate comparable to rCcP, Table 5.2. This implies that the very low turnover number is related to the reaction with ferrocytochrome *c* and not the hydrogen peroxide reaction. E201K has a K_M value

comparable to rCcP, within experimental error, suggesting that there is no alteration in binding affinity due to mutation. This observation is consistent with the crystal structure of yeast cytochrome *c*/CcP complex (13), which identifies no significant electrostatic interaction between Glu-201 and any of the positively charged residues in bound cytochrome *c*. Nevertheless, residue Glu-201 is quite close to Ala-193 and Ala-194 on the surface of CcP, the putative entry point for electron transfer in the cytochrome *c*/ CcP complex (13). Changing the glutamate to lysine may have altered the exact orientation of the two proteins in the complex, slowing the rate of electron entry into CcP.

The other two low-side outliers identified in Figure 6.9, D146K and D217K, have about 43% of the predicted turnover number based on the percentage of inactive enzyme. There appears to be no special considerations as to why the D217K and D146K mutants have significantly lower catalytic turnover than predicted. Both are substantially penta-coordinate mutants, have low percentages of inactive enzyme, and react rapidly with H_2O_2 just as rCcP. D146K does have a very small K_M value, Table 6.1, which might contribute to the lower turnover number if product dissociation were rate limiting. The cause of the increased affinity for cytochrome *c* by D146K is not well understood since it is hard to imagine how an Asp to Lys mutation could increase the binding of a positively-charged protein like cytochrome *c*. There does not appear to be anything special about D217K except that Asp-217 was one of the residues implicated in cytochrome *c* binding by the Brownian dynamic simulations of Northrup *et al.* (18). However, D217K does not appear to affect cytochrome *c* binding, as indicated by the similarity of the K_M values for D217K and rCcP, Table 6.1. D146K and D217K may not be unique in that there is a

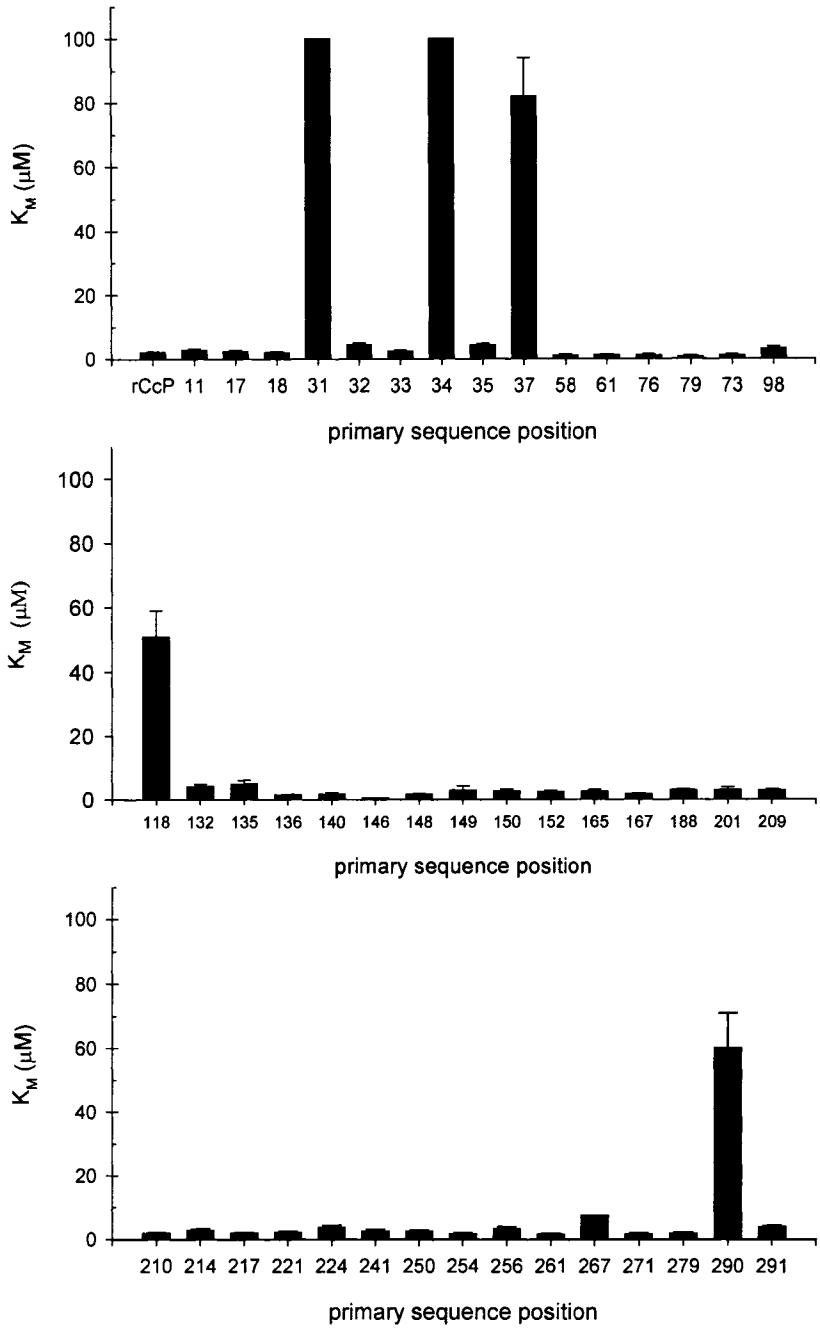

Figure 6.9. Bar graph showing K_M as a function of the primary sequence position. The K_M value for rCcP is shown at the left-hand side of the top panel. Five charge-reversal mutants significantly increase the value of K_M and these are located at primary sequence positions 31, 34, 37, 118, and 290.

large group of mutants that cluster just below the correlation line shown in Figure 6.8. The bias in the plot shown in Figure 6.9 is toward lower maximum turnover than predicted for the estimated amount of H_2O_2-inactive enzyme. This could mean that the rate-limiting step (or steps) at saturating concentrations of cytochrome *c* are affected by the charge-reversal mutations. The current hypothesis for the rate-limiting steps in the CcP mechanism is that either product dissociation or oxidation of the Fe(IV) site in CcP-Compound II, or both, contribute to the rate-limiting turnover of the enzyme (19). Since these charge-reversal mutations should weaken cytochrome *c* binding and increase the rate of product dissociation, the most likely cause of lower turnover is that the rate of oxidation of the Fe(IV) site is lower in most of the charge-reversal mutations.

Five mutants appear to have slightly higher than predicted turnover rates based on the estimated percentage of H_2O_2-inactive enzyme and these appear above the correlation line in Figure 6.8. Again, there is no obvious reason why these mutants should be more active than predicted by the amount of active enzyme except to conclude that there are other factors that affect the turnover rate and these factors have to affect the rate-limiting step or steps in the catalytic mechanism.

Variation in K_M for the Charge-Reversal Mutants

In this study, the Michaelis constants have been used to assess the effects of charge-reversal mutations on the surface of CcP on the interaction of rCcP with yeast iso-1 cytochrome *c* (C102T). The Michaelis constant for the rCcP/yeast iso-1 cytochrome *c* (C102T) reaction is 2.1 ± 0.2 μM under the conditions of these experiments, Table 6.1.

The variation in K_M can be visualized in the bar graph shown in Figure 6.9. Thirty-nine of the forty-five mutants for which K_M values could be determined, have K_M values that are within a factor of two of that of rCcP and these mutations are considered to have no significant effect on cytochrome *c* binding. Two mutants, D79K and D146K, have K_M values that are smaller than that of rCcP, Table 6.1 and Figures 6.4 and 6.5. As presented in the results section, there is no obvious reason why converting a negatively charged aspartate residue to a positively charged lysine residue should enhance the binding of the positively charged cytochrome *c*, and thus the cause of this apparent stronger binding is unknown.

Five of the forty-five mutants have very large K_M values, Figure 6.9. R31E, D34K, D37K, E118K, and E290K, have K_M values that are >24 times larger than that of wild-type rCcP, which indicate low affinity of these mutants for the binding of cytochrome *c*. Among these residues, Arg-31, Asp-37 and Glu-118 are highly conserved and Asp-34 and Glu-290 are moderately conserved. All these mutants, with the exception of Asp-37, are on the front face of CcP near the binding site identified in the crystal structure of the 1:1 complexes, Site 1, Figure 6.10. Asp-37 is on the left-hand face of CcP but near the high-affinity cytochrome *c* binding site, Figure 6.11.

Effect of D34K and E290K on binding The large increase in K_M for both D34K and E290K, Table 6.1, is consistent with the crystal structure of the 1:1 yeast iso-1 cytochrome *c*/ CcP complex, Figure 6.10, determined by Pelletier and Kraut (13), which shows potential interactions between Asp-34 and Glu-290 on CcP with Lys-87 and Lys-73 on cytochrome *c*, respectively. Previous studies have also shown that charge-

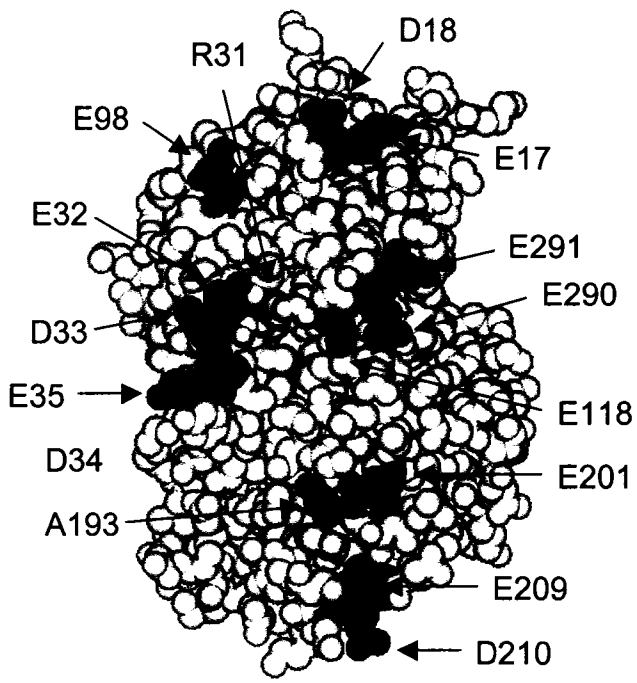

Figure 6.10. Front-face of CcP. Residues in black (Glu-32, Ala-193, and Glu-290) define Site 1, the crystallographically-identified cytochrome *c* binding site (12). Note that Glu-32 and Glu-290 were individually mutated to lysine residues as part of this study. Other negative-to-positive charge reversal mutation sites are shown in blue, either aspartate (D) or glutamate (E) to lysine mutations. The R31E mutation site is shown in yellow.

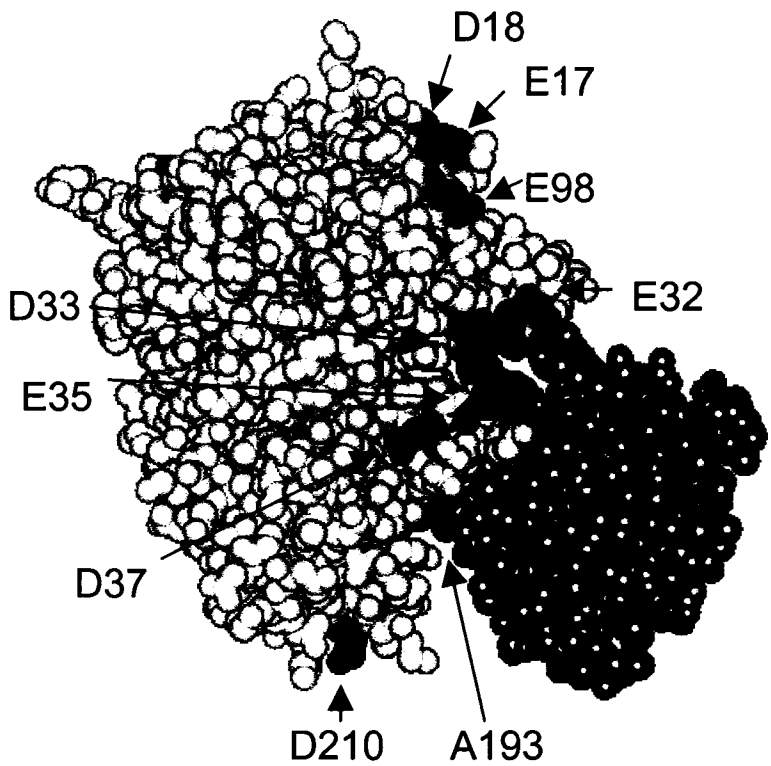

Figure 6.11. Space-filling model of the yeast cytochrome *c*/CcP complex (10). The orientation of the complex is the same as that shown in Figure 6.10 except that it is rotated 90° counter clockwise about a vertical axis. This rotation shows the left-hand face of CcP and the bound cytochrome *c*. The color scheme for CcP is the same as in Figure 6.10. Cytochrome *c* is shown in orange. Asp-32 and Ala-193 are observed in this view and are two of the three residues used to define the cytochrome *c* binding site.

neutralization or charge-reversal mutations at positions 34 and 290 decrease the affinity for binding cytochrome *c*. Steady-state kinetic studies with D34N and E290N mutants show 4- to 18-fold increases in the K_M values for yeast iso-1 ferrocytochrome *c*, depending upon ionic strength (8), while calorimetry studies with these same mutants find a 4-fold decrease in binding affinity for horse cytochrome *c* for both mutants in 50 mM ionic strength buffers, pH 6.0 (20). Photoinitiated electron transfer kinetic studies between E290K and zinc-substituted horse cytochrome *c* indicate that the affinity for horse cytochrome *c* is reduced 20-fold in 18 mM ionic strength buffer, pH 7.0 (21). All these data are consistent with the involvement of both D34 and E290 in binding cytochrome *c* to form the 1:1 complex.

Effect of E118K on Binding The E118K mutation increased K_M for yeast cytochrome *c* by a factor of 24, Table 6.1. E118K is not in direct contact with the bound cytochrome, Figure 6.10, but located near Glu-290 on the surface of CcP between the two protein molecules. Reduction of E118K affinity for cytochrome *c* may be due to the reorientation of the side-chain of residue 118. The carboxylate side-chain of Glu-118 is partially buried with one of the carboxylate oxygens hydrogen bonded to the peptide nitrogen of Leu-289 in the interior of CcP (13). Mutation of Glu-118 to lysine will disrupt the hydrogen bonding to Leu-289 and most likely cause the positively charged lysine side-chain to rotate toward the surface of CcP, which would increase the electrostatic repulsion between CcP and cytochrome *c* weakening the binding as observed. In addition, Glu-118 is highly conserved and may be important for the

structural integrity of the enzyme near the binding interface. No other research group has done mutagenic studies on this residue. This is the first report that indicates that Glu-118, a well-conserved residue near the binding interface, is important for the binding affinity of the enzyme.

Effect of D37K on Binding Previous studies have shown that the D37K mutation decreases the affinity for both horse and yeast cytochrome *c*, with decreases ranging from 5- to 67-fold depending upon experimental conditions (22-24). Current data are consistent with the published literature, showing that the D37K mutant has approximately 40-fold decrease in affinity for yeast cytochrome *c* at pH 7.5, 100 mM ionic strength. However, D37 is not involved in binding cytochrome *c* in the crystal structures of the horse and yeast cytochrome *c*/ CcP complexes (13). The considerations that must be taken into account are the effects of localized charge reversal mutations. D34K causes a 48-fold decrease in cytochrome *c* affinity while mutations at both adjacent residues, D33K and E35K, have almost no effect, Table 6.1. This is also seen with E290K and E291K. The former mutation causes a 30-fold decrease in binding affinity while the latter has essentially no effect because the carboxylate group of Glu-291 points away from the binding site. Assuming that D37K mutation causes a localized effect on cytochrome *c* binding, then these data strongly suggest that cytochrome *c* can bind in a different orientation from that shown in the crystal structure of the 1:1 complex, one that involves direct interaction between Asp-37 and a positively charged residue on cytochrome *c*. Alternatively, Asp-37 could be part of a second binding site that is adjacent to and/or overlaps the crystallographic site, as suggested by Nocek *et al.* (25).

Nocek et al. suggest that the second binding site is essentially that first proposed by Poulos and Kraut (26) involving residues Asp-34, Asp-37, Asp-79, Gln-86, Asn-87 and Asp-217. Asp-37 is at the boundary between the crystallographic site and the Poulos/Kraut site and could affect cytochrome *c* binding at both. The data of Corin *et al.* (22, 23), however, would seem to eliminate Asp-79 and Asp-217 from the second site.

A recent NMR study (27) of the CcP/yeast iso-1 cytochrome *c* complex demonstrates that the bound cytochrome *c* has considerable mobility, but generally corroborates the crystallographic structure, indicating that cytochrome *c* resides at the crystallographic site about 70% of the time and in much more dynamic encounter complexes about 30% of the time. The encounter complexes encompass much of the CcP surface, as first postulated by Northrup *et al.* in their computer simulation study (18). Using covalently attached paramagnetic spin labels, Volkov *et al.* (27) show that encounter complexes exist near residues 38, 200, and 288 on the surface of CcP but not at residues 137 and 263. The spin-label probe at residue 38 should detect cytochrome *c* binding near Asp-37.

There is also the possibility that the D37K mutation decreases the affinity of cytochrome *c* by altering the surface conformation of CcP. The carboxylate side-chain of Asp-37 is rotated toward the interior of CcP, with one of the carboxylate oxygen atoms hydrogen bonding to a nitrogen in the imidazole ring of His-181 (28). His-181 is part of the hydrogen-bonding network that connects residues in the distal heme pocket with those in the proximal heme pocket (29). Disruption of the hydrogen-bonding network by the lysine for aspartate substitution could account for the increased concentration of hexa-coordinate heme in this mutant, Table 3.2, and perhaps for an altered surface formation of

the cytochrome *c* binding site. It is likely that the lysine-for-aspartate substitution would rotate the lysine side-chain toward the surface of CcP, bringing it closer to cytochrome *c* bound at the crystallographic site, increasing the electrostatic repulsion of bound cytochrome *c*, and decreasing the affinity at the crystallographic site.

D37 is a highly conserved residue and the study by Corin *et al.* (22) has shown that D37K affects cytochrome *c* binding. D37 forms a charge-mediated hydrogen bond with the imidazole side chain of H181 and stabilizes the native conformation of the enzyme (29). D37K replacement will result in repulsion between the ε-amino group of lysine and the imidazole of H181. Therefore, decreased affinity due to the Lys-37 mutation may represent binding region perturbation by a more global effect on enzyme structure (20).

Effect of R31E on Binding The fifth mutation with a large effect on the Michaelis constant is the R31E mutation. Arg-31 is a positively charged residue that precedes the string of negatively charged residues, Glu-32 through Asp-37. Arg-31 was mutated to glutamate in anticipation that it might increase the affinity of CcP for cytochrome *c*. Surprisingly, it was found that R31E mutation had a profound effect on the steady-state kinetics, generating a biphasic Michaelis-Menten plot, Figure 6.3, with the major phase having a K_M value so large that only a lower limit of 100 μM could be established. The steady-state data suggests that the R31E mutation decreases the binding affinity for cytochrome *c* by more than a factor of 50. This is difficult to understand based on simple electrostatic considerations and something more profound may be occurring, such as the R31E mutation causing a change in the tertiary structure of CcP.

Van der Waals interactions between CcP and yeast cytochrome *c* include R31 (13), a fairly well conserved residue, and therefore changing Arg-31 to Glu-31 might have contributed to the decreased affinity of the enzyme.

References

1. Erman, J. E., and Vitello, L. B. (2002) Yeast cytochrome *c* peroxidase: mechanistic studies via protein engineering, *Biochim. Biophys. Acta 1597*, 193-220.

2. Yonetani, T., and Ray, G. S. (1966) Studies on cytochrome *c* peroxidase: III. Kinetics of the peroxidatic oxidation of ferrocytochrome *c* catalyzed by cytochrome *c* peroxidase, *J. Biol. Chem. 241*, 700-706.

3. Nicholls, P., and Mochan, E. (1971) Complex-formation between cytochrome *c* and cytochrome *c* peroxidase: Kinetic studies, *Biochem. J. 121*, 55-67.

4. Kang, C. H., Ferguson-Miller, S., and Margoliash, E. (1977) Steady-state kinetics and binding of eukaryotic cytochromes *c* with yeast cytochrome *c* peroxidase, *J. Biol. Chem. 252*, 919-926.

5. Kang, D. S., and Erman, J. E. (1982) The cytochrome *c* peroxidase-catalyzed oxidation of ferrocytochrome *c* by hydrogen peroxide: Steady state kinetic mechanism, *J. Biol. Chem. 257*, 12775-12779.

6. Kim, K. L., Kang, D. S., Vitello, L. B. and Erman, J. E. (1990) Cytochrome *c* peroxidase catalyzed oxidation of ferrocytochrome *c* by hydrogen peroxide: Ionic strength dependence of the steady-state rate parameters, *Biochemistry 29*, 9150-9159.

7. Matthis, A. L., and Erman, J. E. (1995) Cytochrome *c* peroxidase-catalyzed oxidation of yeast iso-1 ferrocytochrome *c* by hydrogen peroxide. Ionic strength dependence of the steady-state parameters, *Biochemistry 34*, 9985-9990.

8. Miller, M. A., (1996) A complete mechanism for steady-state oxidation of yeast cytochrome *c* by yeast cytochrome *c* peroxidase, *Biochemistry 35*, 15791-15799.

9. Nakani, S., Viriyakul, T., Mitchell, R., Vitello, L. B., and Erman, J. E. (2006) Characterization of a covalently-linked yeast cytochrome *c*-cytochrome *c* peroxidase complex: Evidence for a single, catalytically-active cytochrome *c* binding site on cytochrome *c* peroxidase, *Biochemistry 45,* 9887-9893.

10. Mauk, M. R., Ferrer, J. C., and Mauk, A. G. (1994) Proton linkage in formation of the cytochrome *c*-cytochrome *c* peroxidase complex: Electrostatic properties of the high- and low-affinity cytochrome *c* binding sites on the peroxidase, *Biochemistry 33*, 12609-12614.

11. Wang, X., and Pielak, G. J. (1999) Equilibrium thermodynamics of a physiologically-relevant heme-protein complex, *Biochemistry 38*, 16876-16881.

12. Morar, A. S., Wang, X., and Pielak, G. J. (2001) Effects of crowding by mono-, di-, and tetrasaccharides on cytochrome *c* peroxidase binding: Comparing experiment to theory, *Biochemistry 40*, 281-285.

13. Pelletier, H., and Kraut, J. (1992) Crystal structure of a complex between electron transfer partners, cytochrome *c* peroxidase and cytochrome *c*, *Science 258*, 1748-1755.

14. Kolthoff, I. M., and Belcher, R. (1957) Hydrogen peroxide, in *Volumetric Analysis*, Vol. 3, pp 75-76, Interscience, New York.

15. Morar, A. S., Kakouras, D., Young, G. B., Boyd, J., and Pielak, G. J. (1999) Expression of ^{15}N-labeled eukaryotic cytochrome *c* in *Escherichia coli*, *J. Biol. Inorg. Chem. 4*, 220-222.

16. Pollock, W. B. R., Rosell, F. I., Twichett, M. B., Dumont, M. E., and Mauk, A. G. (1998) Bacterial expression of a mitochondrial cytochrome *c*. Trimethylation of Lys72 in yeast iso-1-cytochrome *c* and the alkaline conformational transition, *Biochemistry 37*, 6124-6131.

17. Wang, K., Mei, H., Geren, L., Miller, M. A., Saunders, A., Wang, X., Waldner, J. L., Pielak, G. J., Durham, B., and Millett, F. (1996) Design of a ruthenium-cytochrome *c* derivative to measure electron transfer to the radical cation and oxyferryl heme in cytochrome *c* peroxidase, *Biochemistry 35*, 15107-15119.

18. Northrup, S. H., Boles, J. O., and Reynolds, J. C. L. (1988) Brownian dynamics of cytochrome *c* and cytochrome *c* peroxidase association, *Science 241*, 67-70.

19. Mei, H., Wang, K., McKee, S., Wang, X., Waldner, J. L., Pielak, G. J., Durham, B., and Millett, F. (1996) Control of formation and dissociation of the high affinity complex between cytochrome *c* and cytochrome *c* peroxidase by ionic strength and the low affinity binding site. *Biochemistry 35,* 15800-15806.

20. Erman, J. E., Kresheck, G. C., Vitello, L. B., and Miller, M. A, (1997) Cytochrome *c*/cytochrome *c* peroxidase complex: Effect of binding-site mutations on the thermodynamics of complex formation, *Biochemistry 36*, 4054-4060.

21. Leesch, V. W., Bujons, J., Mauk, A. G., and Hoffman, B. M. (2000) Cytochrome *c* peroxidase-cytochrome *c* complex: locating the second binding domain on cytochrome *c* peroxidase with site-directed mutagenesis, *Biochemistry 39*, 10132-10139.

22. Corin, A. F., McLendon, G., Zhang, Q., Hake, R. A., Falvo, J., Lu, K. S., Ciccarelli, R. B., and Holzschu, D. (1991) Effects of surface amino acid replacements in cytochrome *c* peroxidase on complex formation with cytochrome *c*, *Biochemistry 30*, 11585-11595.

23. Corin A. F., Hake, R. A., McLendon, G., Hazzard, J. T., and Tollin, G. (1993) Effects of surface amino acid replacements in cytochrome *c* peroxidase on intracomplex electron transfer from cytochrome *c*, *Biochemistry 32*, 2756-2762.

24. Zhou, J. S., Tran, S. T., McLendon, G., and Hoffman, B. M. (1997) Photoinduced electron transfer between cytochrome *c* peroxidase (D37K) and Zn-substituted cytochrome *c*: probing the two-domain binding and reactivity of the peroxidase, *J. Amer. Chem. Soc. 119*, 269-277.

25. Nocek, J. M., Zhou, J. S., De Forest, S., Priyadarshi, S., Beratan, D. N., Onuchic, J. N., and Hoffman, B. M. (1996) Theory and practice of electron transfer within protein-protein complexes: application to the multidomain binding of cytochrome *c* by cytochrome *c* peroxidase, *Chem. Rev. 96*, 2459-2489.

26. Poulos, T. L., and Kraut, J. (1980) A hypothetical model of the cytochrome *c* peroxidase · cytochrome *c* electron transfer complex, *J. Biol. Chem. 255*, 10322-10330.

27. Volkov, A. N., Worrall, J. A. R., Holtzmann, E., and Ubbink, M. (2006) Solution structure and dynamics of the complex between cytochrome *c* and cytochrome *c* peroxidase determined by paramagnetic NMR, *Proc. Nat'l. Acad. Sci. USA 103*, 18945-18950.

28. Finzel, B. C., Poulos, T. L., and Kraut, J. (1984) Crystal structure of yeast cytochrome *c* peroxidase refined at 1.7-Å resolution, *J. Biol. Chem. 259*, 13027-13036.

29. Miller, M. A., Hazzard, J. T., Mauro, J. M., Edwards, S. L., Simons, P. C., Tollin, G., and Kraut, J. (1988) Site-directed mutagenesis of yeast cytochrome *c* peroxidase shows histidine 181 is not required for oxidation of ferrocytochrome *c*, *Biochemistry 27*, 9081-9088.

CHAPTER VII

GENERAL DISCUSSION AND CONCLUSION

The primary objective of this dissertation is to make a significant contribution to a detailed understanding of the interaction between yeast iso-1 cytochrome *c* and cytochrome *c* peroxidase. The interaction between these two heme proteins is electrostatic in nature with strong attraction between the positively-charged cytochrome *c* molecule and the negatively-charge peroxidase. The binding is strongly dependent upon ionic strength with 2:1 cytochrome *c*/CcP complexes observed at low ionic strength but only 1:1 complexes observed at ionic strengths of 0.1 M and above (1). With this in mind, it was decided to modulate the binding of cytochrome *c* by mutating the negatively-charged amino acid residues on the surface of CcP, one at a time, to positively-charged lysine residues. It was hypothesized that mutations near the cytochrome *c* binding sites on the surface of CcP would strongly perturb the binding while mutations distant from the binding sites would have only minor effects, allowing for the localization of binding sites. Five specific goals were established for this research project.

1. Construct a library of charge-reversal mutants of CcP in which each of the aspartate and glutamate residues in CcP are individually converted to lysine residues.

2. Characterize each of the charge-reversal mutants with respect to their expression, purification, and electronic absorption spectrum.
3. Determine the hydrogen peroxide reactivity of each of the charge-reversal mutants.
4. Determine the steady-state kinetic parameters for the catalytic oxidation of yeast iso-1 ferrocytochrome *c* by hydrogen peroxide for each of the mutants.
5. Map the interaction site, or sites, for formation of the 1:1 cytochrome *c*/CcP complex using the Michaelis constants from the steady-state catalysis studies.

This chapter comprises a general discussion on how the experiments were carried out to achieve the main objectives of the project and the conclusions based on the experimental data.

Construction of the Single Site Charge-Reversal Mutants

CcP contains 25 aspartate residues and 20 glutamate residues. Forty-two of these carboxylate residues are on the surface of CcP, while three are internal residues. For completeness, it was decided to mutate all forty-five carboxylate residues to lysine residues and to characterize both the surface and the internal residues. For reasons discussed in Chapter II, it was also decided to make two positive-to-negative charge reversal mutations in CcP by constructing R31E and K149D. Plasmids containing the mutant CcP genes for all forty-seven charge-reversal mutants were successfully constructed by site-directed mutagenesis and sequenced to confirm their authenticity.

The plasmids were successfully transformed into *E. coli.* for expression of the proteins and a library of forty-seven charge-reversal mutants of CcP is now available for this project as well as for future projects.

Characterization of Charge-Reversal Mutants

The second goal of this project was to characterize each mutant with respect to expression, purification, and electronic absorption spectrum. Each of the forty-seven transformed *E. coli* cell lines grew well, and under the experimental conditions for cell growth, produced between 7 and 15 g of wet cells per liter of culture. However, upon purification it was discovered that only forty-six cell lines produced detectable quantities of purified enzyme. Cells containing the plasmid for D106K failed to give detectable enzyme. D106K is one of the three internal residues and it is thought that the Asp to Lys mutation disrupts the folding, leading to degradation of the protein during cell growth.

The electronic absorption spectrum is an essential tool for characterization of heme proteins. The UV-visible absorption spectrum for each of the forty-six purified CcP mutants was determined at both pH 6.0 and 7.5 in order to monitor potential changes in the spectrum as a function of pH. The ratio of absorbance at the Soret maximum to the maximum absorption near 280nm is referred to as the purity index or RZ value. It monitors the ratio of the heme absorption to the absorption of the aromatic amino acids in the polypeptide chain. The RZ value for forty-two of the forty-six CcP mutants is similar to that of wild-type recombinant CcP, suggesting that the purity of these preparations is similar. The four exceptions were E11K, E118K, and E201K with low RZ values and

E267K with a high RZ value compared to rCcP, Figure 3.4. The low RZ value is due to incomplete incorporation of heme into the apoprotein of E11K, E118K, and E201K during the purification process. The incomplete heme incorporation is not a problem since all of the remaining properties of these mutants are determined based on the heme absorbance of the holoenzyme and the apoproteins should not interfere with these measurements. The high RZ value for E267K is attributed to a change in heme ligation in this mutant which increases the extinction coefficient at the Soret maximum.

One of the unexpected findings of this research project is that the charge-reversal mutations on the surface of CcP can alter heme ligation in the interior of the protein. The ratio of absorbance at the Soret maximum to that at 380 nm can be used to monitor changes between penta- and hexa-coordinate heme groups. Wild-type rCcP is mainly penta-coordinate at both pH 6.0 and 7.5 with a slight increase in hexa-coordinate forms at pH 7.5. The spectra of four mutants, namely D37K, K149D, D241K, and E267K, show the greatest deviation from the spectrum of rCcP WT at pH6.0, Figure 3.8, and this is attributed to increased amounts of hexa-coordinate forms in these four mutants. At pH 7.5, the A_{Soret}/A_{380} ratio indicates that most of the mutants have some hexa-coordinate heme forms and that the fraction of hexa-coordinate forms is quite variable among the charge-reversal mutants, Figure 3.9.

A mechanism to explain the variable changes in heme ligation in the charge-reversal mutants relative to rCcP was postulated in Chapter III. The most likely sixth heme ligand in CcP and the charge-reversal mutants is the negatively-charged hydroxide ion. A pH dependent equilibrium exists between penta-coordinated CcP and hydroxy-ligated CcP, both in rCcP and in the mutants. Changing the net charge on the surface of

the enzyme perturbs the equilibrium between penta-coordinate heme and hydroxy-ligated heme. For the negative-to-positive mutations, the hydroxy-heme is stabilized relative to the penta-coordinated heme and a greater fraction of hexa-coordinated hydroxy-CcP exists in the charge-reversal mutants in comparison to rCcP at comparable values of pH.

It has not been definitively shown that the sixth ligand is in fact the hydroxide ion. Other potential ligands include a water molecule and a protein-based amino acid residue such as the distal histidine, His-52. Future work could investigate the pH and temperature-dependent changes in the spectrum in of the charge-reversal mutants in order to deconvolute the spectra to determine if multiple hexa-coordinate species exist. In addition, the apparent pK_A for the conversion of the penta- to hexa-coordinate species can be determined as well as the rates of binding and dissociation of the sixth ligand. Dissociation of the hydroxide ion or the distal histidine from the heme iron can have a profound effect upon the reactivity of the heme

Determination of Secondary Structure Changes by Circular Dichroism

With the observation that the charge-reversal mutations could cause a change in heme ligation in CcP and that a potential sixth ligand to the heme could be an amino acid residue such as the distal histidine, an obvious question was whether the change in heme ligation was associated with a change in the secondary structure of the protein. In order to determine if the change in heme ligation is associated with changes in secondary structure, the CD spectra of selected charge reversal mutants were determined. Two

mutants that had UV-visible spectra similar to rCcP, D34K and E290K, were chosen as representative of the penta-coordinate CcP mutants and two mutants that had A_{Soret}/A_{380} values greater than 2.0 at pH 6.0, D37K and K149D, were chosen as representatives of the dominantly hexa-coordinate CcP mutants, Table 4.1. CD spectra were determined at pH 6.0, the middle of the pH stability region for CcP, and the spectra of all four mutants were within experimental error of the CD spectrum for rCcP, Figure 4.1. The conclusion is that there is no significant change in secondary structure between the CcP mutants having predominantly penta-coordinate heme groups and those having predominantly hexa-coordinate heme groups. CcP is a very robust protein and, to date, no single-site mutant for which crystallographic data are available has shown significant alteration in the secondary structure of the protein.

Determination of Hydrogen Peroxide Reactivity

It has previously been noted that formation of hexa-coordinate CcP at alkaline pH is associated with loss of reactivity toward hydrogen peroxide. In order to determine whether or not the hexa-coordinate heme forms in the CcP charge-reversal mutants affected the hydrogen peroxide reactivity, the spectrum of each mutant was determined in the presence and absence of a slight stoichiometric excess of hydrogen peroxide. It was expected that if the charge-reversal mutants reacted completely with hydrogen peroxide, the spectrum in the presence of hydrogen peroxide would be identical to that of yCcP compound I. Some mutants did react completely with hydrogen peroxide to form an intermediate with a Compound I-like spectrum, Figure 5.1, while other mutants did not

react with hydrogen peroxide at all, Figure 5.2. The fraction of H_2O_2-reactive enzyme for each mutant was estimated by calculating the fractional change of the spectrum to that of yCcP Compound I, specifically using the absorbance data at 424 nm, the wavelength of maximum absorbance change for the reaction between yCcP and hydrogen peroxide.

Only four mutants reacted completely with hydrogen peroxide at pH 6.0, E32K, D33K, E35K, and E98K, while only E32K reacted completely with hydrogen peroxide at pH 7.5. The percent conversion to a Compound I-like intermediate ranged from 0 to 100% at both pH 6.0 and 7.5 with the average conversion 67% at pH 6.0, Figure 5.3, and 49% at pH 7.5, Figure 5.4. There is a reasonable but not a perfect correlation between the estimated fraction of H_2O_2-reactive enzyme and the amount of hexa-coordinate enzyme forms as monitored by the A_{Soret}/A_{380} value, Figures 5.8 and 5.9.

In addition to determining the fraction of each mutant that reacted with hydrogen peroxide to form a Compound I-like intermediate, the rate of the reaction with hydrogen peroxide was also determined. The reaction of CcP with hydrogen peroxide is very fast and a stopped-flow instrument is used to measure the rate of reaction. The reaction is monitored at 424nm, the maximum difference in absorbance between the enzyme and Compound I. In many instances, the reaction with hydrogen peroxide is biphasic and the results are fitted to a one or two exponential equation to obtain the observed rate constants, k^{obs}, using the software provided with the stopped-flow instrument.

A plot of k^{obs} as a function of hydrogen peroxide concentration can distinguish whether the reaction is bimolecular or unimolecular. The reaction of rCcP with hydrogen peroxide is biphasic and the rate constant for both the fast and slow phases are dependent

on hydrogen peroxide concentration, giving two bimolecular rate constants. On the other hand, the reaction of mutant enzymes with hydrogen peroxide can be divided into five groups: (1) mutants with biphasic kinetics and both phases dependent on hydrogen peroxide concentration, (2) mutants with biphasic kinetics with the slow phase independent of hydrogen peroxide concentration, (3) mutants with monophasic kinetic with the rate constant similar to the fast phase reaction rate, (4) mutants with monophasic kinetic with the rate constant similar to that of the slow phase, and (5) mutants for which the reaction with hydrogen peroxide cannot be detected during time limit of the experiment.

The slow phase of the hydrogen peroxide/enzyme reaction is most likely due to the presence of hexa-coordinate forms. Whether the slow phase of the hydrogen peroxide reaction is bimolecular or unimolecular may be associated with the rate of dissociation of the sixth ligand. If the ligand is easily displaced by hydrogen peroxide, the slow phase may be dependent upon the hydrogen peroxide concentration giving an apparent bimolecular reaction phase. On the other hand, if the ligand is difficult to displace, the slow phase of the reaction may be determined by the rate of ligand dissociation and will give an apparent unimolecular reaction. The wide variety of observed behavior for the slow phase of the hydrogen peroxide reaction for the charge-reversal mutants provides an opportunity to investigate this aspect of the hydrogen peroxide reactivity in greater detail in future studies.

Steady-State Kinetic Studies

The steady-state kinetic properties for the enzyme-catalyzed oxidation of yeast iso-1 ferrocytochrome *c*(C102T) by hydrogen peroxide were determined for rCcP and the forty-six CcP charge-reversal mutants at 0.10 M ionic strength, pH 7.5. An ionic strength of 0.10 M was used such that 2:1 complex formation between cytochrome *c* and CcP would be negligible. Steady-state velocity plots as a function of the cytochrome *c* concentration followed simple Michaelis-Menten kinetics for forty-three of the forty-six mutants. Two mutants, R31E and D34K, had biphasic kinetic behavior, and one mutant, D235K, was completely inactive. Asp-235 is an internal residue which hydrogen bonds to the proximal histidine, His 175, and to the proximal tryptophan, Trp-191, Figure 1.3 and is a critical residue for catalytic activity. The maximum turnover numbers for the CcP mutants, V_{max}/e_0, vary from a low value of 0.3 ± 0.1 s^{-1} for E267K to a high of 750 ± 20 for E32K, over 2200-fold. The K_M values vary 190-fold, from 0.43 ± 0.11 μM for D146K to 82 ± 12 μM for D37K (excluding the lower limits of 100 μM for the major phases of R31E and D34K).

The variation of V_{max}/e_0 correlates reasonably well with the fraction of H_2O_2-reactive enzyme, Figure 6.8, except for four mutants with mutations in or near Site 1 for cytochrome *c* binding, D34K, D37K, E201K, and E290K, and two additional mutants, D146K and D217K.

This study is most concerned with the effect of charge on the binding of cytochrome *c* as monitored by the Michaelis constants. Forty of the forty-six expressed mutants have K_M values within a factor of five of that for rCcP and these mutants are

considered not to have a significant effect on the binding of cytochrome *c*, Figure 6.9. Of the remaining six mutants, one, D235K, is inactive and no steady-state data are available, and the other five have K_M values that are more than 24 times larger than that of rCcP, indicating significantly reduced affinity for cytochrome *c*, R31E, D34K, D37K, E118K, and E290K. These latter residues map the CcP surface important for 1:1 cytochrome *c*/CcP complex formation.

Mapping the Sites for 1:1 Complex Formation

The steady-state kinetics for oxidation of yeast iso-1 ferrocytochrome *c* by hydrogen peroxide as catalyzed by rCcP and the forty-six charge reversal mutants constructed for this study are affected by formation of the 1:1 complex between enzyme and cytochrome *c*. Most of the mutations have little effect on the Michaelis constant and the sites of these mutations are not involved in binding of cytochrome *c*. Five mutations have been identified as significantly decreasing the affinity of CcP for cytochrome *c* and these are R31E, D34K, D37K, E118K, and E290K. These residues are shown in Figure 7.1 in relation to Site 1, the cytochrome *c* binding sited identified by x-ray crystallography (2).

Four of the mutations occur along the upper perimeter of Site 1, R31E, D34K, E118K, and E290K, Figure 7.1. The view of CcP shown in Figure 7.1 is a 30° counter-clockwise rotation about a vertical axis from the view shown as the front-face of CcP in Figures 1.8 and 2.1. This view simultaneously shows the positions of both Asp-37 and Glu-290. The D37K mutation significantly weakens the binding of cytochrome *c* but is

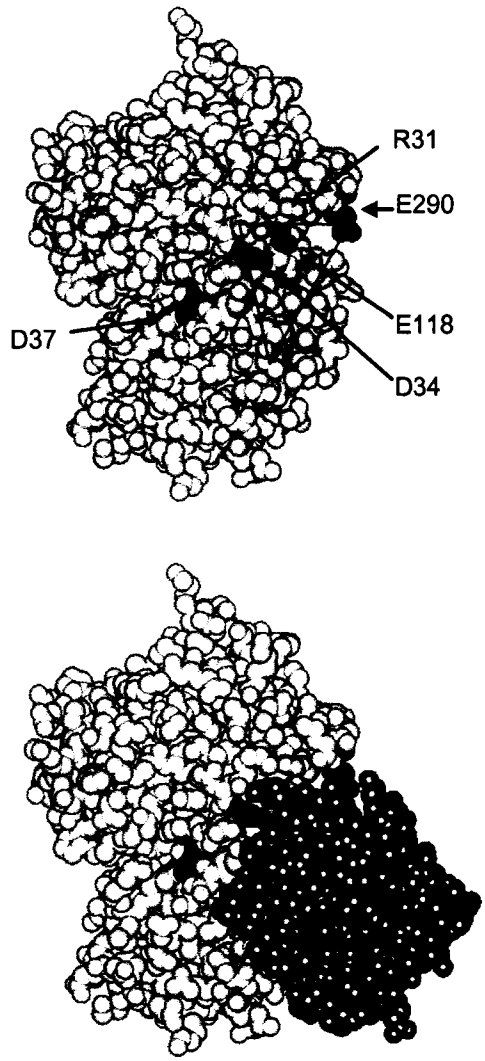

Figure 7.1. Location of binding site. Top Panel – Space-filing model of CcP showing the location of the mutation sites that strongly affect the binding of cytochrome *c*. This orientation of CcP is rotated 30° in a counter-clockwise direction about a vertical axis compared to the front-face of CcP shown in Figure 2.1. The negative-to-positive mutation sites (D34, D37, E118, and E290) are shown in blue and the positive-to-negative mutation site (R31) is shown in yellow. Site 1 is represented by the triangle with the vertices of the triangle located at residues E32, A193, and E290. Bottom Panel – Same orientation as the top panel with yeast iso-1 cytochrome *c* (red) bound to Site 1. Data from reference 2 and the Protein Data Bank (PDB ID: 2PCC).

not within the Site 1 although it is relatively close. A question which still cannot be resolved is whether Asp-37 defines a second cytochrome *c* binding site, Site 2; whether it defines an alternative interaction site for reorientation of cytochrome *c* bound at Site 1, perhaps defining two subsites within a single binding domain, Site 1A and Site 1B; or whether the D37K mutation causes a reorientation of the side chain of residue 37 such that it interacts with cytochrome *c* bound at Site 1. The side-chain carboxyl of Asp-37 is pointed toward the interior of CcP and hydrogen bonds with His-181 in the interior of CcP. Mutating the side chain to a lysine residue will break the hydrogen bond with His-181 and perhaps cause the Lys-37 side chain to flip toward the solvent where it will be in closer proximity to cytochrome *c*, perhaps explaining the weakened interaction with cytochrome *c* in the D37K mutant.

Irrespective of why D37K weakens the binding of cytochrome *c* there does not seem to be a distinct Site 2 that is far removed from Site 1 and important for formation of the 1:1 complex. In this respect, these data support the unique, non-interacting site model for binding of yeast iso-1 cytochrome *c* at 0.10 M ionic strength.

Finally, this work has generated a library of CcP charge-reversal mutants which will be useful in future studies. First, equilibrium studies should be performed to determine the effect of these mutants on the equilibrium dissociation constants for both the 1:1 and 2:1 cytochrome *c*/CcP complexes, K_{D1} and K_{D2}. The effect of the mutations on K_{D1} should be used to confirm the results of this study based on steady-state kinetic results. In addition, determination of the effect of the mutations on K_{D2} will locate the secondary binding site, Site 2, and it will be interesting to see if the secondary binding site is located on the left-hand face of CcP near Asp-37, Figure 2.2, or if it is located on

the back-face of CcP near Asp-146 and Asp-148, Figure 2.4, as suggested by Leesch *et al.* (3).

References

1. Erman, J. E., and Vitello, L. B. (2002) Yeast cytochrome *c* peroxidase: mechanistic studies via protein engineering, *Biochim. Biophys. Acta 1597*, 193-220.

2. Pelletier, H., and Kraut, J. (1992) Crystal structure of a complex between electron transfer partners, cytochrome *c* peroxidase and cytochrome *c*, *Science 258*, 1748-1755.

3. Leesch, V. W., Bujons, J., Mauk, A. G., and Hoffman, B. M. (2000) Cytochrome *c* peroxidase-cytochrome *c* complex: Locating the second binding domain on cytochrome *c* peroxidase with site-directed mutagenesis, *Biochemistry 39*, 10132-10139.

APPENDIX A

EXPERIMENTAL PROTOCOLS

Site Directed Mutagenesis

Primer Design

The Stratagene QuikChange® Site-Directed Mutagenesis Kit (Stratagene, La Jolla, CA) was used throughout this study. This system requires two complementary primers containing the desired mutation. The cloned pET $24a^+$ plasmid with wild type CcP gene is used as the template for designing the mutagenesis primers. The primer length ranges from 24 to 45 bases, with melting temperatures ranging from 60 to 80°C.

1. The desired mutation is placed in the middle of the primer with 10 to 15 bases of correct sequence on both sides.
2. The primers contain a minimum of 40% GC content except in some target regions where the GC content is scarce. The primers terminate in at least two GC bases to ensure binding of the primers to the template.
3. The primer sequence is analyzed using the Oligoanalyzer3.0 available from www.idtdna.com (Integrated DNA Technologies, Coralville, IA). Given the 5' to3' primer sequence, the program generates the complementary sequence, the melting temperature, the % GC content, the possible hair pin, self and hetero dimer structures.
   After careful examination of the results from the Oligoanalyzer, the primers are synthesized by MWG Biotech or Fisher Scientific Company and used without further purification.
4. The primers for both the coding strand and the template strands are centrifuged at 14000rpm for 2 minutes (Eppendorff Centrifuge 5417R, Hamburg, Germany) to ensure that the sample is collected at the bottom of the vials. The samples are then diluted to 1μg/μL stock solution and 100ng/μL working solutions for use in the polymerase chain reaction (PCR).

Polymerase Chain Reaction

1. The Stratagene protocol was followed using thin-walled Thermowell tubes ™ (Corning, Inc. Corning, NY). The control reaction contains: 5μL of 10x reaction buffer
   2μL(10ng) of pWhitescript™ 4.5kb control plasmid (5ng/ μL),
   1.25 μL(125ng) of oligonucleotide control primer #1 [34-mer (100ng/ μL)],
   1.25 μL(125ng) of oligonucleotide control primer #2 [34-mer (100ng/ μL)],
   1 μL of dNTP mix
   Sufficient sterile deionized-distilled water is added to bring the total volume of the reaction to 50 μL.
   Then, 1μL *Pfu Turbo* DNA polymerase (2.5 U/μL) is added to the reaction mixture.

2. The sample reaction contains:
   5 μL of 10x reaction buffer
   1 μL (10ng/ μL) of CcP pET24a+, the double stranded DNA template
   1.25 μL of (100ng/ μL) coding primer
   1.25 μL of (100ng/ μL) template primer
   1 μL of dNTP mix and
   Sufficient sterile deionized-distilled water is added to bring the total volume of the reaction to 50 μL.
   Then, 1μL *Pfu Turbo* DNA polymerase (2.5 U/μL) is added to the reaction mixture.
3. Each reaction mixture is overlaid with 30 μL of mineral oil to prevent evaporation during the reaction.
4. The Stratagene RoboCycler ® gradient 40 Temperature Cycler is used for the PCR. Cycling parameters for the QuikChange Site-Directed Mutagenesis Method are 95°C for melting, 55°C for annealing and 68°C for elongation. The total number of cycles for the reaction is 25. There are two segments in the cycle. Segment 1 is performed once at 95°C for 30s. Segment 2 is performed in cycles 2 through 25. The settings for segment 2 are melting at 95°C for 30s, annealing at 55°C for 1 min and elongation at 68°C for 13 min (2min/kb of plasmid length). The total run time is about 6 hrs. The *pfu turbo* DNA polymerase extends and incorporates the mutagenic primers resulting in nicked circular strands.
5. After the PCR, agarose gel electrophoresis is performed to check whether the reaction was successful and sufficient amplification was made. A 0.9% agarose (SeaKem LE agarose, FMC BioProducts, Rockland, ME) gel, 2μL 1kb ladder, 10μL PCR product and 5x loading dye are used for the electrophoresis.
6. The PCR products are digested with DpnI restriction enzyme to remove methylated parental strands. 1μL of the DpnI restriction enzyme (10U/μL) is added directly to each amplification reaction below the mineral oil overlay.
7. The reaction mixture is gently and thoroughly mixed and centrifuged for 1min at 140000 rpm an Eppendorff microcentrifuge. After centrifugation, the reaction is immediately incubated at 37°C for 1 hour to digest the parental, nonmutated, supercoiled double-stranded DNA.

Transformation Reaction

1. For the transformation reaction, Epicurian Coli XL-1 Blue supercompetent cells are gently thawed on ice. 50μL aliquots of the supercompetent cells are added to a prechilled thin-walled Thermowell™ tube.
2. 1μL of the DpnI-treated DNA from each control and sample reaction is transferred to separate aliquots of the supercompetent cells. The transformation reactions are gently swirled and the reactions are incubated on ice for 30 minutes. XL-1 Blue supercompetent cells repair the nicks in the mutated plasmids.

3. The transformation reactions are heat-pulsed for 45 seconds at 42°C and then placed on ice for 2 minutes.
4. 0.5mL of NZY+ broth preheated to 42°C is added to the reactions and the transformation reactions are incubated at 37°C for 1 hour with shaking at 225-250 rpm.
5. The transformation reactions are plated immediately. The control transformation reaction contains 250μL of the reaction mixture on LB-ampicillin agar plates that have been prepared with 20μL of 10% (w/v) X-gal and 20μL of 100mM IPTG. The sample reaction contains the entire volume of each sample transformation reaction on agar plates containing kanamycin.
6. The transformation plates are incubated at 37°C for at least 16 hours.
7. Then the plates are examined for the presence of bacteria colonies. Successful transformation of the control reaction is indicated by the presence of blue colonies. The sample reaction contains white colonies.
8. A single colony is picked and inoculated in 5mL LB broth containing 5μL of 30mg/mL kanamycin. The mixture is incubated overnight at 37°C with shaking at 250 rpm.
9. Glycerol stocks are prepared by mixing 850μL of the bacteria culture with 150μL of sterile glycerol. The rest is used for plasmid isolation.

Plasmid isolation

1. Plasmid isolation was performed using the QIAprep^{R} Miniprep Kit (QIAGEN Inc. Valencia, CA). The bacterial culture is transferred to 50mL sterilized polycarbonate tubes and centrifuged at 3700rpm (1200xg) at 5°C for 10-15 minutes. The supernatant is decanted and the pellet is used for plasmid extraction.
2. The pelleted bacterial cells are resuspended in 250μL of buffer P1 and transferred to a 1.5mL microfuge tube.
3. 250μL of buffer P2 is added and the tube is inverted gently 4-6 times to mix. This lysis reaction is not allowed to proceed more than 5 minutes.
4. 350μL of Buffer N3 is added and the tube is inverted immediately but gently 4-6 times.
5. The reaction mixture is centrifuged for 10 minutes. During centrifugation, a QIAprep spin column is placed in a 2-mL collection tube.
6. After centrifugation, the supernantant is applied to the QIAprep column by decanting or pipetting.
7. The spin column is centrifuged for 60 seconds and the flow-through is discarded.
8. The QIA prep spin column is washed by adding 0.5mL of Buffer PB and centrifuged for 60 seconds. The flow-through is discarded.
9. The QIAprep spin column is washed again by adding 0.75mL of Buffer PE and centrifuged for 60 seconds. The flow-through is discarded and the column is centrifuged for an additional 1 min to remove residual wash buffer.

10. The QIAprep spin column is placed in a clean 1.5mL microfuge tube. DNA is eluded by adding 50μL of autoclaved water to the center of each spin column. It is allowed to stand for 1 minute and centrifuged for 1 minute. The sample is concentrated by ethanol precipitation.
11. After plasmid isolation, agarose gel electrophoresis is performed to detect the presence of DNA at the correct molecular weight and estimate the approximate concentration of the bands.
12. The concentration DNA concentration is also determined from the absorbance at 260nm. For double stranded DNA, an absorbance equal to 1.0 at 260 nm corresponds to a concentration of 50ng/μL. The ratio of A_{260} /A_{280} is used to determine the purity of the sample. Samples with ratios less than 1.8 indicate the presence of protein contamination. Absorbances are determined using the HP 8452A diode array spectrophotometer.
13. One μg of the sample is sent to Dr. Scott Greyburn, DNA Core Facilities, Department of Biological Sciences, Northern Illinois University or to MWG Biotech (High Point, NC) for sequencing. At least 4 primers are used to determine the sequence.
14. Genecode Sequencher Demo version (www.genecodes.com) is used to verify the DNA sequences.
15. After the correct sequence is obtained the plasmid is transformed into *E.coli* BL21 (DE3) Gold supercompetent cells for protein expression. 1μL of plasmid DNA is added to 100μL of supercompetent cells pre-chilled in a thin-walled 0.5mL tube (Thermowell ™ ,Corning Inc, Corning, NY). The cells are swirled gently and the reaction is incubated on ice for 30 minutes. The transformation reaction is heat-pulsed at 42°C for 20 seconds. Followed by incubation on ice for 2 minutes. 0.9 mL of SOC medium at 42°C is added to the transformation and the reaction is incubated at 37°C for 1 hour with shaking at 225-250 rpm. The entire transformation reaction is then plated onto a LB agar plate containing 1mg/mL kanamycin. The plate is incubated overnight at 37°C.
16. One colony is picked and inoculated in 5mL LB broth that contains 5μL 30mg/mL kanamycin. It is incubated overnight at 37°C with 250rpm shaking.
17. 850μL of the culture is added to 150μL glycerol, mixed using a vortex mixer and frozen in liquid nitrogen. The glycerol stock are stored at -70°C.

Cytochrome c Peroxidase expression, isolation and purification

The following protocol is used for the expression, isolation and purification of wild type as well as mutant proteins.

1. The primary culture contains 5mL LB broth, 5μL 30mg/mL kanamycin and a small amount of an *E. coli* BL21 (DE3) sample from a glycerol stock. The culture tube is incubated overnight at 37°C with 250rpm shaking.
2. 1mL of the 5mL culture is added to 100mL of Terrific Broth (TB) containing 100μL of 30mg/mL kanamycin. The culture is incubated for about 3-4 hrs to an OD of 1-1.2 at 600nm.

3. 24mL of the culture is added to each of four Fernbach flasks containing 1L TB, 1mL of 30mg/mL kanamycin. The cultures are incubated at 37°C with 250rpm shaking to an OD of 1 to 1.2 at 600nm. This process requires about 2-4 hours to reach the desired OD.
4. Protein expression is induced by addition of 2.5mL 0.4M IPTG. The temperature is reduced to 30°C and the cultures are incubated overnight with shaking at 250rpm.
5. To harvest the cells, one of four 500mL centrifuge bottles is weighed and the weight of the bottle is noted.
6. Four 500mL centrifuge bottles are filled half-full with the culture. This method prevents spills and uses the contents of one flask. They are centrifuged at 4000g (5000rpm) for 18 minutes at 4°C in a Beckman J2-21 centrifuge (Beckman, Palo Alto, CA)
7. After each round of centrifugation, the supernatant is poured into the empty flask that contains 200mL of bleach. Centrifugation is continued until all the flasks are empty.
8. The cell pellets are transferred to the weighed bottle and the residual broth is removed by pipetting. The weight of the cells is determined and the cells are stored at -20°C.
9. The cells are thawed at room temperature for 1 hour and 20-30mL of lysis buffer, 0.8mg lysozyme/g cells, 4mg each of DNAse and RNAase are added. If the solution is too viscous, more DNAse is added. The cells are kept on ice and stirred for at least 10 minutes.
10. The cells are frozen at -70°C for 30 minutes. Then they are thawed overnight at 4°C.
11. For 25 to 30g wet cells, 8.3mL of 5% Brij 58 is added and shaken gently at 4°C for 1.5 hour.
12. 50mL polycarbonate tubes are half-filled with the sample and centrifuge at 18000rpm (43000xg) for 35 minutes.
13. The supernatant is collected and dialyzed against 2L deionized water. The pellets are treated with 50% bleach for 30min and are then discarded.
14. The dialyzed sample is centrifuged for 30minutes at 18000rpm (43000xg). The supernatant is collected and the pellet is discarded.
15. Size exclusion chromatography in Sephadex G75 equilibrated with 50mM potassium phosphate buffer, pH 6.2 is used to fractionate the sample into discrete molecular weight fractions. A 25 mL sample is applied to a 90cm x 3cm column kept at 4°C. The sample is eluted with 50mM potassium phosphate buffer, pH 6.2 and 5min fractions, about 5mL) are collected using an LKB 2111 Mulirack fraction collector.
16. The spectra of the fractions are determined in the Cary 3E UV-Vis spectrophotometer (Varian, Australia).
17. The fractions containing apo-CcP are pooled.
18. Fractionation using size exclusion chromatography in using Sephadex G75, is repeated until all the dialyzed sample is used. Apo-CcP fractions are pooled and the total volume is recorded.

19. The concentration of apo-CcP is estimated from the absorbance at 280nm usinf an extinction coefficient of $55mM^{-1}cm^{-1}$.
20. To convert apo-CcP to holo protein, a 5-fold (mol/mol) excess of hemin is added to the pooled fractions. Based on the number of mmol of apo-CcP, the number of mmol of hemin is calculated. Then it is converted to grams by using the molecular weight of hemin, 652g/mol.
21. The calculated amount of hemin is dissolved in 0.5mL 0.1M NaOH, and then diluted with 3.0mL of water. This solution is added to the protein solution which has been adjusted to pH 7.5. The flask is covered with a box to protect it from light and the reaction is allowed to proceed for 2.5 hours.
22. The sample is dialyzed against 2L of deionized water.
23. The dialyzed sample is centrifuged at 18000rpm (39,200xg) for 30 minutes to remove unbound hemin.
24. The sample is loaded into a DEAE Sepharose fast flow column equilibrated in 50mM potassium phosphate buffer, pH 6.
25. After all the sample is loaded, the column is washed with the same buffer to remove any unbound molecule.
26. A 400mL linear gradient is prepared by placing 200mL of 50mM potassium phosphate buffer, pH6 in one beaker and 200mL of 1.0 M potassium phosphate buffer, pH 6 in a second beaker. A salt bridge is created between the two beakers.
27. The sample is eluted with the gradient and 5 to 8mL fractions are collected.
28. The spectra of the heme containing fractions are determined in the Cary 3E UV-Vis double beam spectrophotometer and the fractions containing A_{408}/A_{280} above 1.2 are collected and combined.
29. The pooled fractions are dialyzed against deionized water.
30. Small DEAE Sepharose FF column is prepared and equilibrated in 50mM potassium phosphate buffer, pH 6.
31. The CcP solution is added to the column. The protein binds, making a dark brown band at the top of the column bed.
32. The column is washed with 50mM potassium phosphate buffer, pH 6 to remove any unbound molecules.
33. 1.0M potassium phosphate buffer, pH 6 is added carefully to the top of the column bed. The CcP starts to elute. As soon as the color is visible in the eluent, the fractions are collected.
34. The spectrum of the fraction is taken and the RZ value (A_{408}/A_{280}) is determined.
35. The fractions are dialyzed against water. CcP is not soluble in water; therefore it crystallizes in 3-5 days after 3 to 4 changes of water.
36. The crystals are collected by centrifugation in Oak Ridge centrifuge tubes and the supernatant is discarded or frozen at -20°C for lyophilization.
37. The crystals are stored at -20°C.

Cytochrome c expression, isolation and purification.

1. The primary culture contains 100mL of TB broth and 200uL 50ng/mL ampicillin. and inoculated with a small sample of the BL21 (DE3) glycerol stock transformed with the yeast cytochrome *c* (C102T) gene The primary culture is incubated for 4hrs at 37°C, and 250rpm.
2. Four Fernbach flasks containing doubly concentrated TB broth are prepared and kept at room temperature.
3. 5.0mL of 0.1M, cold sterilized, δ-amino levulinic acid is prepared.
4. After 4 hours of inoculation, 1mL of 0.1M δ-amino levulinic acid, 2mL of 50mg/mL ampicillin, 100mL 0.1 M potassium phosphate buffer and 10mL of the cytochrome *c* culture are added to the TB broth. The culture flasks are incubated at 37C, 250rpm for 48hours.
5. The procedure for centrifuging the cells is the same as for CcP.
6. The cells lysis procedure is the same as for CcP except that no lysozyme is added.
7. The sample is centrifuged at 18,000 rpm (39,200xg) for 30 minutes. The supernatant, pink-red in color, is saved.
8. The pellet is washed with lysis buffer and is centrifuged. The supernatant is saved. This step is repeated 3 times.
9. The supernatant is dialyzed in a special dialysis tube (molecular weight cutoff 4000-8000) in a 4L flask with at least 3 changes of water.
10. The sample is centrifuged at 18,000rpm (39,200xg), 4°C for 35 minutes before loading to the CM FF column in the 4°C cold room.
11. The13x3.5cm CMFF column is equilibrated with 10mM potassium phosphate buffer, pH 7.2.
12. The sample is loaded to the column and washed with 10mM potassium phosphate buffer, pH 7.2 until the yellowish color disappears and the clear color of the buffer is observed.
13. Cytochrome c is eluted with 500mM potassium phosphate buffer, pH 7.2. The sample is collected when the red-colored sample starts to elute.
14. The sample is then dialyzed against several changes of distlled water. The small molecular weight cut-off special dialysis tubes are used.for the dialysis. The samples are lyophilized, sealed properly and stored at -20°C.
15. After elution of the sample, the CMFF column is washed with two column volumes of 1M potassium phosphate buffer pH 7.2 to remove anything that is bound to the column. Then the column is re-equilibrated with 10mM potassium phosphate buffer and is ready for the next use.

Buffers, Broths and other Reagents Used in the Site-directed Mutagenesis and Protein Expression:

1. LB Agar (kanamycin plates for bacteria culture) – 1L
   40g LB Agar,Miller or 5g Triptone, 10g NaCl, 5g yeast extract and 15g agar.
   Add deionized H_2O to a final volume of 1L
   Autoclave
   Cool down to 60°C and add 1mL of 30mg/mL kanamycin
   Pour into Petri dishes (~25 ml/100mm plate)

2. LB Agar (Ampicillin plates for bacteria culture) -1L
   40g LB Agar,Miller or 5g Triptone, 10g NaCl, 5g yeast extract and 15g agar.
   Add deionized H_2O to a final volume of 1L
   Autoclave
   Cool down to 60°C and add 1.2mL of 50mg/mL ampicillin
   Pour into Petri dishes (~25 mL/100mm plates)

3. NZY+ Broth (per Liter)
   10g of NZ amine (casein hydrolysate)
   5g of yeast extract
   5g of NaCl
   Adjust to pH 7.5 using NaOH
   Autoclave
   Add the following supplement prior to use
   12.5mL of 1M $MgCl_2$ and 12.5 mL of 1M $MgSO_4$
   20mL of 20% (w/v) glucose
   Filter sterilize

4. Ethanol Precipitation
   To a 50μL sample add 5μL 3M sodium acetate.
   Add 110μL cold, molecular biology grade, 100% ethanol
   Allow to react at -20°C for at least 2hours
   Centrifuge for 15minutes at 14,000 rpm (23,700xg) at 4°C
   Decant and invert on a paper towel
   Add 500μL 70% cold ethanol
   Vortex at maximum speed
   Centrifuge at 14,000 rpm for 15 minutes, 4°C
   Decant and invert on a paper towel
   The sample is dried using the Savant Speed Vac® Plus (SC110A) for approximately 10 to 30 minutes.
   Dissolve the dried plasmid in approximately 50μL of water
   Record the spectrum between 240 and 700nm. The absorbance at 260nm is used to determine concentration. For double stranded DNA, 1 absorbance unit corresponds to 50μg/mL. The A_{260}/A_{280} is used to assess the purity of the sample.

The molecular weight and purity are determined by agarose gel electrophoresis.

5. LB Broth (per Liter)
   25g of LB powder or 10g triptone, 10g NaCl, 5g yeast extract in 1L of water
   Adjust to pH 7.5 with NaOH
   Autoclave

6. SOB Medium (per Liter)
   20.0g of tryptone
   5.0 g of yeast extract
   0.5g of NaCl
   Autoclave
   Add 10mL of 1M $MgCl_2$ and 10mL of 1M $MgSO_4$ prior to use
   Filter sterilize

7. SOC Medium(per 100mL) – This medium should be prepared immediately before use
   2mL of filter-sterilized 20% (w/v) glucose
   SOB medium to a final volume of 100mL
   Filter sterilize

8. Tris-Borate Electrophoresis buffer(5x) – 1L
   54g Tris base
   27.5g boric acid
   20mL 0.5M EDTA
   Adjust to pH 8.0 (use HCl)

9. 0.9% Agarose gel
   0.54 g agarose, SeaKem LE agarose (FMC BioProducts, Rockland, Maine)
   60mL of 0.5x TBE
   Microwave for 2minutes
   Allow to cool to 60°C
   Add 3μL ethidium bromide
   Mix by swirling and pour into gel chamber
   Insert eight-well comb
   Allow to cool for approximately 30minutes

10. Kanamycin:
    0.9g in 30mL Milli-Q plus grade deionized water
    Cold sterilized
    Store in sterilized vial at 4-5°C

11. Ampicillin:
    1.5g in 30mL Milli-Q plus grade deionized water
    Cold sterilized
    Store in sterilized vial at 4-5°C

12. Terrific broth (for CcP isolation) -1L
    24g yeast extract
    12g tryptone
    4mL glycerol
    900mL Milli-Q plus deionized water
    The ingredients are autoclaved in a 2.8L Fernbach flask
    Potassium phosphate buffer containing 2.31g potassium phosphate monobasic and 12.5g potassium phosphate dibasic in 1L Milli-Q plus grade deionized water is distributed into 10, 150mL Erlenmeyer flasks and autoclaved.
    The broth and buffer are kept separate and mixed just before use for inoculation.

13. Terrific broth (for cytochrome *c* isolation) -1L
    48g yeast extract
    24g tryptone
    8mL glycerol
    900mL Milli-Q plus grade deionized water
    The ingredients are autoclaved in a 2.8L Fernbach flask
    Potassium phosphate buffer containing 2.31g potassium phosphate monobasic and 12.5g potassium phosphate dibasic in 1L Milli-Q plus grade deionized water is distributed into 10, 150mL Erlenmeyer flasks and autoclaved.
    The broth and 100mL buffer are mixed just before inoculation.

14. 1M, pH 6.0 potassium phosphate buffer – 1L
    103.41g anhydrous K_2HPO_4, MW 174.18g/mol
    41.82g anhydrous KH_2PO_4, MW 136.09g/mol

15. 100mM, pH 7.5 potassium phosphate buffer for steady-state kinetic studies.
    Solution A: 0.1M KH_2PO_4 (13.6g/L)
    Solution B: 0.0333M K_2HPO_4

Sodium Dodecyl Sulfate- Polyacrylamide Gel Electrophoresis (SDS- PAGE) PhastSystem

1. The Pharmacia LKB PhastSystem unit is used for the analysis of protein purification. The sensitivity of the technique is about 30ng/μL for each protein in the sample using Coomassie Blue stain. More than 2μg/μL of each protein can overload the gel.
2. Sample preparation
3. 70μL protein in TE buffer
4. 30μL 10%SDS
5. 5μL bromophenol blue (2% in water)

6. The samples are centrifuged for 2min.
7. The electrophoresis e procedure is that described in the PhastSystem manual.

Agarose gel electrophoresis

1. Agarose gel electrophoresis is used for the analysis of DNA samples. For the 5.4kb plasmid, a 0.9% gel is used for the analysis. Protective gloves are needed during the entire process.
2. The gel is cast as described in the reagent section.
3. 2μL of 1kb DNA ladder are mixed with 3μL autoclaved Milli-Q-plus water and 1μL of 6x loading dye.
4. Each sample contains 5μL sample and 1μL 6x loading dye. The samples are centrifuged for 1 min before loading onto the gel.
5. When the gel is molded, the comb and rubber guards are removed and the electrophoresis chamber is filled with 0.5x TBE buffer to about 2mm above the gel. The samples and standard are loaded in the wells and their position noted. About 7μL ethidium bromide is added to the chamber with the positive charge, the lid and electrodes are attached and the electrophoresis is carried out at 90-95mV for 1.25 to 1.5 hrs.
6. After electrophoresis, the gel is viewed in the UV light box. Polaroid pictures are taken . The gel and all buffers are disposed in the designated container. Since ethidium bromide is a probable mutagenic reagent, careful handling and disposal are necessary.

Steady-State Kinetics, 100mM ionic strength, pH7.5

1. The following protocol is used to perform the steady-state kinetic studies on wild type and mutant recombinant enzymes, as well as ionic strength dependence studies on wild type yeast CcP and recombinant yeast CcP.

Day one:

1. The potassium phosphate buffer is prepared in Milli-Q plus deionized water.
2. The Sephadex G25 column, 30cm in height and 1.5cm in diameter, is equilibrated with the buffer at room temperature. The buffer is bubbled with argon to maintain a reduced environment. 2 scoops of sodium hydrogen sulfite are dissolved in 1mL buffer. Remove buffer from the top of the column and load the sodium hydrogen sulfite solution to the column. The buffer is allowed to percolate (penetrate) into the column and a small amount of buffer is layered on the column bed. The column is washed with 2 to 3 column volumes.
3. The top of the column is sealed thoroughly with Parafilm until the next day.

Day two:

The HP diode array spectrophotometer is used for the absorbance measurements of the steady state kinetic studies. The lamp is turned on at least 15 to 20 minutes before the beginning of the experiment.

A – Preparation of reduced cytochrome *c*:

1. The Sephadex G25 column is washed with 1-2 volumes of potassium phosphate buffer bubbled with argon.
2. The cytochrome *c* C102T is dissolved in 2mL buffer in a Corex tube and centrifuged at 15°C, 12000rpm for 20 minutes to remove any undissolved materials.
3. A scoop of sodium hydrosulfite is added to the cytochrome *c*. There is a change in cytochrome *c* color from dark red to pinkish red.
4. The buffer on top of the column bed is removed and the cytochrome *c* sample is carefully loaded. It is allowed to penetrate into the column completely and re-layered with a small amount of buffer to make sure all the sample is in. The sample is passed through the G25 column and the reduced cytochrome *c* is collected in a tube with side arm to keep it under argon while collecting the reduced cytochrome *c*.
5. The column is washed with buffer to remove the sodium hydrosulfite.
6. Both the cytochrome *c* and buffer are kept under argon at room temperature throughout the entire experiment.

B – Preparation of CcP mutant and wild type enzymes

1. A small amount of CcP sample is dissolved in 1mL of potassium phosphate buffer. It is labeled as CcP1.
2. The CcP solution is centrifuged at 10-15°C, 14000 rpm for 10 minutes.
3. The supernate is used for the concentration measurement.
4. The HP diode array spectrophotometer standard mode is used for the measurement of the absorbance between 240nm and 700nm.
5. A 2mL quartz cuvette with 1cm path length is filled with 1mL buffer and the blank absorbance is measured.
6. 300-500uL of CcP is added to the buffer and mixed well. The absorbance is measured.
7. The concentration in the cuvette is calculated using Beer's law. The extinction coefficient, $98mM^{-1}cm^{-1}$ at 408nm is used.
8. The sample in cuvette is used to prepare CcP 2 which is about 0.2-0.5uM.

C – Determination of Cytochrome *c* concentration and percent reduction

1. A 3mL quartz cuvette with 1cm path length is filled with 2mL buffer and the blank absorbance is measured.
2. 40uL of cytochrome *c* is added to the cuvette and mixed well. The absorbance is measured.
3. A few grains of sodium hydrosulfite are added to the cuvette, mixed well and the absorbance is measured at 548nm. This step is repeated until the maximum absorbance is achieved, which indicates the presence of excess sodium hydrosulfite that reduces the cytochrome *c* to the highest percent possible. The ideal for this step is 100% reduction of cytochrome *c*.

4. The concentration in the stock is calculated by using Beer's law and the diluting factors. The extinction coefficient at 548nm, 30.90 $mM^{-1}cm^{-1}$, is used for the calculation.
5. The percent reduction is calculated.

D - Preparation of Hydrogen Peroxide Solutions:

1. 0.1mL of 30% hydrogen peroxide is added to 9.9mL of Milli-Q plus deionized water and mixed well. The sample, $H_2O_2(1)$, is kept on ice.
2. 1mL of $H_2O_2(1)$ is added to 4.2mL of Milli-Q plus deionized water and mixed well. The sample, $H_2O_2(2)$ is kept on ice. This gives a final concentration of 20mM.

E – Steady-State Kinetic Experiment

1. The parameters for steady state kinetics are set up before the actual run in the kinetic mode. The absorbances at 314, 362, 548, 418nm are followed for very low cytochrome *c* concentration (1-7uM),the absorbances at 362, 448, 468, 548nm are followed for 7-32uM cytochrome *c* concentration and absorbances at 362, 448, 468, 564 and 478nm are followed for the 32-100uM cytochrome *c* concentrations. These wavelengths are followed to observe the progress of the reaction and the oxidation of the cytochrome *c*. The reaction time is 1minute for each run and it is recorded every second. The overall absorbance range is 240-700nm. The temperature is set at 25°C. The instrument is set in Kinetics Mode.
2. The buffer and cytochrome *c* are kept under argon at room temperature. CcP and H_2O_2 are kept on ice.
3. The volume of 20mM H_2O_2 (2) is constant at 20uL for the entire experiment.
4. The concentrations of cytochrome *c* vary from 1uM to 100uM. The volume of CcP is adjusted to give a good reaction rate, which also gives good initial slopes.
5. The reaction is initiated by the addition of 20uLof 20mM H_2O_2 to the cuvette which contains buffer, cytochrome *c* and CcP.
6. The change in absorbance is followed at the appropriate wavelengths.
7. The data in the kinetic mode is exported as CSV files to do further calculation.

APPENDIX B

PRIMERS FOR SITE-DIRECTED MUTAGENESIS

Primers for Site Directed Mutagenesis

E11K
Coding
5' CGT TCA TGT CGC CTC TGT CAA AAA AGG GAG GTC ATA CG 3'
Template
5' CGT ATG ACC TCC CTT TTT TGA CAG AGG CGA CAT GAA CG 3'

E17K
Coding
5' GGG AGG TCA TAC AAG GAC TTC CAA AAG G 3'
Template
5' CCT TTT GGA AGT CCT TGT ATG ACC TCC C 3'

D18K
Coding
5' GGA GGT CAT ACG AGA AGT TCC AAA AGG TG 3'
Template
5' CAC CTT TTG GAA CTT CTC GTA TGA CCT CC 3'

R31E
Coding
5' GCA CTC AAG CTG GAG GAA GAT GAC G 3'
Template
5' CGT CAT CTT CCT CCA GCT TGA GTG C 3'

E32K
Coding
5' GCG ATT GCA CTC AAG CTG AGG AAA GAT GAC GAA TAT GAC AAC TAT ATA GGC TAT GGG CCC 3'
Template
5' GGG CCC ATA GCC TAT ATA GTT GTC ATA TTC GTC ATC TTT CCT CAG CTT GAG TGC AAT CGC 3'

D33K
Coding
5' GCT GAG GGA AAA GGA CGA ATA TGA CAA CTA TAT AGG CTA TGG GCC CG 3'
Template
5' CGG GCC CAT AGC CTA TAT AGT TGT CAT ATT CGT CCT TTT CCC TCA GC 3'

D34K
Coding
5' GCT GAG GGA AGA TAA GGA ATA TGA CAA CTA TAT AGG CTA TGG GCC CG 3'
Template
5' CGG GCC CAT AGC CTA TAT AGT TGT CAT ATT CCT TAT CTT CCC TCA GC 3'

E35K
Coding
5' GCT GAG GGA AGA TGA CAA ATA TGA CAA CTA TAT AGG CTA TGG GCC CG 3'
Template
5' CGG GCC CAT AGC CTA TAT AGT TGT CAT ATT TGT CAT CTT CCC TCA GC 3'

D37K
Coding
5' GAG GGA AGA TGA CGA ATA TAA GAA CTA TAT AGG CTA TGG GCC CG 3'
Template
5' CGG GCC CAT AGC CTA TAT AGT TCT TAT ATT CGT CAT CTT CCC TC 3'

D58K
Coding
5' CAC TTC AGG GAC CTG GAA GAA GCA CGA CAA TAC AGG 3'
Template
5' CCT GTA TTG TCG TGC TTC TTC CAG GTC CCT GAA GTG 3'

D61K
Coding
5' CCT GGG ACA AGC ACA AGA ATA CAG GCG GGT CAT ACG 3'
Template
5' CGT ATG ACC CGC CTG TAT TCT TGT GCT TGT CCC AGG 3'

E76K
Coding
5' CAG ATT CAA AAA GAA GTT TAA CGA TCC ATC C 3'
Template
5' GGA TGG ATC GTT AAA CTT CTT TTT GAA TCT G 3'

D79K
Coding
5' GGA GTT TAA CAA GCC ATC CAA TGC G 3'
Template
5' CGC ATT GGA TGG CTT GTT AAA CTC C 3'

E93K
Coding
5' GGC TTT AAG TTC CTG AAG CCC ATT CAC AAA GAG TTT CCC 3'
Template
5' GGG AAA CTC TTT GTG AAT GGG CTT CAG GAA CTT AAA GCC 3'

E98K
Coding
5' GCC CAT TCA CAA AAA GTT TCC CTG GAT CTC CTC GGG 3'
Template
5' CCC GAG GAG ATC CAG GGA AAC TTT TTG TGA ATG GGC 3'

D106K
Coding
5' GGA TCT CCT CGG GTA AGC TGT TCA GTC TAG GG 3'
Template
5' CCC TAG ACT GAA CAG CTT ACC CGA GGA GAT CC 3'

E118K
Coding
5' GCT GTG CAG AAG ATG CAG GGT CC 3'
Template
5' GGA CCC TGC ATC TTC TGC ACA GC 3'

D132K
Coding
5' GGA GAT GTG GTA GAG TCA AGA CGC CAG AGG ATA CTA CC 3'
Template
5' GGT AGT ATC CTC TGG CGT CTT GAC TCT ACC ACA TCT CC 3'

E135K
Coding
5' GGT AGA GTC GAC ACG CCA AAG GAT ACT ACC CCT GAC 3'
Template
5' GTC AGG GGT AGT ATC CTT TGG CGT GTC GAC TCT ACC 3'

D136K
Coding
5' CGA CAC GCC AGA GAA GAC TAC CCC TGA CAA CG 3'
Template
5' CGT TGT CAG GGG TAG TCT TCT CTG GCG TGT CG 3'

D140K
Coding
5' GGA TAC TAC CCC TAA GAA CGG GAG ACT GCC 3'
Template
5' GGC AGT CTC CCG TTC TTA GGG GTA GTA TCC 3'

D146K
Coding
5' GGG AGA CTG CCT AAG GCT GAT AAG GAC GC 3'
Template
5' GCG TCC TTA TCA GCC TTA GGC AGT CTC CC 3'

D148K
Coding
5' CGG GAG ACT GCC TGA CGC TAA GAA GGA CGC 3'
Template
5' GCG TCC TTC TTA GCG TCA GGC AGT CTC CCG 3'

K149D
Coding
5' GCC TGA CGC TGA TGA TGA CGC TGA C 3'
Template
5' GTC AGC GTC ATC ATC AGC GTC AGG C 3'

D150K
Coding
5' CGC TGA TAA GAA GGC TGA CTA TGT CAG AAC G 3'
Template
5' CGT TCT GAC ATA GTC AGC CTT CTT ATC AGC G 3'

D152K
Coding
5' CGC TGA TAA GGA CGC TAA GTA TGT CAG AAC G 3'
Template
5' CGT TCT GAC ATA CTT AGC GTC CTT ATC AGC G 3'

D165K
Coding
5' GAC TTA ATA TGA ATA AGA GAG AAG TAG TTG C 3'
Template
5' GCA ACT ACT TCT CTC TTA TTC ATA TTA AGT C 3'

E167K
Coding
5' GAC TTA ATA TGA ATG ACA GAA AAG TAG TTG CTC TTA TGG GGG C 3'
Template
5' GCC CCC ATA AGA GCA ACT ACT TTT CTG TCA TTC ATA TTA AGT C 3'

E188K
Coding
5' GAA CTC TGG ATA CAA GGG GCC ATG GGG AGC 3'
Template
5' GCT CCC CAT GGC CCC TTG TAT CCA GAG TTC 3'

E201K
Coding
5' CGT CTT TAC CAA TAA GTT TTA CTT G 3'
Template
5' CAA GTA AAA CTT ATT GGT AAA GAC G 3'

E209K
Coding
5' GAA CTT GTT GAA TAA GGA CTG GAA ATT GG 3'
Template
5' CCA ATT TCC AGT CCT TAT TCA ACA AGT TC 3'

D210K
Coding
5' CTT GTT GAA TGA AAA GTG GAA ATT GG 3'
Template
5' CCA ATT TCC ACT TTT CAT TCA ACA AG 3'

E214K
Coding
5' GAC TGG AAA TTG AAA AAG AAC GAC GCG 3'
Template
5' CGC GTC GTT CTT TTT CAA TTT CCA GTC 3'

D217K
Coding
5' GAA ATT GGA AAA GAA CAA GGC GAA CAA CGA AC 3'
Template
5' GTT CGT TGT TCG CCT TGT TCT TTT CCA ATT TC 3'

E221K
Coding
5' CGA CGC GAA CAA CAA ACA GTG GGA CTC TAA GAG C 3'
Template
5' GCT CTT AGA GTC CCA CTG TTT GTT GTT CGC GTC G 3'

D224K
Coding
5' CAA CGA ACA GTG GAA GTC TAA GAG CGG 3'
Template
5' CCG CTC TTA GAC TTC CAC TGT TCG TTG 3'

D235K
Coding
5' CAT GAT GCT GCC CAC TAA GTA TTC TTT GAT TCA GG 3'
Template
5' CCT GAA TCA AAG AAT ACT TAG TGG GCA GCA TCA TG 3'

D241K
Coding
5' GAT TAT TCT TTG ATT CAG AAG CCC AAG TAC TTA AGC 3'
Template
5' GCT TAA GTA CTT GGG CTT CTG AAT CAA AGA ATA ATC 3'

E250K
Coding
5' GCA TTG TGA AAA AAT ACG CTA ATG ACC 3'
Template
5' GGT CAT TAG CGT ATT TTT TCA CAA TGC 3'

D254K
Coding
5' GAA TAC GCT AAT AAG CAG GAC AAG TTC 3'
Template
5' GAA CTT GTC CTG CTT ATT AGC GTA TTC 3'

D256K
Coding
5' GCT AAT GAC CAG AAG AAG TTC TTC AAG G 3'
Template
5' CCT TGA AGA ACT TCT TCT GGT CAT TAG C 3'

D261K
Coding
5' GGA CAA GTT CTT CAA GAA GTT TTC CAA AGC 3'
Template
5' GCT TTG GAA AAC TTC TTG AAG AAC TTG TCC 3'

E267K
Coding
5' CCA AAG CTT TTA AAA AAC TGT TGG AAA ACG G 3'
Template
5' CCG TTT TCC AAC AGT TTT TTA AAA GCT TTG G 3'

E271K
Coding
5' GCT TTT GAA AAA CTG TTG AAA AAC GGT ATC ACT TTC CC 3'
Template
5' GGG AAA GTG ATA CCG TTT TTC AAC AGT TTT TCA AAA GC 3'

D279K
Coding
5' CGG TAT CAC TTT CCC TAA AAA GGC GCC CAG TCC ATT TAT TTT C 3'
Template
5' GAA AAT AAA TGG ACT GGG CGC CTT TTT AGG GAA AGT GAT ACC G 3'

E290K
Coding
5' CAA GAC TTT AAA GGA ACA AGG 3'
Template
5' CCT TGT TCC TTT AAA GTC TTG 3'

E291K
Coding
5' GAC TTT AGA GAA GCA AGG TTT ATA GG 3'
Template
5' CCT ATA AAC CTT GCT TCT CTA AAG TC 3'

Primers to sequence CcP

99111 - 5' CGA TCC ATC CAA TGC GGG C 3'
99223 - 5' GAC GCT GAC TAT GTC AGA AC 3'
99245 - 5' GAG CGT GAG CCC CCA TAA GAG 3'
99262 - 5' CTT TTC GGG CTT TGT TAG 3'

APPENDIX C

SPECTRA OF rCcP AND 46 CHARGE-REVERSAL MUTANTS

(FIGURES C.1 to C.47)

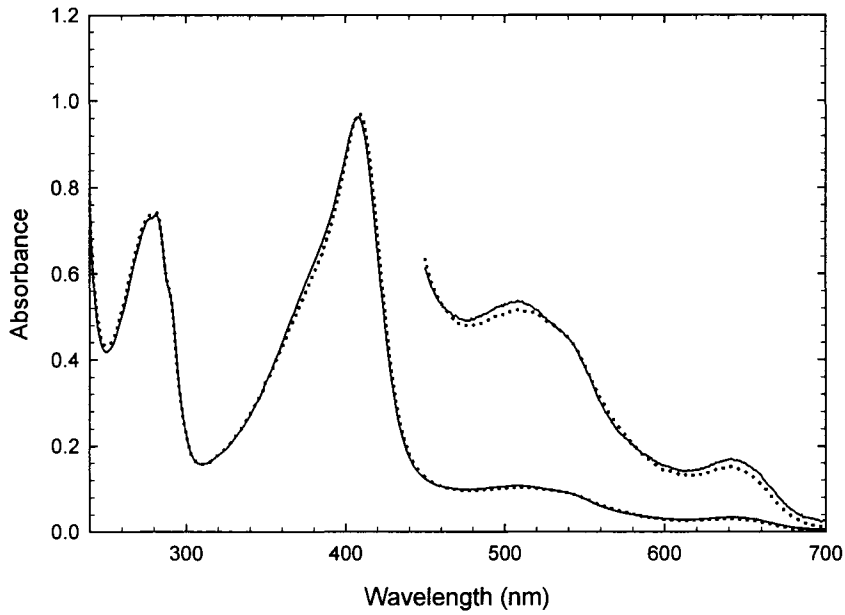

Figure C.1. A comparison of the spectra of 9.67μM rCcP at pH6.0 (solid line) and 7.5 (dotted line) in 100mM potassium phosphate buffer

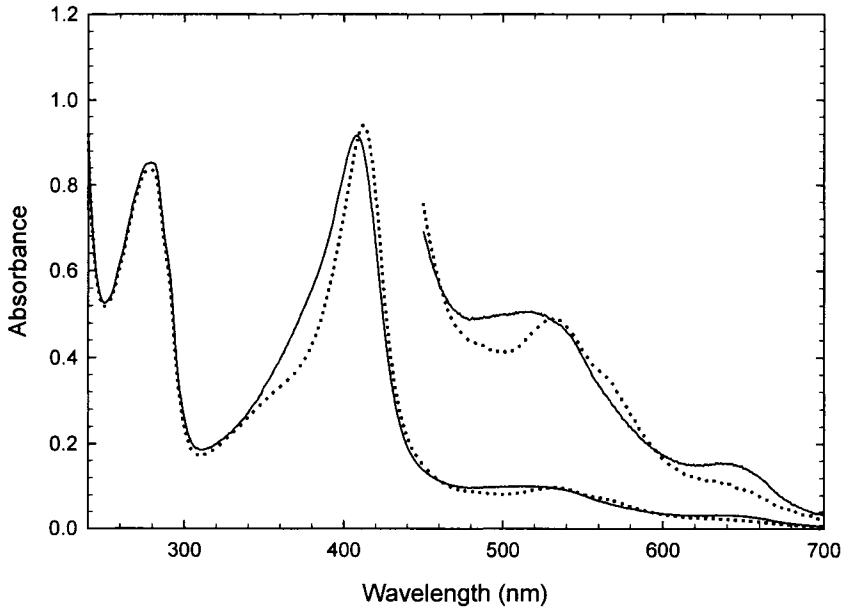

Figure C.2. A comparison of the spectra of 9.38μM E11K at pH6.0 (solid line) and 7.5 (dotted line) in 100mM potassium phosphate buffer

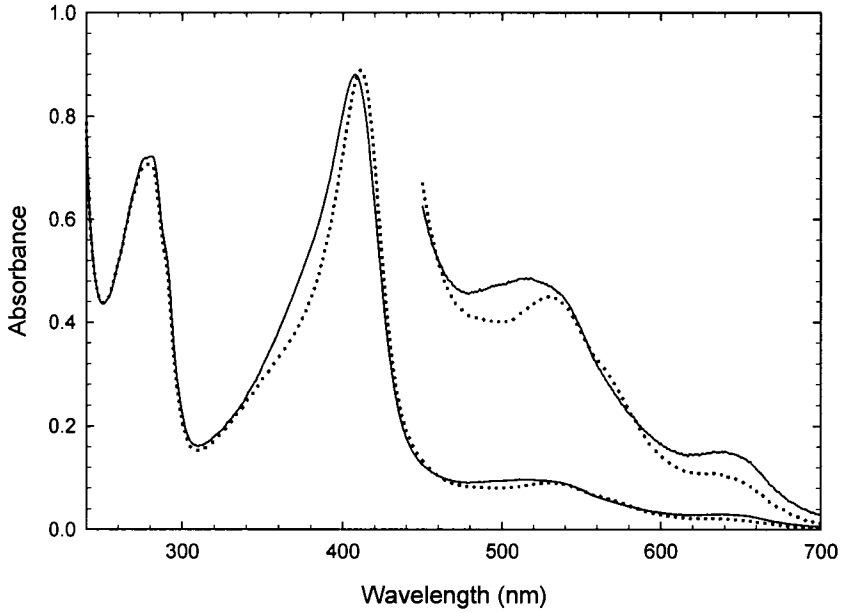

Figure C.3. A comparison of the spectra of 8.93μM E17K at pH6.0 (solid line) and 7.5 (dotted line) in 100mM potassium phosphate buffer

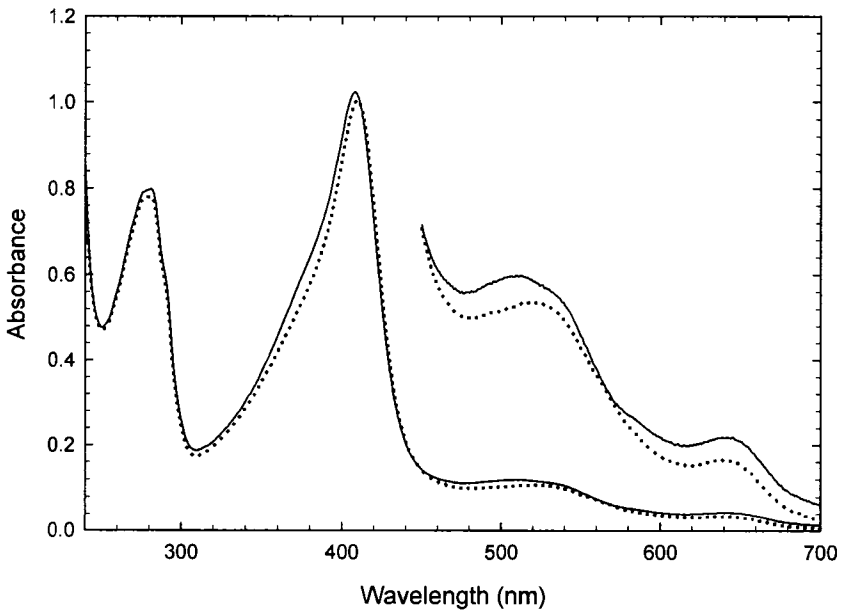

Figure C.4. A comparison of the spectra of 10.3μM D18K at pH6.0 (solid line) and 7.5 (dotted line) in 100mM potassium phosphate buffer

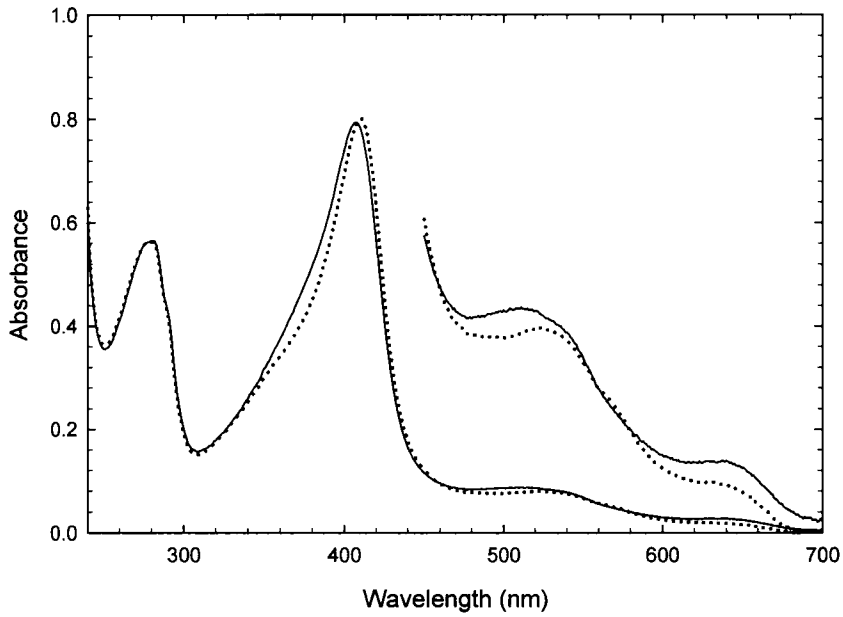

Figure C.5. A comparison of the spectra of 8.01μM R31E at pH6.0 (solid line) and 7.5 (dotted line) in 100mM potassium phosphate buffer

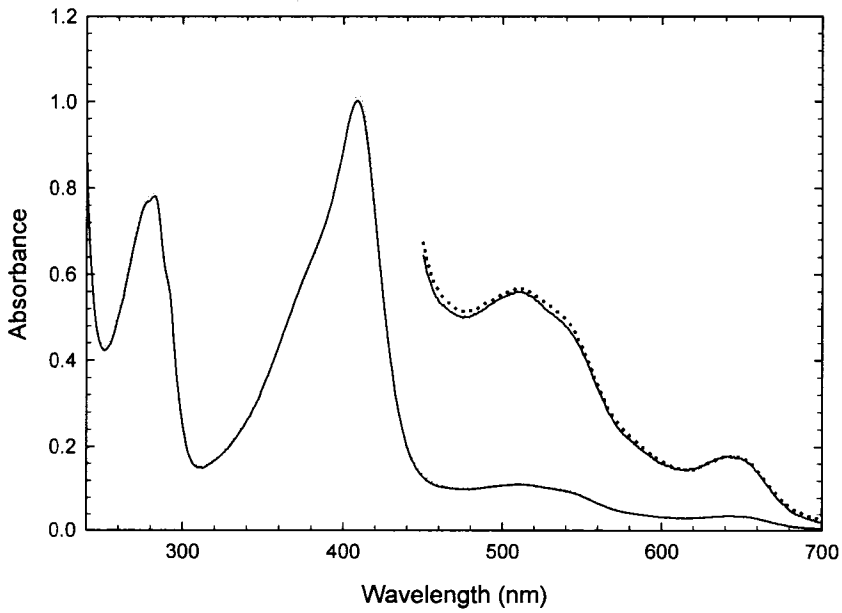

Figure C.6. A comparison of the spectra of 10.1μM E32K at pH6.0 (solid line) and 7.5 (dotted line) in 100mM potassium phosphate buffer

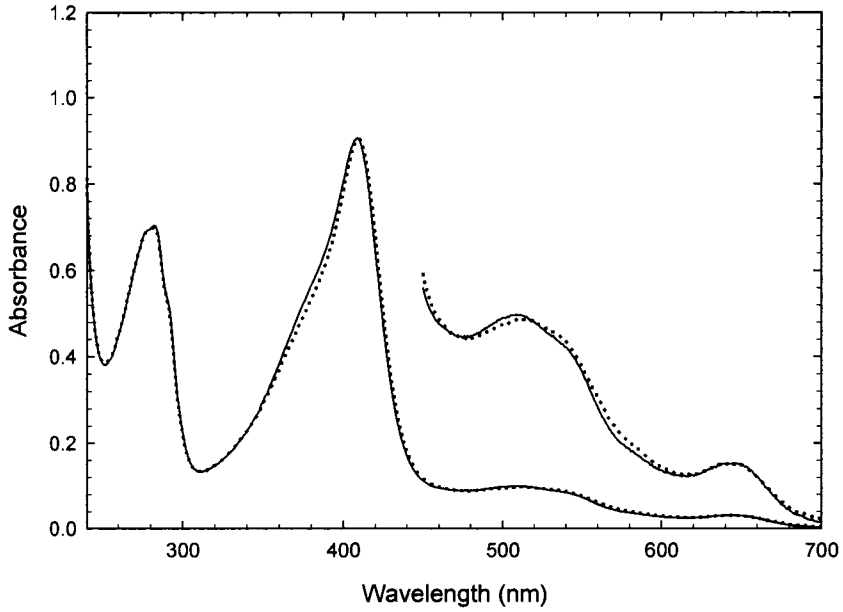

Figure C.7. A comparison of the spectra of 9.13μM D33K at pH6.0 (solid line) and 7.5 (dotted line) in 100mM potassium phosphate buffer

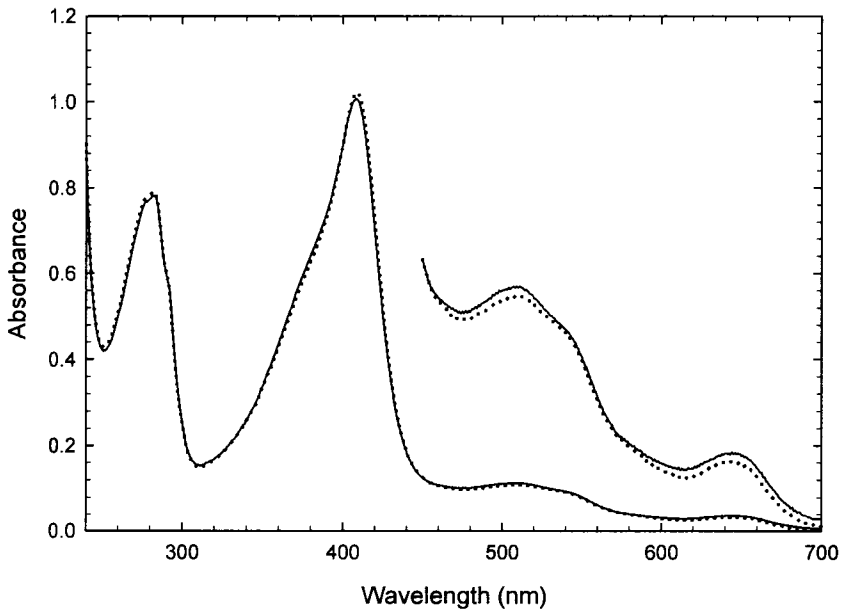

Figure C.8. A comparison of the spectra of 10.2μM D34K at pH6.0 (solid line) and 7.5 (dotted line) in 100mM potassium phosphate buffer

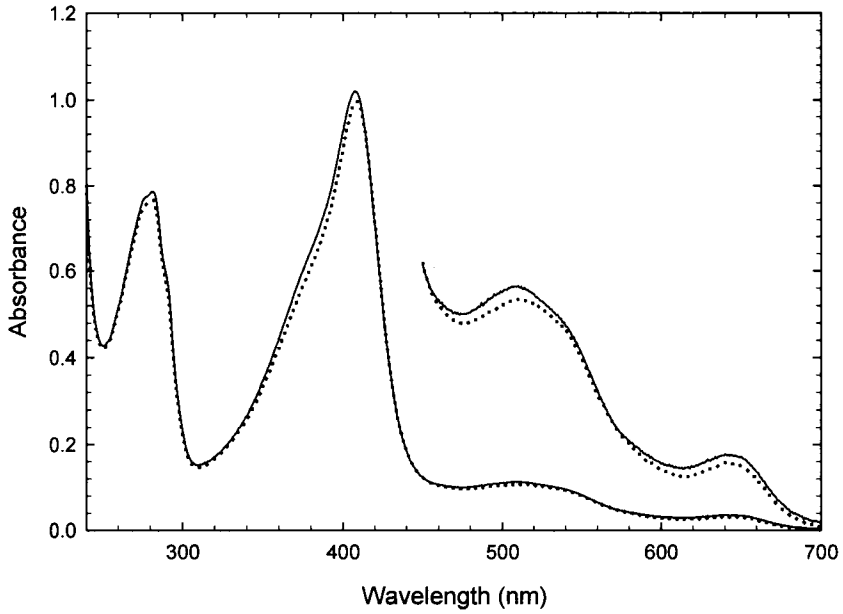

Figure C.9. A comparison of the spectra of 10.3μM E35K at pH6.0 (solid line) and 7.5 (dotted line) in 100mM potassium phosphate buffer

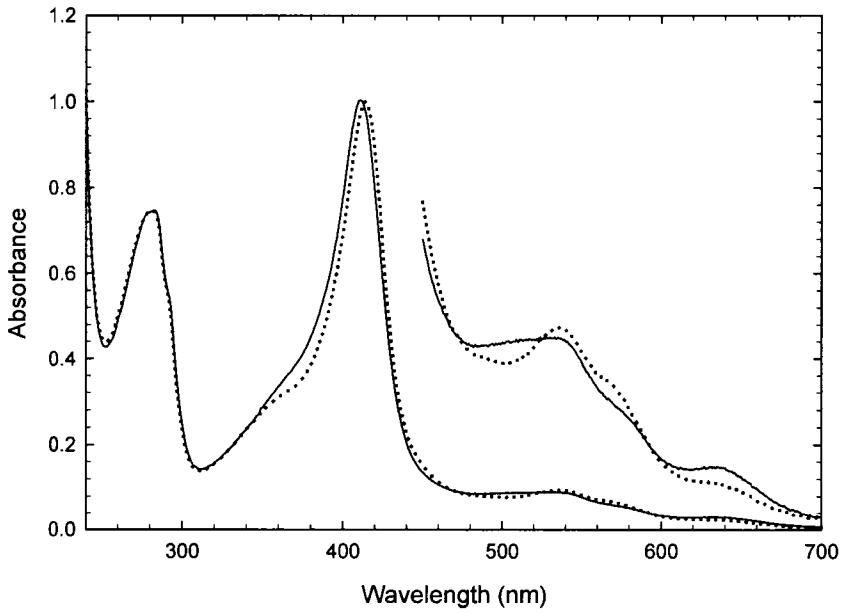

Figure C.10. A comparison of the spectra of 10.3μM D37K at pH6.0 (solid line) and 7.5 (dotted line) in 100mM potassium phosphate buffer

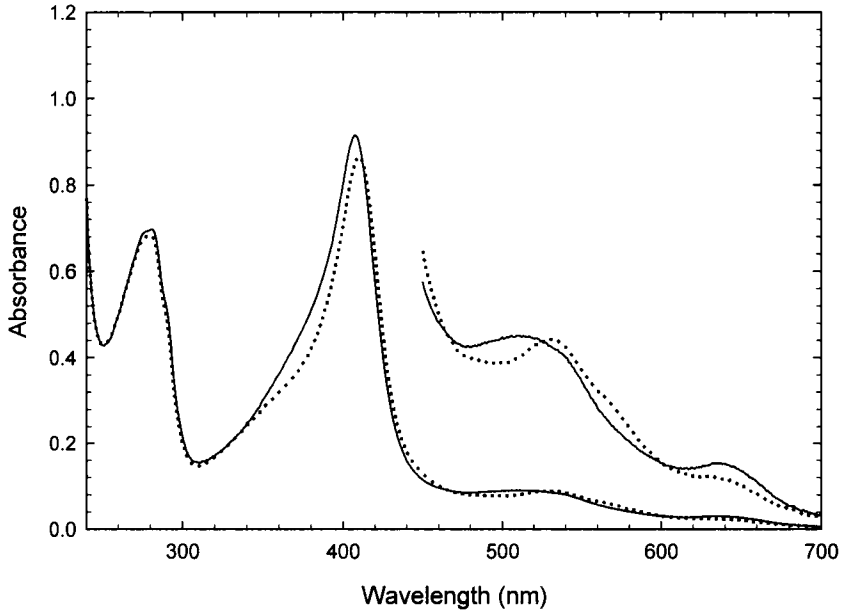

Figure C.11. A comparison of the spectra of 9.28μM D58K at pH6.0 (solid line) and 7.5 (dotted line) in 100mM potassium phosphate buffer

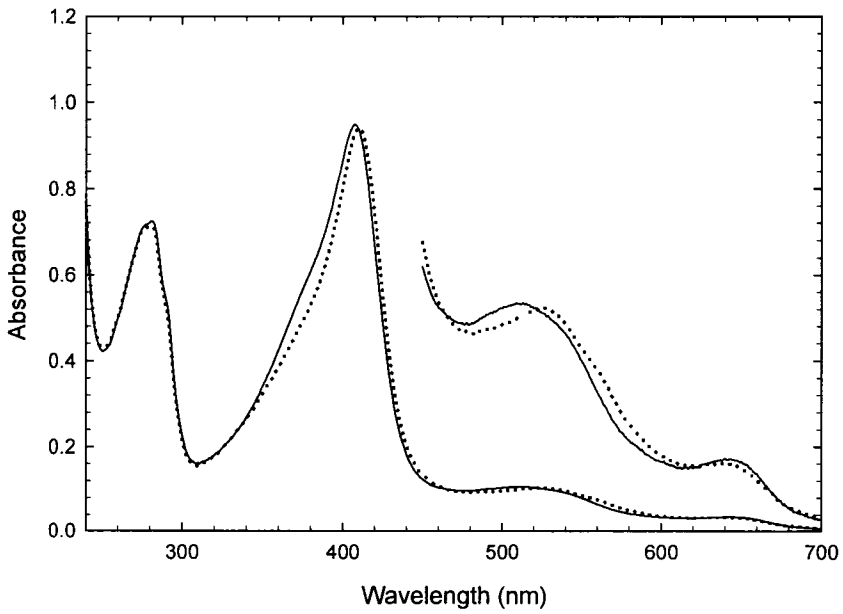

Figure C.12. A comparison of the spectra of 9.60μM D61K at pH6.0 (solid line) and 7.5 (dotted line) in 100mM potassium phosphate buffer

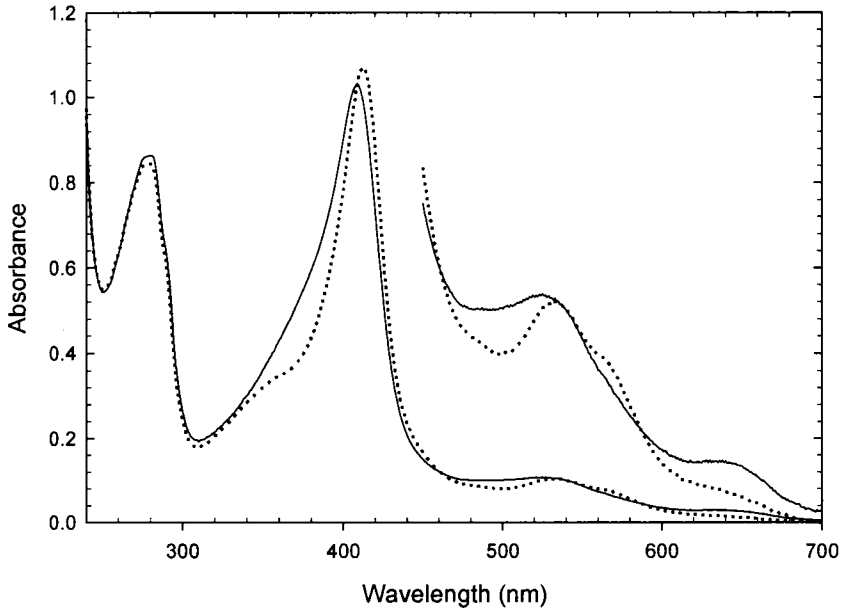

Figure C.13. A comparison of the spectra of 10.5μM E76K at pH6.0 (solid line) and 7.5 (dotted line) in 100mM potassium phosphate buffer

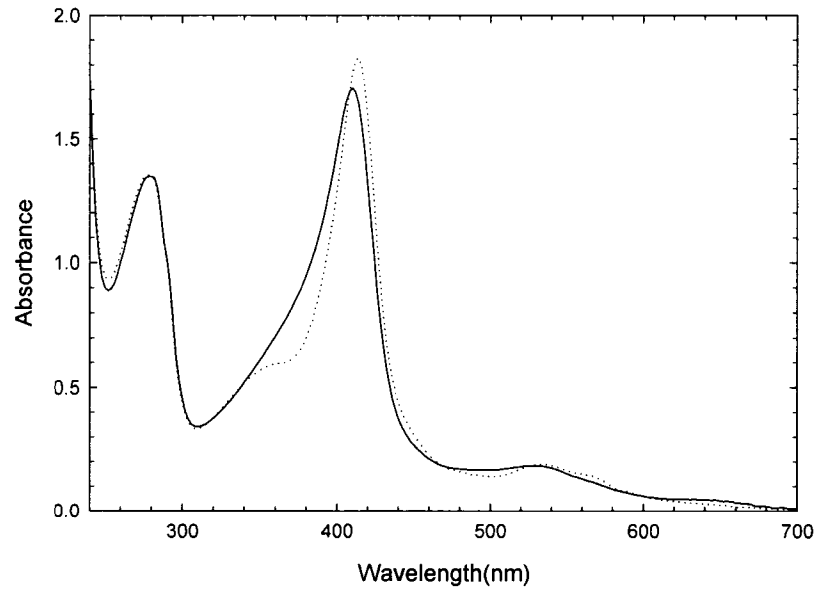

Figure C.14. A comparison of the spectra of 17μM D79K at pH6.0 (solid line) and 7.5 (dotted line) in 100mM potassium phosphate buffer

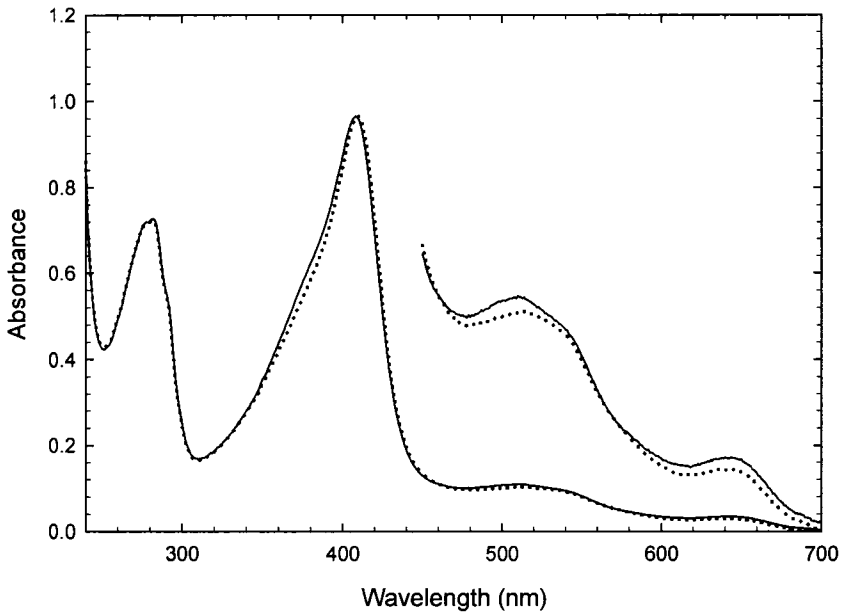

Figure C.15. A comparison of the spectra of 9.79μM E93K at pH6.0 (solid line) and 7.5 (dotted line) in 100mM potassium phosphate buffer

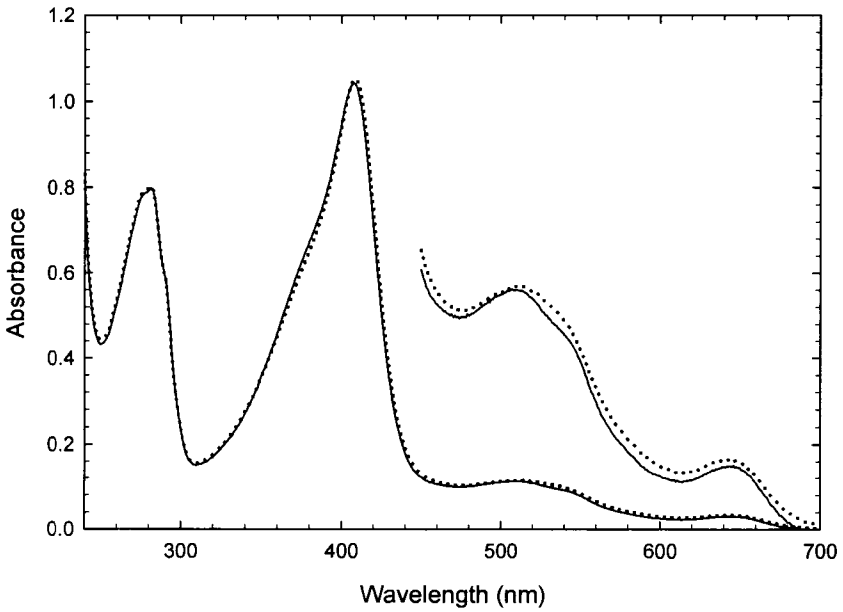

Figure C.16. A comparison of the spectra of 10.6μM E98K at pH6.0 (solid line) and 7.5 (dotted line) in 100mM potassium phosphate buffer

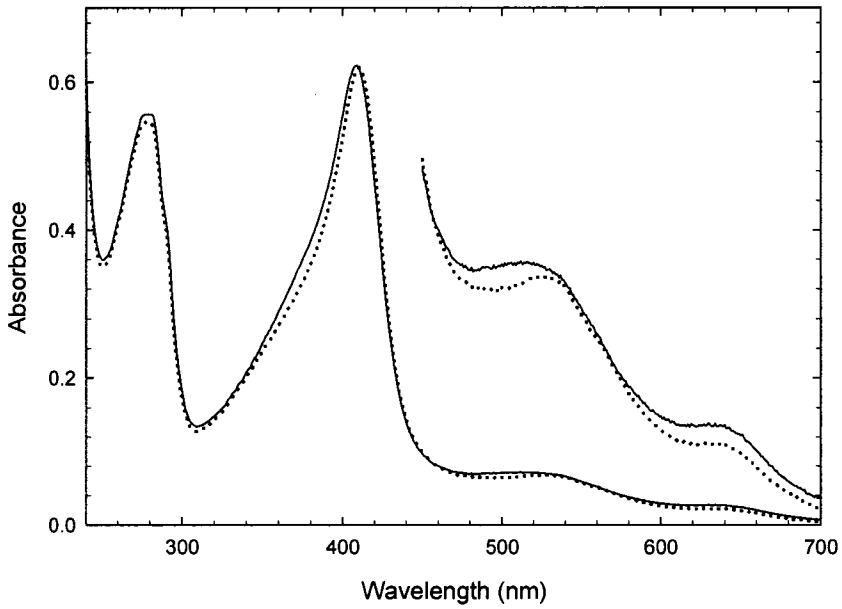

Figure C.17. A comparison of the spectra of 6.35μM E118K at pH6.0 (solid line) and 7.5 (dotted line) in 100mM potassium phosphate buffer

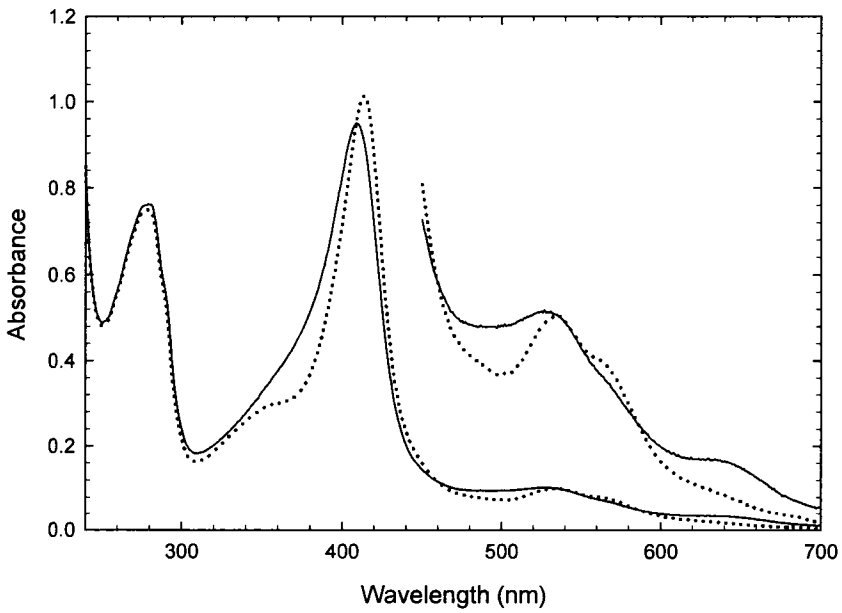

Figure C.18. A comparison of the spectra of 9.66μM D132K at pH6.0 (solid line) and 7.5 (dotted line) in 100mM potassium phosphate buffer

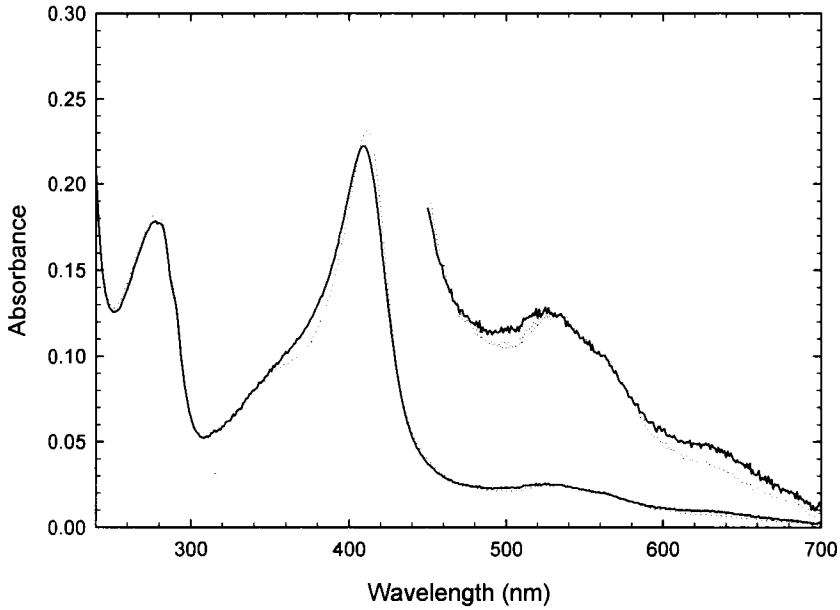

Figure C.19. A comparison of the spectra of 3.15μM E135K at pH6.0 (solid line) and 7.5 (dotted line) in 100mM potassium phosphate buffer

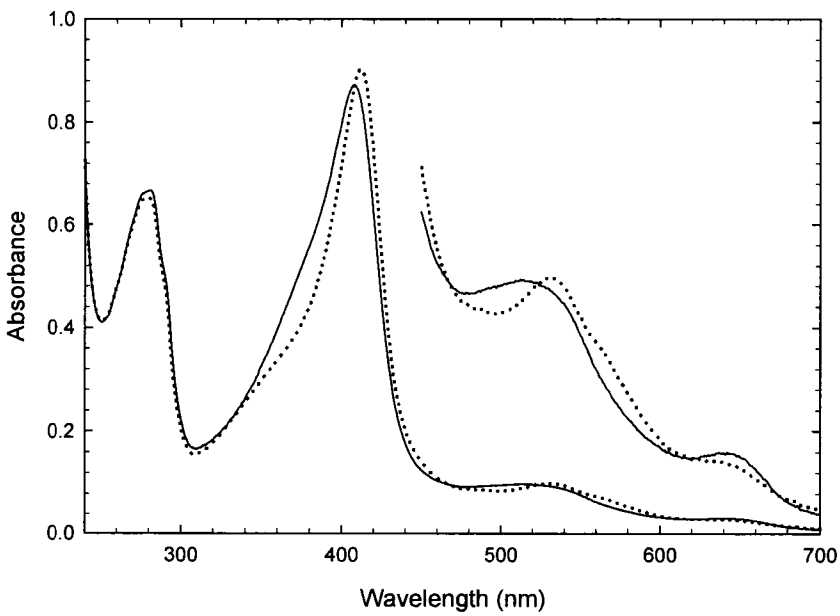

FigureC.20. A comparison of the spectra of 8.79μM D136K at pH6.0 (solid line) and 7.5 (dotted line) in 100mM potassium phosphate buffer

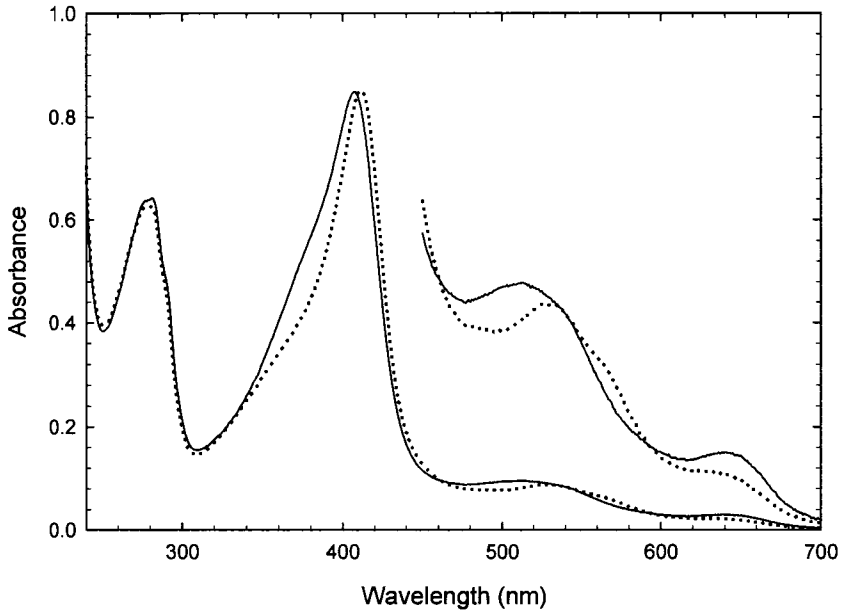

Figure C.21. A comparison of the spectra of 8.57μM D140K at pH6.0 (solid line) and 7.5 (dotted line) in 100mM potassium phosphate buffer

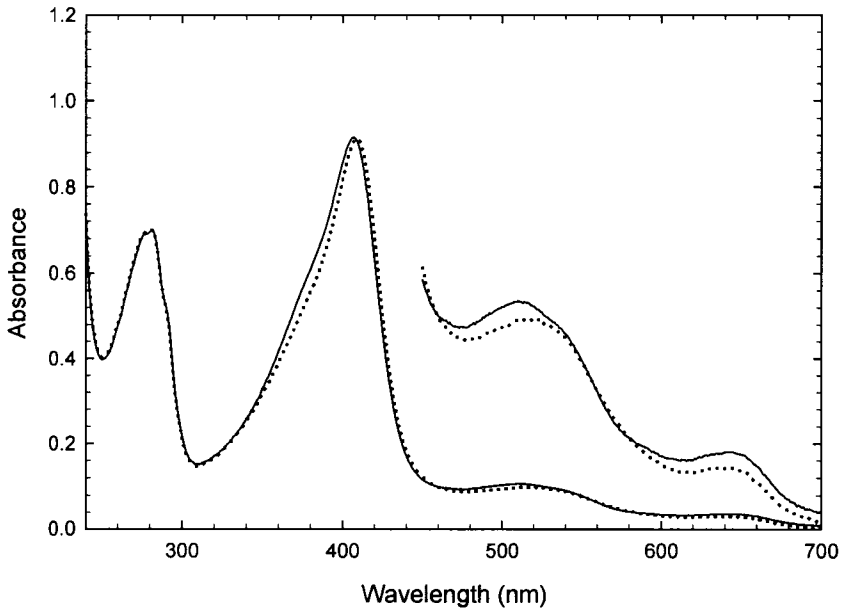

Figure C.22. A comparison of the spectra of 9.20μM D146K at pH6.0 (solid line) and 7.5 (dotted line) in 100mM potassium phosphate buffer

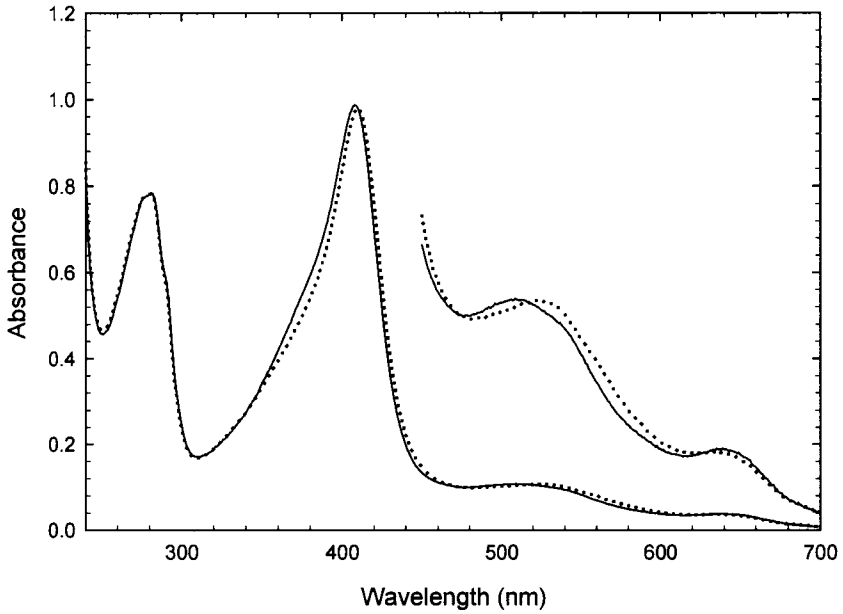

Figure C.23. A comparison of the spectra of 9.99μM D148K at pH6.0 (solid line) and 7.5 (dotted line) in 100mM potassium phosphate buffer

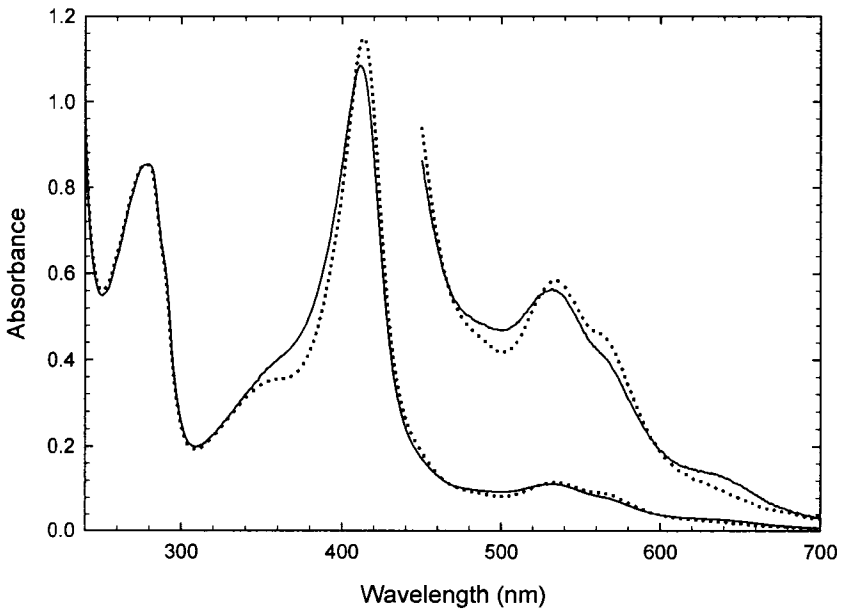

Figure C.24. A comparison of the spectra of 10.9μM K149D at pH6.0 (solid line) and 7.5 (dotted line) in 100mM potassium phosphate buffer

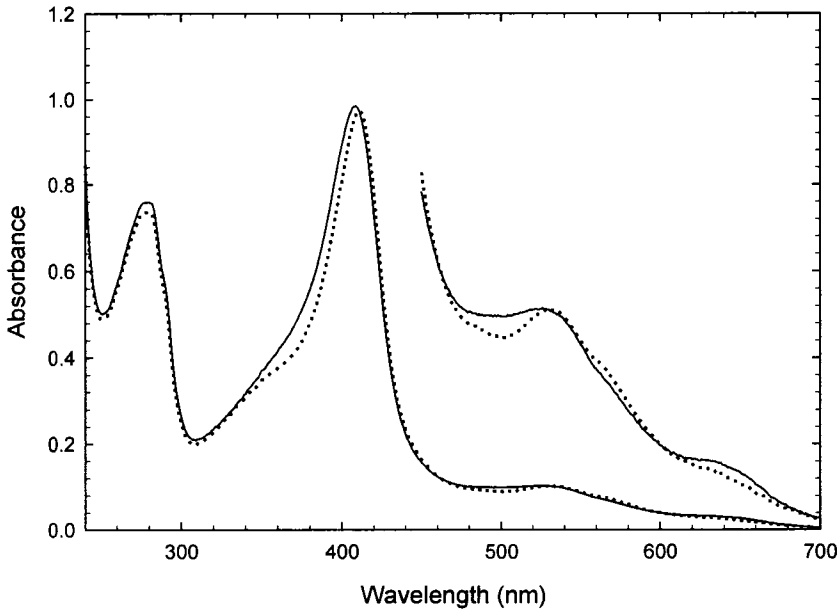

Figure C.25. A comparison of the spectra of 10.0μM D150K at pH6.0 (solid line) and 7.5 (dotted line) in 100mM potassium phosphate buffer

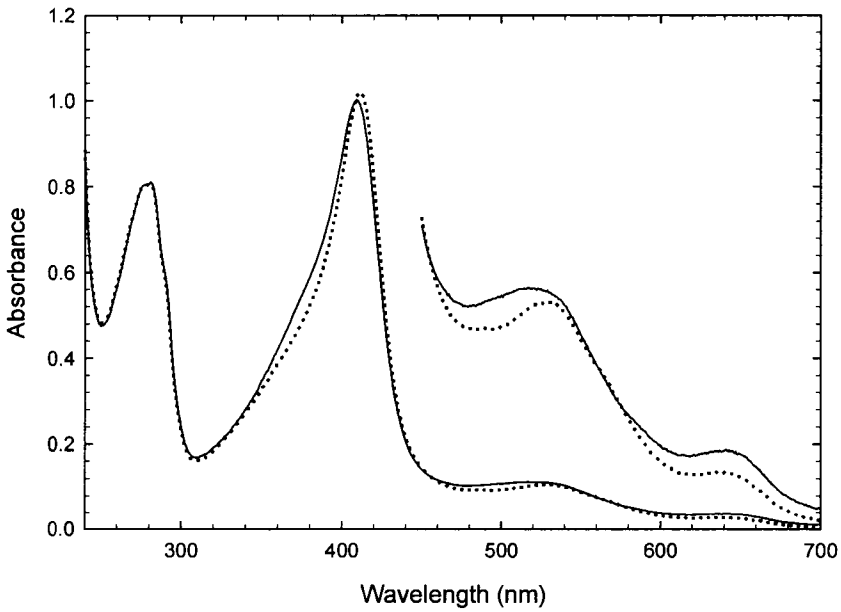

Figure C.26. A comparison of the spectra of 10.1μM D152K at pH6.0 (solid line) and 7.5 (dotted line) in 100mM potassium phosphate buffer

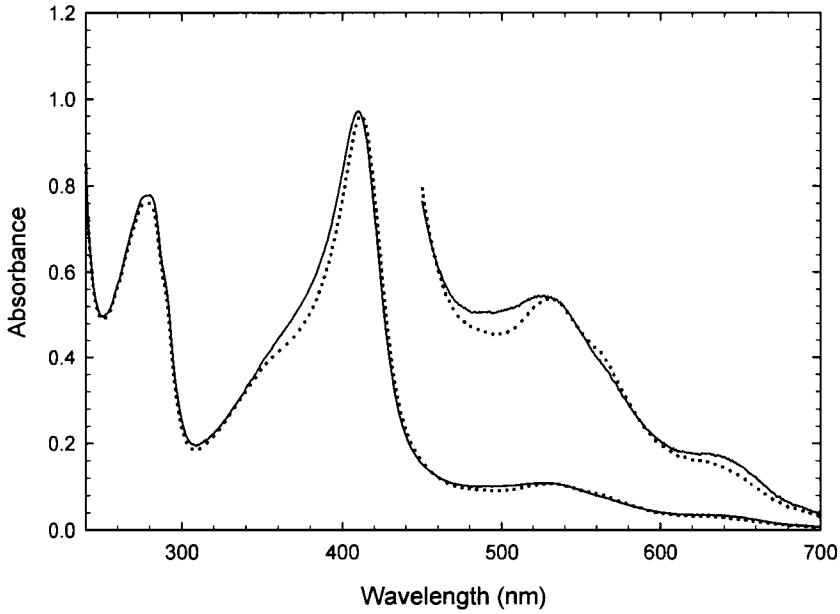

Figure C.27. A comparison of the spectra of 9.91μM D165K at pH6.0 (solid line) and 7.5 (dotted line) in 100mM potassium phosphate buffer

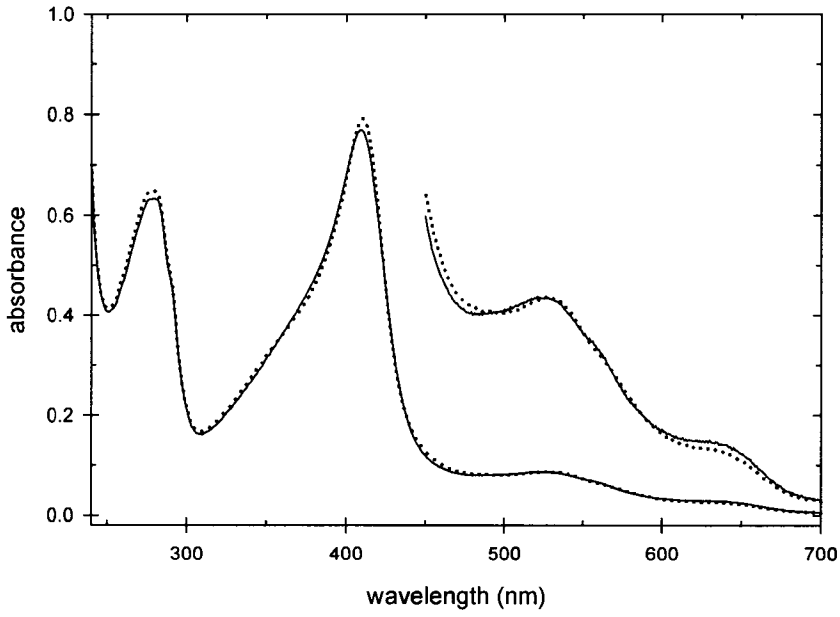

Figure C.28. A comparison of the spectra of 7.61 μM E167K at pH6.0 (solid line) and 7.5 (dotted line) in 100mM potassium phosphate buffer

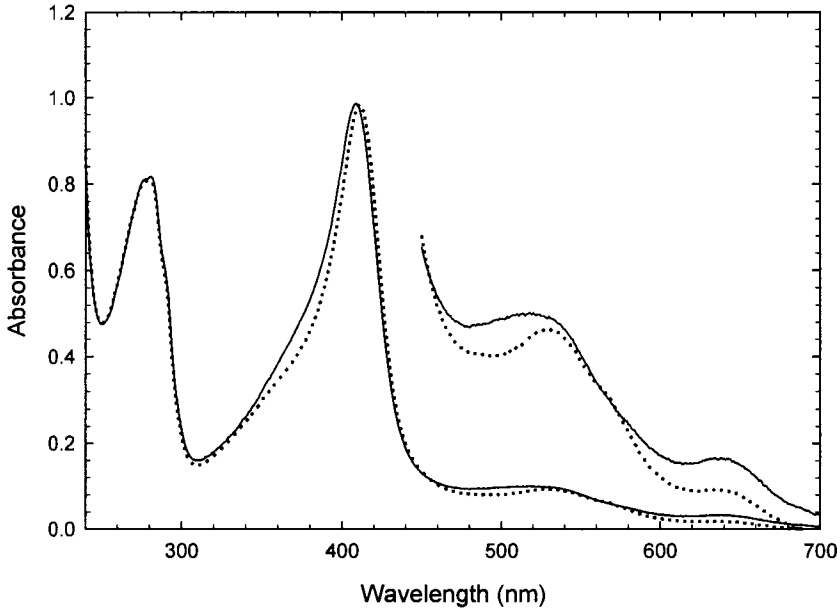

Figure C.29. A comparison of the spectra of 10.0μM E188K at pH6.0 (solid line) and 7.5 (dotted line) in 100mM potassium phosphate buffer

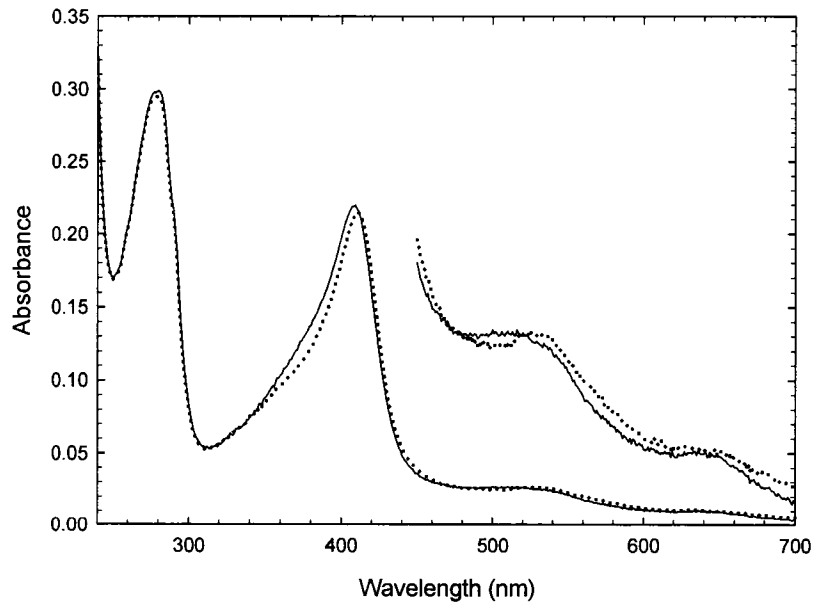

Figure C.30. A comparison of the spectra of 2.23μM E201K at pH6.0 (solid line) and 7.5 (dotted line) in 100mM potassium phosphate buffer

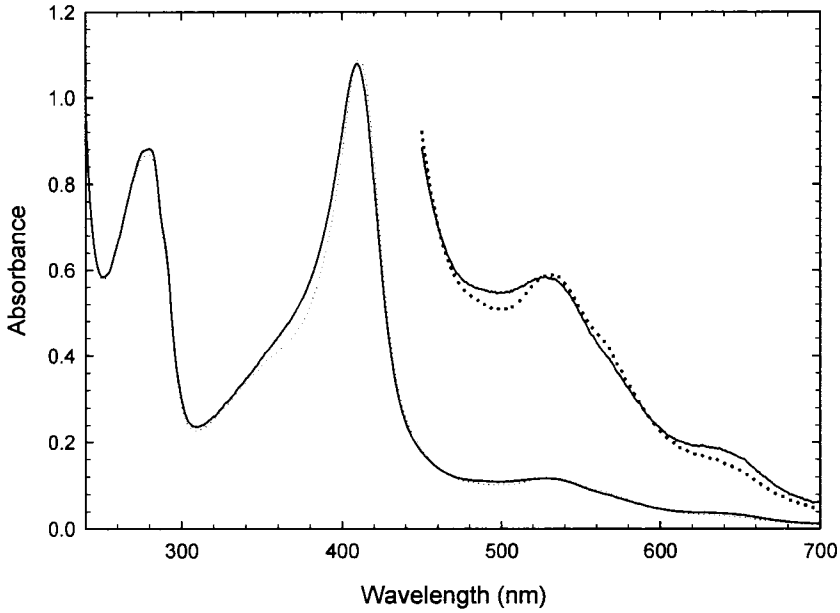

Figure C.31. A comparison of the spectra of 10.9μM E209K at pH6.0 (solid line) and 7.5 (dotted line) in 100mM potassium phosphate buffer

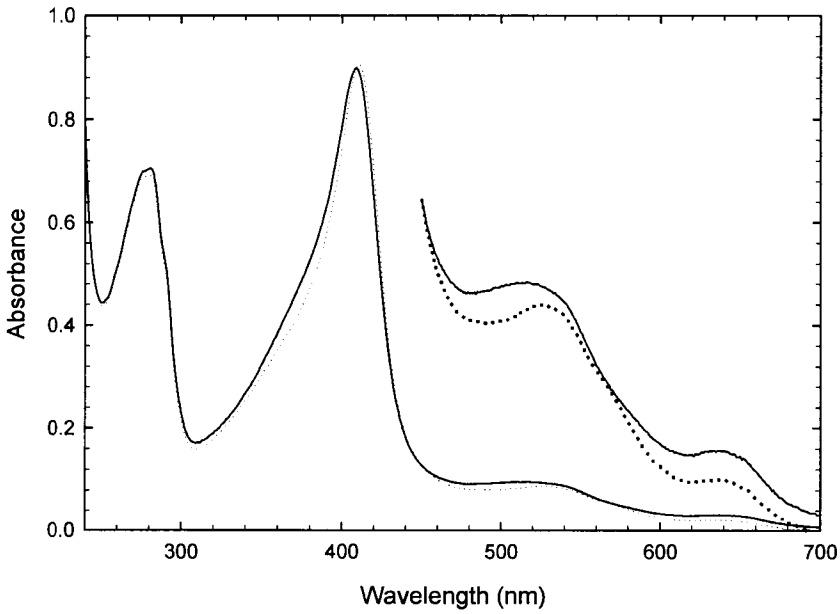

Figure C.32. A comparison of the spectra of 9.05μM D210K at pH6.0 (solid line) and 7.5 (dotted line) in 100mM potassium phosphate buffer

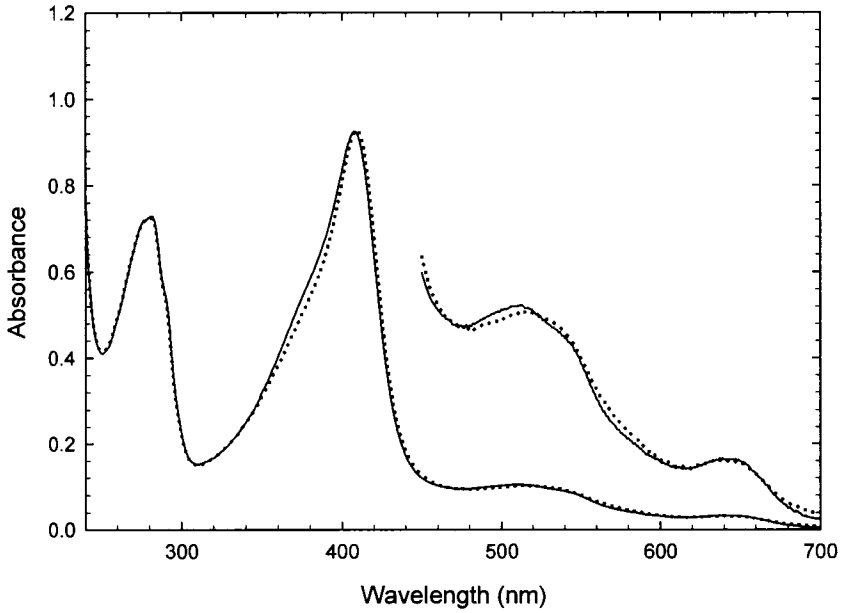

Figure C.33. A comparison of the spectra of 9.39μM E214K at pH6.0 (solid line) and 7.5 (dotted line) in 100mM potassium phosphate buffer

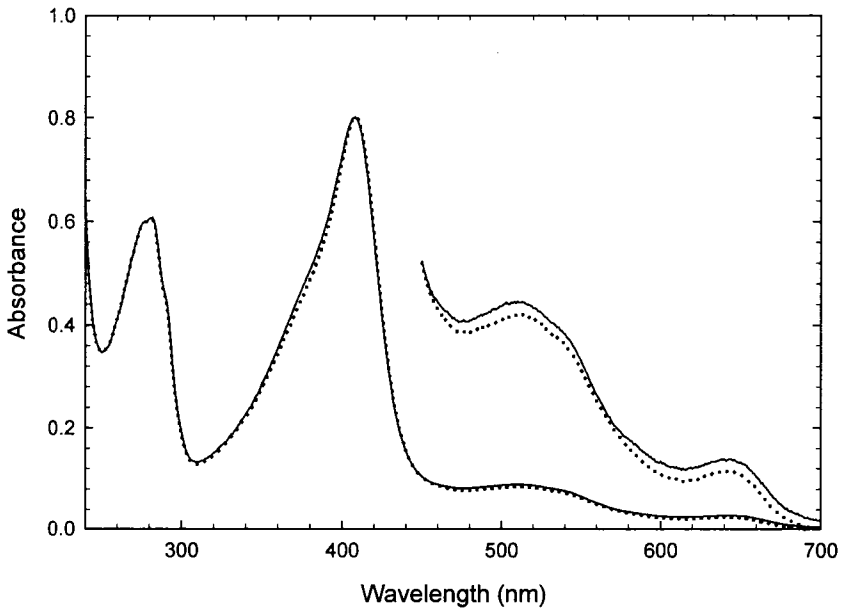

Figure C.34. A comparison of the spectra of 8.13μM D217K at pH6.0 (solid line) and 7.5 (dotted line) in 100mM potassium phosphate buffer

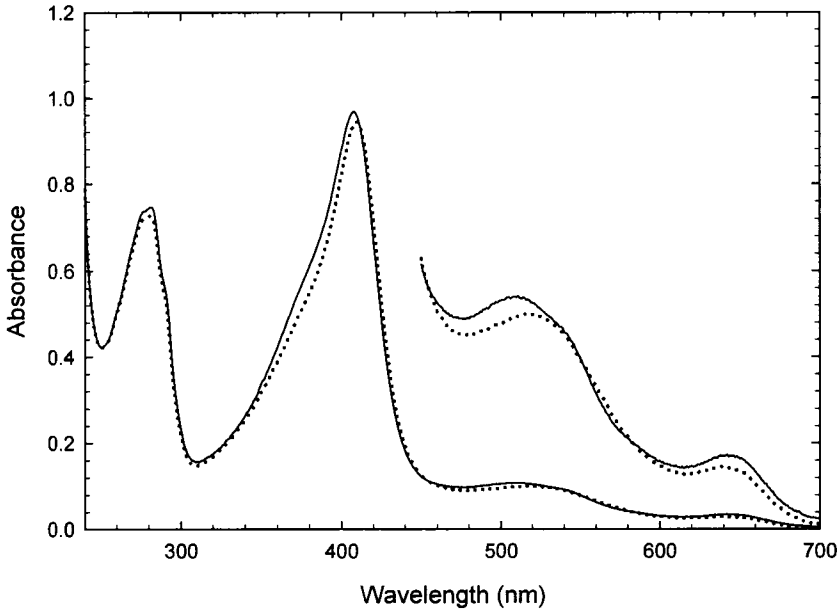

Figure C.35. A comparison of the spectra of 9.75μM E221K at pH6.0 (solid line) and 7.5 (dotted line) in 100mM potassium phosphate buffer

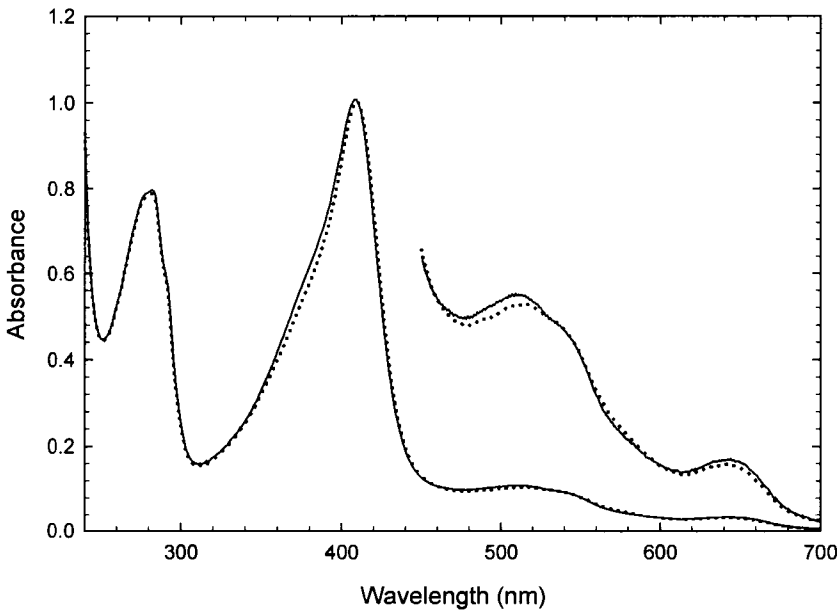

Figure C.36. A comparison of the spectra of 10.3μM D224K at pH6.0 (solid line) and 7.5 (dotted line) in 100mM potassium phosphate buffer

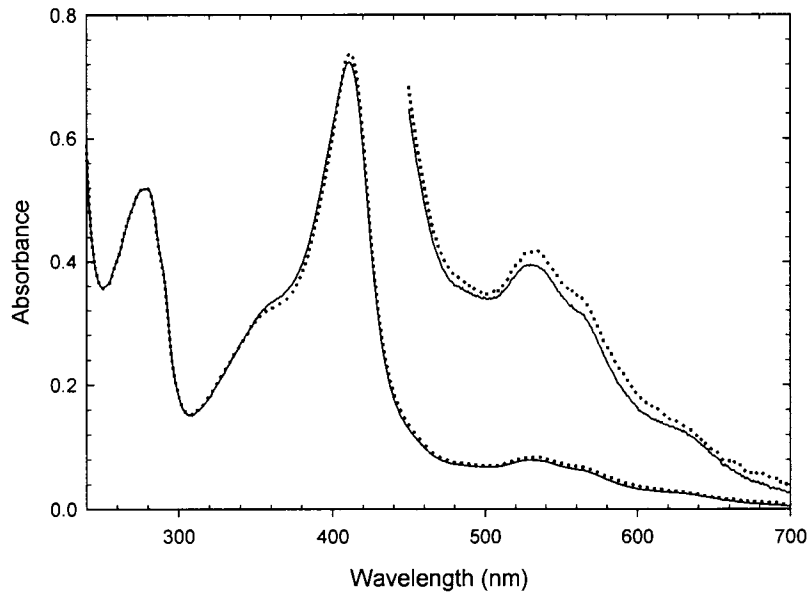

Figure C.37. A comparison of the spectra of 7.324μM D235K at pH6.0 (solid line) and 7.5 (dotted line) in 100mM potassium phosphate buffer

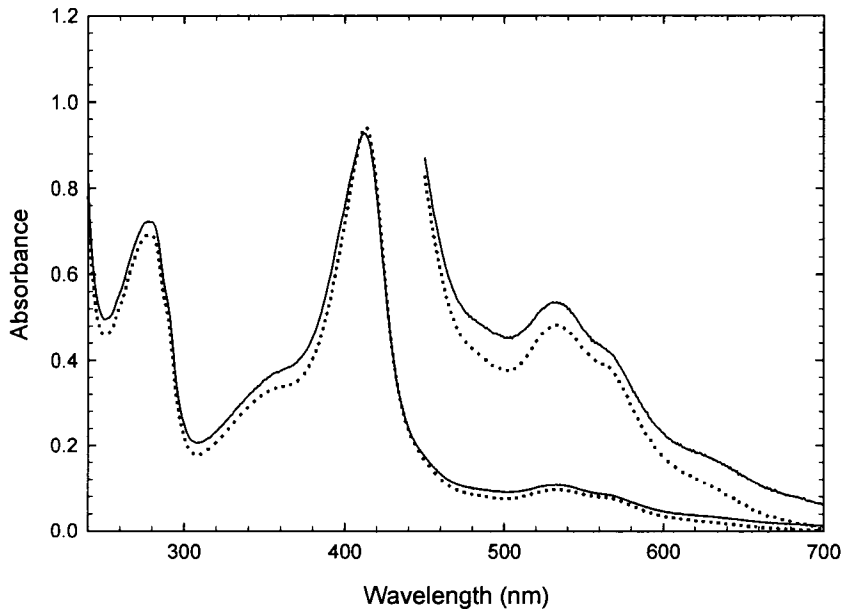

Figure C.38. A comparison of the spectra of 9.53μM D241K at pH6.0 (solid line) and 7.5 (dotted line) in 100mM potassium phosphate buffer

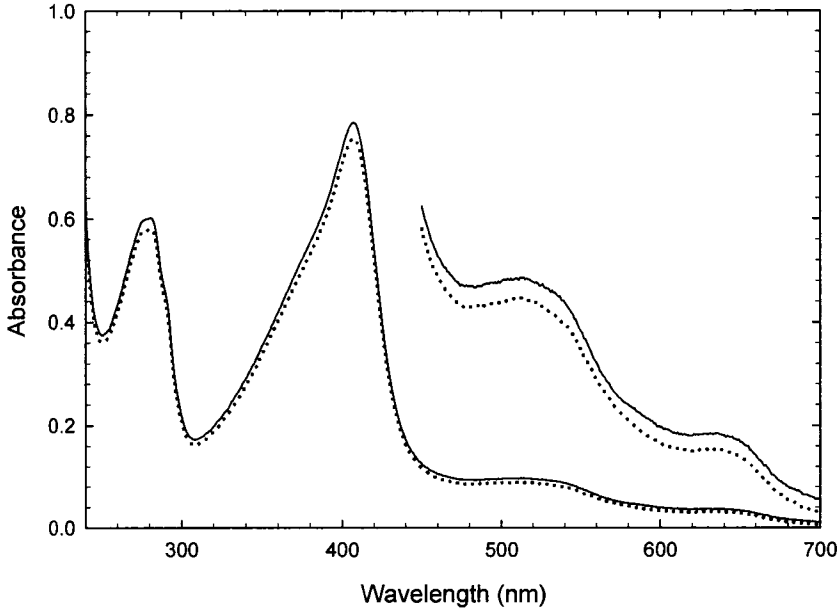

Figure C.39. A comparison of the spectra of 7.89μM E250K at pH6.0 (solid line) and 7.5 (dotted line) in 100mM potassium phosphate buffer

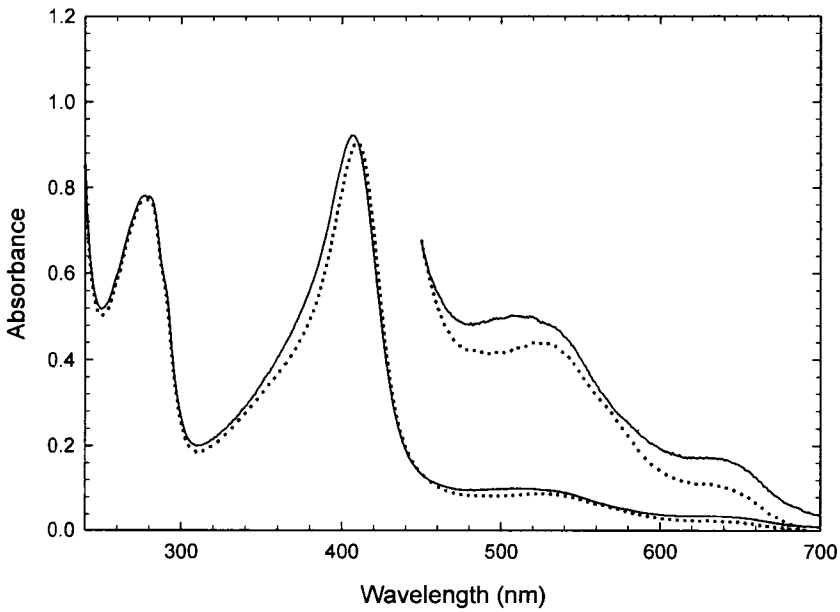

Figure C.40. A comparison of the spectra of 9.40μM D254K at pH6.0 (solid line) and 7.5 (dotted line) in 100mM potassium phosphate buffer

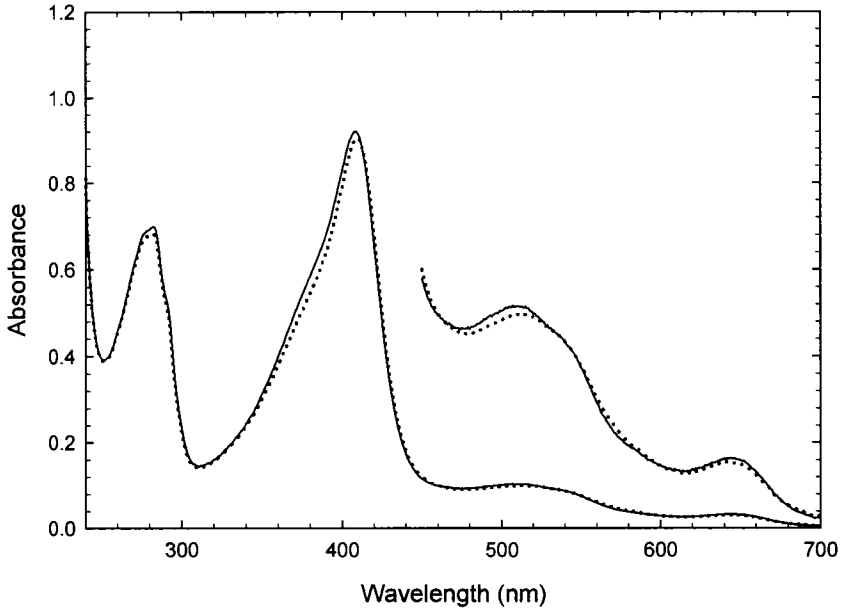

Figure C.41. A comparison of the spectra of 9.32μM D256K at pH6.0 (solid line) and 7.5 (dotted line) in 100mM potassium phosphate buffer

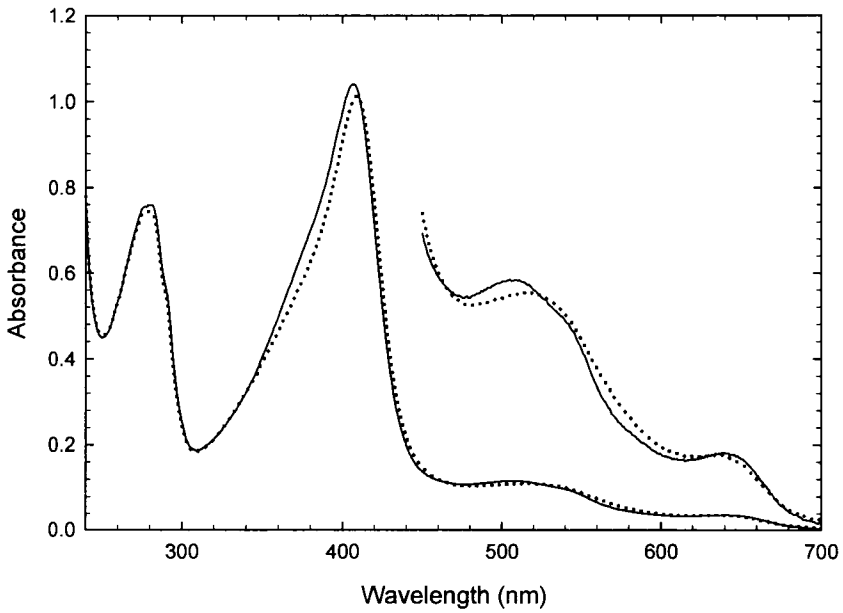

Figure C.42. A comparison of the spectra of 10.5μM D261K at pH6.0 (solid line) and 7.5 (dotted line) in 100mM potassium phosphate buffer

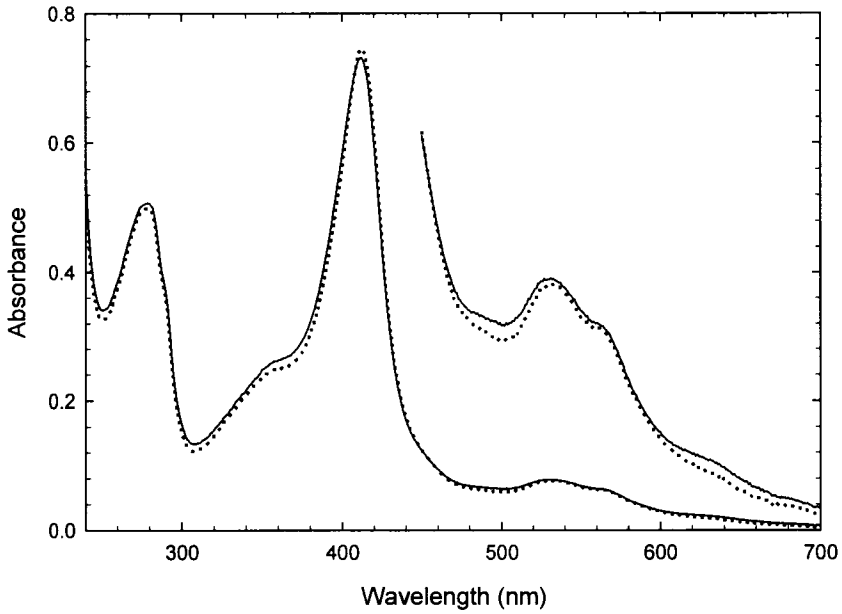

Figure C.43. A comparison of the spectra of 7.44μM E267K at pH6.0 (solid line) and 7.5 (dotted line) in 100mM potassium phosphate buffer

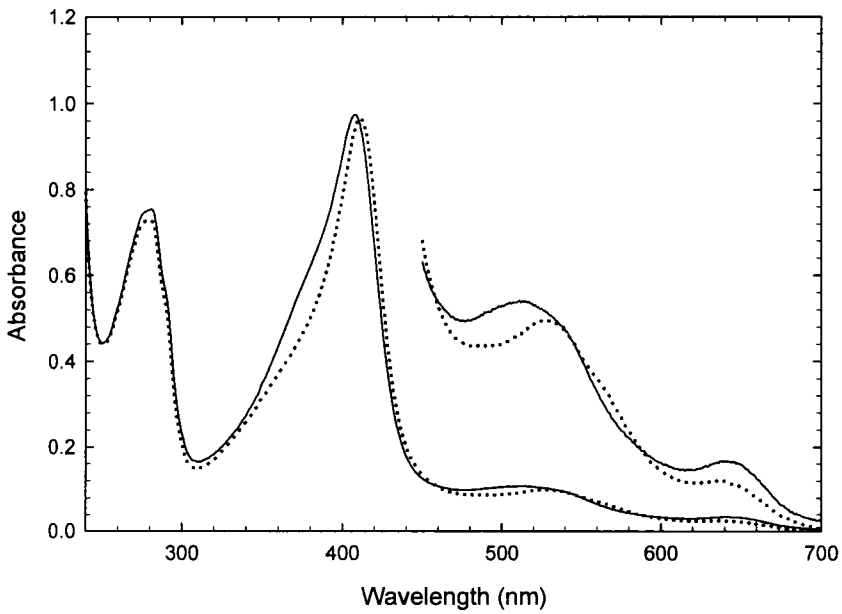

Figure C.44. A comparison of the spectra of 9.83μM E271K at pH6.0 (solid line) and 7.5 (dotted line) in 100mM potassium phosphate buffer

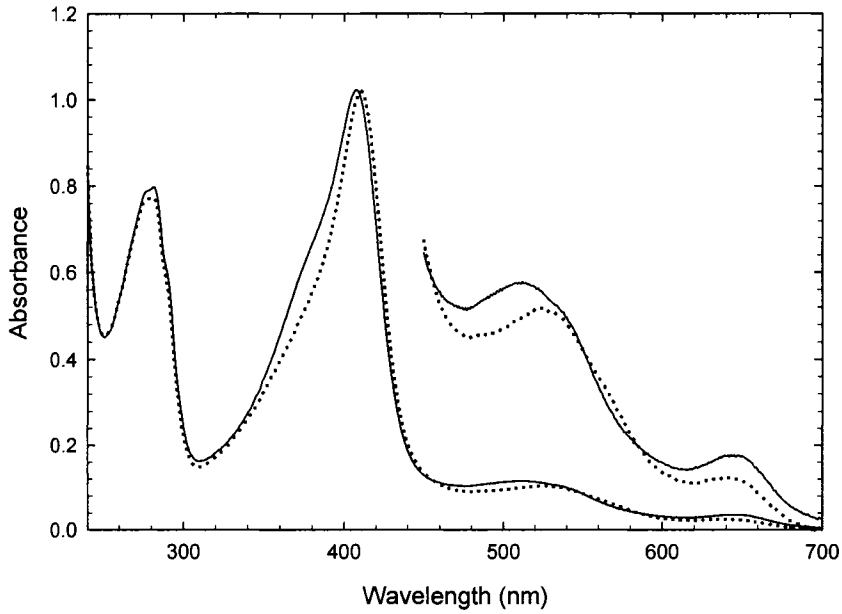

Figure C.45. A comparison of the spectra of 10.3μM D279K at pH6.0 (solid line) and 7.5 (dotted line) in 100mM potassium phosphate buffer

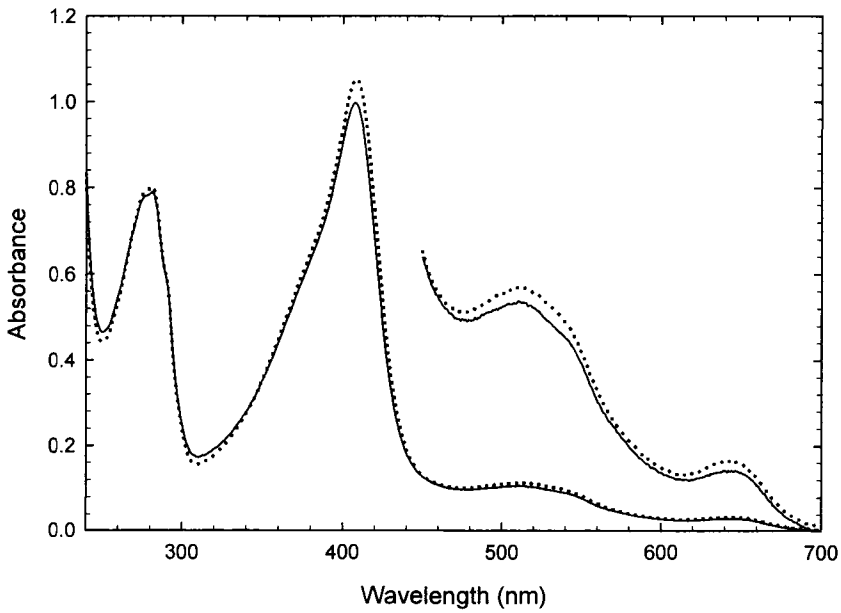

Figure C.46. A comparison of the spectra of 10.2μM E290K at pH6.0 (solid line) and 7.5 (dotted line) in 100mM potassium phosphate buffer

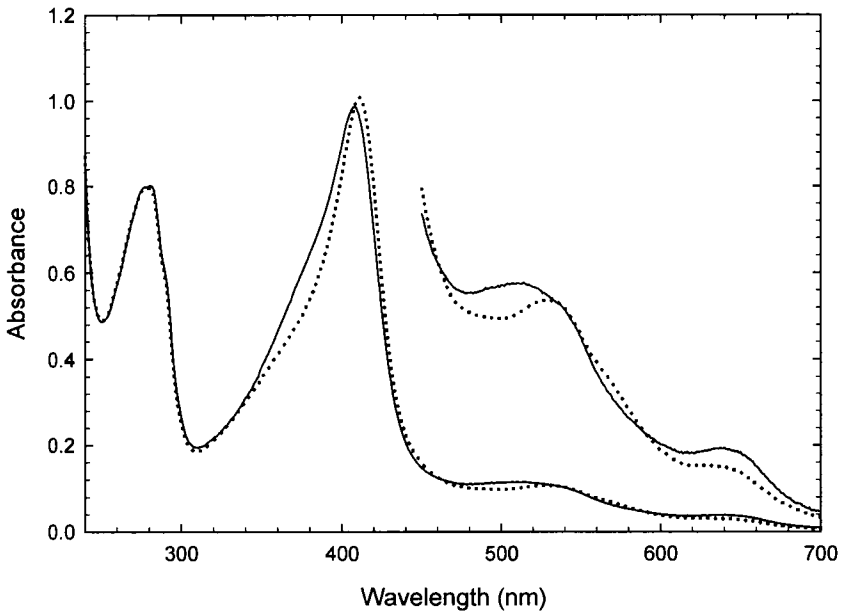

Figure C.47. A comparison of the spectra of 10.0μM E291K at pH6.0 (solid line) and 7.5 (dotted line) in 100mM potassium phosphate buffer

APPENDIX D

ANALYSIS OF CD SPECTRA

APPENDIX D

ANALYSIS OF THE CIRCULAR DICHROISM SPECTRA OF rCcP AND FOUR CHARGE-REVERSAL MUTANTS

Introduction

The estimation of the secondary structure of rCcP and the four charge-reversal mutants D34K, D37K, K149D, and E290K by the CDNN 2.1 software package provided with the AVIV Model 215 Circular Dichroism spectrophotometer did not agree with the amount of secondary structure calculated from the X-ray crystal structure of yCcP (1). With the discrepancy between the CD analysis of secondary structure using the CDNN 2.1 program and that based on the crystal structure of CcP, a number of other methods were used to estimate the secondary structure of rCcP and the four charge-reversal mutants from their CD spectra. These methods were those of Chen *et al.* (2) and the CDPro software package developed by Sreerama and Woody (3), which contains three different programs for secondary structural analysis, namely the CDSSTR, CONTIN/LL and SELCON3 programs. The CDPro package can be used with five different reference protein data sets ranging from 29 to 48 proteins and the protein data sets vary in the wavelength ranges they cover and whether they include or exclude denatured proteins (3). The detailed analyses using each of these additional software packages are given below.

The Chen Method

The Chen method (2) uses least squares analysis for the determination of the secondary structures. The mean residue ellipticity at any given wavelength is given by Equation D.1 where X_i is the experimentally determined mean residue ellipticity at a

$$X_i = f_H X_H + f_\beta X_\beta + f_R X_R \qquad \text{D.1}$$

given wavelength. X_H, X_β and X_R are the reference values at the same wavelength for the pure helix (H), β form (β), and unordered form (R), respectively. The fraction of each form is represented by the f values. The CD spectra of five proteins with known values of X_H, X_β and X_R are used along with the experimental value of X_i to determine the fraction of helix, beta and unordered structure in the protein under analysis. Chen *et al.* (2) also indicated that the equation only applies when the contributions of non-peptide chromophores are insignificant in the wavelength under study. Chen *et al.* included the 3_{10} helix and distorted helix in the f_H values and indicated that their assumption seems to be supported by the theoretical calculations of the optical activity of the helical segments in four proteins. Contributions due to the presence of β turns are included in the values of f_R.

The reference protein set contains 5 proteins and the analysis is done every three nm between 190 and 243 nm. Since the CD spectrum of CcP is taken between 195 and 450 nm, there are 17 data points for the secondary structure estimation. The results

obtained using the Chen analysis are collected in Table D.1. For comparison, the values predicted by the X-ray crystallographic data for yCcP are also included.

Table D.1. Secondary Structure of CcP Predicted by X-ray Crystallography and the Chen Method

Protein	% Helix	% β Structure	% Random Coil	Coordination State
yCcP X-ray	50	6	44	5
rCcP	26	40	34	5
D34K	25	49	26	5
E290K	26	42	32	5
D37K	24	43	33	6
K149D	27	29	44	6

A comparison of the data in Table D.1 indicates underestimation of helix and overestimation of beta structure by the Chen method. As did the CDNN2.1 secondary structure analysis from the CD data, the Chen method of analysis does not agree well with the crystallographic structure of yCcP but does predicts similar secondary structures for rCcP and the mutant enzymes.

CDPro Software Package

The CDPro software package developed by Sreerama and Woody (3) contains three programs, namely CDSSTR, CONTIN/LL and Self-Consistent Method

(SELCON3) for secondary structure analysis. Five reference protein data sets ranging from 29 to 48 proteins are included in the software package. The protein data sets vary in the wavelength ranges they cover and the inclusion or exclusion of denatured proteins.

CDSSTR

This method requires a minimum of only eight reference proteins for a good analysis. Proteins are selected randomly from the reference set and a large number of combinations are made among the eight proteins. This makes the method extremely flexible but may adversely affect the results by making the solution unstable depending on the eight reference proteins selected. A singular value decomposition (SVD) algorithm is used to obtain the solution in CDSSTR method. The results of this analysis using 43 and 37 reference proteins are collected in Tables D.2 and D.3, respectively. Reference values obtained from X-ray crystallography are also included in these tables.

For CDSSTR, ordered helix and distorted helix make up the % helix, ordered strand and distorted strand make up the %β structure, and β turn and unordered forms make up the % unordered form. Four residues per α-helix and two residues per β-strand are regarded as the distorted structures. Again, the secondary structural analysis from the CD data using the CDSSTR program for both the 43 protein basis set, Table D.2 and the 37 protein basis set, Table D.3 underestimate the amount of helix and overestimate the amount of β sheet in comparison to the x-ray analysis just as does the CDNN2.1 and the

Chen analyses. And again, the CDSSTR programs indicate that the secondary structure of rCcP and the four surface mutants are essentially the same.

Table D.2. Comparison of CcP Secondary Structures Predicted by X-ray and CDSSTR Using 43 Reference Proteins

Protein	% Helix	% β Structure	% Unordered	Coordination State
yCcP (X-ray)	50	6	44	5
rCcP	42	25	33	5
D34K	33	23	44	5
E290K	31	23	46	5
D37K	34	20	46	6
K149D	36	17	47	6

Table D.3. Comparison of CcP Secondary Structures Predicted by X-ray and CDSSTR Using 37 Reference Proteins

Protein	% Helix	% β Structure	% Unordered	Coordination State
yCcP (X-ray)	50	6	44	5
rCcP	25	38	37	5
D34K	23	29	48	5
E290K	24	28	48	5
D37K	21	29	50	6
K149D	24	28	48	6

SELCON3

SELCON3 is the latest version of the self-consistent method, SELCON. The analyzed sample is included in the matrix of CD spectral data, and the initial guess, the reference protein structure with the CD spectrum most similar to that of the protein analyzed, is made for the unknown secondary structure. The solution is used to replace the initial guess and iteration is continued until convergence. A singular-value decomposition (SVD) algorithm is used to solve the secondary structure. Reference proteins and SVD coefficients are varied to obtain solutions. Tables D.4 and D.5 show the results of this analysis using 43 and 37 reference proteins. Values from the X-ray analysis are also included in the tables.

Table D.4. Comparison of CcP Secondary Structures Predicted by X-ray and SELCON3 Using 43 Reference Proteins

Proteins	% Helix	% β Structure	% Unordered	Coordination State
yCcP (X-ray)	50	6	44	5
rCcP	21	28	51	5
D34K	26	24	50	5
E290K	28	22	50	5
D37K	25	26	49	6
K149D	26	25	49	6

Table D.5. Comparison of CcP Secondary Structures Predicted by X-ray and SELCON3 Using 37 Reference Proteins

Protein	% Helix	% β Structure	% Unordered	Coordination State
yCcP (X-ray)	50	6	44	5
rCcP WT	22	26	52	5
D34K	23	27	50	5
E290K	25	25	50	5
D37K	21	31	48	6
K149D	24	26	50	6

The results obtained using the 43 and 37 reference proteins data sets show underestimation of the % helix, overestimation of the β structure, and good agreement on the % unordered forms as compared with the X-ray data analysis. Although there is a difference in secondary structures between X-ray and CD analysis, the structures determined by the analysis of the CD are consistent for both five and six coordination states.

CONTIN/LL

CONTIN/LL is a variant of the CONTIN method, the ridge regression procedure. It fits the CD spectrum of the test protein as a linear combination of the CD spectra of the reference proteins. In CONTIN/LL, the reference set is arranged so that the proteins are in the order of increasing RMS distance of the CD spectra from that of the protein

analyzed. Tables D.6 and D.7 give the results of this analysis using 43 and 37 reference proteins, respectively. Also included are the values obtained from analysis of the X-ray crystallographic data. For both reference protein sets used, the results show underestimation of the % helix, overestimation of the % β structure, and good agreement in the % unordered forms compared to the X-ray data. As is the case with the other analyses, the secondary structures determined from the CD data give comparable results for rCcP and the mutants.

Table D.6. Comparison of CcP Secondary Structures Predicted by X-ray and CONTIN/LL Using 43 Reference Proteins

Protein	% Helix	% β Structure	% Unordered	Coordination State
yCcP (X-ray)	50	6	44	5
rCcP WT	24	27	49	5
D34K	27	25	48	5
E290K	28	23	49	5
D37K	27	23	50	6
K149D	28	21	51	6

Table D.7. Comparison of CcP Secondary Structures Predicted by X-ray and CONTIN/LL Using 37 Reference Proteins

Protein	% Helix	% β Structure	% Unordered	Coordination State
yCcP (X-ray)	50	6	44	5
rCcP WT	21	29	50	5
D34K	22	28	50	5
E290K	25	25	50	5
D37K	21	30	49	6
K149D	23	26	51	6

Summary

In general, all of the software packages for the analysis of CD spectra give essentially identical results for the secondary structure of rCcP and the four charge-reversal mutants, and none of the software packages agree with the X-ray structure of yCcP. All of the CD analysis programs underestimate the amount of helix structure in CcP and overestimate the amount of beta sheet structure. A summary of the results for secondary structure prediction from the various software packages is given in Table 4.4 of Chapter 4.

References

1 Finzel, B. C., Poulos, T. L.,and Kraut, J. (1984) Crystal structure of yeast cytochrome *c* peroxidase refined at 1.7 Å resolution, *J. Biol. Chem 259*, 13027-13036

2. Chen, Y. H., Yang, J. T., Chau, K. H., (1974), Determination of the helix and β form of proteins in aqueous solution by circular dichroism, *Biochemistry 13*, 3350-3359.

3. Sreerama, N., and Woody, R.W., (2000), Estimation of protein secondary structure from circular dichroism spectra: Comparison of CONTIN, SELCON, and CDSSTR methods with an expanded reference set, *Analytical Biochem. 287*, 252-260.